UNIVERSITY OF LIVERPOOL

Design of Gold Nanoparticles with Controllable Phase Transfer Properties

Thesis submitted in accordance with the requirements of the University of Liverpool for the degree of Doctor in Philosophy by

Alexander Paul Hill

September 2018

Acknowledgements

First and foremost, I would like to thank my supervisor Prof Mathias Brust for the opportunity to do this project and his continued help and assistance throughout it. It was a pleasure to work with him on trying to develop something both unique and interesting.

My thanks also go out to every member of the Brust group, past and present, for their advice and practical and emotional support throughout my entre PhD. Special thanks go to both Dr Casper Kunstmann and Dr Marcin Grzelczak who provided both support and motivation throughout.

Big thanks also go to Dr Domagoj Belic, Alison Beckett, Mike Craven, Adam Michael Davidson, Stephen Danks, Faye Hern and Malte Strozyk; Domagoj for his invaluable help in cryo-TEM, for which the use of the analytical tool would not have been possible without his high level of experience and determination; Alison for teaching me how to use TEM and helping me out every time the machine misbehaved. Mike, Adam, Stephen, Faye and Malte, thanks for being pillars of emotional support when I was struggling to see the light.

Huge thanks go to my entire family, the Hills and the Booths, for all their emotional support and motivational speeches during those hard moments, with a special mention for my parents Dr Kathryn Booth and Dr Steven Hill, for their unwavering assistance in helping me reach the end of writing my thesis. I would never have reached this moment without them.

Finally, my greatest thanks go to my partner Megan. Always there when I lost my way, always ready to comfort me and get me smiling once more on those hard days, always providing support, you were my rock.

Abstract

The University of Liverpool

Doctor of Philosophy

Design of Gold Nanoparticles with Controllable Phase Transfer Properties

Alexander Paul Hill

This project was aimed at initiating the development of gold nanoparticles (AuNP) functionalised in such a way that allowed for the mimicking of biological systems, those that effectively couple uphill processes with downhill processes to transfer charge across an organic interface (the phospholipid membrane). The hope was to utilize a specific functional group adhered to the gold surface to achieve cation transfer, whilst attempting to achieve electron transfer via the exposed gold core.

Via the application of the cyclic oligomers better known as crown ethers, taking advantage of their selective cation association properties, the transfer of cations from the aqueous phase to the organic phase via the use of small functionalised gold nanoparticles was successfully demonstrated. The most effective system (18-Crown-6-modified AuNPs) was identified via comparative studies between the rates of phase transfer with various cations. These studies were then later used to achieve complimentary cation transfer across an artificial membrane, evidenced by both cryo-TEM and fluorescence spectroscopy data.

This idea was then taken further by implementing the same crown ether (18-Crown-6) upon larger AuNPs (7.5nm), a gold core volume with a much greater potential for allowing the transfer of electrons. Not only did AuNPs modified in this way result in similar phase transfer and membrane adherence of the 3nm particles, but also presented a unique process; entropically driven reversible agglomeration with changes in temperature. This system was characterized in full to further advance our understanding, to maximise the potential of using it for both cation and electron transfer.

Preliminary work on the interaction of the larger AuNPs with a redox couple (potassium ferro/ferri cyanide) was briefly undertaken, in the hopes of transferring an electron from one redox partner to the other, via the coupling of a downhill reaction, the formation of Barium Sulphate. However, this system was not fully realised within this thesis, but a solid foundation was laid for future work.

List of Abbreviated Acronyms

AuNP – Gold Nanoparticle

ATR – Attenuated Total Reflection

DDT – Dodecanethiol

DLS – Dynamic Light Scattering

DOPC – Dioleoylphosphatidylchline

FTIR – Fourier Transform Infra-Red

ITC – Isothermal Titration Calorimetry

LCST – Lower Critical Solution Temperature

MUC - Mercapto Undecane Carboxylate

MUDA – Mercaptoundecanoic Acid

MUS - Mercapto undecane sulfonate

OT - Octanethiol

PEG – Polyethylene Glycol

SEM – Scanning Electron Microscopy

SPR – Surface Plasmon Resonance

TEM – Transmission Electron Microscopy

TOAB – Tetraoctylammoniumbromide

UCST – Upper Critical Solution Temperature

UV-Vis – Ultraviolet – Visible Spectroscopy

Contents

Chapter 1 Introduction and Background Literature Review

1.1 Introduction

Biological systems have often been regarded as having superior performance when compared to anything non-biological; this is believed to be down to the nanoscale organisation at which these systems operate[1]. Deliberate nano-structuring of artificial materials has therefore been widely explored in an attempt to replicate the efficiency of biological systems; what these systems are attempting to replicate is a biological model that is stable and close to thermodynamic equilibrium. Such attempts at replicating passive biological structures have resulted in great success; examples being lotus leaves, gecko feet and morpho butterfly wings, resulting in self-cleaning surfaces[2, 3], novel adhesive materials[4, 5] and optical coatings[6, 7]. It is these passive nanostructures that represent current state-of-the-art nanotechnology.

Whilst the development of such materials is extremely useful, what is commonly overlooked when referring to bio-inspired nanotechnology is that biological systems use predominantly active nanostructures that are capable of fulfilling energy consuming functions such as signal processing, active transport[8] and uphill chemical processes[7].

Whilst these processes rely on the biological systems' nano-organisation, they also rely on the ability of the system to operate under conditions that are far from chemical equilibrium. This essential feature is generally considered to be the definition of a living object; a human being only functions because it uses processes that constantly keep the system from reaching equilibrium. A good example is an ion transporter. Ion transporters, also called an ion pump, are transmembrane proteins that move ions across a plasma membrane against their concentration gradient. Such proteins are capable of driving the system against its natural equilibrium due to the consumption of fuel, which can vary from Adenosine triphosphate (ATP) to sunlight and other redox reactions. Because the system is consuming energy to drive a system out of equilibrium it is considered an active process. The development of synthetic ribosomes by Andrew Tuberfield[9, 10] is a perfect example of we can attempt to replicate nature's own processes to further our understanding.

The research discussed and described in this thesis is about the development, characterisation and implementation of gold nanoparticles (AuNPs) coated in crown-ether moieties which could become capable of behaving as artificial active nano-structures by combining the cation binding affinity of crown ethers with the potential for electron conduction through the gold core. This opens a pathway to potentially creating an artificial nano-system capable of transporting both cations and electrons across barriers; opening avenues into artificial nano-batteries capable of mimicking the active processes that occur within biological cells.

1.1.1 Publications

Journals

Grzelczak, Marcin P, Hill, Alexander P, Belic, Domagoj, Bradley, Dan F, Kunstmann-Olsen, Casper and Brust, Mathias (2016) Design of artificial membrane transporters from gold nanoparticles with controllable hydrophobicity. FARADAY DISCUSSIONS, 191. 495 - 510.

Hill, Alexander, Brust, Mathias, Kunstmann-Olsen, Casper and Grzelczak, Marcin (2018) Entropy-Driven Reversible Agglomeration of Crown Ether Capped Gold Nanoparticles. Chemistry: A European Journal, 24 (13). 3151 - 3155.

Conferences

July 2015: 7th International Gold Conference, Cardiff Catalysis Institute, Cardiff University, Cardiff, UK: Poster presentation on 18-Crown-6-modified AuNPs and phase transfer.

July 2016: Nanoparticles with Morphological and Functional Anisotropy, Glasgow, UK: Discussed the Faraday Discussion paper as seen in above publications.

March 2018: 255th ACS National Meeting & Exposition, New Orleans Convention Centre, New Orleans, Louisiana, USA: Presenting published work from Chemistry-A European Journal.

1.1.2 Structure of the Thesis

Chapter 1

The rest of this chapter will introduce the background to the different properties that we will be attempting to exploit to promote cation/electron transport across systems set far from equilibrium. This will be followed by a brief discussion of characterisation techniques used and a discussion of some of their pros and cons.

Chapter 2

Describes the successful (and failed) attempts at functionalisation of both small (3nm) and larger (7.5, 15.5 and 25.7 nm) AuNPs coated in either pure crown ether ligand or achieved through secondary functionalisation (15.5 and 25.7 nm with PEG 5000), all stable within pure aqueous media. The chapter also goes into detail about their characterisation and general properties.

Chapter 3

Effectively demonstrates that after phase transfer testing with various cations (K^+, Na^+, Li^+ and Ba^{2+}) that 3 nm 18-Crown-6-modified AuNPs show high degrees of selectivity for both K^+ and Ba^{2+} in relation to the other cations, even when in pure aqueous media that was shown in literature to reduce the stability constant and binding selectivity of the crown ether moieties. The 3 nm 18-Crown-6-modified AuNPs are then shown to successfully transport K^+ passively across lipid membranes in the form of vesicles, with the AuNPs showing no interest in membrane penetration until the addition of the complimentary cation K^+, resulting in an on-off trigger style mechanism where by the particles hydrophobicity can be directly controlled and activated. This chapter also discusses preliminary attempts at creating larger 18-Crown-6-modified AuNPs.

Chapter 4

Discusses and characterises the both interesting and unique properties of the 7.5 nm 18-Crown-6-modified AuNPs which is the reversible agglomeration of the particles to one another and/or nearby surfaces upon heating and cooling of the aqueous solution. A property that appears to show the basic principle of Gibbs free energy in a unique experimental form. This interesting property was then shown to potentially be usable in

controlling the hydrophobicity of the particle, with lower temperatures showing little sign of membrane penetration and higher temperatures showing potential membrane penetration, as the particle stability lowers in the aqueous media with increasing temperature. Preliminary phase transfer experiments were undertaken to determine whether the 7.5 nm 18-Crown-6-modified AuNPs were capable of achieving similar phase transfer properties as the 3 nm AuNPs, with the addition of a redox couple (potassium ferro/ferri cyanide) to set a foundation for further experimentation to determine whether electron transfer can be coupled with cation transfer (Ba^{2+}) between two aqueous phases surrounded by an organic interface.

Chapter 5

Discusses potential avenues for advancing this work in the future by laying out ideas that could be utilized to plan and develop more experiments capable of providing further insight into how these particles can effectively transfer charge across membranes/interfaces. There are also a few examples of more niche experiments that could be utilized to try and find other potential avenues of use for the 18-Crown-6-modified AuNPs. These future work proposals are followed by a brief conclusion summarizing the successes of the project, with milestones that were reached and goals that can be met with further work.

1.2 Background Literature Review

This section reviews the background literature relevant to the challenges of the work discussed in this thesis, namely the synthesis, stabilisation and functionalisation of gold nanoparticles, the properties of crown ethers, the use of crown ethers as membrane transports and the interaction of gold nanoparticles and lipid membranes.

This body of work forms the starting point for the research that is subsequently presented. The historic development of AuNPs is needed to further explore potentially effective methods of developing a suitable conductive core, followed by exploitation of this property within a vesicle membrane, which retains its stability in a variety of environments. The crown ether literature review was undertaken in order to better understand the molecule, with its selective cation binding and phase transfer properties, including cation transfer through membranes in suitably structured compounds; the compound would prove extremely useful if these properties were able to be attached to a conductive core such as gold. The interaction of AuNPs with membranes, including both active and passive insertion was explored in this section to further understand the properties that are required for successful integration, otherwise the whole line of research would prove fruitless if the particle was never able to interact with a membrane in the first place.

1.2.1 Synthesis, Stabilisation and Functionalisation of Gold Nanoparticles (AuNPs)

As the size of gold structures is progressively decreased, significant changes to both its chemical reactivity and physical properties are observed, chiefly due to the larger ratio of surface atoms to bulk atoms. The reasoning behind this is well known from the field of surface science and electrochemistry, which show the importance and unique chemistry of surface, edge and defect atoms[11] . The incomplete configuration of the atoms leads them to become highly reactive, which under normal circumstances results in a short lifespan due to the large entropic drive to limit the number of atoms within a system with an incomplete electron configuration. The typical solution to this entropic drive is for smaller nuclei to merge with one another, forming larger particulates with reduced ratios of surface to bulk atoms. This process, when left unchecked, would continue to occur until the system had properties that essentially resemble that of bulk gold.

To stop the aggregation of smaller particulates to such a size that mimics bulk gold prevention methods must be implemented. This can be achieved via one of three ways; charge stabilisation[12], encapsulation[13, 14] and steric/ligand stabilisation[14].

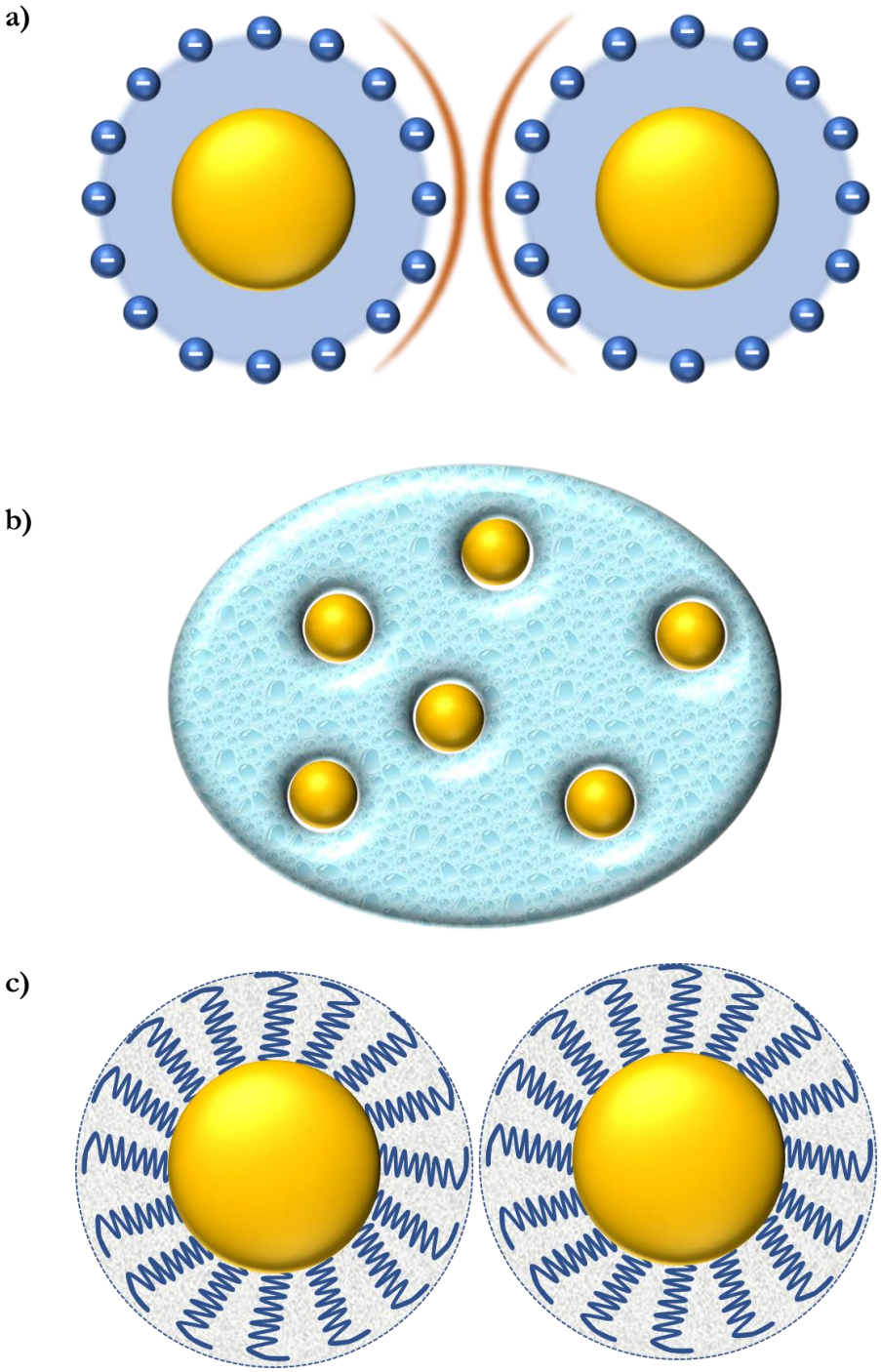

Figure 1.1: Illustrations showing a) Electrostatic stabilisation, b) Encapsulation and c) Ligand stabilisation of AuNPs

Charge stabilisation is a method whereby a charged compound is either electrostatically bound to the AuNP surface, a process well demonstrated by the Turkevich synthesis method involving citrate[15], or by the covalent bonding of a ligand stabilised shell with a charged end group[16]. The charge that is now situated on or around the AuNP causes the GNPs to electrostatically repel one another when coming within close proximity, preventing them from being able to effectively aggregate.

Encapsulation is a method whereby the particles are trapped in a solid medium of some form which physically prevents the particles from being able to move closer to one another, therefore preventing aggregation. Well known examples of this type of stabilisation are red stained glass windows and polymer gels[17].

Ligand stabilisation works by chemically binding a compound to the surface of the AuNP, resulting in the creation of a physical shell around the particles, sterically preventing them from coming into close enough contact with one another to allow aggregation to occur. This type of stabilisation can also be achieved by fixing the particles to a surface using rigid connector ligands which prevents the particles from aggregating whilst not entirely encapsulating them. This anchoring method is commonly used due to the ability to affix a wide range of end groups, and therefore functionalities, to the external end of the ligand attached to the AuNPs. There are a several types of functional group that can be used to bind to the gold surface, with some of the possibilities being alcohols[18] and amine groups[19]. The most common however is the gold-thiol bond. The gold-thiol bond has an average enthalpy of formation (ΔH_f) of approximately 418 $KJmol^{-1}$ [20], with the next strongest bond being that for gold-boron at approximately 368 $KJmol^{-1}$ [21]. This high enthalpy of formation for the gold-thiol bond results in thiolated compounds readily replacing other ligands situated upon the AuNP surface, swiftly forming self-assembled mono-layers[22]. The scientific literature is filled with examples of various types of ligands being bound to an AuNPs surfaces this way, including long chain poly-ethylene glycol (PEG)[23], Oligomers[24] and polymers[25] to name a few.

Encapsulation, whilst useful within scientific research, is not effective for the work discussed within this thesis and so shall not be discussed in detail.[26, 27]

The earliest detailed report of such a AuNP being developed in this way was known as the Schmid's cluster, $[Au_{55}(PPh_3)_{12}Cl_{16}]$, which was reported in 1981 and showed, at that

time, unique properties of highly monodisperse (1.4 nm ± 0.4 nm) AuNPs, despite its precarious and delicate synthesis[28]. This process was then improved upon by Mulvaney and Giersig in 1993[29] when it was first reported in the stabilisation of AuNPs via the use of alkanethiols, with the chain length being variable, giving rise to the potential for modification[29]. In 1994 the Brust-Schiffrin method was developed, with a modified procedure used within this thesis . A synthesis that has had considerable impact in the field due to the allowance of facile synthesis of both thermally- and air-stable AuNPs whilst still being monodisperse, with the size of the AuNPs created ranging from 1.5 to 5.2 nm in size; the increasing size of the AuNPs made in this manner did result in higher dispersity values however. The technique used was initially inspired by Faraday's two-phase system[30], combined with the use of thiols that strongly bind gold due to the soft character of both Au and S[23, 31]. The experimental procedure, briefly described, involved the transfer of $AuCl_4^-$ into toluene by extraction from the aqueous phase by tetraoctylammoniumbromide (TOAB). The toluene mixture was then vigorously mixed with an aqueous $NaBH_4$ solution whilst in the presence of dodecanethiol, resulting in the formation of monodisperse, stable dodecanethiol coated AuNPs. It was found that larger thiol:gold molar ratios gave smaller average core sizes, and fast addition of the reducing agent into cooled solutions gave more monodisperse AuNP formation.

From this moment on the modifications to both the experimental procedure and thiolated ligands used advanced quickly. Brust *et al.* further improved the synthetic procedure via the use of p-mercaptophenol, resulting in the development of a single phase system[23], opening the avenue for a more diverse range of ligands to be utilized[32, 33], which then resulted in a plethora of published literature on analysis of various ligands being placed upon AuNPs[34, 35]. The original work is therefore of immense importance both in terms of the role it has played in the scientific literature over the last two decades, and for providing a starting point for the work produced for this thesis; The research within this thesis uses a modification of this method, with a successful publication being the outcome[36].

The next step is to move on to the synthesis of larger AuNPs (10-200 nm); this is where the Turkevich synthesis, developed in 1951[37], or modifications thereof [38-43] are used; desired for its lack of toxic reactants, allowing for use in medical experimentation, but also for the production of highly monodisperse samples. The source of the gold in this method is tetrachloroauric acid ($HAuCl_4$), with the reducing agent being citrate, which

also acts as the stabilising agent once it has been reduced to its ketone form[44] The use of citrate as both the stabilising agent and the reducing agent is not essential, however, as different compounds are also capable of achieving the same outcome[45-48].

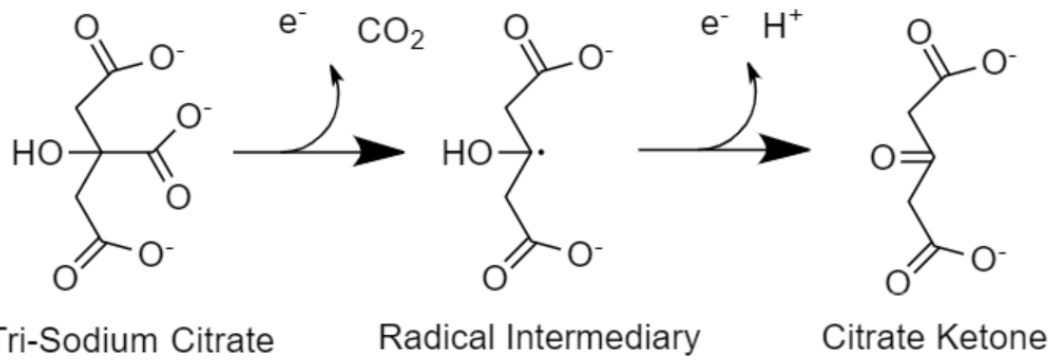

Figure 1.2: Reaction mechanism showing how Tri-Sodium Citrate reduces the Au(III) to Au(0), with the product (the ketone) acting as the stabilising agent.

The process for this method is as follows (Figure 1.2): The reduction of Au(III) to Au(0), resulting in precipitation, requires three electrons. The oxidation of citrate however only provides two electrons upon formation of the stabilising ketone agent, resulting in the ratio of citrate to gold being 3:2 as a bare minimum. The concentration of citrate within the solution can be increased to control the size of particle created, with higher concentrations citrate resulting in smaller particle sizes, with reports of ~10 nm particles being formed at around 5.2 mM concentration. Evidence suggests that higher concentrations of citrate within solution results in the destabilisation of the colloidal solution[49].

Other important factors that have been shown to contribute to the synthesis process are: pH[50], solvent[51], perpetually homogenous solution (vigorous stirring) and a static temperature. The controlled stirring and temperature are necessary to initiate AuNP nucleation across the whole system simultaneously, giving rise to AuNP growth rates across the system being similar, resulting in monodispersed samples. The pH of the system is important as it dictates the stability of the solution; decreasing the pH will result in aggregation due to the loss of electrostatic stability, whilst increases in pH result in typically more stable systems, to a degree.

The key steps to synthesising highly monodisperse AuNPs are fast nucleation which, as stated previously, is where all nucleation sites and seed growths are formed

simultaneously; followed by slow propagation to allow for currently existing AuNPs seeds to grow into highly monodisperse spherical AuNPs. These steps are achieved through the Turkevich method by heating the gold salt solution above the reacting temperature and then quickly and homogenously adding a pre-warmed reducing agent to initiate nucleation. Modifications of the process such as the reverse Turkevich method[49] heat the reducing agent up to temperature first to achieve AuNPs smaller than what are obtainable through the standard method. Providing that the ratio of citrate to gold is at or above 3:2 then rapid reduction can occur, and seeds develop which is then swiftly followed by the propagation step.

Other modifications to the standard method of larger AuNP preparation involve the addition of further chemical compounds to achieve properties typically outside of normal parameters. The use of tannic acid for example allows for the generation of <10 nm citrate-tannic acid stabilised particle due to improved reduction kinetics of the stronger reducing agent as well as the provision of a much bulkier ligand, effectively combining both electrostatic and steric stabilisation[40].

The advantage of larger particles (10-200 nm) is that they are much easier to observe, analyse and characterise. This is due to their increased size allowing for efficient cleaning via centrifugation (providing they do not lack the necessary stability once cleaned to stay as separate entities), and sharper resolution when analysed via electron microscopes, allowing for the general shape and size to be characterised as well as being much more efficient at the conduction of electrons through the gold core[52] .

The major benefit of developing AuNPs this way, apart from the high degree of control over a wide range of nanoparticle sizes, is that the stabilizing agent (the citrate ketone) acts as a rather loose ligand shell, allowing for ligand exchange with components that could prove more useful upon the gold nanoparticle surface. The challenge that arises here is being able to successfully exchange the ligands without the aggregation of the AuNPs.

AuNPs with both excellent optical sensitivity and stability can supposedly be created if a suitably sized AuNP, created via the Turkevich method or a modification thereof, can undergo chemisorption of thiols onto the surface of the gold core. For this to be facilitated the initial stabilizing agent, usually a highly charged species (citrate ketone), must be readily displaced; smaller anionic species are preferable for this. Under normal

circumstances, upon chemisorption of the thiolated capping agent, the desorption of the charged species sacrifices the electrostatic stability and causes irreversible aggregation[53-56]. In almost all cases, if the newly added chemisorbing thiolated agent is not negatively charged the result is aggregation of the colloidal gold, with the solution undergoing a characteristic colour change from bright red to steel blue, as the plasmon resonance of the AuNPs red-shifts, a result of the dramatically increased size. The ability to preserve the stabilising charge upon the AuNP whilst assembling a suitably large protective monolayer is not trivial.

An approach introduced by Aslan and Perez-Luna was the successful steric stabilisation of AuNPs by mixing Tween 20 into the solution prior to the addition of a thiolating agent[56], with the non-ionic surfactant preventing aggregation long enough for the thiolated agent to chemisorb onto the AuNP surface and develop a stable protective monolayer. It is believed that the reason for this success was the slowing down of the rate of removal of the charged species during ligand exchange. This idea was taken further by the use of thioctic acid as an intermediary functionalisation step[56]. The doubly thiolated species added to the AuNP solution at a pH of 11, resulted in the deprotonation of the thioctic acid during ligand exchange, retaining stability. The role of the extra Au-thiol bond within this experiment was to slow down the rate of exchange between the chemisorbed thioctic acid and the desired species for ligand exchange. The overall result was successful, with the exchange ratio of thioctic acid to a new capping agent being dependant on the capping agent in question, with 11-MUDA showing a 100% exchange ratio and a long chained 15-Crown-5 (15-Crown-5-SH) showing 64%. The issue with this procedure, whilst very effective, is that there is an incomplete ligand exchange, resulting in the presence of the intermediary ligand still upon the AuNP surface. Also, the chain length of each of the final stage thiolated compounds is quite long, once again potentially limiting access to the gold core for effective charge transfer.

Another potential method of intermediary functionalisation is to use thiolated polyethylene glycol compounds (PEG). The functionalisation of AuNPs with PEG has become well known within scientific literature[57-60], chiefly due to its almost uncanny ability to chemisorb onto the gold surface and successfully stabilise the system with little-to-no complications, but also due to PEG being a principle component in different classes of therapeutic agents currently in clinical use. Due to the high stability granted to the AuNPs by the presence of PEG molecules chemisorbed to the surface it is potentially possible

to utilize this an intermediary functionalisation step for the addition of a desired ligand, much like the work with thioctic acid discussed previously. The same issue arises again however, in that there will still be PEG present upon the surface even after ligand exchange, one again contaminating the purity of the AuNP.

Prior to the work of this thesis there was no universal solution to the successful direct functionalisation of larger (>5 nm) AuNPs with smaller thiolated ligands. The capping agents are typically extremely large polymers (such as PEG) or ligands capable of holding a negative charge in a basic solution in order to retain the electrostatic stability. Issues created by this are discussed in Chapter 2 of this thesis whereby multiple attempts at functionalising larger AuNPs with crown ethers were attempted; culminating in the successful synthesis of 7.5nm 18-Crown-6-modified AuNPs as described in Chapter 2.

1.2.2 The inherent properties of Crown Ethers

Crown ethers are heterocycles that, in their simplest form, are cyclic oligomers of dioxane, with the essential repeating unit of any simple crown ether being ethyleneoxy (-CH_2-CH_2O-) which repeats twice in dioxane and six times in 18-Crown-6, as an example. Macrocycles of the repeating ethyleneoxy type (-CH_2-CH_2O-)$_n$ in which n ≥ are generally referred to as crown ethers instead of their generic names, with the reasoning being due to them being part of a special group of heterocycles that bind cations, many of which have appeared in literature[61-64]. In the mid-1960s Pedersen was trying to prepare a complexing agent that worked with divalent cations with the strategy of linking two catechols through on hydroxyl on each molecule. The intent was to create a compound that could partially envelop and, by ionisation of the phenolic hydroxyls, neutralize the bound dication. Pederson then found that one of the by-products, when successfully isolated, was capable of complexing with the potassium cation, yet had no ionizable hydroxyl groups. This new material was called dibenzo-18-crown-6. It was realized that these polyethers represented a new class of complexing agents that were capable of binding alkali-metal cations with only a neutral complexer, a product that was highly desirable for multiple fields of research such as phase-transfer catalysis[65, 66] and biological ion transport[67].

Crown ether compounds possess multiple remarkable attributes, with their most important property being the ability to complex cations yet being neutral in nature, a

property that is highly sought after and exploited. Taking 18-Crown-6 as an example, 18-Crown-6 has 6 oxygen donor groups that have the potential to orientate inwards towards the centre of the macrocylic ring, in free form this is not the case. Solid state structures show that crowns typically crystalize in a parallelogram arrangement in the absence of a guest cation[68], meaning that a conformational reorganisation occurs to accept a guest within the internal compartment of the ring structure. 18-Crown-6, in the presence of K^+, forms a host-guest complex with solid state structures indicating that the result is a symmetrical complex with the K^+ present within the centre[69], with the unit cell showing that the six crown ether oxygens are bound to both the K^+ cation and a singular water molecule, with several water molecules also occupying space outside the crown ether but within the unit cell. Another potential structure of the unit cell is having the water molecule present within the crown ether cavity being replaced by the cations counter anion, with the above literature showing that the MoO_4 anion replaces the water molecule, indicating that the counter anion can either be present internally or externally around the crown ether.

The complexation of ions by crown ethers has been extensively studied within scientific literature and through reviews[70-75], resulting in important principles that are worth mentioning here. It was stated previously that the crown ether complex might show a direct interaction between the bound cation and the now un-associated counter anion or an interaction of the cation with the solvent and perhaps even both simultaneously. A common arrangement is for the water of solvation to coordinate to the ring-bound cation and then hydrogen bond to the counter anion with the solvent and/or the counter anion providing suitable solvation to the otherwise two-dimensionally coordinated cation. It was found in literature that the equilibrium constant for the complexation of reaction (K_s), better known as the stability constant, was generally observed to be higher in lower polarity solvents over higher polarity solvents, with K_s showing a dramatic increase between 80% methanol and pure methanol[76], and then even higher when present in solvents such as chloroform. Unfortunately, due to the inability to dissolve salts within non-polar solvents without the presence of crown ether the true determination of binding within these types of media can prove difficult. The stability constant of these host-guest complexes can also be affected by the ability of the surrounding solvent to H-bond to the solute, an example being that acetonitrile and methanol have very similar dielectric constants, yet the latter has a stronger H-bond donor, which can make it difficult to assess binding strengths and experimental findings.

So, observations from previous scientific literature indicate that the K_s value for a large majority of crown ethers will be reduced when in water, the main solvent used for experiments within this thesis, due to the higher polarity of the solvent. That does not mean that these will not be a strong enough association between the crown ether and the complimentary cation of interest, but a reduced selectivity and drive to associate. This can be seen from the binding data shown in Table 1.1[67]. The data indicates that whilst cation transport from water to various organic phases will not be as selective and/or effective compared to methanol, it is still possible.

Compound	**Solvent**	**Dielectric constant, ε**	**Log K_s**	
			Na^+	**K^+**
12-Crown-4	methanol	33	1.7	1.3
15-Crown-5	methanol	33	3.24	3.43
18-Crown-6	methanol	33	4.35	6.06
18-Crown-6	acetonitrile	37	4.8	5.7
18-Crown-6	water	80	1.8	2.06

Table 1.1[67]: Stability constants for the three major crown ethers used within this thesis: 12-Crown-4, 15-Crown-5 and 18-Crown-6 when in various solvents of increasing polarity, showing how the degree of binding, Log K_s, is reduced as the polarity of the solvent increases.

It should be remembered that the equilibrium constant is the ratio between the binding and release rates of the cation from the crown ether cavity, meaning that the cation is not permanently bound within the crown ether cavity but is subsequently bound and released. In this regard the reduced stability constant in water can be exploited to increase the rate of cation transfer across membranes, as a larger number of cations will be released back into the surrounding environment at any given time.

With the understanding of crown ethers, and their complimentary binding to specific cations, growing due to more in-depth studies over time it seems intuitively reasonable to postulate that when the crown ether's interior cavity (hole) is about the same size as a given cation (guest), binding between the two constituents will be optimal, which gave rise to the "hole size relationship". Unfortunately, the amount of comparative data obtained under identical conditions, to further explore this postulation, has not been studied in depth, with one study showing that the ring sizes ranging from 12-Crown-4 to 24-Crown-8 in methanol all preferred K^+ (chloride as the counter anion), indicating that

the relationship was irrespective of ring size[77]. Whilst this work proves insightful in regard to deciding which system is most likely to work for transporting cations across a membrane on crown ether coated AuNPs, the work discussed in this thesis uses a system whereby the crown ether has been thiolated and then attached to a gold surface and experimented on in water as the solvent. The properties of the crown ethers within the system described in this thesis, when attached to nanoparticles, have not been studied in detail previously. Therefore, a range of cations (K^+, Na^+, Li^+, Ba^{2+} and H^+) has been studied with a range of crown ethers (12-Crown-4, 15-Crown-5 and 18-Crown-6) to confirm whether K^+ was still the most consistent cation for hole-cation association.

The examples of crown ethers being used as sensors within scientific literature are numerous[67, 78-84], with their selective receptor properties in conjunction with the relative ease of synthesis and structural modification making them desirable ionophores. Although a large number of crown-based sensors are developed for the use in ion-selective electrodes[85-88] there are many other applications for such structures, the first example being crown ether dyes; the first compound[89] was reported in the late 1970s, with these dyes being mostly insoluble within aqueous media. This resulted in the compounds being capable of efficiently extracting cations at the aqueous-organic interface, resulting in a colour change that could be detected spectrophotometrically. This thesis does not directly involve the use of crown ethers in such a manner and so this topic shall not be discussed further but was mentioned as an acknowledgment of the potential uses for crown ether complexes, and how their selectivity can prove useful.

With the early applications of crown ethers having been discussed thanks to their inherent ability to selectivity bind to specific cations, this review will now move onto the application of such crown ether compounds in the transport of molecules across membranes.

1.2.3 Crown Ethers as Membrane Transporters

It was found in the 1960s[90] that certain natural antibiotics had the ability to transport cations through cellular membranes, resulting in the death of the cell. One of the compounds studied was Valinomycin, the reason being its prominent ability to transport K^+ at extremely high rates (10^4 ions per second) and with extremely high selectivity over other ions commonly present in vivo such as Na^+ [91-95]. This combination of selective and

rapid cation transfer across cellular membranes is the reason why valinomycin was taken as the control for the membrane transport work discussed in this thesis. Valinomycin is a cyclododecadepsipeptide that folds around the K^+ ion in a structure much resembling that of a "tennis ball seam" arrangement, with the carbonyl oxygens serving as electron donors within the three dimensional complex[96, 97]. It should be noted that the reason why valinomycin has a much higher selectivity than the crown ethers used within this work is due to the ability to conform around the cation in three dimensions rather than two. The cost of such a structure is an increase in size relative to the crown ether moiety; as the intent of this research was to also allow for electron transport across the gold core, the core could not be masked by large capping agents, and so valinomycin was not investigated as an alternative capping agent. Other reasons for not using valinomycin was due to there being no obvious literature on how to thiolate the structure, making it incapable of binding to the gold as well as it being extremely toxic.

The development of crown ethers as described previously in this review allowed for the opportunity to mimic such natural antibiotics with synthetically variable host molecules. One of the most obvious applications for these easily modified synthetic macrocycles was for the transport of different ions through membranes of various types[98]. A large majority of the ion-binding macrocycles were designed to mimic natural carriers such as: valinomycin, enniatin, nonactin and others; with studies conducted in a wide range of membrane systems where, for the most part, synthetic membranes were used, with natural bilayers sometimes taking the spotlight.

Early studies involving membranes consisted of aqueous phases separated by an immiscible organic phase[99] with the membrane layer typically being formed out of CH_2Cl_2 or $CHCl_3$ followed by charging with the ionophore. The transport of the cation was generally detected by colorimetric assay of a counterion such as picrate, with such studies proving highly informative but lacking relevance to natural membranes. Although bulk organic solvents can mimic membrane behaviour to some extent, synthetic vesicles or liposomes constitute a far better model. Liposomes are spherical vesicles with at least one lipid bilayer, with the bilayer being built up of amphiphilic molecules with both a hydrophilic head and a hydrophobic tail; the latter collecting together to form the internal hydrophobic section, and the prior acting as the protective surface. These artificial liposomes can be constructed from a single amphiphilic molecule such as dioleoylphosphatidylchline (DOPC) or as a complex mixture of lipids such as cholesterol and azolectin, with the advantage of the former pure DOPC example being that the composition of the membrane is more accurately known and therefore highly reproducible.

Typically, these experiments are conducted in vesicles that have been prepared especially for the studies in question, for which the vesicles will be formed by either sonication or extrusion in an aqueous suspension of water, buffer or an aqueous mixture intended to be encapsulated, such as differing salt concentrations. The resulting vesicles are then purified either through dialysis or filtration through a Sephadex column. The work discussed in this thesis used dialysis due to the lack of experience in column filtration and a high degree of experience in dialysis.

These types of transport experiments in and out of vesicles typically employed fluorescent dyes, with the experiment conducted being altered depending on the dye that is being used. Typically, the dyes are entrapped within the vesicle during formation. Carboxyfluorescein[100] is a good example. Within the vesicle it self-quenches due to high concentrations and fluoresces very little. However, upon release it is readily detected as it moves into the bulk solution and the quenching is stopped. Dyes such as [6-methoxy-N-(3-sulfopropyl)quinolinium] (SPQ)[101] and lucigenin are both fluorescent within vesicles that can become quenched when in the presence of Cl^- [102]. These types of dyes are extremely useful as analytical measurements of ionophoric activity in membrane systems. Safranin-O was the fluorescent dye used within the vesicle transport experiments

discussed in this thesis due to its ease of use, availability and relative insensitivity to compounds present in solution that were used through the experiments.

With the preparation of artificial membranes becoming easier to develop and reproduce reliably, along with suitable ion sensing fluorescent dyes becoming more mainstream, experiments involving the use of crown ethers as ion transporters became much more prominent. Earlier designs for synthetic cation transporting channels typically incorporated a macrocycle within the structures centre. Tabushi, a pioneer in the field of synthetic pore design, successfully prepared an amphiphilic cyclodextrin that was capable of demonstrating the transport of Co^{2+} across a membrane[103] with examples incorporating the macrocyclic compounds of interest within this thesis being developed further on down the line[104-107], with these compounds directing the movement of alkali metal ions through artificial membranes. In order for these compounds to successfully insert within a phospholipid membrane they had to have a certain set of characteristics which are better described as "Hydraphiles", a designated class of synthetic ion channels, with the central structure typically being crown ethers and the terminal groups being either crown ethers or polar moieties to allow for the structure to orientate itself correctly and have the channel like structure parallel with the phospholipid architecture, whilst the central crown ether acted as an energy lowering "central relay" [108]. A large number of structural variations were prepared in this manner to ascertain a better understanding of the structure activity relationship between the compounds and the ability to insert into the membrane and transport cations[109-113], with these experiments proving that cation selective synthetic pores could be successfully developed and implemented via the application of macrocyclic molecules.

The "Hydraphiles" described in this review section are extremely efficient at doing their proposed job, the transport of cations across membranes. Thus, the work described in this thesis intends to incorporate the success shown within the scientific literature described but with the extra potential for electron transport to occur at the same time, potentially opening avenues into coupling cation and electron transport between two previously confined systems. To do so a suitably redox-active compound must also be incorporated into a macrocycle system in order to allow electron transport to occur. This is an avenue that AuNPs may be able to open up due to the ability to modify the external properties of the gold via various capping agents

1.2.4 Nanoparticles and Lipid Membranes

Monolayer-protected inorganic nanoparticles (NPs) have been used within the scientific literature for target selective drug vectors[114, 115], nanothermal agents[116, 117] and diagnostic devices[117, 118]. For such uses to become effective it requires that we achieve control of the NP interaction with different biological environments, with the interaction between NP and cell membranes being crucial for the delivery of molecules into cells, resulting in intense research efforts aimed at understanding active endocytic pathways as well as passive membrane permeation. The work in this thesis is aimed at working with the latter principle, passive membrane permeation. Such a process has been shown to be relevant for the smallest NPs (< 10 nm) when interacting with plasma membranes and model lipid bilayers[119-121].

The ability for a NP to penetrate a lipid membrane passively is a result of a complex interplay of both thermodynamics and kinetics; from a thermodynamic perspective the degree of hydrophilicity of the NP determines its "want" to reside either within the aqueous phase or within the hydrophobic core of the membrane[120, 122, 123].

Recent literature has given rise to a wide array of experimental papers[121, 122, 124, 125] which have focused on a select number of charged, monolayer-protected AuNPs and their interactions with model lipid bilayers as well as living cellular membranes. These AuNPs in question are typically functionalised by a mixture of hydrophobic and negatively charged ligands such as mercapto undecanesulfonate (MUS) and mercapto undecane carboxylate (MUC), which results in non-destructive penetration, proven via the use of neutron reflectivity data for floating zwitterionic bilayers[125], of the lipid bilayer with viable mechanisms being stated by both Stellacci[120] and Katz[122]. Another common mixture of ligands is neutral hydrophobic ligands such as octanethiol and dodecanthiol (OT and DDT). Potential mechanisms of penetration were investigated further with more advanced computational studies which fit well with previously collected data, indicating that there are three main stages of anionic/neutral AuNP membrane penetration[126]. The commonality between most of these membrane-penetrating particles is: 1) They are all relatively small (<5nm), this is necessary in terms of thermodynamic favourability for passive membrane insertion (without membrane destruction), 2) they all incorporate well-packed hydrophobic chains (end groups can still be polar) that will mask and inhibit access to the gold core itself, essentially removing the functionality of the gold surface from further use. This results in AuNPs that are effectively sitting within the membrane,

but potentially losing a very valuable pathway for charge transfer across the membrane, the gold core.

1.2.5 Contribution of this Thesis

So far, this review has discussed the general characteristics of gold nanoparticles and how they can potentially be exploited, including the most famous synthesis methods and further modifications thereof. It then moves on to the characteristic properties of macrocyclic molecules (crown ethers) and how they can effectively be used as selective phase transfer agents for complimentary cations, with the stability constant for the host-guest complexation depending on a variety of factors such as: solvent polarity, solvent H-bonding potential, ring size, ring conformation, cation size and charge, counter anion size and charge. Literature involving their use as highly selective membrane transporters for cations, via the mimicking of nature's ionic transporters such as valinomycin, was then discussed and described how they can effectively be placed into membranes via the development of "Hydraphile" type structures. Further scientific literature was then reviewed discussing the general principles of passive NP penetration into lipid membranes and the factors that affect this such as NP size and shape, ligand charge and hydrophilicity and ligand flexibility, with a heavy emphasis on long chained capping agents to give the particle an amphiphilic nature, resulting in the masking of the Au surface.

The research described and discussed within this thesis was aimed at creating a hybrid between the cationic transfer properties of crown ethers across lipid membranes, with the ability to insert AuNPs passively into a lipid membrane while, at the same time, keeping the ligand shell surrounding the AuNP surface relatively small in an attempt to retain the functionality of the Au core, thereby opening a pathway to additionally achieving electron transfer.

1.3 Characterisation Techniques

The remaining sections of this chapter will present the characterisation techniques used in the following chapters.

1.3.1 UV-Vis Spectroscopy

As stated previously, because of the small size of metallic nanoparticles and their high surface to bulk atom ratio they exhibit unique optical properties that can be exploited in order to effectively characterise them in solution. This section will briefly discuss relevant properties and the way in which they are used for characterisation.

The configuration of gold is [Xe] $f4^{14}$ $5d^{10}$ $6s^{1}$, resulting in each atom within the gold particle having a singular valence electron. These valence electrons are delocalised throughout the particle within the conduction band, resulting in the formation of an electron cloud that is referred to as the surface plasmon, Figure 1.3.

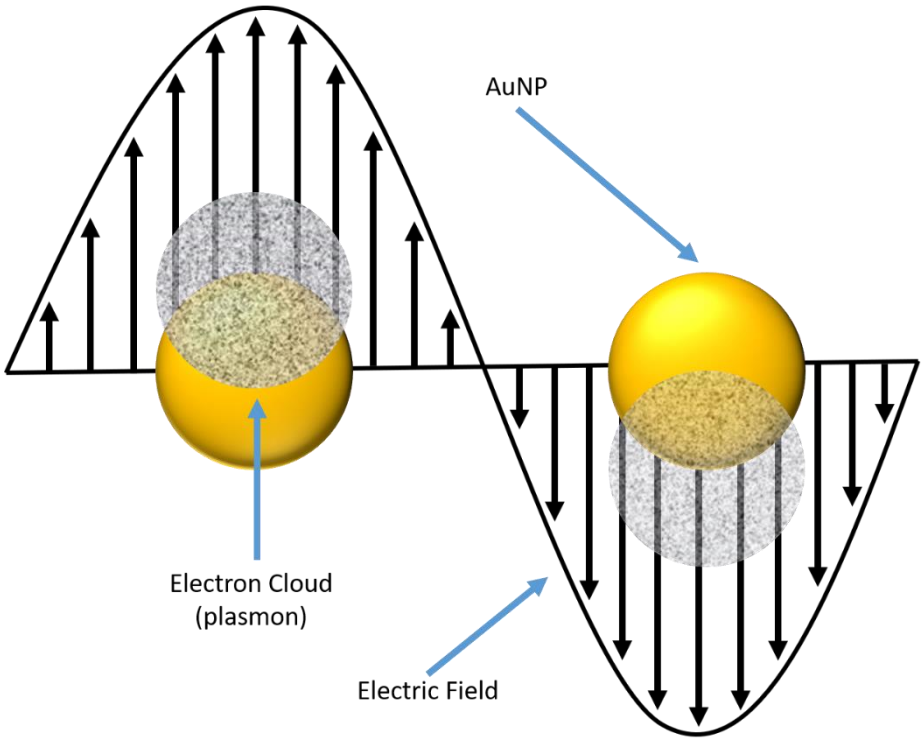

Figure 1.3: Illustration of the surface plasmon's interaction of a metal nanoparticle with an electromagnetic field.

Particles that have a plasmon resonance, when smaller than the wavelength of the electric component of an electromagnetic field, can exhibit a resonance between the plasmon and the field; such that the plasmon begins to oscillate in the opposing direction of the electric field, with the effect being known as the surface plasmon resonance (SPR). This SPR

results in the enhancement of both absorption and scattering of visible light frequencies that initially cause the oscillation. These interactions can be readily observed spectroscopically using UV-Vis absorption spectroscopy, or even physically by the distinctive colouration of metal nanoparticles exhibiting such an effect, as shown in Figure 1.4[127, 128].

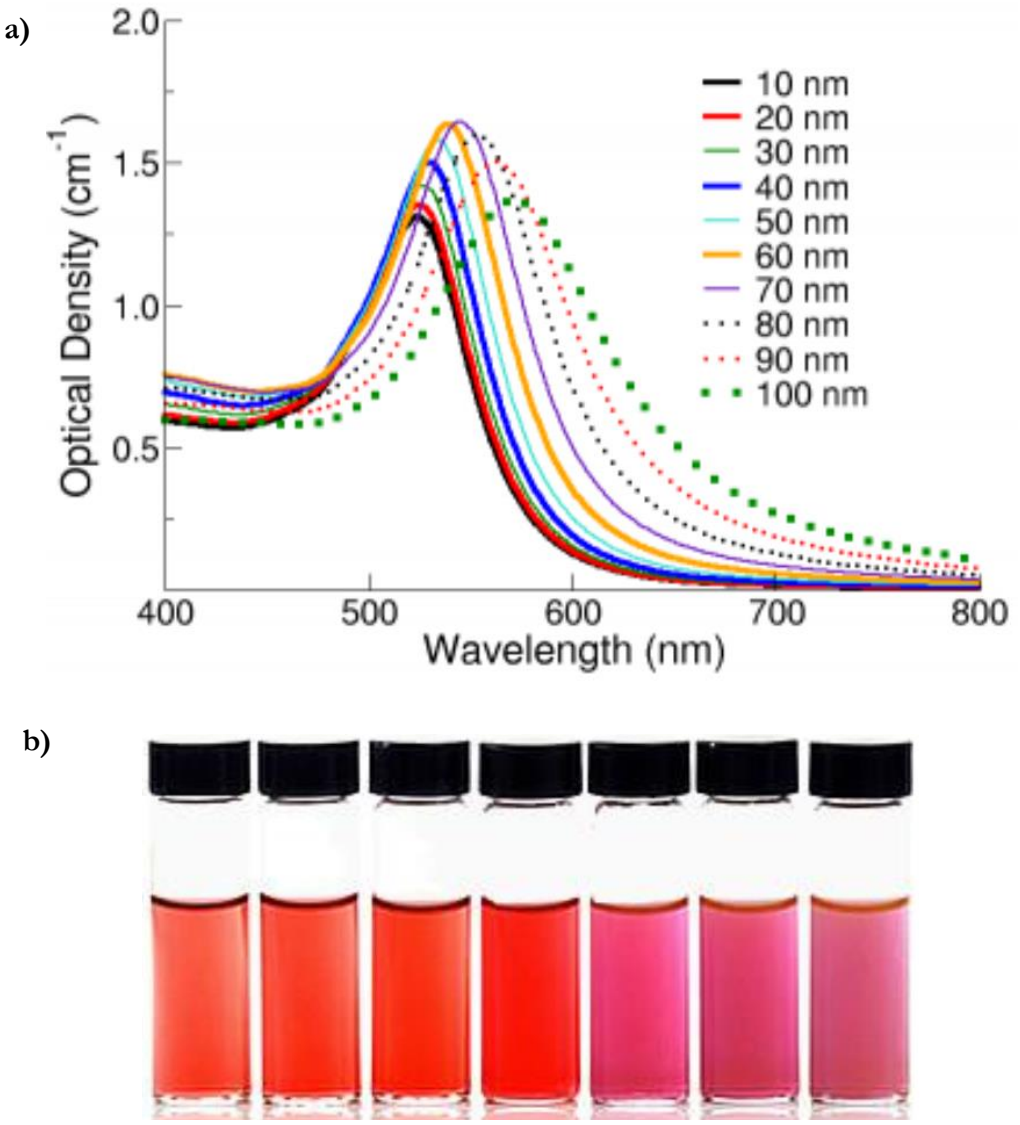

Figure 1.4: a) UV-Vis spectra of the SPR of increasing sizes of AuNPs[127], b) Image of the observed colour change with increasing sizes of AuNPs[128]

The surface plasmon and its frequency are highly dependent on many variables, such as the material in question, the size, the shape, the protective coating and the surrounding media the particle is presented in, with the latter two being better known as the dielectric

medium. The result is the unequivocal use of UV-Vis spectroscopy to characterise such particles, due to it being both quick and inexpensive as a tool for collecting qualitative and quantitative characterisation data; using the method described by Haiss *et al.*[129] the approximate size and concentration of a metallic colloidal sample can be quickly determined. In brief, Haiss *et al.* modelled theoretically, via the use of Mie's solutions to the Maxwell light equations[130], the relationship between the size of spherical AuNPs and the expected amount of scattered/absorbed light, which was found to be experimentally accurate for a wide range of AuNPs sizes.

It was determined from this correlation that the absorbance at the SPR (ASPR) and the absorbance at 450nm (A450) have a direct relationship allowing for the development of the Haiss formula:

$$d = \exp(B_1 \frac{A_{SPR}}{A_{450}} - B_2)$$

where B_1 and B_2 are constants taken from the experimental fitting. Using these two absorbance values and a list of ratios taken from the supplementary information of the paper, the approximate size of AuNPs coated in citrate in an aqueous solution can be quickly determined. The calculated extinction coefficients for each size of AuNP (also calculated in the Heiss paper) can be entered into the Beer-Lambert Law[131] with the ASPR to give an estimated concentration of AuNPs. Upon functionalisation with a protective coating/capping agent the exact frequency of the SPR changes (typically only by a few nanometers), allowing for a quick qualitative verification of successful ligand exchange. The broadening of the SPR can also be highly informative with regard to the stability of the colloidal solution before and after modification, again giving quick insight into the stability of AuNPs of interest. UV-Vis was used extensively in this thesis due to these highly informative results which are quick to produce. Unfortunately, the usefulness of UV-Vis at smaller sizes of nanoparticle (<3 nm) starts to deteriorate as the plasmon resonance of such particle sizes is subdued and so characterisation from optical analysis becomes difficult and less informative.

1.3.2 Dynamic Light Scattering

Dynamic light scattering (DLS) is a very common method of sizing nanoparticle samples (down to a size of ~10-15 nm). The technique works by directing a polarized light source at a colloidal solution and then using an automated correlation function to analyse the light scattering picked up by the receiver, as shown in Figure 1.5[132]. This allows the technique to provide dynamic data on even relatively small particles in complex solutions. The correlation function that is used, however, is dependent upon the cross-section of the particles in question, resulting in the technique being highly size dependant[133]; the dependence upon the nanoparticle cross-section results in larger particles contributing much more to the scattering signal that is collected, thus a sample measured by DLS is always skewed towards larger particles present in the sample. This is notorious for decreasing the accuracy of the technique should any large particulates be present within solution, such as dust. Whilst the accuracy of DLS comes into question with smaller AuNPs the technique can still be readily used as secondary proof of the approximate size of a nanoparticle/agglomeration in solution.

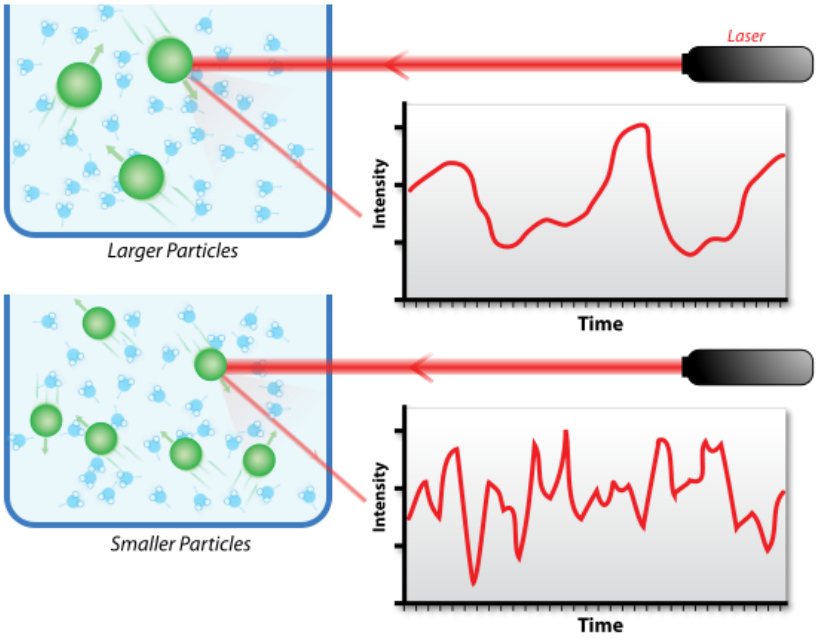

Figure 1.5: Illustration showing how the degree of scattering of the incident laser light is dependent upon the size of the particles in solution, allowing for size differentiation to be achieved[132].

1.3.3 Zeta Potential

Particles within a colloidal suspension or emulsion typically carry an electrical charge. The charge is often more negative than positive, and the development of the charge can occur via a number of ways. Sometimes it is due to the ligands upon the surface containing certain chemical groups that can ionize and produce a charged surface. It may also be due to the selective association of a specific charge close to the particle surface, much like the crown ethers used within this thesis and their association with complimentary cations, or even the addition of chemisorbing agents that are already charged and then relocate that charge to the surface.

In science it is typically stated as particles being electrically charged. However, it is important to realize that the charge on the surface of each particle is counterbalanced by charges (ions) of the opposite sign in the surrounding solution, resulting in the overall suspension being as close to neutral as possible and the actual size of the "whole" particle system being somewhat larger than just the solid core.

Typically, the charge that is associated to the particle surface is quite firmly attached and so will remain there indefinitely, with the surrounding charge within the medium (better known as the electrochemical double layer) being much more loosely associated with the particle. Thermal motion of both the solvent molecules and surrounding ions results in this electrochemical double layer being spread in a diffuse layer which stretches out for some distance away from the particle surface, with the distribution of charge changing from a rather steep gradient by the particle surface (as opposing charges of the particle surface are drawn to it, and similar charges repelled) which eventually smoothens out into an evenly balanced distribution of cationic and anionic charge, essentially the continuous mobile phase.

This method works by applying an electric field to the suspension and measuring how fast the particles move within the solution as a result; a process better known as electrophoresis. The higher the charge that the particles carry, the faster the particles will migrate through the applied electric field, with the electric potential measured being that of the slipping plane illustrated in Figure 1.6.

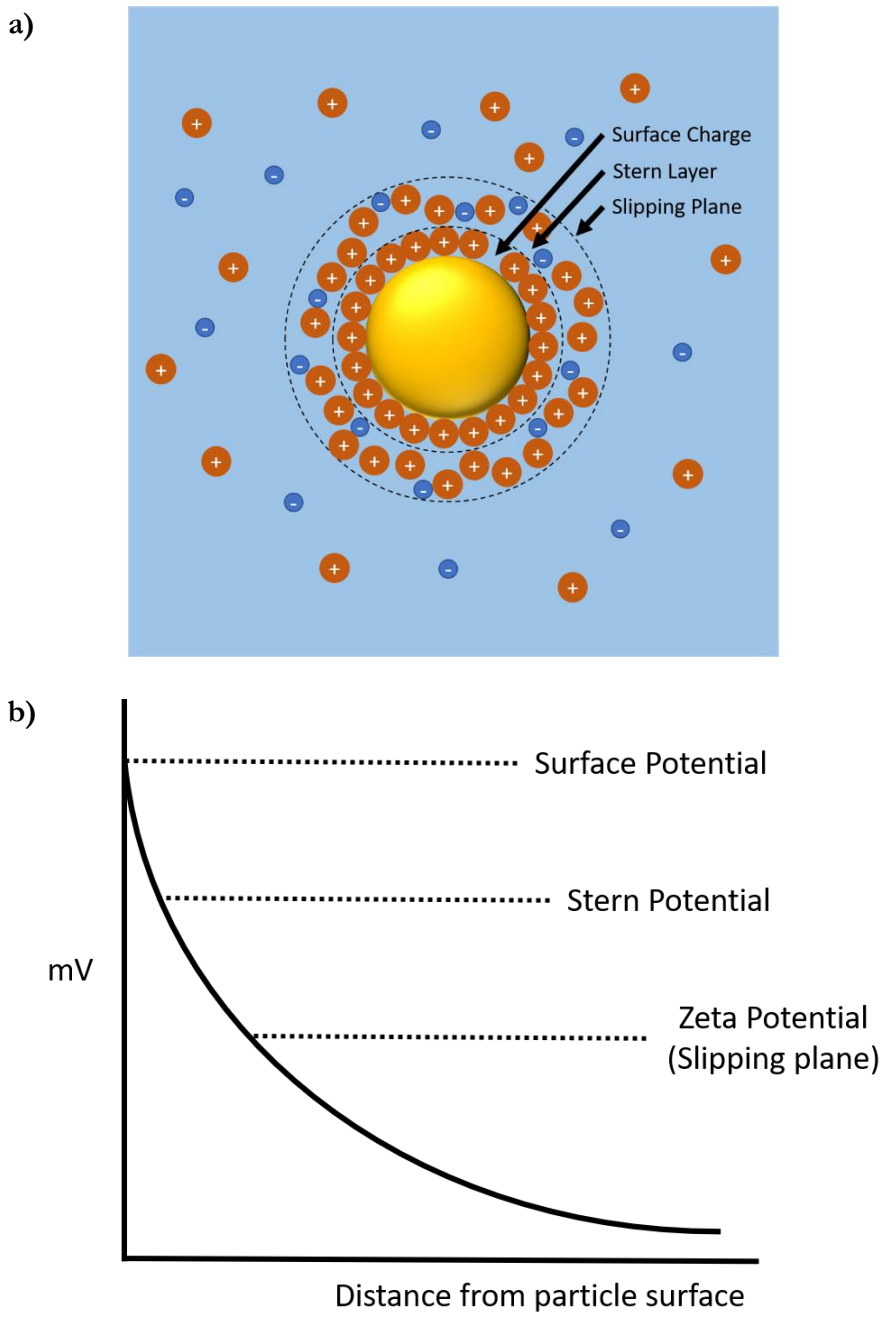

Figure 1.6: a) Schematic showing the difference in the surface layer, the stern layer and the slipping plane, b) Graph showing how the electric potential surrounding the particle decreases with increasing distance from the particle surface.

It should be noted that the Zeta potential (ζ) is not equal to that of the Stern potential or the electric surface potential within the double layer[134], so such assumptions should be applied with caution; ζ is often the only path to effectively characterise the double layer properties of particles in solution.

Zeta potential is not measurable directly but is calculated from the velocity that a particle experiences when placed within an electric field, as described previously. The particle velocity is typically measured using a technique called laser Doppler anemometer[135], where the frequency/phase shift of the incident laser, caused by moving particles, is measured. This is then converted into the ζ by inputting the dispersant viscosity and dielectric permittivity (water in the case of all experiments undertaken in this thesis) and applying Smoluchowski theories[136].

ζ is used quite extensively within this thesis in order to validate explanations as to why crown ether modified AuNPs are capable of transferring to an organic phase upon associating with complimentary cations. The fact that the ζ is not directly measuring the surface potential of the particle, but the slipping plane (Figure 1.6) has been taken into consideration. The charge that is effectively measured reflects more realistically what a singular particle "sees" as it approaches another particle/phase boundary, which is what actually determines the properties the particles exhibit. Whilst ζ is not widely used within the scientific community, it is extremely useful for the topics and processes discussed in this thesis, essentially providing a solid understanding of how these systems work.

1.3.4 Fourier Transformed Infra-Red Spectroscopy

Fourier transform infra-red spectroscopy (FTIR) exposes a sample to a source of infra-red light, with the absorption and emissions spectrum being recorded and analysed. Not only can the technique be used to determine the approximate concentration and surface coverage of molecules on the surface of the nanoparticles, but it can be particularly useful in determining whether ligand exchange upon a particle was a success and what degree of ligand exchange had occurred (complete exchange or partial exchange). The reason why FTIR is good at validating the effective association of a desired ligand to the nanoparticle surface is because different chemical structures (such as ligands) produce different spectral fingerprints, meaning that certain frequencies of IR light are absorbed by the sample as vibrational frequencies inherent to the compounds molecular bonds resonate with similar frequencies in the IR spectrum.

The benefit of using FTIR is that the spectrum contains a large amount of information about the sample, the Attenuated Total Reflectance (ATR) sampling is quick, resulting in validation in a short period of time, is highly sensitive and can detect very low concentrations of molecules present within solution.

FTIR was used to a minor degree within this thesis, only as a tool to check whether certain nanoparticle functionalisation had occurred and whether any unwanted compounds were still present in solution or on the particle itself. FTIR will not be discussed further as a result.

1.3.5 Electron Microscopies

1.3.5.1 Transmission Electron Microscopy

Transmission electron microscopy (TEM) is a microscopy technique where a beam of electrons is transmitted through a specimen of interest to form an image. More often than not the specimen is an ultra-thin section (100 nm or less in thickness) and is suspended upon a grid. The image is formed from the interaction of electrons with the sample as they pass through it, with much denser material resulting in scattering/a reduction in energy of the electron. These electrons then hit a detection device which is typically a fluorescent screen, photographic film or a charge-coupled sensor.

Theoretically, the maximum resolution, *d*, that can be obtained with a light microscope is limited by the wavelength of the photons being used to probe the sample, λ, as well as the numerical aperture of the system, *NA*.

$$d = \frac{\lambda}{2n\,sin\alpha} \approx \frac{\lambda}{NA}$$

where *n* is the index of refraction of the medium in which the lens is working, and α the maximum half-angle for the cone of light that can enter the lens[137]. It was theorised that methods of getting around the resolution limitations was by using electrons, allowing for the new particle beam to behave like a beam of electromagnetic radiation with the wavelength of the electrons being related to their kinetic energy via the de Broglie equation:

$$\lambda_e = \frac{h}{\sqrt{2m_0E(1 + \frac{E}{2m_0c^2})}}$$

where h is the Planck's constant, m_0 is the rest mass of an electron and E is the energy of the accelerated electron, with these electrons being generated from a heated tungsten filament, and then accelerated by an electric potential.

To increase the mean free path of the electron gas interaction TEM is done under vacuum at around 10^{-4} Pascal (Pa) or less; this also prevents any arcing discharges from the cathode. These are just the basic principles for the initial development of TEM as an analytical tool, the mathematical manipulations and engineering required to develop the TEM instruments used today is extremely vast and will not be covered here.

TEM is extremely useful for characterising AuNP systems ex-situ; due to the need for vacuum. Any solution that the particles were once present in will rapidly evaporate off, lowering its potential for a detailed analysis of the whole system, yet it is still highly informative. The density of gold results in very strong degrees of electron scattering/absorption, resulting in a very sharp contrast between the particles present upon a grid and the background film. This allows for TEM to be used to directly observe the shape and size of particles, with enough resolution and accuracy that, when a suitable sample size is taken, the approximate size of the particle can be determined, which fits nicely with the calculated sizes taken from UV-Vis. Thus, the techniques can be used to validate each other. The limitation of TEM is the ability to observe particles within their original environment, i.e. suspended in solution, as stated previously, resulting in it being a valuable technique when combined with other validation methods, such as UV-Vis, DLS and FTIR. The technique was used extensively throughout this thesis to ascertain whether particles were of a desired size and dispersity, the correct shape and the properties of agglomeration (as seen in Chapter 4).

1.3.5.2 Cryo-TEM

It was noted above that a major limitation of TEM is the inability to observe colloidal systems in-situ; instead the particles are presented on a 2D plane that, whilst providing detail characterisation upon the particle size, shape and stability, gives no insight into their behaviour when in solution. A perfect example of this in this thesis would be the

interaction of artificial vesicles discussed in Chapters 3 and 4; in a standard TEM the vesicles would be destroyed as their surrounding solution is removed, leaving only the particles and a lipid residue upon the grid.

Cryo-TEM is an effective answer to that limitation, using a process known as the Dubochet's vitrification method[138], developed by Dubochet, a process for which he was awarded a Nobel prize for his contribution to science, whereby the droplet that is placed upon the TEM grid is frozen so rapidly that the water forms disordered glass, rather than crystalline ice (Figure 1.7). This change in the ice structure is essential as ice crystals would strongly diffract the microscopes electron beam, obscuring any information about the molecules being studied. An example of this is shown in Figure 1.7, which is a failed attempt at observing 18-Crown-6-modified AuNPs with vesicles where the formation of ice was allowed to occur over an extended time period, resulting in huge ice crystals that masked any valuable data.

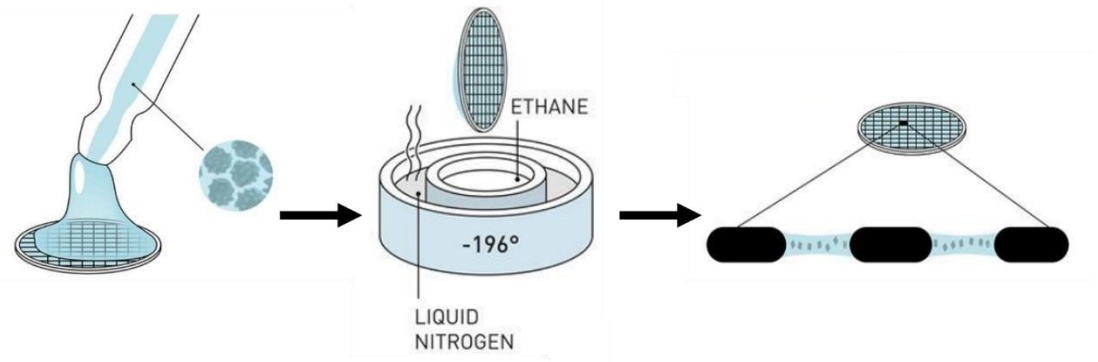

Figure 1.7: An illustration created by Johan Jarnestad at the Royal Swedish Academy of Sciences depicting the technique used to effectively freeze a sample in situ in order to allow for EM imaging[139]. The solution is placed upon the TEM grid, excess solution removed by briefly dabbing the grid with filter paper, followed by the grid being rapidly plunged into liquid ethane in order to instantly freeze the remaining solution present within the grid's cavities.

This analytical technique was essential in this thesis for attempting to observe the interaction of the variously sized 18-Crown-6-modified AuNPs with artificial vesicles, allowing for accurate validation of whether the particles were interacting with the membrane or not. The limitations of this technique are that is requires considerable experience and skill in order to achieve any substantial data, with even the most skilled of EM specialists having failure rates of over 50% for every sample created. The other problem is that the process is very intensive and time consuming but, if done properly, very worthwhile.

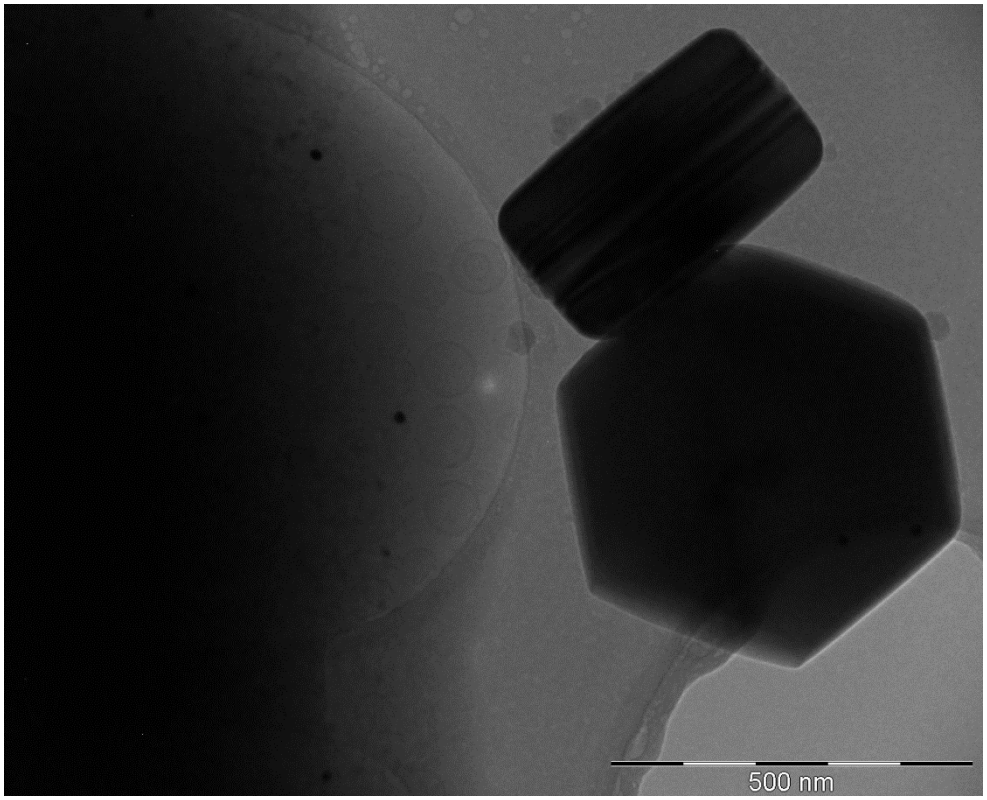

Figure 1.8: A Cryo-TEM image showing how the formation of traditional ice crystals can heavily obscure the sample of interest, showing that the rapid freezing process developed by Dubochet is essential for Cryo-TEM imaging.

Figure 1.8 shows that if the freezing process is done incorrectly you obtain formations of structured ice appearing upon the grid; with the darkened area on the right-hand side of the image being a thick layer of structured ice, and the large symmetrical structures on the left large being ice crystals. The disordered glass ice can be seen beneath, with vesicles captured in it, but the much larger structured ice makes analysis difficult.

1.3.5.3 Scanning Electron Microscopy

Scanning electron microscopy (SEM) is an analytical tool like TEM in that it uses an electron beam to probe a sample, except that it creates an image by scanning the surface with a focused dynamic beam of electrons rather than a static beam as used in TEMs. The most common SEM mode used for imaging is the detection of secondary electrons emitted by atoms within the sample of interest that became excited when exposed to the electron beam. The number of secondary electrons that can be detected is dependent on sample topography, which allows for the generation of highly detailed images of the

surface structure of samples, providing that they are of a suitable density to provide sufficient contrast from the background. An example of this is shown in Figure 1.9.

The advantages of SEM over TEM is that it is possible to obtain much more information about the topography of a sample. This typically comes at the cost of resolution, however, meaning that attempting to resolve singular particles of <10 nm in anything other than perfect conditions is a challenge. The other disadvantage of basic SEM is one that is shared with TEM, in that it is required to observe the sample in vacuum, to allow for the electrons to efficiently probe only the sample surface and not molecules found in the atmosphere.

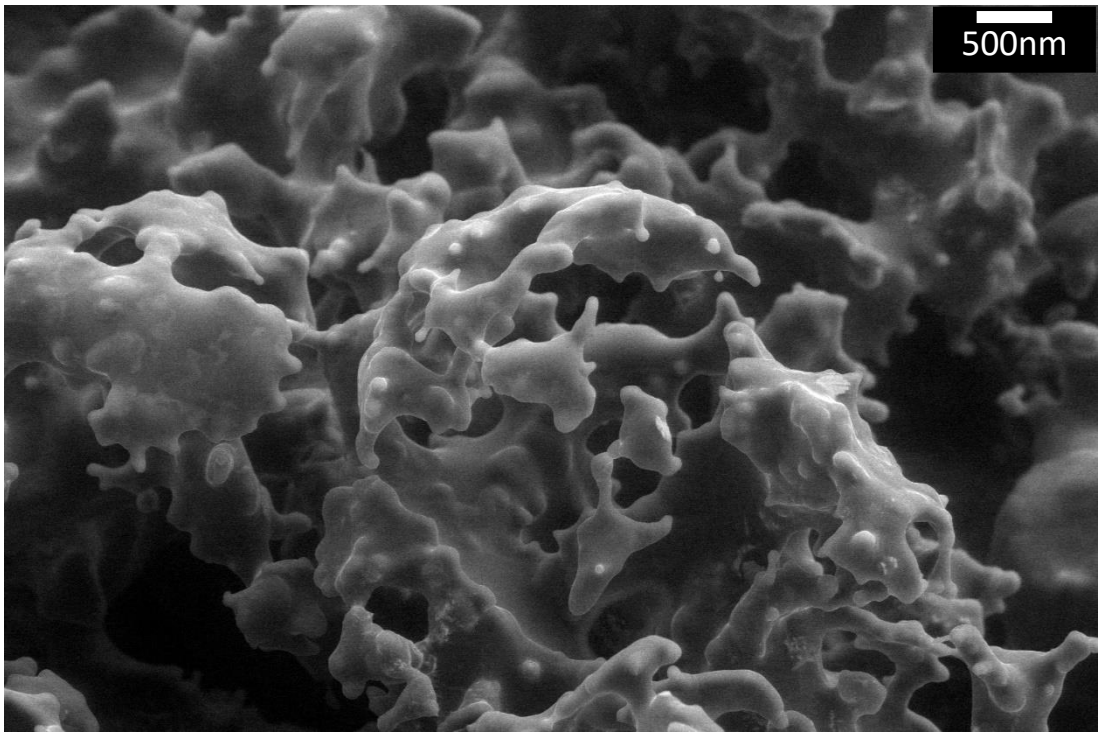

Figure 1.9: An ESEM image of the frozen water-in-chloroform emulsion showing off the detailing and resolution of SEM, allowing for real insight into a sample structure.

1.3.5.4 Environmental SEM

This is an analytical technique that utilizes the same principles as traditional SEM but allows for the collection of data on "wet" specimens, similar to Cryo-TEM in the sense that it allows for the presence of liquid within the sample, providing more information on the sample when in-situ.

The specimen chamber which sustains the desired high-pressure environment is separate from the high vacuum environment in which the electron optics column resides, with only two small orifices known as pressure-limiting apertures (PLA). Any leakage of the high-pressure environment through the PLA is swiftly evacuated from the system with a pump that maintains a much lower pressure immediately above the aperture; this is known as differential pumping. The gas flow fields created by this setup are characterised and validated in a range of experiments in order to quantify how the electron beam behaves in various pressure environments[140] in order for the data to be effectively built into an image. The exact details as to how ESEM works are incredibly complex and shall not be discussed further in this thesis.

1.4 Summary

This chapter started with an overview of the goal of this research, and why it could prove useful within the future. This was then followed by three topics of background literature, being: the history and synthesis of various sizes of AuNPs, the properties of crown ethers and their use as cation transporters within membranes and aqueous organic interfaces, and the ability for AuNP to penetrate lipid membranes depending on their size and structure of the stabilising cell. This background research enabled the development of a baseline from which to work up from in order to move towards successfully developing a system capable of achieving both cation and charge transfer across organic interfaces.

1.5 References

1. M. Sarikaya, C. Tamerler, A. K. Y. Jen, K. Schulten and F. Baneyx, *Nature Materials*, 2003, **2**, 577.
2. J.-S. Sun, J.-W. Jiang, H. S. Park and S. Zhang, *Nanoscale*, 2018, **10**, 312-318.
3. Y. Wang, Y. Zhao, W. Zheng, M. Duan, H. Chen and Y. Du, *Journal of Nanoscience and Nanotechnology*, 2017, **17**, 8623-8639.
4. M. Brogly, O. Noel, H. Awada, G. Castelein and J. Schultz, *Comptes Rendus Chimie*, 2006, **9**, 99-110.
5. X.-Z. Liu, Q. Li, P. Egberts and R. W. Carpick, *Advanced Materials Interfaces*, 2014, **1**, 1300053.
6. S. A. Maier, M. L. Brongersma, P. G. Kik, S. Meltzer, A. A. G. Requicha and H. A. Atwater, *Advanced Materials*, 2001, **13**, 1501-1505.
7. A. J. Haes and R. P. Van Duyne, *Journal of the American Chemical Society*, 2002, **124**, 10596-10604.
8. A. B. Pardee, *The Journal of General Physiology*, 1968, **52**, 279-295.
9. B. Yurke, A. J. Turberfield, A. P. Mills Jr, F. C. Simmel and J. L. Neumann, *Nature*, 2000, **406**, 605.
10. W. Meng, R. A. Muscat, M. L. McKee, P. J. Milnes, A. H. El-Sagheer, J. Bath, B. G. Davis, T. Brown, R. K. O'Reilly and A. J. Turberfield, *Nature Chemistry*, 2016, **8**, 542.
11. G. A. Somorjai, *Langmuir*, 1991, **7**, 3176-3182.
12. D. Grasseschi, R. A. Ando, H. E. Toma and V. M. Zamarion, *RSC Advances*, 2015, **5**, 5716-5724.
13. R. B. Grubbs, *Polymer Reviews*, 2007, **47**, 197-215.
14. P. Thoniyot, M. J. Tan, A. A. Karim, D. J. Young and X. J. Loh, *Advanced Science*, 2015, **2**, 1400010.
15. J. Turkevich, P. C. Stevenson and J. Hillier, *The Journal of Physical Chemistry*, 1953, **57**, 670-673.
16. G. Rossi and L. Monticelli, *Biochimica et Biophysica Acta (BBA) - Biomembranes*, 2016, **1858**, 2380-2389.
17. M. S. Strozyk, S. Carregal-Romero, M. Henriksen-Lacey, M. Brust and L. M. Liz-Marzán, *Chemistry of Materials*, 2017, **29**, 2303-2313.
18. W. Chang-Hai, L. Chi-Jen, W. Cheng-Liang, H. Tzu-En, M. O. Judy, K. H. Lee, Y. Hwu, Y. Chung-Shi, L. Ru-Shi, L. Hong-Ming, J. Jung-Ho and G. Margaritondo, *Journal of Physics D: Applied Physics*, 2008, **41**, 195301.
19. S. H. Lee, K. H. Bae, S. H. Kim, K. R. Lee and T. G. Park, *International Journal of Pharmaceutics*, 2008, **364**, 94-101.
20. E. Pensa, E. Cortés, G. Corthey, P. Carro, C. Vericat, M. H. Fonticelli, G. Benítez, A. A. Rubert and R. C. Salvarezza, *Accounts of Chemical Research*, 2012, **45**, 1183-1192.

21. J. A. Dean, *Lange's handbook of chemistry*, McGraw-Hill, New York, N.Y., 1999.
22. J. C. Love, L. A. Estroff, J. K. Kriebel, R. G. Nuzzo and G. M. Whitesides, *Chemical Reviews*, 2005, **105**, 1103-1170.
23. M. Brust, J. Fink, D. Bethell, D. J. Schiffrin and C. Kiely, *Journal of the Chemical Society, Chemical Communications*, 1995, DOI: 10.1039/C39950001655, 1655-1656.
24. A. K. R. Lytton-Jean and C. A. Mirkin, *Journal of the American Chemical Society*, 2005, **127**, 12754-12755.
25. M. K. Corbierre, N. S. Cameron and R. B. Lennox, *Langmuir*, 2004, **20**, 2867-2873.
26. E. Boisselier, A. K. Diallo, L. Salmon, C. Ornelas, J. Ruiz and D. Astruc, *Journal of the American Chemical Society*, 2010, **132**, 2729-2742.
27. Y. Yang and P. Burkhard, *Journal of Nanobiotechnology*, 2012, **10**, 42.
28. S. Günter, P. Reinhard, B. Roland, B. Friedhelm, M. Sonja, C. G. H. M. and W. A. van der Velden Jan, *Chemische Berichte*, 1981, **114**, 3634-3642.
29. M. Giersig and P. Mulvaney, *Langmuir*, 1993, **9**, 3408-3413.
30. M. Faraday, *Philosophical Transactions of the Royal Society of London*, 1857, **147**, 145-181.
31. M. Brust, M. Walker, D. Bethell, D. J. Schiffrin and R. Whyman, *Journal of the Chemical Society, Chemical Communications*, 1994, DOI: 10.1039/C39940000801, 801-802.
32. S. Chen, *Langmuir*, 1999, **15**, 7551-7557.
33. S. Chen and R. W. Murray, *Langmuir*, 1999, **15**, 682-689.
34. M. J. Hostetler, S. J. Green, J. J. Stokes and R. W. Murray, *Journal of the American Chemical Society*, 1996, **118**, 4212-4213.
35. M. J. Hostetler, A. C. Templeton and R. W. Murray, *Langmuir*, 1999, **15**, 3782-3789.
36. M. P. Grzelczak, A. P. Hill, D. Belic, D. F. Bradley, C. Kunstmann-Olsen and M. Brust, *Faraday Discussions*, 2016, **191**, 495-510.
37. J. Turkevich, P. C. Stevenson and J. Hillier, *Discussions of the Faraday Society*, 1951, **11**, 55-75.
38. G. Frens, *Kolloid-Zeitschrift und Zeitschrift für Polymere*, 1972, **250**, 736-741.
39. G. Frens, *Nature Physical Science*, 1973, **241**, 20.
40. J. Piella, N. G. Bastús and V. Puntes, *Chemistry of Materials*, 2016, **28**, 1066-1075.
41. S. Zeng, K.-T. Yong, I. Roy, X.-Q. Dinh, X. Yu and F. Luan, *Plasmonics*, 2011, **6**, 491.
42. J. Kimling, M. Maier, B. Okenve, V. Kotaidis, H. Ballot and A. Plech, *The Journal of Physical Chemistry B*, 2006, **110**, 15700-15707.
43. N. G. Bastús, J. Comenge and V. Puntes, *Langmuir*, 2011, **27**, 11098-11105.

44. H. Al-Johani, E. Abou-Hamad, A. Jedidi, C. M. Widdifield, J. Viger-Gravel, S. S. Sangaru, D. Gajan, D. H. Anjum, S. Ould-Chikh, M. N. Hedhili, A. Gurinov, M. J. Kelly, M. El Eter, L. Cavallo, L. Emsley and J.-M. Basset, *Nature Chemistry*, 2017, **9**, 890.
45. N. R. Jana, L. Gearheart and C. J. Murphy, *Langmuir*, 2001, **17**, 6782-6786.
46. M. Aslam, L. Fu, M. Su, K. Vijayamohanan and V. P. Dravid, *Journal of Materials Chemistry*, 2004, **14**, 1795-1797.
47. K.-S. Kim, D. Demberelnyamba and H. Lee, *Langmuir*, 2004, **20**, 556-560.
48. H. Otsuka, Y. Akiyama, Y. Nagasaki and K. Kataoka, *Journal of the American Chemical Society*, 2001, **123**, 8226-8230.
49. S. K. Sivaraman, S. Kumar and V. Santhanam, *Journal of Colloid and Interface Science*, 2011, **361**, 543-547.
50. S. Adem, *Effect of pH on the Stability of Gold Nanoparticles and Their Application for Melamine Detection in Infant Formula*, Journal of Applied Chemistry, 2014, 8, 2278-5736.
51. I. Ojea-Jiménez, F. M. Romero, N. G. Bastús and V. Puntes, *The Journal of Physical Chemistry C*, 2010, **114**, 1800-1804.
52. E. Yuliza, R. Murniati, A. Rajak, K. Khairurrijal and M. Abdullah, *Effect of Particle Size on the Electrical Conductivity of Metallic Particles*, 2014.
53. C. S. Weisbecker, M. V. Merritt and G. M. Whitesides, *Langmuir*, 1996, **12**, 3763-3772.
54. H. Fujiwara, S. Yanagida and P. V. Kamat, *The Journal of Physical Chemistry B*, 1999, **103**, 2589-2591.
55. P. V. Kamat, *The Journal of Physical Chemistry B*, 2002, **106**, 7729-7744.
56. K. Aslan and V. H. Pérez-Luna, *Langmuir*, 2002, **18**, 6059-6065.
57. J. Spadavecchia, D. Movia, C. Moore, C. M. Maguire, H. Moustaoui, S. Casale, Y. Volkov and A. Prina-Mello, *International Journal of Nanomedicine*, 2016, **11**, 791-822.
58. P. Ghosh, G. Han, M. De, C. K. Kim and V. M. Rotello, *Advanced Drug Delivery Reviews*, 2008, **60**, 1307-1315.
59. K. Rahme, L. Chen, R. G. Hobbs, M. A. Morris, C. O'Driscoll and J. D. Holmes, *RSC Advances*, 2013, **3**, 6085-6094.
60. J. Manson, D. Kumar, B. J. Meenan and D. Dixon, *Gold Bulletin*, 2011, **44**, 99-105.
61. X. X. Zhang, A. V. Bordunov, J. S. Bradshaw, N. K. Dalley, X. Kou and R. M. Izatt, *Journal of the American Chemical Society*, 1995, **117**, 11507-11511.
62. G. W. Gokel, *Chemical Society Reviews*, 1992, **21**, 39-47.
63. H. Tsukube, *Coordination Chemistry Reviews*, 1996, **148**, 1-17.
64. Y. Nakatsuji, K. Kita, H. Inoue, W. Zhang, T. Kida and I. Ikeda, *Journal of the American Chemical Society*, 2000, **122**, 6307-6308.
65. T. Jeng-Yu and S. Jeng-Shong, *Journal of the Chinese Chemical Society*, 1994, **41**, 81-87.

66. P. E. Stott, J. S. Bradshaw and W. W. Parish, *Journal of the American Chemical Society*, 1980, **102**, 4810-4815.
67. G. W. Gokel, W. M. Leevy and M. E. Weber, *Chemical Reviews*, 2004, **104**, 2723-2750.
68. J. D. Dunitz and P. Seiler, *Acta Crystallographica Section B*, 1974, **30**, 2739-2741.
69. O. Nagano, *Acta Crystallographica Section B*, 1979, **35**, 465-467.
70. R. M. Izatt, J. S. Bradshaw, S. A. Nielsen, J. D. Lamb, J. J. Christensen and D. Sen, *Chemical Reviews*, 1985, **85**, 271-339.
71. R. M. Izatt, K. Pawlak, J. S. Bradshaw and R. L. Bruening, *Chemical Reviews*, 1991, **91**, 1721-2085.
72. K. Shimojo, N. Kamiya, F. Tani, H. Naganawa, Y. Naruta and M. Goto, *Analytical Chemistry*, 2006, **78**, 7735-7742.
73. L. S. Mizoue and J. Tellinghuisen, *Biophysical Chemistry*, 2004, **110**, 15-24.
74. M. Ali, I. Ahmed, P. Ramirez, S. Nasir, S. Mafe, C. M. Niemeyer and W. Ensinger, *Analytical Chemistry*, 2018, **90**, 6820-6826.
75. R. Mohammadzadeh Kakhki and M. Rakhshanipour, *Arabian Journal of Chemistry*, 2015, DOI: https://doi.org/10.1016/j.arabjc.2015.07.012.
76. D. M. Dishong and G. W. Gokel, *The Journal of Organic Chemistry*, 1982, **47**, 147-148.
77. G. W. Gokel, D. M. Goli, C. Minganti and L. Echegoyen, *Journal of the American Chemical Society*, 1983, **105**, 6786-6788.
78. M. J. Marsella and T. M. Swager, *Journal of the American Chemical Society*, 1993, **115**, 12214-12215.
79. S. J. K. Pond, O. Tsutsumi, M. Rumi, O. Kwon, E. Zojer, J.-L. Brédas, S. R. Marder and J. W. Perry, *Journal of the American Chemical Society*, 2004, **126**, 9291-9306.
80. J. H. Holtz and S. A. Asher, *Nature*, 1997, **389**, 829.
81. W. Wei, C. Xu, J. Ren, B. Xu and X. Qu, *Chem Commun (Camb)*, 2012, **48**, 1284-1286.
82. Y.-H. Kim and J.-I. Hong, *Chem Commun (Camb)*, 2002, DOI: 10.1039/b109596j, 512-513.
83. H. Kuang, W. Chen, W. Yan, L. Xu, Y. Zhu, L. Liu, H. Chu, C. Peng, L. Wang, N. A. Kotov and C. Xu, *Biosensors and Bioelectronics*, 2011, **26**, 2032-2037.
84. S.-Y. Lin, S.-W. Liu, C.-M. Lin and C.-h. Chen, *Analytical Chemistry*, 2002, **74**, 330-335.
85. K. Kimura, T. Maeda, H. Tamura and T. Shono, *Journal of Electroanalytical Chemistry and Interfacial Electrochemistry*, 1979, **95**, 91-101.
86. H. Tamura, *Anal. Chem.*, 1982, **54**, 1224-1227.

87. D. Siswanta, K. Nagatsuka, H. Yamada, K. Kumakura, H. Hisamoto, Y. Shichi, K. Toshima and K. Suzuki, *Analytical Chemistry*, 1996, **68**, 4166-4172.
88. I. H. A. Badr, M. Diaz, M. F. Hawthorne and L. G. Bachas, *Analytical Chemistry*, 1999, **71**, 1371-1377.
89. M. Takagi, H. Nakamura and K. Ueno, *Analytical Letters*, 1977, **10**, 1115-1122.
90. B. C. Pressman, E. J. Harris, W. S. Jagger and J. H. Johnson, *Proceedings of the National Academy of Sciences of the United States of America*, 1967, **58**, 1949-1956.
91. B. Hans and S.-K. Günter, *Chemische Berichte*, 1955, **88**, 57-61.
92. H. W. Huang and C. R. Williams, *Biophysical Journal*, 1981, **33**, 269-273.
93. M. Ohnishi and D. W. Urry, *Science*, 1970, **168**, 1091.
94. W. L. Duax, H. Hauptman, C. M. Weeks and D. A. Norton, *Science*, 1972, **176**, 911.
95. M. A. Bush and M. R. Truter, *Journal of the Chemical Society D: Chemical Communications*, 1970, DOI: 10.1039/C29700001439, 1439-1440.
96. I. L. Karle, *Karle IL. Conformation of valinomycin in a triclinic crystal form. J Am Chem Soc 97: 4379-4386*, 1975.
97. N.-L. Katarina and D. Max, *Helvetica Chimica Acta*, 1975, **58**, 432-442.
98. B. G. Cox and H. Schneider, *Coordination and transport properties of macrocyclic compounds in solution*, Elsevier Science Publishers, Amsterdam, 1992.
99. J. D. Lamb, R. M. Izatt, D. G. Garrick, J. S. Bradshaw and J. J. Christensen, *Journal of Membrane Science*, 1981, **9**, 83-107.
100. Z.-Y. Liu, R. Solow and V. W. Hu, *Biochimica et Biophysica Acta (BBA) - Biomembranes*, 1988, **945**, 253-262.
101. C. D. Geddes, *Sensors and Actuators B: Chemical*, 2001, **72**, 188-195.
102. Y. Li, H. Zhu, P. Kuppusamy, V. Roubaud, J. L. Zweier and M. A. Trush, *Journal of Biological Chemistry*, 1998, **273**, 2015-2023.
103. I. Tabushi, Y. Kuroda and K. Yokota, *Tetrahedron Letters*, 1982, **23**, 4601-4604.
104. L. Jullien and J.-M. Lehn, *Tetrahedron Letters*, 1988, **29**, 3803-3806.
105. L. Jullien and J.-M. Lehn, *Journal of inclusion phenomena and molecular recognition in chemistry*, 1992, **12**, 55-74.
106. V. E. Carmichael, P. J. Dutton, T. M. Fyles, T. D. James, J. A. Swan and M. Zojaji, *Journal of the American Chemical Society*, 1989, **111**, 767-769.
107. A. Nakano, Q. Xie, J. V. Mallen, L. Echegoyen and G. W. Gokel, *Journal of the American Chemical Society*, 1990, **112**, 1287-1289.
108. C. L. Murray, H. Shabany and G. W. Gokel, *Chemical Communications*, 2000, DOI: 10.1039/B005431N, 2371-2372.
109. E. Abel, M. F. Fedders and G. W. Gokel, *Journal of the American Chemical Society*, 1995, **117**, 1265-1270.

110. E. Abel, G. E. M. Maguire, E. S. Meadows, O. Murillo, T. Jin and G. W. Gokel, *Journal of the American Chemical Society*, 1997, **119**, 9061-9062.
111. G. Srinivas, C. F. Lopez and M. L. Klein, *The Journal of Physical Chemistry B*, 2004, **108**, 4231-4235.
112. A. L. Sisson, M. R. Shah, S. Bhosale and S. Matile, *Chemical Society Reviews*, 2006, **35**, 1269-1286.
113. T. M. Fyles, *Chemical Society reviews*, 2007, **36**, 335-347.
114. S. Rana, A. Bajaj, R. Mout and V. M. Rotello, *Advanced Drug Delivery Reviews*, 2012, **64**, 200-216.
115. J. D. Gibson, B. P. Khanal and E. R. Zubarev, *Journal of the American Chemical Society*, 2007, **129**, 11653-11661.
116. X. Sun, G. Zhang, R. S. Keynton, M. G. O'Toole, D. Patel and A. M. Gobin, *Nanomedicine: Nanotechnology, Biology and Medicine*, 2013, **9**, 1214-1222.
117. Y.-S. Yang, R. P. Carney, F. Stellacci and D. J. Irvine, *ACS Nano*, 2014, **8**, 8992-9002.
118. E. C. Dreaden, A. M. Alkilany, X. Huang, C. J. Murphy and M. A. El-Sayed, *Chemical Society Reviews*, 2012, **41**, 2740-2779.
119. Y. Jiang, S. Huo, T. Mizuhara, R. Das, Y.-W. Lee, S. Hou, D. F. Moyano, B. Duncan, X.-J. Liang and V. M. Rotello, *ACS Nano*, 2015, **9**, 9986-9993.
120. R. C. Van Lehn, P. U. Atukorale, R. P. Carney, Y.-S. Yang, F. Stellacci, D. J. Irvine and A. Alexander-Katz, *Nano Letters*, 2013, **13**, 4060-4067.
121. S. Sabella, R. P. Carney, V. Brunetti, M. A. Malvindi, N. Al-Juffali, G. Vecchio, S. M. Janes, O. M. Bakr, R. Cingolani, F. Stellacci and P. P. Pompa, *Nanoscale*, 2014, **6**, 7052-7061.
122. R. C. Van Lehn and A. Alexander-Katz, *The Journal of Physical Chemistry A*, 2014, **118**, 5848-5856.
123. P. Gkeka, L. Sarkisov and P. Angelikopoulos, *The Journal of Physical Chemistry Letters*, 2013, **4**, 1907-1912.
124. A. Verma, O. Uzun, Y. Hu, Y. Hu, H.-S. Han, N. Watson, S. Chen, D. J. Irvine and F. Stellacci, *Nature Materials*, 2008, **7**, 588.
125. S. Tatur, M. Maccarini, R. Barker, A. Nelson and G. Fragneto, *Langmuir*, 2013, **29**, 6606-6614.
126. S. Salassi, F. Simonelli, D. Bochicchio, R. Ferrando and G. Rossi, *The Journal of Physical Chemistry C*, 2017, **121**, 10927-10935.
127. nanoComposix, The Effect of Size on Optical Properties, https://nanocomposix.com/pages/gold-nanoparticles-optical-properties).
128. nanoComposix, Gold Nanospheres Precisely Engineered, https://nanocomposix.com/collections/gold).
129. W. Haiss, N. T. K. Thanh, J. Aveyard and D. G. Fernig, *Analytical Chemistry*, 2007, **79**, 4215-4221.

130. M. Born and E. Wolf, Principle of optics: Electromagnetic theory of propagation, interference and diffraction of light, Cambridge University Press, 1970.
131. P. A. Annis, J. H. Campbell, A. Matsukura, A. Senentz and A. D. King Jr, *Coloration Technology*, 2007, **123**, 242-247.
132. M.Jones,DyanmicLightScattering https://en.wikipedia.org/wiki/Dynamic_light_scattering#/media/File:DLS.svg).
133. WI. Goldburg, *American Journal of Physics*, 1999, **67**, 1152-1160.
134. B. J. Kirby, Electrophoresis, 2004, 25, 187-202.
135. I. Nezu and W. Rodi, *Journal of Hydraulic Engineering*, 1986, **112**, 335-355.
136. HX. Zhou, A. Szabo, *The Journal of Chemical Physics*, 1991, **95**, 5948-5952.
137. M. W. D. Douglas B. Murphy, Fundamentals of Light and Microscopy and Electronic Imaging, WILEY-LISS, 2002.
138. Dubochet. J., *Journal of Microscopy*, 2012, **245**, 221-224.
139. P. Broadwith, *Chemistry World*, 2017, article 300809.
140. G. D. Danilatos, M. R. Phillips and J. V. Nailon, *Microscopy and Microanalysis*, 2001, **7**, 397-406.

Chapter 2 Synthesis and Characterisation of Crown Ether Coated AuNPs

In this chapter the variety of methods and procedures used to prepare gold nanoparticles with various functional groups in the attempt to develop AuNPs capable of transporting cations and/or electrons across an artificial membrane will be discussed. There will be a combination of successes and failures in regard to synthesising such AuNPs, in order to demonstrate that the development of such systems was no easy task.

The nature of the research meant that the procedures carried out here were not completed in a block, prior to characterisation and testing of the resulting particles. Rather, they were carried out over the period of the research, as it progressed. They are presented all together in this chapter so that the logic of each step in the successful synthesis can be more clearly understood.

The format which shall be observed throughout the following chapters, whereby the methodology is incorporated into each section, instead of being present as one large block, was used to provide a smoother transition between the results and the parameters under which they were obtained. This was done to reduce the need for excessive page turning when linking the methodology with the results.

2.1 Preparation of 3 nm thiolated 18-Crown-6 AuNPs

The development of 3 nm AuNPs via the Brust-Schiffrin method[1] and modifications thereof are well documented and readily used due to the relative ease in which it is possible to incorporate new ligands upon the gold surface, allowing for properties characterized and analysed without having to also handle the instability and challenge of functionalising particles stabilised via electrostatic stabilisation[2]. This is the reason that the development of the smaller particles discussed in this thesis were prepared first, to develop a baseline understanding of how the crown ethers behave upon a gold nanoparticle surface, allowing for further advancements later on.

2.1.1 18-CROWN-6-C-CH_2-SH Coated Au NPs

Small, 2.5-3 nm, Au/18-C-6-CH_2-SH were synthesised by a modified literature method[1, 2] where a 1:1 Au^{III} : capping agent ratio was used. Pure 18-C-6-CH_2-SH (5.2 μl), purchased from ProChimia Surface, with a purity of 98%, was added to a 25 mM solution of hydrogen tetrachloroaurate (III) hydrate in methanol (3 ml) resulting in a clear yellow solution. The mixture was stirred for 10 minutes at room temperature which resulted in no change in the colour/composition of the mixture, indicating the ligand was successfully incorporated. Then 1.5 ml of a freshly prepared 0.056 M solution of $NaBH_4$ in methanol was rapidly injected under vigorous stirring. Upon injection, the solution instantly became a deep brown in colour and was left for 20 minutes to allow the reaction to proceed to completion. The resulting solution was then rotary evaporated at 28ºC to yield a black residue coating the flask. The residue was washed first with toluene for a total of three times, then with diethyl ether for a total of 3 times. The residue was then re-dissolved in iso-propanol in order to remove excess hydrophilic reaction products which were then subsequently filtered off. The solution was then rotary evaporated at 30ºC resulting in the final product which was obtained as a black solid coating the flask, which was subsequently dissolved in 2 ml of MQ water.

These particles were characterised by the following techniques: UV-Vis, TEM (including high resolution) and FTIR, as shown in Figure 2.1

The UV-Vis spectrum, Figure 2.1a shows that there is only a very minor plasmon resonance peak, a slight hump upon the spectrum at 500 nm. This is indicative of particles with a diameter of <5 nm due to their lack of plasmon resonance[3, 4] and is further reinforced by the high resolution TEM image, Figure 2.1b, showing a relatively monodisperse sample with a few larger particles being present. It is more than likely that the slight hump seen at 500 nm is due to this small population of larger particles as the change in the plasmon resonance absorption coefficient is quite dramatic at smaller particle sizes

The FTIR spectra, Figure 2.1c, compares the absorbance spectra of the pure 18-C-6-CH_2-SH oil and the freshly functionalised GNPs. Peaks of note within the pure oil are the sharp C-O ether stretch at 1150 cm^{-1} and the sharp C-H alkane stretch at 2850 cm^{-1}. This fits nicely with what was to be expected based on the structure of the compound.

The functionalised particles show very similar sharp peaks again at 1150 cm^{-1} and 2850 cm^{-1} which correspond to the C-O and C-H stretches respectively, with a third prominent peak arising at 3500 cm^{-1}. This peak can be attributed to the presence of water, however, due to this being the solvent the particles are based in after preparation.

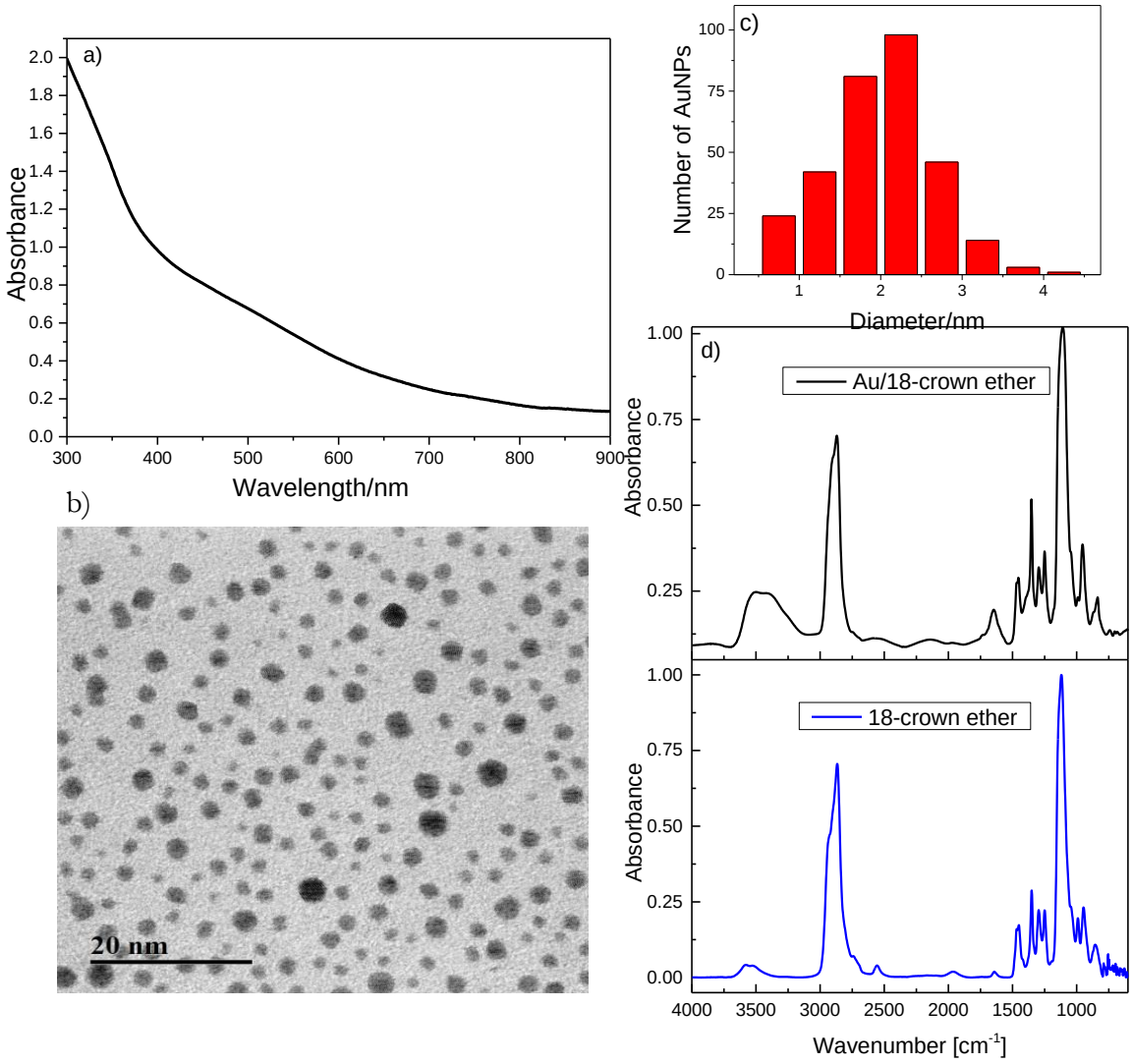

Figure 2.1: a) UV-Vis spectrum of 3nm 18-Crown-6-modified AuNPs, b) High resolution TEM image of the 18-Crown-6-modified AuNPs, c) Histogram showing the size distribution of the 3nm 18-Crown-6-modified AuNPs, d) FTIR spectra of the pure thiolated crown ether oil and the 3nm 18-Crown-6-modified AuNPs.

2.1.2 15-C-5-CH_2-SH Coated Au NPs

These particles were prepared in the same way as the 18-C-6-CH_2-SH particles in Section 2.1.1 except that the volume of crown ether oil added was changed from 5.2 µl to 4.46 µl in order to retain the same Au(III): capping agent ratio.

These particles were characterised by the following techniques: UV-Vis, TEM and FTIR, as shown in Figure 2.2.

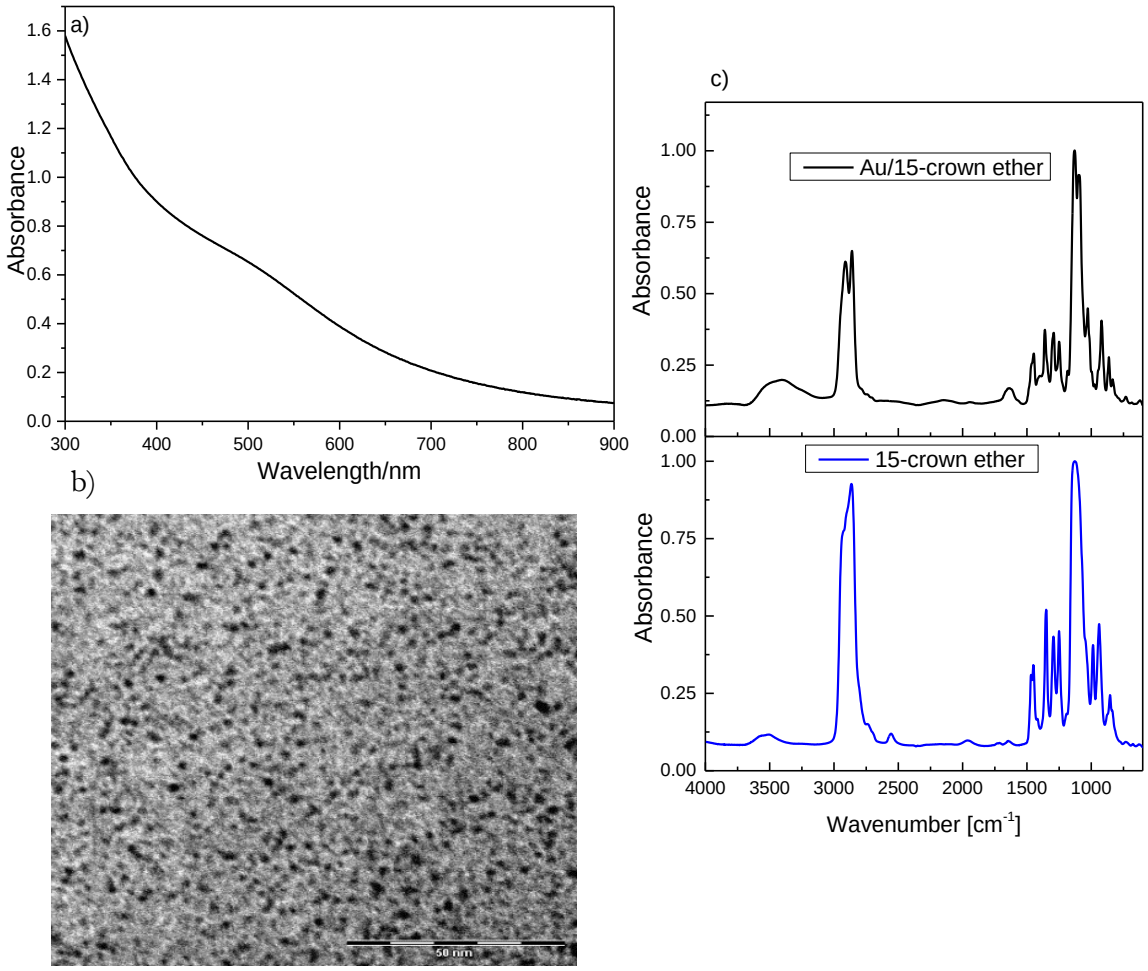

Figure 2.2: a) UV-Vis spectra of 3nm 15-Crown-5-modified AuNPs, b) TEM image of 3nm 15-Crown-5-modified AuNPs, c) FTIR spectra of the pure thiolated 15-Crown-5 oil and the 3nm 15-Crown-5-modified AuNPs.

The UV-Vis spectrum seen in Figure 2.2a shows that there is only a very minor plasmon resonance peak, albeit it is slightly more pronounced than that seen in Figure 2.1a. This difference is not caused by a change in ligand however; the prominence of the hump varies slightly for each separate batch of particles. What is important to take note of is that the overall trend of the curve is like that seen in Figure 2.1a, indicating particles of a similar size. The TEM image, Figure 2.2b gives a rough idea of the particle size; due to the 15-Crown-5 modified AuNPs not being taken forward as the best candidate (see Chapter 3) no high resolution TEM was done, showing they are roughly 3-5 nm, which corresponds nicely with the UV-Vis data. Unfortunately achieving high resolution with

particles of this size is a challenge in normal TEM, the UV-Vis does indicate that they are a similar size to that of the 18-Crown-6-modified AuNPs however.

The FTIR spectra shown in Figure 2.2c compares the absorbance spectra of the pure 15-C-5-CH_2-SH oil and the freshly functionalised GNPs. Much like the 18-C-6-CH_2-SH oil the two prominent peaks are a C-O stretch at 1180 cm^{-1} and a C-H stretch at 2850 cm^{-1}. This similarity is to be expected as the change in the structure and composition going from 18-C-6 to 15-C-5 is very minimal, being just the removal of three carbons and one oxygen. The functionalised particles show very similar sharp peaks again at 1140 cm^{-1} and 2850 cm^{-1}, with an extra peak at 3500 cm^{-1} which has already been attributed to the presence of water.

2.1.3 12-C-4-CH_2-SH Coated Au NPs

These particles were prepared in the same way as the previous particles except that the volume of oil added was changed from 5.2 μl to 3.72 μl in order to retain the same Au (III) : capping agent ratio.

These particles were characterised by the following techniques: UV-Vis, TEM and FTIR, as shown in Figure 2.3, overleaf.

The UV-Vis spectrum shown in Figure 2.3a shows a smooth curve with a slight hump around 500nm, with the TEM (Figure 2.3b) and the FTIR (Figure 2.3c) showing similar properties as the previous two particle systems indicating that the functionalisation with 12-Crown-4 was successful.

2.2 Preparation and Functionalisation of Citrate Stabilised AuNPs

After the success of developing the 3 nm crown ether particles, with all three crown ether types 18-Crown-6, 15-Crown-5 and 12-Crown-4 giving rise to highly stable colloidal aqueous solutions, it was decided that larger AuNPs needed to also be functionalised with the crown ether ligand to open an avenue for charge conductance across the gold core. Only 18-Crown-6 thiolations are described from this point on as it was deemed to be the most likely candidate for achieving the main goal of the thesis; Chapter 3 discusses in more detail why this was decided.

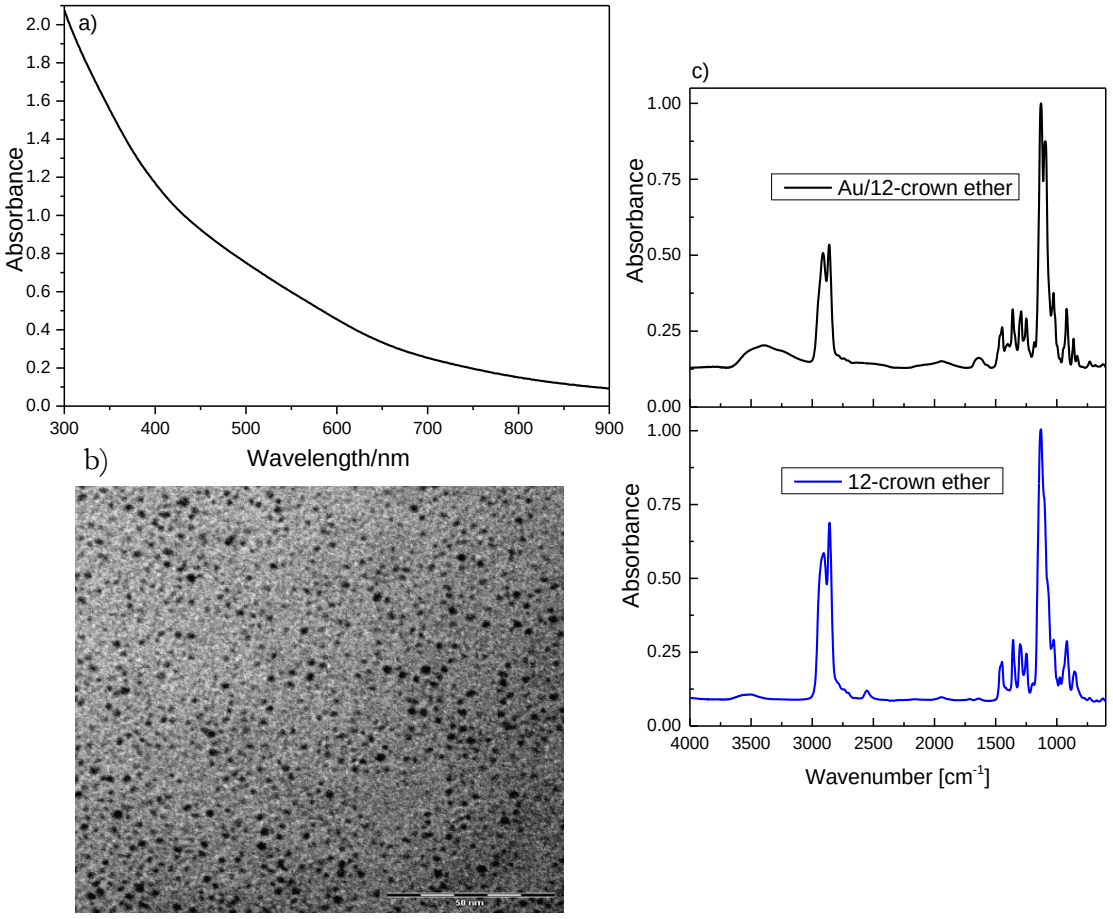

Figure 2.3: a) UV-Vis spectra of 3nm 12-Crown-4-modified AuNPs, b) TEM image of 3nm 12-Crown-4-modified AuNPs, c) FTIR spectra of pure thiolated 12-Crown-4 oil and 3nm 12-Crown-4-modified AuNPs.

It is important to note that the synthesis of AuNPs via the Turkevich method, or modifications thereof[5, 6] (except for those explicitly mentioned), were not successful with regards to directly functionalising the AuNP with thiolated 18-Crown-6. Numerous variations in pH, ligand density, solvent exchanges, temperature and addition speeds were attempted, all resulting in the inevitable aggregation of the colloidal solution, destroying the sample. It became apparent that the size of the thiolated 18-Crown-6 ligand was simply too small to provide any suitable steric stabilisation during ligand exchange[7]. This resulted in other methods of functionalisation having to be investigated to try and develop these larger crown ethers coated AuNPs.

2.2.1 Thioctic Acid as an intermediary ligand

Within the background literature covered in Chapter 1 there was a brief discussion about the use of thioctic acid as an intermediary functionalisation ligand by Chen *et al*[8] resulting in successfully exchanging a proportion of intermediary ligand (the % of ligand exchange varied with ligand type), with that of a desired ligand, one of which included a long chain thiolated crown ether moiety which showed an exchange percentage of ~64%. This was achieved by a combination of retaining a strong negative charge upon the thioctic acid during the initial ligand exchange with a solution pH of 11 followed by the exploitation of the double thiol bound found upon thioctic acid to slow the rate of the secondary ligand exchange, as shown in Figure 2.4.

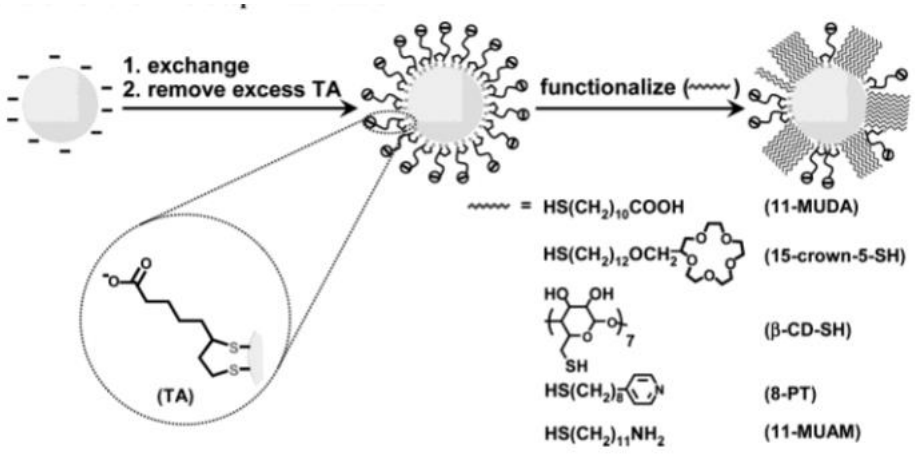

Figure 2.4: Illustration by Chen et al[8], showing the stages involved in the two-step ligand process involving thioctic acid as the intermediary stage.

Due to challenges occurring when attempting to functionalise larger citrate-stabilised AuNPs it was decided that a suitable size particle to attempt this on initially was ~10nm in size. This was achieved by following a method of synthesis by Puntes[9], briefly summarised below:

A solution of trisodium citrate (150ml, 2.2 mM) in MQ water was heated in an oil bath within a 250mL three-necked round-bottom-flask for 15 minutes with vigorous stirring. Upon reaching boiling point a solution of $HAuCl_4$ was rapidly injected (1ml, 25 mM). The colour of the solution immediately changed from yellow to bluish grey, followed by a gradual transition to soft pink within 10 minutes. The solution was then left to cool and analysed via TEM and UV-Vis to determine the size of the particles (~10nm) with a concentration of ~$3x10^{12}$ NPs/mL, Figures 2.5a and 2.5c.

40 ml of ~10 nm citrate-stabilised AuNPs was placed into a falcon tube and the basicity of the solution was adjusted via the addition of NaOH (400 μL, 0.5 M) dropwise under vigorous stirring; the solution remained stable up to this point with no indication of any change. After being left to equilibrate for 2 hours an ethanol solution of thioctic acid (50mg, 1 mL) was slowly added dropwise under vigorous stirring and left overnight to undergo complete ligand transfer. The resulting solution, showing no change in colouration, was centrifuged at 14,600 rpm and 10°C for 45 minutes, resulting in the pelleting of the AuNPs at the bottom of the falcon tube. The supernatant was removed and fresh MQ water added, re-dispersing the AuNPs. The particles were then subjected to a second round of centrifugation to ensure that all excess ligands within the solution were removed. The fact that the AuNPs could be centrifuged, cleaned and centrifuged again indicated that the functionalisation was successful. The particles were then analysed by UV-Vis and TEM to check for any loss of stability. The results are shown Figures 2.5b and 2.5c.

Figures 2.5 a) and b) show that after successful functionalisation the ~10 nm AuNPs showed no sign of stability loss or aggregation, with no change in the ordering upon the TEM grid and no increase in size or the appearance of large agglomerates, this is also backed up by the UV-Vis spectra, c), showing very little change in the colloidal solution spectra.

Upon successfully obtaining the thioctic acid functionalised 10 nm AuNPs a number of experiments were undertaken, varying the pH and excess ligand values from 7-11 and 10-500/nm^2 respectively.

Unfortunately, every combination involving the addition of thiolated 18-Crown-6 to the thioctic acid stabilised 10 nm AuNPs resulted in the rapid aggregation of the colloidal solution. The number of ligands added per nm^2 showed no change, only resulting in faster aggregation with increasing amounts, and the change in pH having no effect upon the rate of aggregation. Further changes within the experimental procedure such as: addition speed, temperature and solvent exchange (ethanol) proved unsuccessful in changing the outcome. It was therefore decided that while this method proved effective for Chen *et al.* with relatively long chained thiolation groups, the thiolated 18-Crown-6 was still too small to effectively stabilise the AuNPs in solution. This avenue of research was not taken any further as the ability to functionalise larger AuNPs in this manner was deemed not attainable.

a) b)

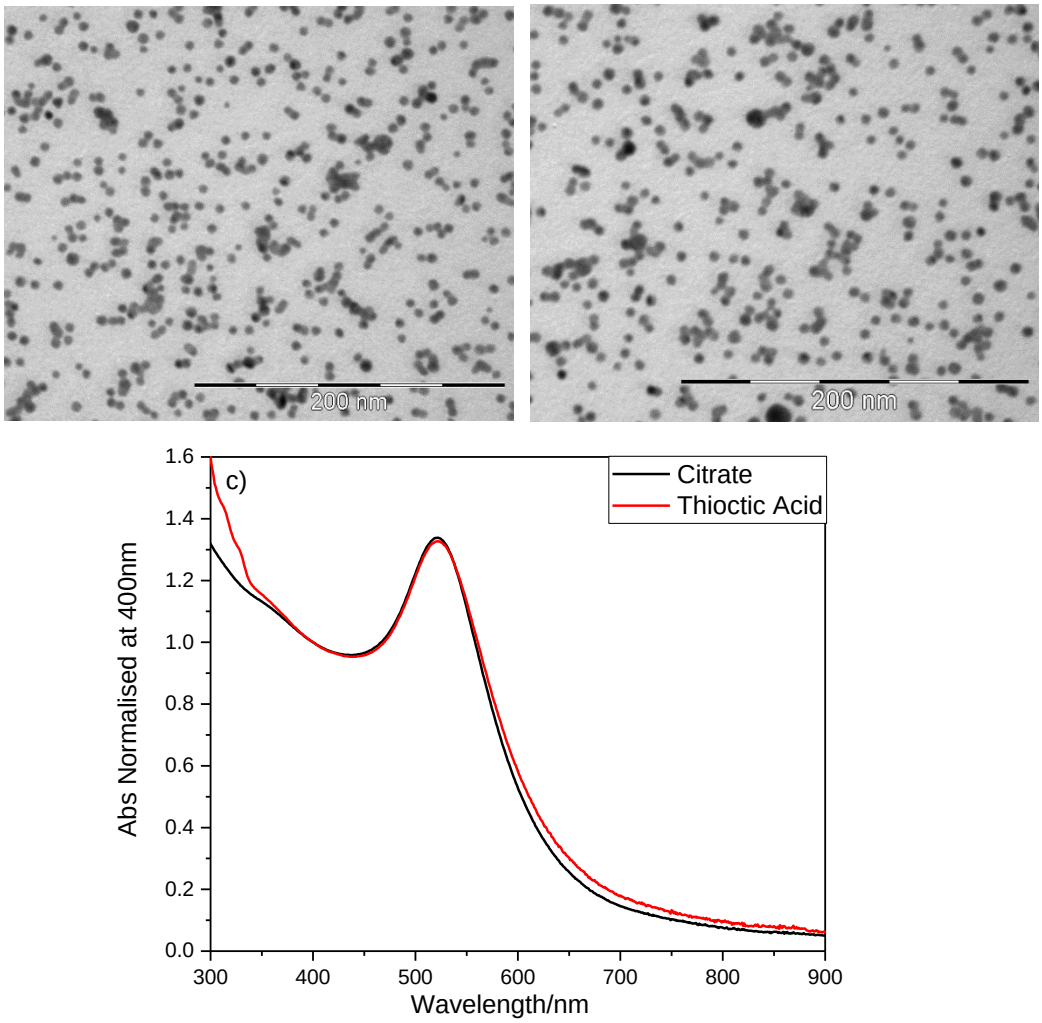

Figure 2.5: a) TEM image of the freshly made 10nm citrate AuNPs, b) TEM image of the freshly functionalised thioctic acid AuNPs, c) UV-Vis of each solution and normalised at 400nm for direct comparison.

2.2.2 mPEG-SH 5000 as an intermediary ligand

With the experiments attempting the two-step functionalisation with thioctic acid proving unsuccessful in achieving larger 18-Crown-6-modified AuNPs other approaches had to be investigated. As discussed briefly in Chapter 1, the use of thiolated polyethylene glycol (PEG) has been shown to be hugely successful in directly functionalising and stabilising AuNPs initially stabilised via the citrate ketone[3,4,5]. It was then postulated as to whether a thiolated PEG molecule could be used as an intermediary ligand exchange agent. O-[2-2(mercaptopropionylamino)ethyl] -O-methyl-poly(ethylene glycol) (mPEG-SH, Mw 5000) was chosen for several reasons: 1) it was suitably sized such that only a small number of ligands would have to be chemisorbed upon the gold surface in order to achieve a strong degree of stability[10-12], 2) the resulting small quantity of ligands chemisorbed to the gold surface would mean an increased degree of ligand exchange

when in the presence of the thiolated crown ether, and 3) any remaining m-PEG-SH present upon the surface could provide the essential stability that is needed for the 18-Crown-6-modified AuNPs to be successfully made. The same procedure laid out by Bastus *et al*[6]. as described in section 3.2.2 was again implemented here, except rather than using the seeds, the resulting growth steps were followed to achieve larger particles. The procedure is summarised below:

Upon obtaining the ~10nm seeds as discussed in section 3.2.2, the colloidal solution was cooled down to 90°C then 2 ml of the colloid solution was removed and replaced by trisodium citrate (1 ml, 60 mM) and left to equilibrate for 5 minutes followed by a secondary injection of $HAuCl_4$ (1 ml, 25 mM). The solution initially developed a deep red colouration before reverting to a bright ruby red over a period of 10 minutes. It was left to stir for 1 hour and then the solution was then removed and analysed via UV-Vis and TEM (Figure 2.6).

For the synthesis of larger (25.5 nm) AuNPs the same process was repeated, except that the number of solution removal-reactant addition steps was increased to a 6 rather than 1.

The initial functionalisation with m-PEG-SH 5000 was then achieved as follows: 30 ml of 15.1 nm AuNP solution was mixed with m-PEG-SH 5000 (4 molecules per nm^2 of surface gold) under vigorous stirring. The solution was left to stir for 40 minutes at room temperature to ensure complete functionalisation had occurred. The solution was then centrifuged at 14600 rpm for 30 minutes at 10°C, resulting in the pelleting of the particles. The supernatant was then removed and the particles re-dispersed into ethanol (5 ml). The centrifugation process was repeated a total of three times [13] to ensure that all water and excess ligand was removed.

The same process was repeated for the 25.5 nm AuNPs, functionalised with the same number of ligands per nm^2 (4), and centrifuged at: 13000 rpm for 30 minutes at 10°C. The resulting solutions were then analysed again using UV-Vis and TEM.

In order to replace the intermediate m-PEG 5000 ligand with the desired thiol 18-Crown-6, a solution of 18-C-6-CH_2-SH (400 molecules per nm^2 of surface gold) was dissolved in ethanol (1 ml), the crown ether solution was then slowly added drop wise under vigorous stirring to the ethanolic dispersion of both 15.7 and 25.5 nm m-PEG 5000 AuNP solutions (25 ml). The mixtures were then sonicated for 20 minutes and left at room

temperature, under stirring, for 12 hours. The product was then isolated via centrifugation at 13000 rpm for 1 hour at 10°C for the 15.7 nm AuNPs and 12000 rpm for 1 hour at 10°C for the 25.7 nm AuNPs. The pelleted AuNPs were re-dispersed in MQ water and then the centrifugation process was repeated a total of three times, to ensure the removal of ethanol and any excess ligand.

The UV-Vis spectra and TEM images are shown for the 15.7 and 25.5 nm particles in Figures 2.6 and 2.7 respectively. Figure 2.6 shows the TEM of the 15.7nm 18-Crown-6-modified AuNPs and the UV-Vis spectra throughout each stage of functionalisation. The UV-Vis has a slight broadening of the right-side slope indicating a slightly lower stability of the particles in water than the initial citrate particles, with a small peak shift from 521 nm to 530 nm, which again could be related to a slight loss in stability, but the overall stability of the newly made 18-Crown-6-modified AuNPs in water appears to be sufficient.

Figure 2.7 shows the same layout of images and spectra for the 25.7 nm 18-Crown-6-functionalised AuNPs, with the same general change in the UV-Vis spectra occurring; a slight broadening of the right-hand side slope and a minor increase in the PRS, but again overall showing good stability within aqueous media.

Unlike the thioctic acid two-step functionalisation described in Section 2.2.1, upon the addition of the thiol 18-Crown-6 the solutions remained a bright red in colouration, showing no signs of stability loss. The m-PEG-SH 5000 coated AuNPs were inherently unstable within pure water, slowly aggregating over a few hours, with the 18-Crown-6-modified AuNPs showing no sign of loss of stability in water was a strong indication that the ligand exchange was successful.

This synthesis was the first successful functionalisation of larger AuNPs with thiolated 18-Crown-6, enabling their use as potential cation transporters in Chapter 3 of this thesis. Unfortunately, it was found that they did not successfully achieve cation transport when in the presence of vesicles, with Cryo-TEM also showing that there was little interaction with the lipid membrane. This meant that another approach to developing smaller and 100% pure crown ether AuNPs was needed, which is described in Chapter 3.

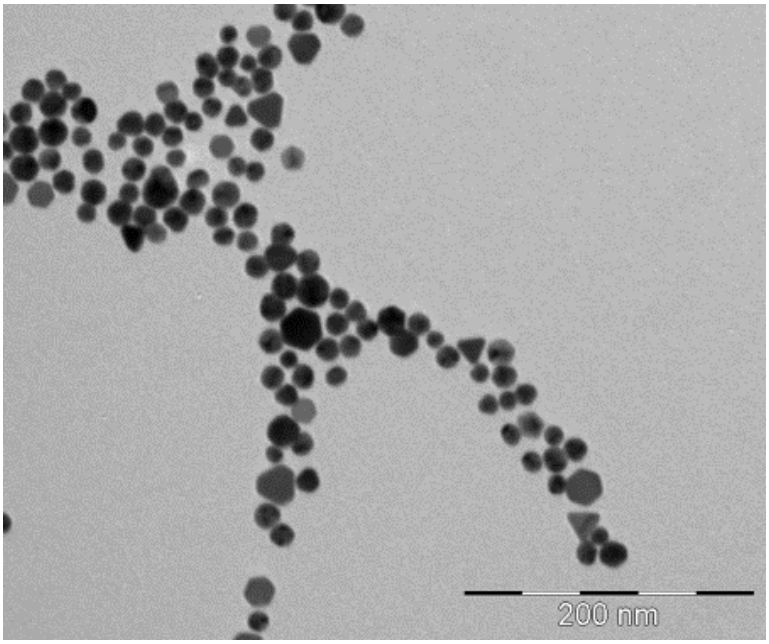

a)

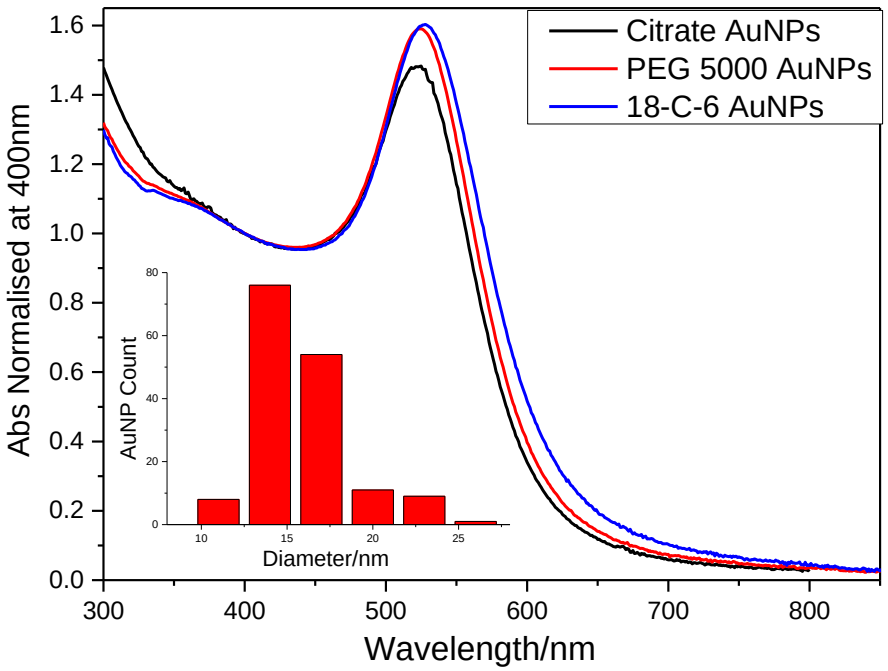

b)

Figure 2.6: a) TEM image of the 15.7nm 18-Crown-6-modified AuNPs, b) UV-Vis Spectra of the 15.7nm Citrate AuNPs (Black), the m-PEG-SH 5000 AuNPs (Red) and the 18-Crown-6-modified AuNPs (Blue)

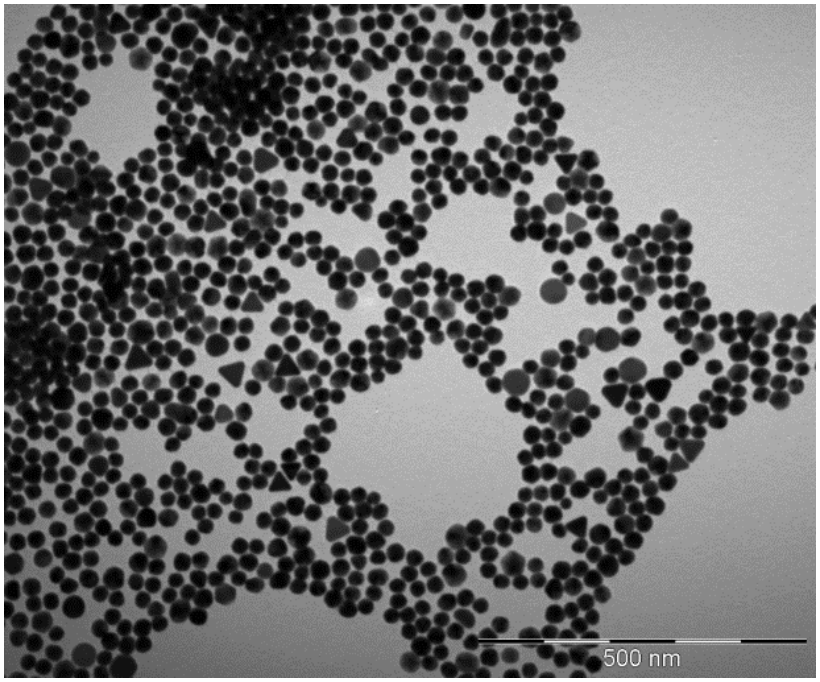

a)

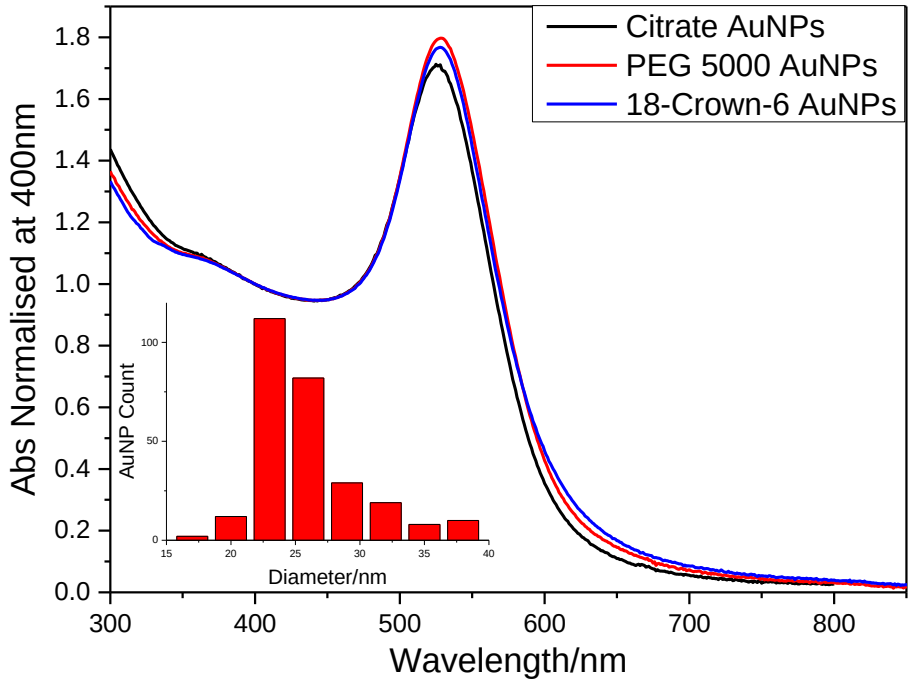

b)

Figure 2.7: a) TEM image of the 25.5nm 18-Crown-6-modified AuNPs, b) UV-Vis Spectra of the 25.5nm Citrate AuNPs (Black), the m-PEG-SH 5000 AuNPs (Red) and the 18-Crown-6-modified AuNPs (Blue)

2.2.3 Direct Functionalisation of 7nm AuNPs with 18-C-6-CH_2-SH

It became apparent at this point that in order for the goal of the thesis, developing an AuNP capable of instigating both cation and electron transport whilst being in a lipid membrane, required certain compromises. Whilst the use of m-PEG-SH 5000 as discussed in Section 2.2.2 provided the first avenue to a successful development of an 18-Crown-6-modified AuNP larger than 3nm, the original property of transporting complimentary cations across a lipid membrane was lost, as will be seen in Chapter 3. This could have been for reasons such as, firstly, the AuNPs were too large, resulting in the passive insertion in the membrane being inhibited and the remnants of m-PEG-SH 5000 upon the gold surface was inhibiting the ability of the particles to interact with the membrane after cation association. Secondly, it was also highly possible that even if the particles did sit in the membrane and achieve cation transfer, the presence of m-PEG-SH 5000 would inhibit the ability of the gold surface to pass charge through the membrane.

This meant that the AuNP would have to be both smaller than previously made, but also functionalised with pure thiolated 18-Crown-6, meaning two-step functionalisation was not viable.

Further research was undertaken into finding a suitable AuNP synthesis that could allow for the direct functionalisation of AuNPs with thiolated 18-Crown-6 to occur yet be smaller than 10 nm in diameter to allow for passive lipid membrane insertion. Puntes *et al*[14] released a paper in 2016 showing that sub-10-nanometer citrate stabilized AuNPs could be developed with a newly developed procedure. This procedure is briefly described below:

A trisodium citrate solution (150 mL, 2.2 mM) was added to a three-necked round-bottom flask. Under vigorous stirring tannic acid (0.1 mL, 2.5 mM) and potassium carbonate (K_2CO_3) (1 ml, 150 mM) were added. The solution was heated up to 70°C and under vigorous stirring $HAuCl_4$ (1 ml, 25 mM) was added, turning the solution from pale yellow to blue-grey, followed by the gradual transition to light orange. 55 ml of the colloidal dispersion was removed, followed by the addition of trisodium citrate (55 mL, 2.2 mM). The resulting solution was left to heat up to 70°C again, at which point $HAuCl_4$ (0.5 mL, 25 mM) was added under vigorous stirring, resulting in the solution darkening briefly before returning to a pale orange after 5 minutes. After 15 minutes a second injection of $HAuCl_4$ (0.5 mL, 25 mM) was added, again leaving the solution for 15 minutes. The removal and addition of extra reactants was repeated for one more complete

cycle (a total of 2 growth steps). The solution was then left to cool to room temperature, collected and analysed by UV-Vis and TEM, resulting in 7nm AuNPs at $2.8x10^{13}$ NP/mL.

A solution of 7 nm AuNPs (40 mL) was placed into a falcon tube and stirred vigorously as pure thiolated 18-Crown-6 dissolved in ethanol (10 ligands/cm^2 of surface gold) was slowly injected. The resulting solution quickly darkened followed by a gradual return to bright red after 15 minutes. The solution was left to stir for 4 hours, to ensure a complete ligand transfer had occurred.

The solution was then centrifuged in 20x2 mL lo-Bind Eppendorfs, to prevent surface sticking, at 14600 rpm for 1 hour at 2°C. The resulting AuNP pellet had the supernatant removed and fresh MQ water added and the particles re-dispersed. The solution was then centrifuged again at 13000 rpm for 1 hour at 2°C. The supernatant was again removed, and the remaining particles collected to gather and re-dispersed into fresh MQ water. The resulting colloidal solution was then analysed via UV-Vis, TEM and FTIR. The results are shown in Figure 2.8.

The TEM images shown in Figure 2.8a and b are a comparison between the 7 nm AuNPs before and after direct functionalisation with thiolated 18-Crown-6. It is obvious that the particles have not lost any noticeable amount of stability, with the AuNPs actually starting to develop more ordered structures upon the TEM grid whilst the original citrate AuNPs were quite randomly distributed across the surface. The UV-Vis shown in Figure 2.8c, shows a similar trend to the UV-Vis spectra discussed in Figure 2.6 and Figure 2.7, with the spectra after functionalisation red shifting slightly (515 nm to 518 nm), with a slight broadening of the right-hand side slope of the plasmon resonance, again indicating a slight broadening in the particle size. Even with this slight broadening the 7 nm 18-Crown-6-modified AuNPs are stable within aqueous media (providing they are kept below their phase transition temperature, see Chapter 4 for further details).

The stability of the particles after this method of synthesis was somewhat surprising, as the only additions to the reactant mixture were tannic acid, a stronger reducing agent than citrate resulting in the reduced size of the AuNPs, and K_2CO_3, present within solution to keep the pH on the basic side to retain colloidal stability[7]. Whilst ligand exchange is generally easier on smaller AuNPs in relation to larger ones, this is chiefly due to the effective coverage of the particle surface that can be achieved in the vital electrostatic to

steric stabilisation exchange, the relative ease at which these particles were functionalised was unusual.

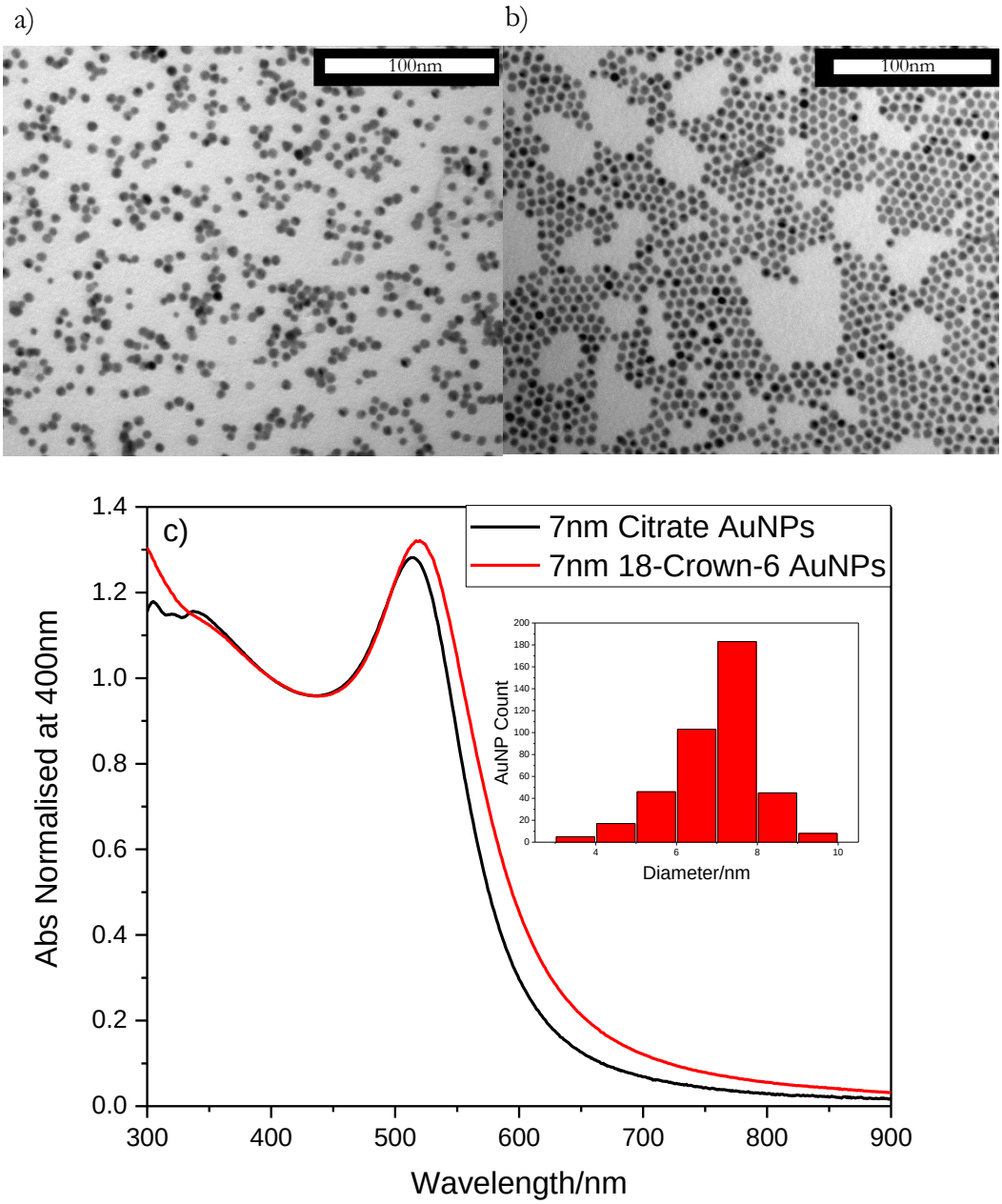

Figure 2.8: a) TEM image of the 7nm Citrate AuNPs, b) TEM image of the 7nm 18-Crown-6-modified-AuNP, c) UV-Vis spectra showing the change in the absorbance of the colloidal solution before and after thiol 18-Crown-6 functionalisation.

It was then postulated that perhaps the presence of the K^+ cation from the K_2CO_3 played a much larger role during ligand exchange than previously imagined. The strength of the association between 18-Crown-6 and K^+ has been well studied, both in literature and within this thesis (see Chapters 3 and 4). Whilst not as effective in water as other organic solvents[15], it still shows a strong degree of binding and selectivity. As stated at the start of

Section 1.2, most of the experiments involving the addition of thiolated 18-Crown-6 to citrate particles resulted in immediate irreversible aggregation but when in the presence of K_2CO_3 the crown ether can essentially become "charged", due to the K^+ cation picked up by the freshly injected thiolated crown ether. It then begins to make sense as to why these 7 nm AuNPs do not aggregate as seen previously. They are undergoing ligand exchange but rather than losing the electrostatic stability for steric stability, they are effectively retaining both, allowing for the system to be stable enough to achieve full functionality before aggregation can occur.

The K^+ is then readily washed away during the centrifugation purification stage, but by that time the AuNPs are already sterically stable, resulting in the AuNPs shown discussed in this section. This is only a theory however; whilst further work would need be done in order to clarify if this is the mechanism for stabilisation during ligand exchange. the FTIR results shown in Figure 2.9 indicate that the thiolated 18-Crown-6 has successfully chemisorbed to the gold surface, displacing the original ligand citrate. This is especially obvious by the disappearance of the two sharp C-H stretches/bends present in in the spectrum in Figure 2.9a at 1480 cm^{-1} and 1290^{-1} which is entirely absent in the pure crown ether spectrum, Figure 2.9b and the spectrum of the 7 nm 18-Crown-6-modified AuNPs, Figure 2.9c. An extra validation of the successful ligand exchange is the appearance of the sharp C-O peak at 1100 cm^{-1} in the 7 nm 18-Crown-6-modified AuNP spectrum, which is also highly prominent in the pure crown ether spectrum. The C-H stretch at 2860 cm^{-1} for the pure crown ether is also present for the AuNPs, but much less prominent. It is believed that the broad O-H peak that is present in both the citrate AuNPs and the 18-Crown-6-modified AuNPs is chiefly due to the presence of water.

Unfortunately, due to time constraints further investigation into how this process occurs was not covered in the work of this thesis, however a suitable experiment for achieving such a feat would be to use the smaller 15-Crown-5 and 12-Crown-4 moieties; their selectivity for K^+ is much lower than that of 18-Crown-6 in water (see Chapter 3), which should result in reduced stability of the particles during the ligand exchange injection.

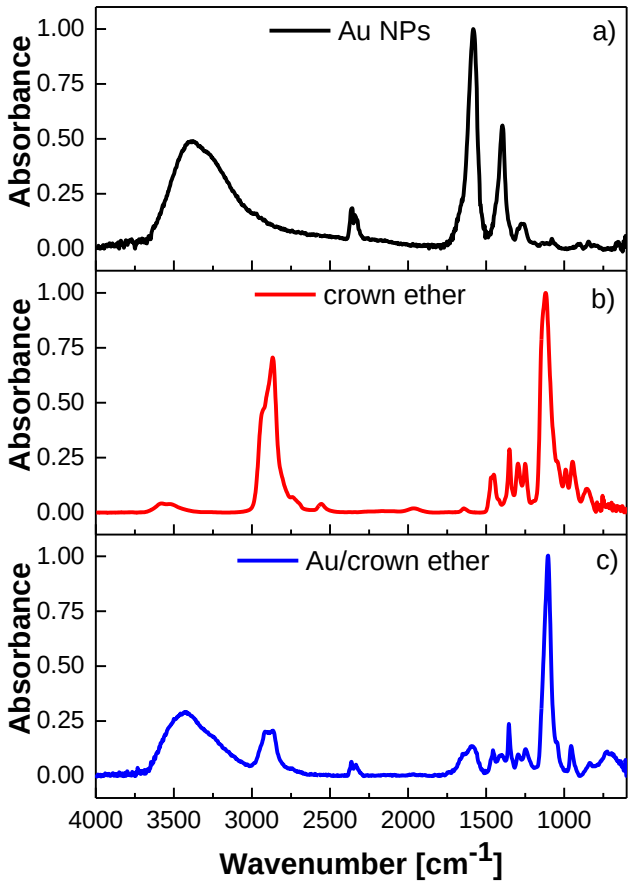

Figure 2.9: a) FTIR of the 7nm citrate stabilised AuNPs, b) FTIR of the pure thiolated 18-Crown-6, c) FTIR of the 7nm 18-Crown-6-modified AuNPs

2.3 Summary

The aim of this chapter was to show the synthetic procedures for the crown ether modified AuNPs that were used extensively within this thesis, including an overview on the thought process of how the development of these particles could be achieved. The development of the 3 nm AuNPs coated in various crown ethers was a success, with these particles then being discussed and experimented with in Chapter 3. Standard functionalisation experiments were done over a broad spectrum and resulted in failure every time, followed by more advanced two-step functionalisation methods either resulting in failure or partial success, until finally achieving the first >5 nm 18-Crown-6-modified AuNPs which are also discussed in Chapter 3. The final and most significant synthesis in terms of achieving a difficult task was the functionalisation of the 7 nm 18-Crown-6-modified AuNPs with pure crown ether; no intermediary steps were used yet a

ligand as small as 18-Crown-6-CH_2-SH was successfully placed upon the gold surface and remained stable within aqueous media. The unique properties that these particles exhibit is discussed in Chapter 4, along with further characterisation due to their strong potential for furthering the goal of this project, namely- achieving both cation and electron transfer across a lipid membrane.

2.4 References

1. M. Brust, J. Fink, D. Bethell, D. J. Schiffrin and C. Kiely, *Journal of the Chemical Society, Chemical Communications*, 1995, DOI: 10.1039/C39950001655, 1655-1656.
2. A. M. Cioran, A. D. Musteti, F. Teixidor, Ž. Krpetić, I. A. Prior, Q. He, C. J. Kiely, M. Brust and C. Viñas, *Journal of the American Chemical Society*, 2012, **134**, 212-221.
3. U. Kreibig and C. von Fragstein, *The Limitation of Electron Mean Free Path in Small Silver Particles*, 1969.
4. U. Kreibig, *Kramers-Kronig Analysis of the Optical Properties of Small Silver Particles*, 1970.
5. J. Turkevich, P. C. Stevenson and J. Hillier, *The Journal of Physical Chemistry*, 1953, **57**, 670-673.
6. J. Turkevich, P. C. Stevenson and J. Hillier, *Discussions of the Faraday Society*, 1951, **11**, 55-75.
7. E. M. Hotze, T. Phenrat and G. V. Lowry, *Journal of environmental quality*, 2010, **39**, 1909-1924.
8. S.-Y. Lin, Y.-T. Tsai, C.-C. Chen, C.-M. Lin and C.-h. Chen, *The Journal of Physical Chemistry B*, 2004, **108**, 2134-2139.
9. N. G. Bastús, J. Comenge and V. Puntes, *Langmuir*, 2011, **27**, 11098-11105.
10. L. Unsworth, H. Sheardown and J. Brash, *Polyethylene oxide surfaces of variable chain density by chemisorption of PEO-thiol on gold: Adsorption of proteins from plasma studied by radiolabelling and immunoblotting*, 2005.
11. A. Wijaya and K. Hamad-Schifferli, *Langmuir*, 2008, **24**, 9966-9969.
12. J. V. Jokerst, T. Lobovkina, R. N. Zare and S. S. Gambhir, *Nanomedicine (London, England)*, 2011, **6**, 715-728.
13. C. Fernández-López, C. Mateo-Mateo, R. A. Álvarez-Puebla, J. Pérez-Juste, I. Pastoriza-Santos and L. M. Liz-Marzán, *Langmuir*, 2009, **25**, 13894-13899.
14. J. Piella, N. G. Bastús and V. Puntes, *Chemistry of Materials*, 2016, **28**, 1066-1075.
15. V. P. Solov'ev, N. N. Strakhova, O. A. Raevsky, V. Rüdiger and H.-J. Schneider, *The Journal of Organic Chemistry*, 1996, **61**, 5221-5226.

Chapter 3 The Design of Artificial Membrane Transporters from Gold Nanoparticles with Controllable Hydrophobicity

The work discussed in this chapter will be focused on comparing the three types of crown ether-functionalised nanoparticles (18-C-6-CH_2-SH, 15-C-5-CH_2-SH and 12-C-4-CH_2-SH) developed and characterised within Chapter 2, Section 2.1.1 of this thesis and attempts to induce phase transfer into organic media via the complexation of alkali metals. Upon determining which of the crown ether functionalised particles shows the most efficient rate of phase transfer and cation selectivity, further phase transfer experiments will be undertaken to better understand the system. This will be followed by experiments involving the use of the most suitable particles for attempts at cation transfer across an artificial membrane, a vesicle in this case, whereby we monitor the effectiveness of this by applying Safranin O, a permeant cationic dye capable of fluorescence that changes with membrane potential.

3.1 Phase Transfer of Crown Ether Particles with K+, Na+ and Li+

Once the 3 nm crown ether particles were successfully developed the next phase of experiments were used to determine whether the crown ethers, organic compounds known for selectively binding alkali salts from aqueous media and readily dispersing them into organic media[1], retain their unique and useful properties once thiolated and bound upon a gold surface.

In the following sections, phase transfer and zeta-potential results will be presented for each of the three types of crown ether-functionalised nanoparticles in turn.

3.1.1 18-Crown-6-CH2-SH (18-C-6-CH2-SH)

Phase Transfer: Three 0.25 ml aliquots of an aqueous solution of 18-C-CH_2-SH 3 nm coated AuNPs (1.52 x10^{16} NP/mL) were placed into three separate Lo-Bind Eppendorfs (2 ml), to which each solution had 0.75 mL of fresh MQ water added (1 ml total volume, 3.8x10^{15} NP/mL). Each solution was vortexed thoroughly for 15 seconds followed by the addition of 4 mM KCl, NaCl or LiCl. All solutions were then vortexed for 15 seconds and then left to equilibrate for 5 minutes. Chloroform (1 ml) was placed into three separate glass vials (4 ml) on to the top of which the AuNP solutions were steadily injected. The solutions were then left undisturbed and pictures taken at various time intervals.

Figure 3.1 visually shows the transfer of particles from the aqueous phase to the organic phase (in this case chloroform) with each image being taken at a set period of time after adding the aqueous solution of particles to the organic phase. At t=0 there is no apparent difference between each solution, after a short period of time (t=90 minutes) there is an obvious change when comparing each solution. The vial with 4 mM KCl has developed a depletion layer next to the aqueous-organic interface, and particles previously present within the aqueous phase have now transferred into the organic phase. The solutions containing 4 mM NaCl and 4mM LiCl however show no obvious change relative to t=0.

As time progresses the difference in the solutions becomes more pronounced, with the depletion layer of the KCl solution rising upwards as more particles transfer into the organic phase. The NaCl and LiCl solutions however show very little change except for a slight build-up of particles around the edges of the vial (420 minutes). After 18 hours the KCl solution shows that a majority of the particles are now present within the organic phase, with the remaining particles positioned at the top of the depletion layer. The NaCl and LiCl solutions show no signs of transfer to the organic phase, just an increased build-up particle around the interface. After 3 full days it is now undeniable that in the presence of KCl the thiolated 18-C-6 particles readily transfer to the organic phase but show no inclination to do this when presented with 4 mM NaCl and LiCl.

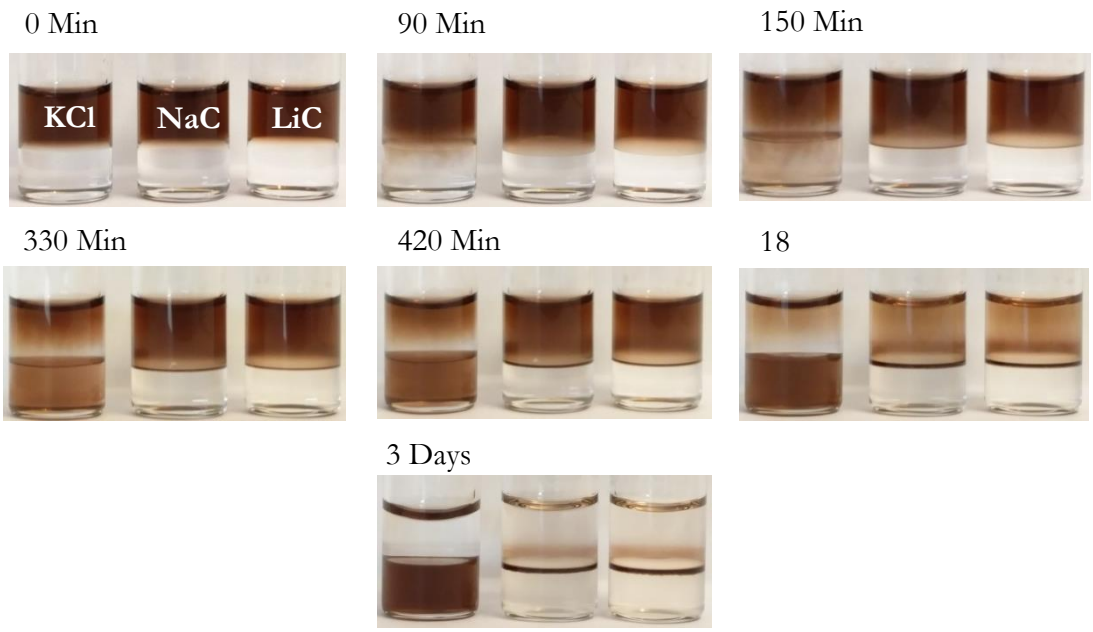

Figure 3.1: Images showing the phase transfer as a function of time for 18-C-6-CH_2-SH coated 3nm AuNPs when in the presence of 4mM KCl, NaCl and LiCl respectively.

It is important to note at this point that whilst the images shown in Figure 3.1 give very insightful information on how the particles phase transfer from the aqueous phase to the organic phase, the rate at which they transfer across the interface cannot be easily obtained. This is due to the development of the depletion layer, which can be readily seen. This depletion layer arises due to the rate of phase boundary transfer occurring faster than the rate of diffusion, resulting in the kinetics of transfer being limited by diffusion in these experiments.

To better understand the process occurring in the phase transfer images shown in Figure 3.1 the particles zeta-potential was measured to determine whether the complexation of a complementary cation changes the observed charge surrounding the AuNP.

Zeta Potential (ζ) Measurements: Three 0.125 ml aliquots of an aqueous solution of 18-C-CH_2-SH 3 nm coated AuNPs (1.52 x10^{16} NP/mL) were placed into three separate Lo-Bind Eppendorf's (2ml), to which each solution had 0.875 ml of fresh MQ water added (1 mL total volume, 1.9x10^{15}). The solutions were vortexed thoroughly for 15 seconds. To the first solution KCl was added to achieve a final concentration of 0.1 mM, the solution was shaken vigorously for 1 minute and then placed into a DTS-1070

Zetasizer disposable cuvette. The solution's ζ was measured with a minimum of 10 scans per run for 3 runs. Upon completion of the measurement the solution was removed and further KCl added to achieve a final concentration of 0.25 mM, mixed thoroughly and the ζ measured again. This process was repeated for 0.5, 1, 2, 3, 4 and 5 mM final concentrations of KCl. The conductivity of the solution was also measured for every sample to ensure that there were no unusual effects taking place and/or an error had occurred during the salt addition process. The experiment was then repeated for NaCl and LiCl.

The error for each ζ and conductivity measurement was calculated by taking the standard deviation of the three measurements (10 runs per measurement) for each sample point. The error was then plotted on the same axis to determine the reliability of each result.

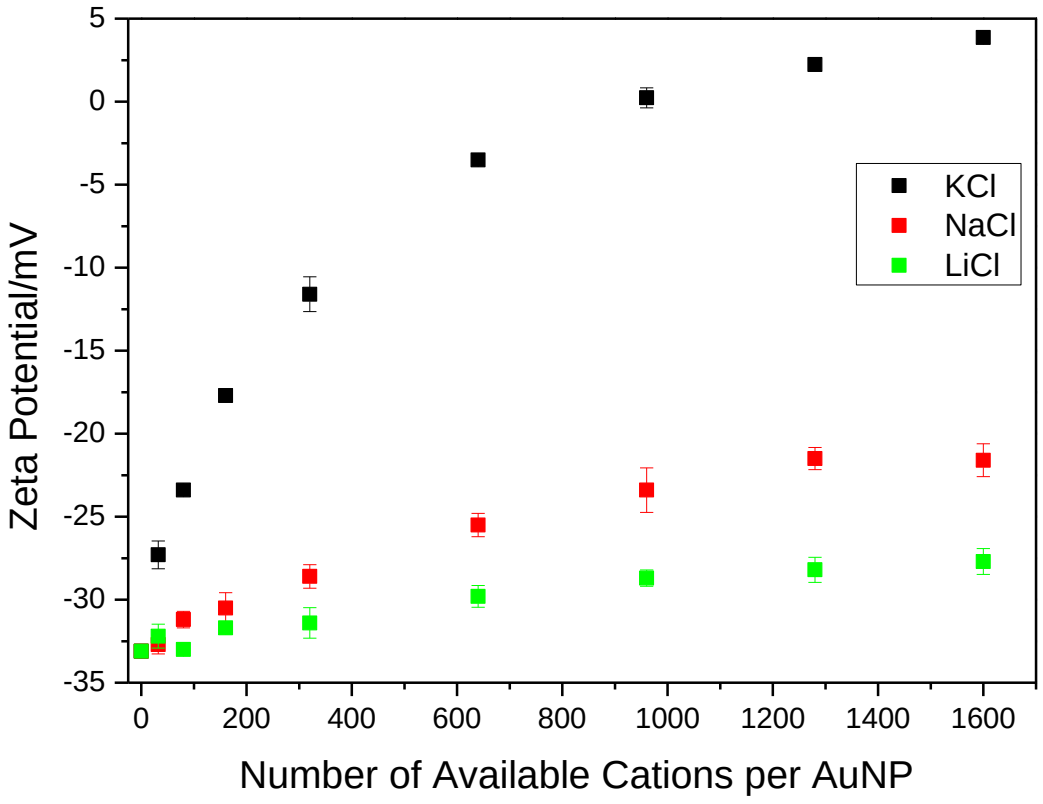

Figure 3.2: The change in ζ of 18-C-6-CH_2-SH coated 3nm AuNPs when in the presence of increasing ratios of alkaline metals (KCl, NaCl and LiCl)

Figure 3.2 shows the change in ζ and Figure 3.3 shows the change in conductivity as a function of increasing ratios of alkaline metals. Note that due to the concentration of

particles used in the phase transfer ($3.8x10^{15}$ NP/mL) and ζ ($1.9x10^{15}$) measurements differing by a factor of two. The X-axis of both ζ and conductivity have been modified to the "Number of Available Cations per AuNP" to allow for easier comparison between the data sets and the phase transfer images with the ratio of available cations per AuNP equalling 640 for the phase transfer experiments. The conversion to "Number of Available Cations per AuNP is done simply by dividing the number of cations present within the solution by the number of 18-Crown-6-modified gold nanoparticle in solution.

From the results it can be seen that the hypothesis regarding complexation is true; in Figure 3.2 the 18-C-6-CH_2-SH 3 nm coated particles in this batch have an initial ζ of -33.1 mV. Upon adding KCl to the particle solution the ζ tends towards the positive, with initial additions of KCl resulting in a steep change, followed by a more gradual increase which tails off towards a plateau. The same trend is observed for both NaCl and LiCl, where a gradual positive shift in ζ is observed followed by a plateau; it is the overall change upon the ζ of each system that varies dramatically.

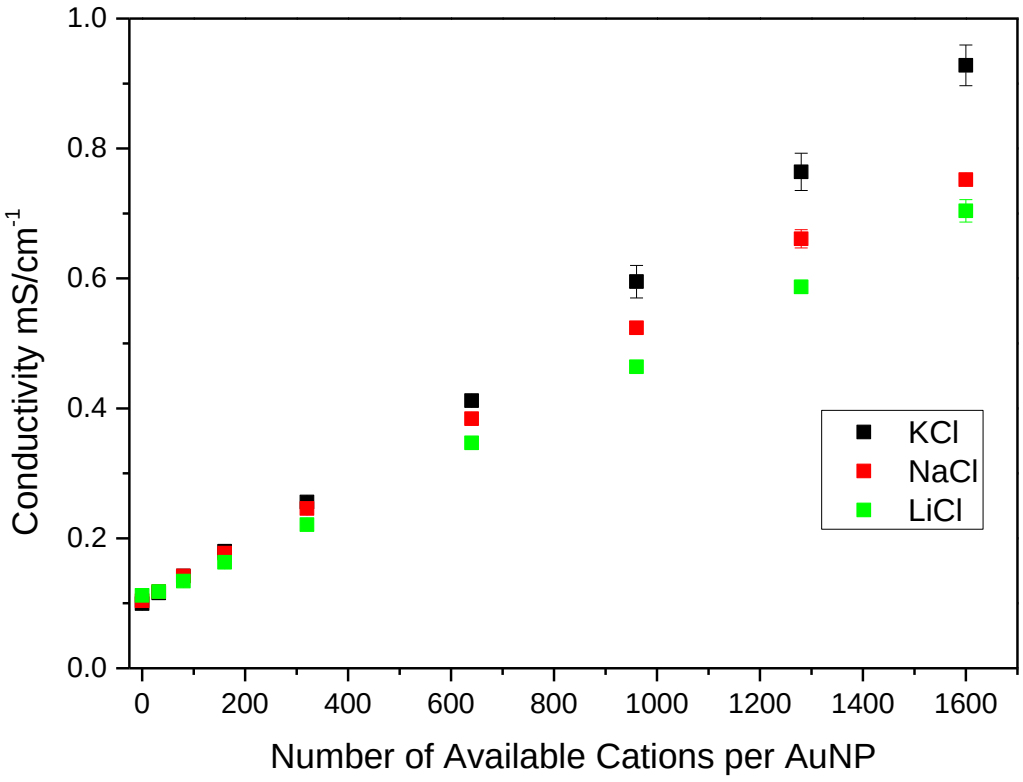

Figure 3.3: The change in conductivity of 18-C-6-CH_2-SH coated 3nm AuNPs when in the presence of increasing ratios of alkali metals (KCl, NaCl and LiCl)

Figure 3.3 shows that the conductivity of each solution rises linearly with increasing salt concentration, which is to be expected when plotting the conductivity of an aqueous

solution verses electrolyte concentration. It is noted that the final conductivity of each system varies depending on the cation present. However this effect is not one induced by the presence of the AuNPs, but is mainly dictated by the ionic size of each cation, including their hydration shells, whereby Li^+ (aq) > Na^+ (aq) > K^+ (aq) [2, 3] which alters their relative conductivities when in solution, fitting the variations observed in this system nicely.

When comparing the ζ measurements to the phase transfer images shown in Figure 3.1 a pattern begins to emerge. At the cation : AuNP ratio of 640, the ratio used in the phase transfer experiment, the ζ of the KCl, NaCl and LiCl solutions are -3.51 mV, -25.5 mV and -29.8 mV respectively. In the presence of KCl at 640 cations : AuNPs the ζ of the solution comes close to zero, whilst in the presence of NaCl and LiCl, at 640 cations : AuNPs, the ζ remains above -25 mV, far from zero. From these initial observations it becomes possible to start to develop a hypothesis to explain the above processes.

It has already been shown and stated that the ζ of the particles is highly negative to begin with (-33.1 mV), with this charge being attributed to electrons present upon the gold core. As previously stated, 18-C-6 is well known to have a high affinity to bind K^+ over other alkali metals such as Na^+ and Li^+. This is seen within the literature[4] and readily explains the effects upon ζ and phase transfer seen in the above data.

In the absence of any cations the particles retain their initial charge of -33.1 mV, resulting in hydrophilic particles which are stable within an aqueous media. This is represented in Figure 3.4a. Upon adding a cation that is highly complementary (K^+) to the crown ether in question (18-C-6-CH_2-SH) it is expected that the crown ether will take up the cation into its cavity, Figure 3.4b. This would result in the lone pairs of electrons present upon the oxygens within the crown ether rings interacting with the new positive charge present within the cavity. With the presence of positively charged cations so close to the gold nanoparticle surface, a result of the strong complimentary binding, the negative charge of the AuNPs become masked, resulting in a more positive ζ, Figure 3.4c, with the positive increase of the ζ being related to the population of complementary cations present around each crown ether ring. This is seen within Figure 3.2 where we observe the steep rise in ζ with only small concentrations of complementary cation present followed by the gradual plateau as each crown ether ring becomes saturated with positive charge, Figure 3.4d.

In the case of non-complementary cations (Na^+ and Li^+) the crown ether (18-C-6-CH_2-SH) does not effectively bind them within its cavity, which results in a much lower degree of interaction with the lone pairs of electrons which further results in very little change in the ζ, which is clearly shown in Figure 3.2.

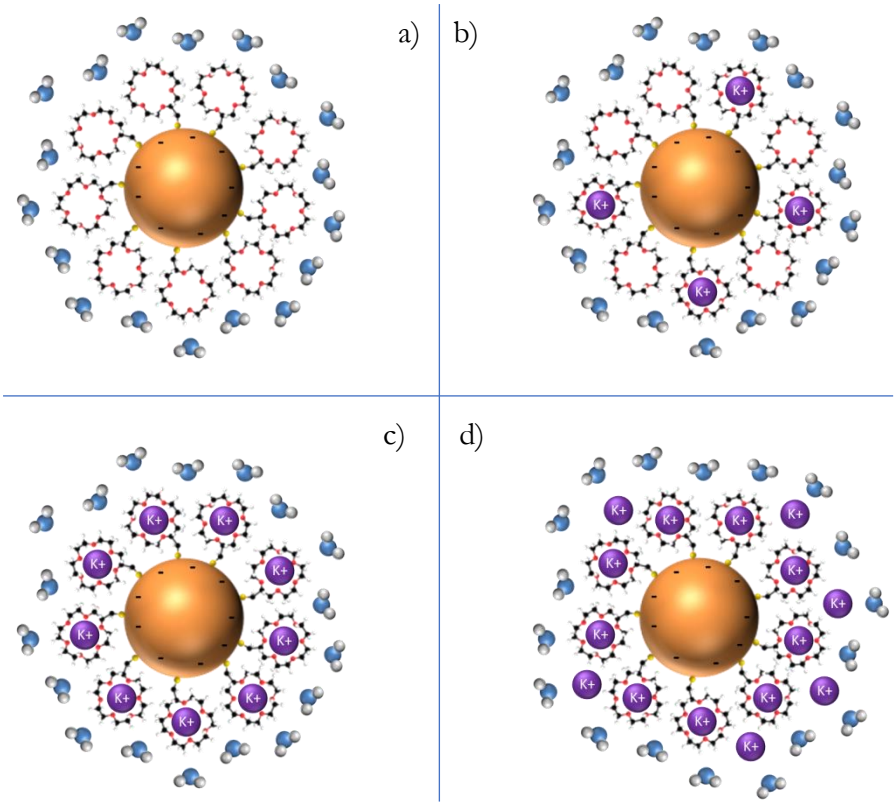

Figure 3.4: Graphical Illustration describing the 18-C-6-CH_2-SH 3nm Coated AuNPs when: a) No Complementary cation is present, b) Small quantity of complementary cation is present, c) The amount of complementary cation present is adequate to mask the entire AuNPs charge, d) The amount of complementary cation exceeds the negative charge, resulting in a positive ζ.

At the present time this hypothesis explains the ζ nicely, but without further explanation the effect of increased phase transfer is still not clearly described. This is where the phenomenon known as the hydrophobic effect[5] plays a part. This phenomenon is also used to explain properties exhibited by larger 18-C-6-CH_2-SH coated AuNPs which are described in Chapter 4 of this thesis, implying it plays a large role in controlling the hydrophobicity of these types of particles.

As with all solutes placed within aqueous media, the water molecules undergo a conformational change, forming structured cages around each solute in order to lower the overall energy of the system. Such cages can be highly favoured if the solute present is highly charged, allowing for strong electrostatic bonds to be formed between the solute and its local water molecules. However, the drive to develop an ordered cage around a solute drops as the charge of the solute drops. This results in relatively low charged or neutral solutes either being forced together (flocculation) to lower the surface area of the solute, or outright evicting the solute from the system if this is an avenue the system can take.

In the phase transfer system observed in Figure 3.1 such an avenue is available; the organic phase. The initial ζ (-33.1 mV) is adequate enough to allow the formation of a solvent shell around each particle as a separate entity, as shown in Figure 3.5a; if this were not the case a more prominent plasmon resonance peak would appear within the UV-Vis spectra due to the flocculation of nanoparticles giving rise to a larger entity. It should be noted that when the aqueous dispersion of AuNPs is presented with an organic interface (chloroform) they build up upon the interface, even in the absence of complementary cations. This is shown clearly in Figure 3.5. Such an interaction indicates that the particles, whilst stable in water, are inherently drawn towards a less polar solvent, which is to be expected due to traditional pure crown ethers being insoluble in aqueous media[6, 7]

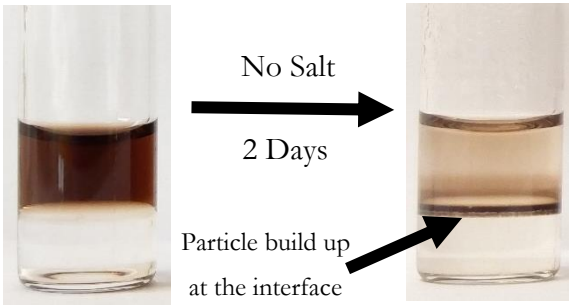

Figure 3.5: 3nm 18-Crown-6-modified gold nanoparticles presented with an aqueous-organic interface in the absence of complimentary cations, resulting in the gradual build-up of particles are the interface but no transfer into the organic phase.

Upon addition of the complementary cation the ζ of the particle is reduced, lowering the electrostatic interactions between the particle and its solvent cage, resulting in the drive for the water to create a solvent cage to be reduced. This reduction in overall charge, combined with the reduced drive to develop a solvent cage, results in pushing the particle

across the aqueous-organic interface, Figure 3.6b, resulting in eventual complete phase transfer, Figure 3.6c. The closer the system tends towards zero ζ the more pronounced this effect should become; the opposite should also be observed when the particles become overly saturated with positive charge, Figure 3.2 and 3.4d. This process is described further in Section 3.3.2; with the current model fitting our data trends and observations.

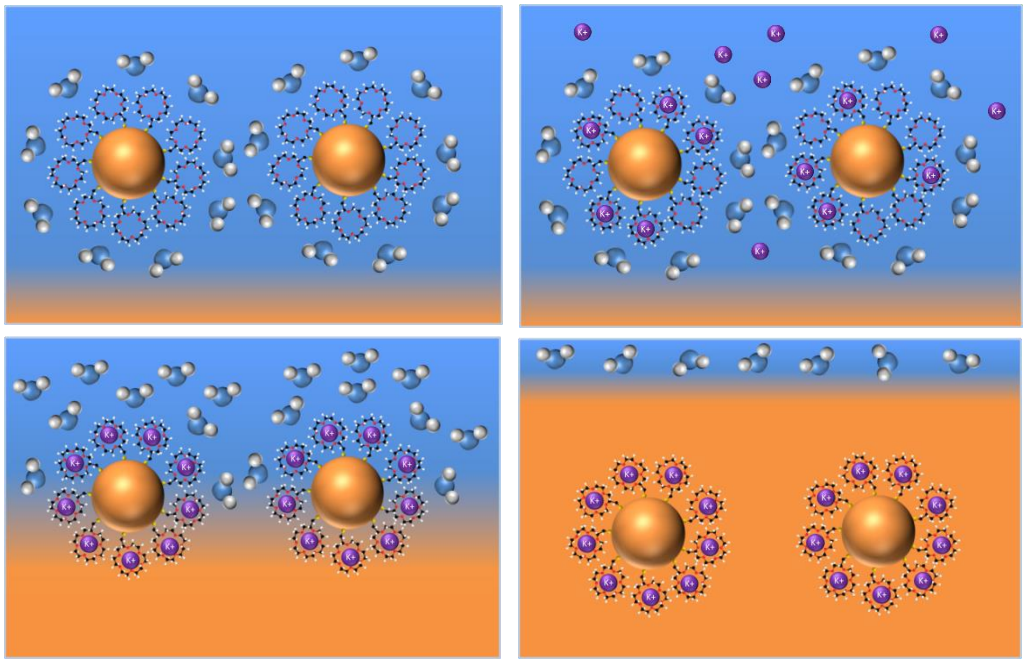

Figure 3.6: Graphical Illustration describing: a) Solvent shells surrounding un-complexed particles, b) The beginning of complimentary cation association, resulting in reduced interaction with the solvent shell, c) Gradual loss off solvent shell as particles phase transfer, c) Complete loss of solvent shell once particles are completely transferred.

Now that a simple model has been developed in order to understand the properties of the 18-C-6-CH_2-SH coated 3nm AuNPs, it is possible to apply this to similar phase transfer experiments done with both 15-C-6-CH_2-SH and 12-C-4-CH_2-SH.

3.1.2 15-Crown-5-CH2-SH (15-C-5-CH2-SH)

The experimental procedure for the following data is a replication of the experimental discussed in Section 3.1.1, with the only change being the type of particle used (15-Crown-5-CH_2-SH coated 3nm AuNPs).

As shown in Figure 3.7, the phase transfer for the 15-C-5-CH_2-SH coated 3nm AuNPs was monitored similarly to the 18-C-6-CH_2-SH coated 3nm particles. At t=0 there is no

obvious differences between the three solutions. However, at t=90 minutes the 4 mM KCl solution resulted in a surprisingly rapid transfer of particles from the aqueous to the organic phase, which continued throughout the experiment, with the reduction in transfer being limited only by the rate of diffusion to the aqueous-organic interface. The 4 mM NaCl solution shows gradual transport of particles from the aqueous phase to the organic phase, with a slight discolouration in the organic phase at t=330 minutes; but becoming more obvious after 18 hours. The 4 mM LiCl solution shows no transport to the organic phase, just the settling of the particles upon the interface, a similar process as seen by the 18-C-6-CH_2-SH particles in Figure 3.1.

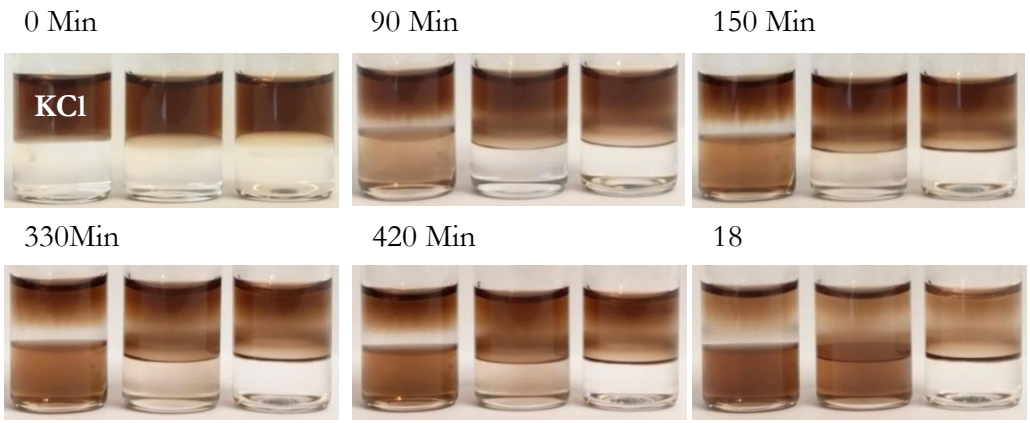

Figure 3.7: Images showing the phase transfer as a function of time for 18-C-6-CH_2-SH coated 3nm AuNPs when in the presence of 4mM KCl, NaCl and LiCl respectively.

This outcome was slightly unexpected. It is stated in the literature[8, 9] that the binding constants of K^+ to 18-Crown-6 and 15-Crown-5 in methanol are 6.08 and 3.43 respectively, suggesting that the 15-Crown-5 should bind to K^+ to a lesser extent than 18-Crown-6, even when attached to an AuNP and in the presence of water rather than methanol this dramatic shift in apparent binding seems amiss. It has, however, also been stated in the literature[10, 11] that 15-Crown-5 moieties attached to nanoparticles show a strong affinity to bind to K^+ by sandwiching a singular K^+ ion between two 15-Crown-5 rings. Upon further inspection with both ζ, Figure 3.8, and UV-Vis, Figure 3.9, it is strongly indicated that such a process occurs within this system.

Figure 3.8 shows the change in ζ with relation to the number of available cations per AuNP. Upon adding a small population of KCl (160 cations : AuNP) the ζ changes dramatically, with an increase of +23mV. This rapid change in the ζ swiftly abates

however as further additions of KCl result in very slight changes in the ζ resulting in a plateau. The ζ for the NaCl solution shows the expected result; a relatively sharp change in the initial ζ followed by a gradual plateau as the particle becomes saturated with the complimentary cation. The LiCl solution shows no obvious signs of binding with only a very gradual trend towards zero in the ζ, which correlates nicely with the phase transfer experiment shown in Figure 3.6, where we see no phase transfer for the LiCl solution.

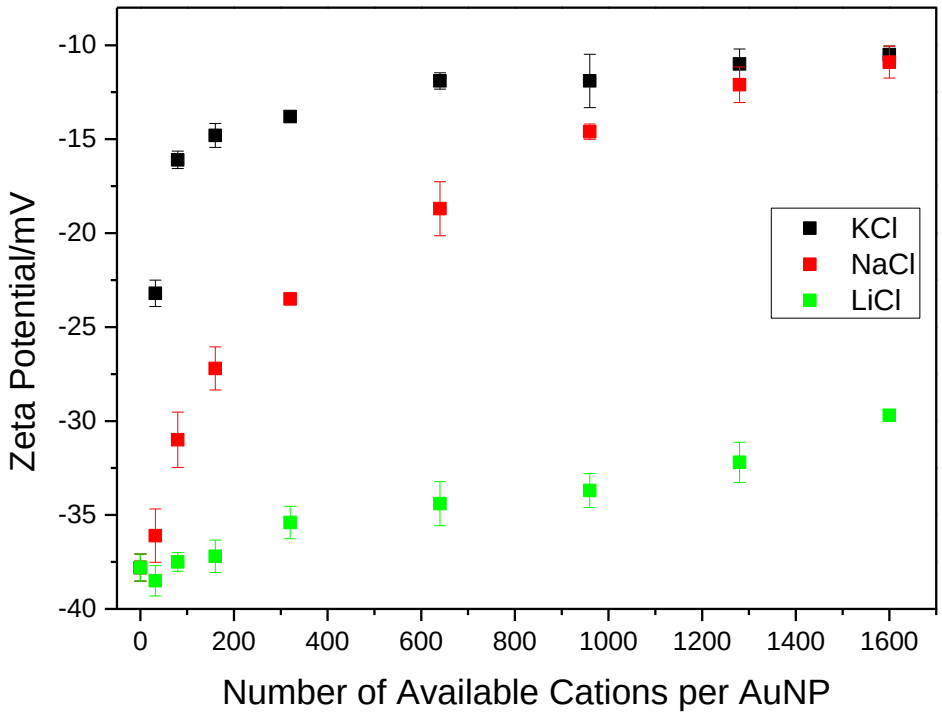

Figure 3.8: The change in zeta potential of 15-C-5-CH_2-SH coated 3nm AuNPs when in the presence of increasing ratios of alkaline metals (KCl, NaCl and LiCl)

For K^+, the sharp rise in the ζ followed by the rapid onset of a plateau seems to agree with the literature in that the particles have to sandwich the K^+; this can be postulated by looking at the values of cation : AuNP at which both the K^+ and Na^+ plateaus start to occur. In the case of K^+ the plateau is observed to start at 640 cations : AuNP, whilst the Na^+ plateau is observed to begin at 1600 cations : AuNP indicating that the crown ethers are saturated at much lower ratios of cation : AuNP in the presence of K^+ over Na^+. This could indeed be due to having to accommodate a singular K^+ with two or more crown ethers. This is of course only an approximation; no specific data values/experiments have been done in order to further prove this relationship, but the current trend observed seems to fit well with both literature and data shown within this thesis. Additionally,

further evidence for the sandwiching process is shown when comparing the UV-Vis spectra of the 15-C-5-CH_2-SH coated 3nm AuNP with and without K^+ ions present, Figure 3.9. A slight hump has developed upon the slope. This hump is the beginning of a plasmon absorbance peak which is typical of particles >3 nm in size. This slight change in the UV-Vis spectrum also supports the presence of larger AuNPs within the solution when in the presence of K^+. With the development of the hump being an indication of particle flocculation, as the close proximity of the AuNPs would result in a more pronounced plasmon resonance; experimental evidence has shown, for the most part, that when in the presence of alkali salts the AuNPs show no obvious signs of losing stability as separate entities within solution. So, this unexpected change in the plasmon resonance peak for this specific experiment is a strong indication that this sandwiching effect is the cause, an interesting observation that should be researched further.

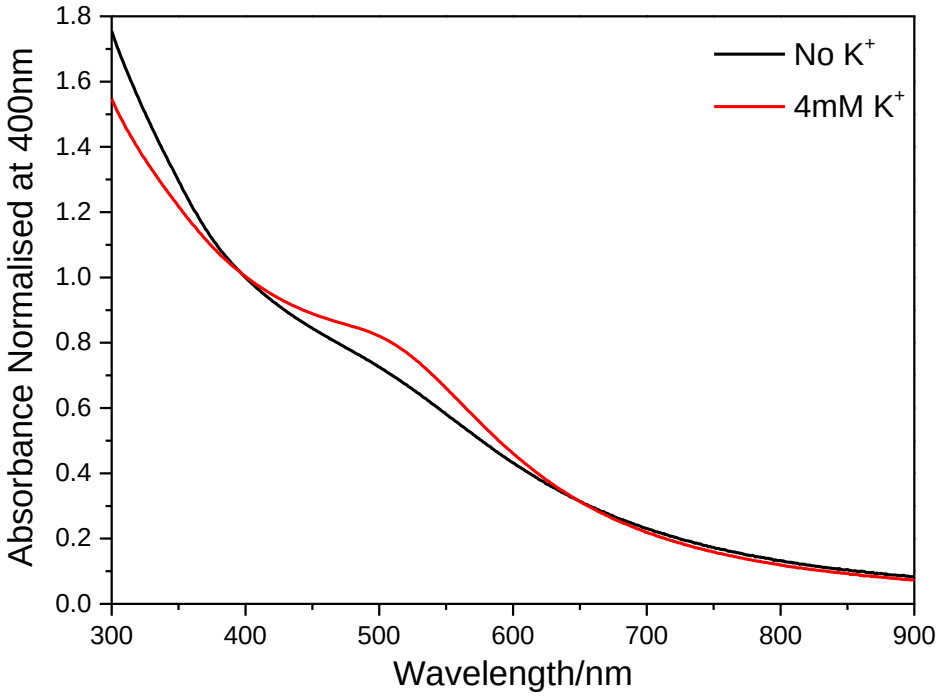

Figure 3.9: UV-Vis spectra of the 15-C-5-CH_2-SH coated 3nm AuNP with and without 4mM K^+

Figure 3.10 shows the expected linear trend of increasing conductivity with increasing concentration of electrolyte and follows the same trend as seen in Figure 3.3 which was to be expected, with the hydration radii of each cation resulting in slight shifts in their relative conductivities.

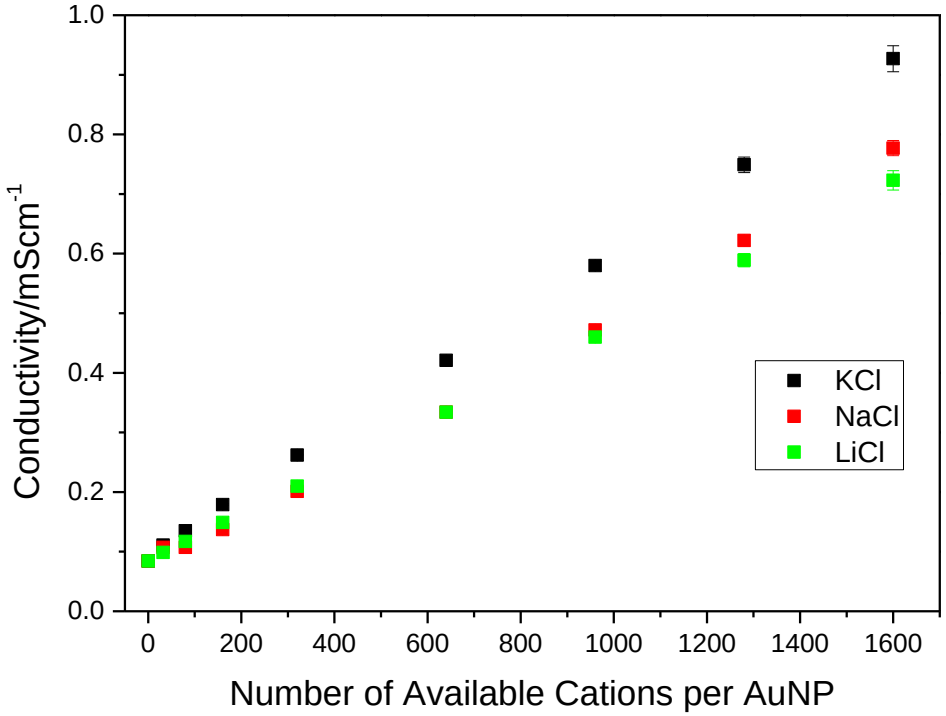

Figure 3.10: The change in conductivity of 15-C-5-CH_2-SH coated 3nm AuNPs when in the presence of increasing ratios of alkaline metals (KCl, NaCl and LiCl)

3.1.3 12-Crown-4-CH2-SH (12-C-4-CH2-SH)

The experimental procedure for the following data is a replication of the experimental discussed in Section 3.1.1, with the only change being the type of particle used (12-Crown-4-CH_2-SH coated 3 nm AuNPs).

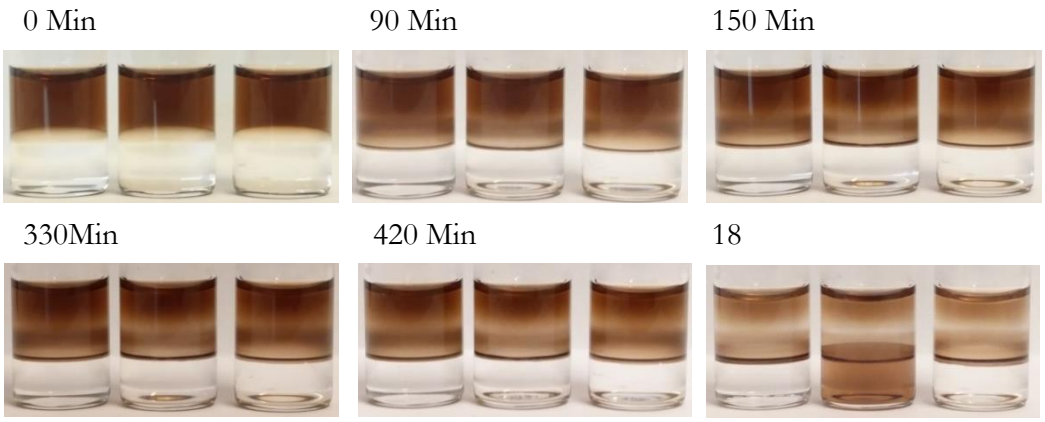

Figure 3.11: Images showing the phase transfer as a function of time for 12-C-4-CH_2-SH coated 3nm AuNPs when in the presence of 4mM KCl, NaCl and LiCl respectively

As shown in Figure 3.11, the phase transfer for the 12-C-4-CH_2-SH coated 3 nm AuNPs was monitored similarly to the 18-C-6-CH_2-SH coated 3 nm particles. At t=0 there is very little difference between the solution and there is no apparent difference between each particle solution until the image taken at t=18 hours, where the 4 mM NaCl solution has phase transferred into the organic phase, albeit not very well. The majority of the particles appear to sit upon the interface. This behaviour, again, was noted when particles with no cations present are able to interact with the aqueous-organic interface, which can be seen in Figure 3.5, indicating that there is little interaction between the cations and the 12-Crown-4 present upon the AuNP surface.

This low degree of interaction between the cations and the particles becomes apparent when looking at the ζ in Figure 3.12. Unlike the smooth saturation curves observed for ζ with both the 18-C-6-CH_2-SH AuNP and 15-C-5-CH_2-SH AuNP when presented with complementary cations, the ζ obtained for the 12-C-4-CH_2-SH AuNPs shows no such thing. Most of the changes in ζ follow a linear trend, including for Li^+, the cation that is supposedly complementary for 12-Crown-4[12] Interestingly the presence of Li^+ in solution results in lower values of the ζ when compared to both Na^+ and K^+, with the Na^+ showing a relatively steep rise at 320 cations : AuNP but then is caught up by K^+. Such a change in the ζ for the larger cations could indicate that the 12-Crown-4 is attempting to sandwich each cation[13], similar to the 15-Crown-5 seen in Figures 3.8 and 3.9. This could explain why the Na^+ solution shows some degree of transfer respectively to both the K^+ and Li^+. Combined with no dramatic change in the ζ it is not possible to explain this data away as a sandwiching effect. In Figure 3.12 we can see that the conductivity of the system mimics that of both Figures 3.3 and 3.8, so the presence of salt within this system is unchanged with respect to the others.

With the ζ showing very little change between each cation, combined with the slow/no transfer of 12-C-4-CH_2-SH AuNP it can be concluded that the overall selectivity of these AuNPs is quite poor, showing a small interaction with every cation (K^+, Na^+ and Li^+), resulting in these linear increases in ζ, and no effective transport of the particles, as seen in Figure 3.12, with the conductivity showing the expected linear relationship with increasing salt concentration, Figure 3.13.

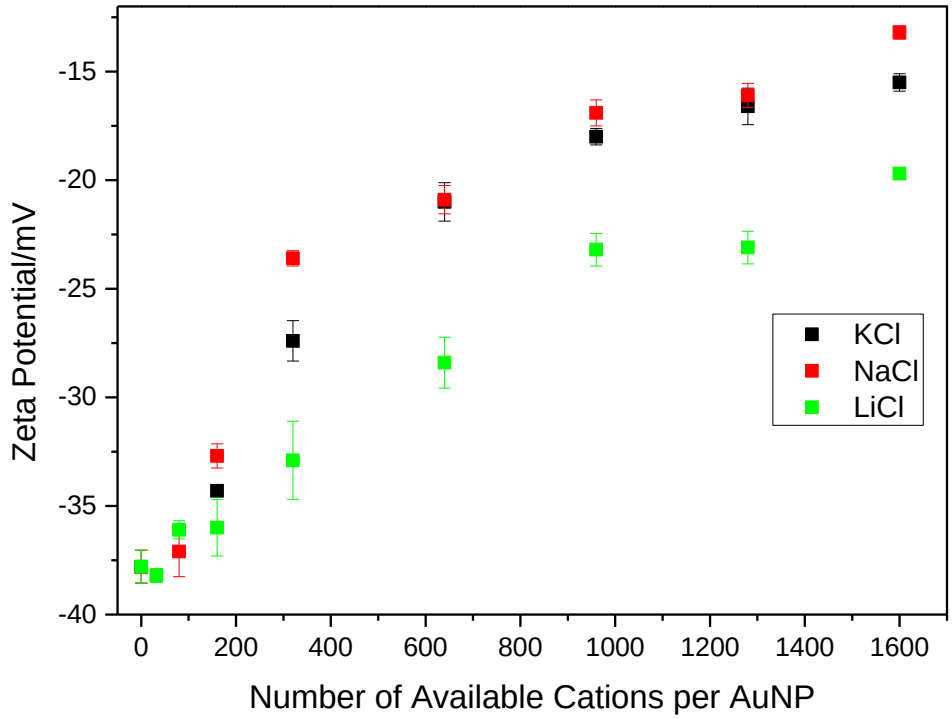

Figure 3.12: The change in zeta potential of 12-C-4-CH_2-SH coated 3nm AuNPs when in the presence of increasing ratios of alkaline metals (KCl, NaCl and LiCl)

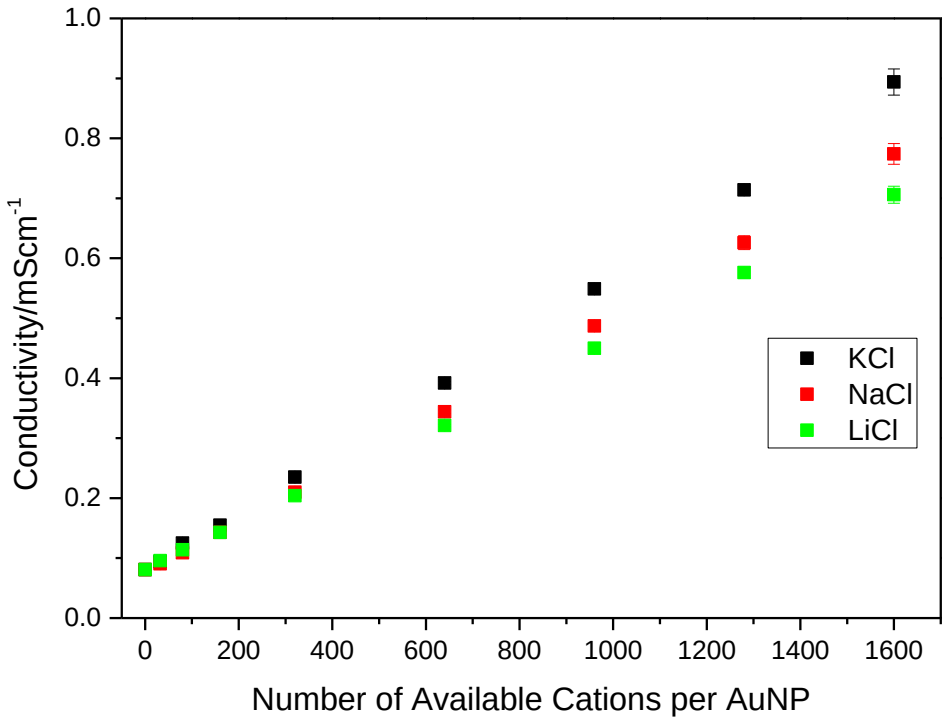

Figure 3.13: The change in conductivity of 12-C-4-CH_2-SH coated 3nm AuNPs when in the presence of increasing ratios of alkaline metals (KCl, NaCl and LiCl).

3.1.4 Zeta Potential Comparisons for Each Crown Ether

In order to develop of a greater understanding of which crown ether AuNP was most suitable for successfully transporting cations across a membrane the change in the zeta potential (Δζ) for each cation in the presence of each crown ether was plotted against the cation : AuNP. In Figure 3.14a firstly it is observed that in the presence of K^+ the 18-C-6 AuNPs eventually show the highest degree of association, with the 15-C-5 AuNPs initially showing a greater degree of association; this observation has already been explained in section 3.1.2 via the sandwiching of multiple crown ethers over a singular cation. Secondly, the early plateau experienced by the 15-C-5 AuNPs compared to the much smoother plateau of the 18-C-6 AuNPs also suggest that a larger proportion of the binding sites are used up at low cation : AuNPs ratios, which is then followed by rapid saturation. Finally, the 12-C-4 AuNPs also show a degree of association but the overall curve does not follow the trend now associated with a strong affinity to bind, as seen by the 18-C-6 and 15-C-5 AuNPs.

In Figure 3.14b it is observed that in the presence of Na^+ the 18-C-6 AuNPs show a very gradual Δζ, a large change in comparison to the K^+ values, indicating a low degree of cation association. The 15-C-5 AuNPs show a similar Δζ change as to that seen with K^+ except the curve is much smoother, as seen by 18-C-6 AuNPs in the presence of K^+. The 12-C-4 AuNPs show a slightly higher Δζ than observed with K^+ and follow a similar curve as previously seen.

In Figure 3.14c it is observed that in the presence of Li^+ the 18-C-6 AuNPs show only a very small Δζ, indicating a low degree of cation association. The 15-Crown-5 AuNPs also show only a small Δζ, again indicating a low degree of cation association. The 12-Crown-4 AuNPs however show a moderate Δζ which indicates a moderate degree of association.

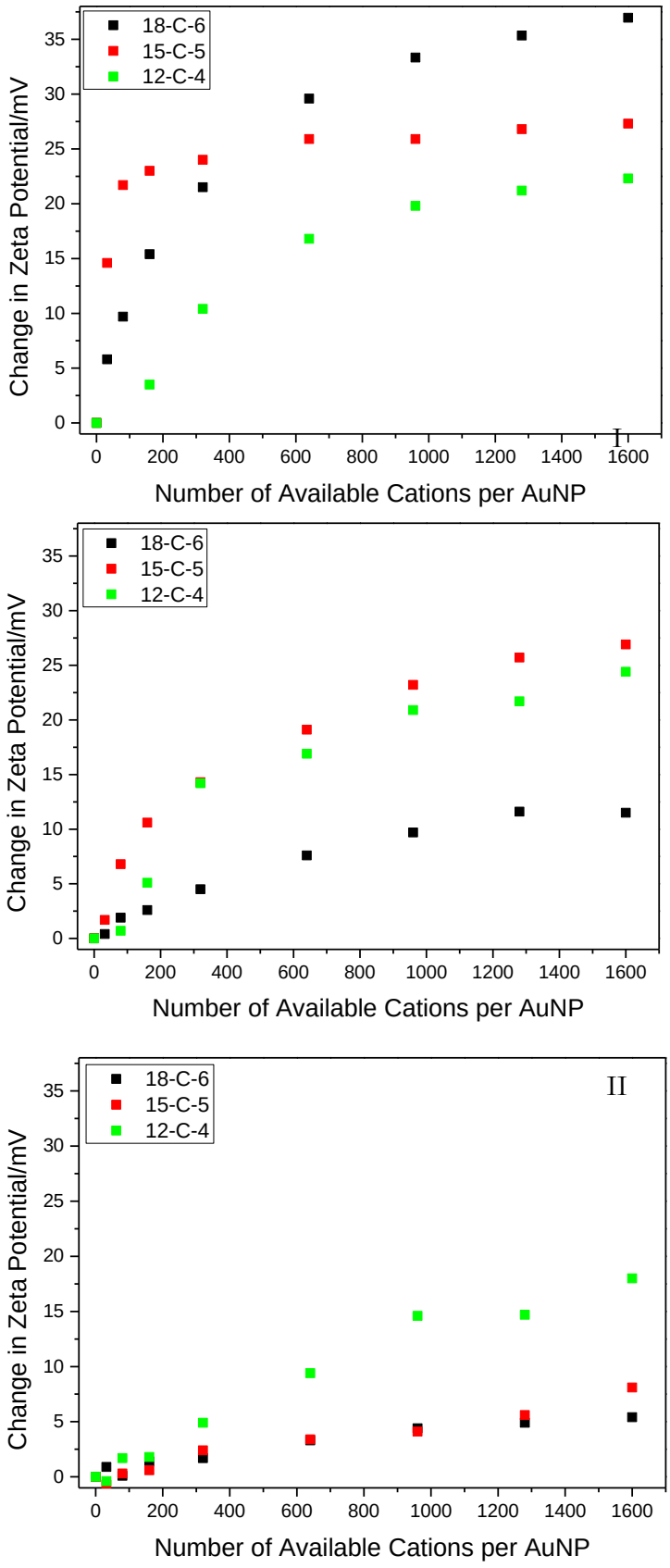

Figure 3.14: $\Delta\zeta$ for 18-C-6-CH_2-SH, 15-C-5-CH_2-SH and 12-C-4-CH_2-SH coated 3nm AuNPs when in the presence of increasing ratios of alkaline metals, a)KCl, b) NaCl and c)LiCl).

It becomes clear after analysing the current data for each crown ether in the presence of the cations of interest that the 18-Crown-6 AuNPs show the most promise for selective cation transport across a membrane, with K^+ association resulting in fast particle transfer, whilst Na^+ and Li^+ result in no particle transfer and very minor $\Delta\zeta$ (Figure 3.1), which indicates very little association. The 15-Crown-5 AuNPs, whilst showing very fast transfer in the presence of K^+, potentially due to crown ether sandwiching, also show transport with Na^+, making them undesirable for cation selective transport. The 12-Crown-4 AuNPs show no obvious preference for any singular cation, with no strong association observed at lower cation : AuNP ratios, resulting in very slow/no phase transfer, making them, like the 15-Crown-5, undesirable for cation selective transport.

In summary the 18-Crown-6-CH_2-SH 3 nm AuNPs developed and prepared in Chapter 2 of this thesis showed the highest potential to achieve selective cation transport across an artificial membrane.

3.2 Phase Transfer of Crown Ether Particles with $BaCl_2$

It has been previously stated that the high binding affinity of 18-Crown-6 for K^+ cations is due to the complementary nature between hole size and ionic radii. Similarly, the ionic radii of K^+ (1.37 Å) and Ba^{2+} (1.35 Å) has been shown to result in association of Ba^{2+} within the 18-Crown-6 cavity[14-16]. Due to the double charge present upon the barium cation it would be interesting to observe how this alters the phase transfer of each crown ether particle.

Phase Transfer: The phase transfer experiments shown within this section were prepared in a similar method as stated in section 3.1.1 with the following changes: 0.25 ml of each AuNP solution was taken and diluted with 0.75 ml fresh MQ water and 4 mM of $BaCl_2$

Zeta Potential: ζ measurements were collected as described in section 3.1.1 except for the addition of $BaCl_2$ to each crown ether solution.

Figure 3.15 shows the phase transfer as a function of time for 3 nm 18-Crown-6, 15-Crown-5 and 12-Crown-4 modified AuNPs when in the presence of 4 mM $BaCl_2$. It should be noted that the differences in colour of each solution is due to slight variations in the size of each nanoparticle and not an alteration in concentration, with the slight

variation in size arising from having to prepare each solution in small batches. The ratios of cation : AuNP are approximately the same for each solution.

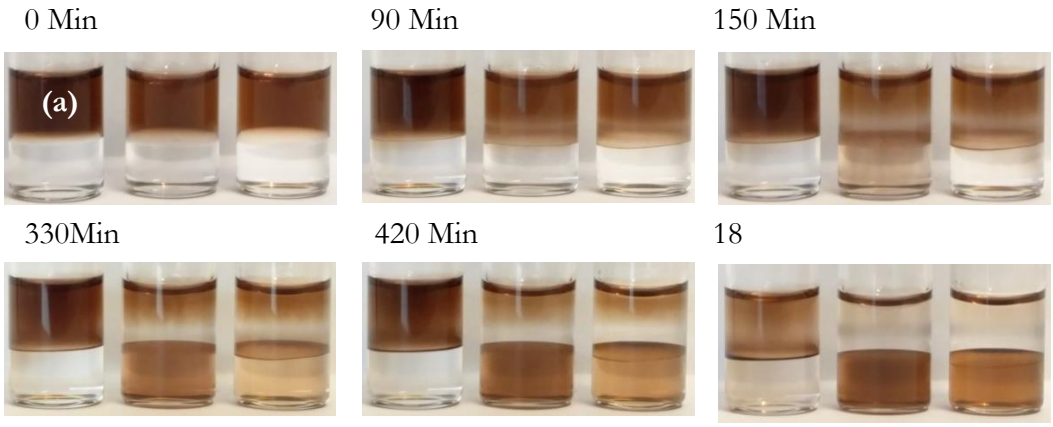

Figure 3.15: Images showing the phase transfer as a function of time for 3nm a) 18-Crown-6, b) 15-Crown-5 and c) 12-Crown-4 modified AuNPs when in the presence of 4mM $BaCl_2$

It is observed in Figure 3.15 that the 3 nm 15-Crown-5-modified AuNPs show the highest rate of transfer into the organic phase, showing almost complete transfer after 18 hours. The 3 nm 12-Crown-4-modified AuNPs also exhibit phase transfer but at a reduced rate, with a large majority of the particles appearing to sit upon the interface before undergoing phase transfer. The 3 nm 18-Crown-6-modified AuNPs only a very small rate of phase transfer, with the organic phase showing only a small population of particles after 18 hours.

The cause of the unexpected behaviour of the 3 nm 18-Crown-6-modified AuNPs showing reduced rates of transfer in the presence of a complementary cation with respect to the other crown ether AuNPs becomes apparent once ζ measurements were taken, Figure 3.16. The steep rise in ζ for the 3 nm 18-Crown-6-modified AuNPs with only small values of $BaCl_2$ indicates that Ba^{2+} is complexed in a similar fashion to that of K^+, with the initial sites becoming rapidly filled followed by a gradual saturation with increasing cation concentration. The Δζ is much more prominent in comparison to K^+ however, with 640 cations : AuNPs resulting in a change of 47.1 mV, with K^+ giving only a change of 29.6 mV. This can be attributed to the divalent nature of the Ba^{2+} cation, resulting in a higher population of positive charge present around the particle at similar cations : AuNPs ratios. The most important aspect of this change in the ζ is that at 640 cations : AuNPs the ζ is +14 mV, well above zero. Earlier in this chapter it was postulated that the rate of transfer from the aqueous to the organic phase was related to the charge of the

particle. The lower the charge present around each particle, the more pronounced the phase transfer will be. The positive charging of the particle with Barium resulting in very slow phase transfer strongly supports this theory.

As stated earlier both the 3 nm 15-Crown-5-modified and 12-Crown-4-modified AuNPs undergo phase transfer in the presence of 4 mM $BaCl_2$, with the 15-Crown-5-modified AuNPs showing a higher rate of transfer than the 12-Crown-4-modified AuNPs. Once again, the ζ provides insight into this behaviour. At 640 cations : AuNP the ζ for the 15-Crown-5-modified and 12-Crown-4-modified AuNPs are -7.07 and -17.4 mV respectively. The charge present upon the 3 nm 15-Crown-5-modified AuNP is closer to zero, hence resulting in the increased rate of transfer.

Of noticeable interest is the variance in the plateau levels for each crown ether-coated AuNP. The 3 nm 18-Crown-6-modified AuNPs show a saturation curve that has become typical of these particles when in the presence of complementary cations, with the plateau occurring at approximately +18 mV. The 15-Crown-5 AuNPs show a similar saturation curve but result in a plateau at approximately -3 mV, whilst the 12-Crown-4 AuNPs appear to become saturated very quickly, resulting in a sharp plateau at approximately -14 mV. Interestingly, the conductivity for both the 12-Crown-4 /15-Crown-5-modified gold nanoparticles behaves linearly, which is the expected outcome, but the 18-Crown-6-modified gold nanoparticle solution conductivity measurements has a reduced rate of increase during the addition of the first Ba^{2+} cations, Figure 3.17. This slower rate of conductivity correlates perfectly with the initial huge increase in the ζ seen in Figure 3.16. Indicating that due to the uptake of Ba^{2+} cations into the crown ether cavities the overall conductivity of the solution is reduced as those associated cations can no longer take part in passing charge through the solution. This serves as an added validation that the cations within these systems are indeed being snatched up by the crown ethers providing they are complimentary cations.

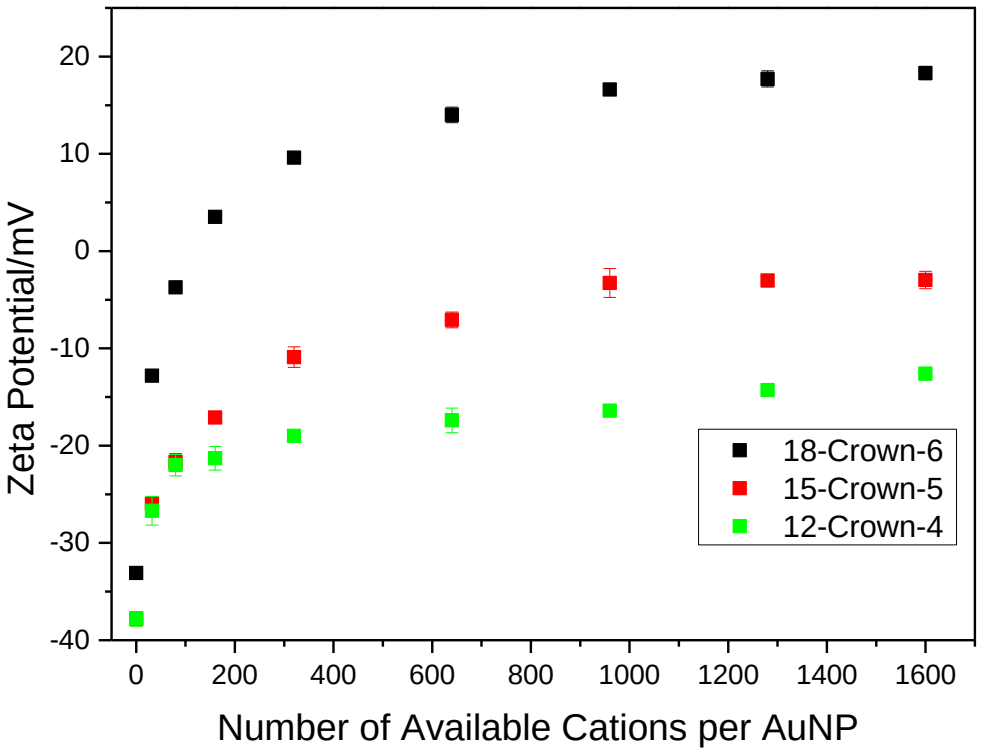

Figure 3.16: The $\Delta\zeta$ of crown ether-coated 3nm AuNPs when in the presence of increasing ratios of $BaCl_2$

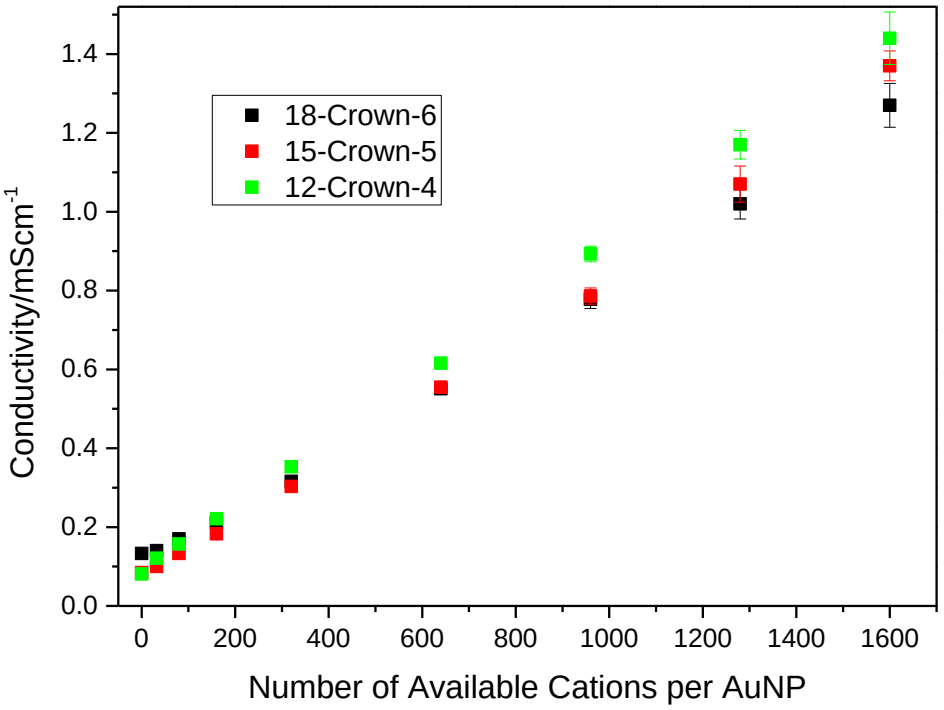

Figure 3.17: The change in conductivity of 3nm crown ether modified AuNPs when in the presence of increasing ratios of $BaCl_2$

3.3 Phase Transfer of Crown Ether Particle with Protons

With the crown ether modified AuNPs showing overall a successful phase transfer from the aqueous phase to the organic phase when presented with cations complimentary to the specific crown ethers, interest was given to the ability of the crown ether modified AuNPs to transport protons (H^+) as well, or at least observe a behaviour change upon interaction with increasing concentrations of H^+. The interaction between crown ethers and protons has been previously studied[17], with particular attention being paid to both 15-Crown-5 and 18-Crown-6[18] as well as modified crown ether complexes[19]. So, there is no reason for effects on the phase transfer properties of the crown ether-modified AuNPs to not occur when in the presence of H^+.

Phase Transfer: The phase transfer experiments shown within this section were prepared in a similar method as stated in section 3.1.1 with the following changes: 0.25 ml of each AuNP solution was taken and diluted with 0.75 ml fresh MQ water and 4 mM of HCl

Zeta Potential: ζ measurements were collected as described in section 3.1.1 except for the addition of HCl to each crown ether solution, up to 4 mM instead of 5 mM due to conductivity limitations within the Zetasizer.

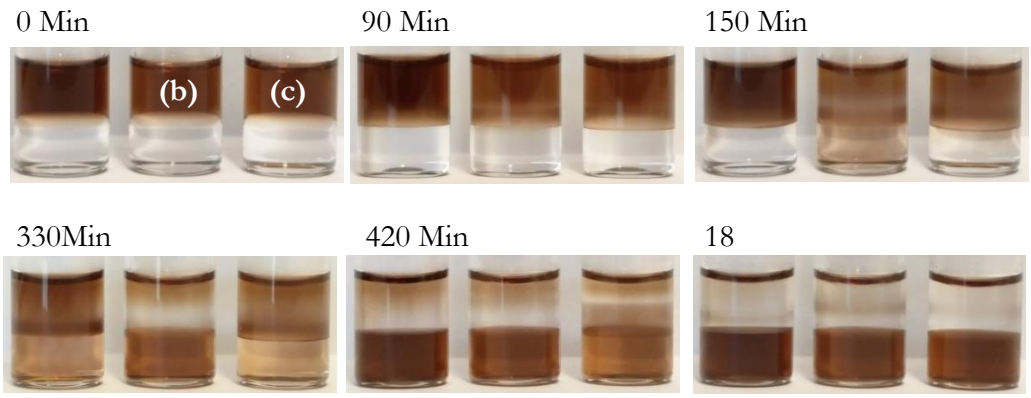

Figure 3.18: Images showing the phase transfer as a function of time for 3nm a) 18-Crown-6, b) 15-Crown-5 and c) 12-Crown-4 modified AuNPs when in the presence of 4mM HCl

Figure 3.18 shows how the presence of 4 mM HCl effects the phase transfer of each type of crown as a function of time. Only upon reaching 150 minutes a noticeable difference between the solutions, with the 15-Crown-5-modified AuNPS appearing to transfer into the chloroform first; the other two solutions do start to show signs of phase transfer after 330 minutes has passed, ending with all three types of crown ether AuNP readily transferring into the chloroform phase after 420 minutes. After 18 hours there is very

little evidence of the particles remaining within the aqueous phase, and all three solutions appear to have resulted in complete phase transfer to the chloroform. Interestingly the ζ result shown in Figure 3.19 deviate slightly from those previously seen with other various salts. Both the 15-Crown-5 and 12-Crown-4-modified AuNPS show prominent association curves, already readily observed previously when involving complimentary cations, while the 18-Crown-6-modified AuNPS show what can be best described as a hysteresis shape. The initial change in ζ is relatively small in comparison to the large changes 180 and 360 Cations : AuNP; with further increases in H^+ resulting in a gradual plateau.

With regards to previous phase transfer experiments this is the first set to show all three particles systems phase transfer within roughly the same time frame. It is also the first time that two of the crown ether species (12-Crown-4 and 15-Crown-5) have shown similar affinities to interact with a positive ion in solution. As to why the 18-Crown-6-modified AuNPS do not show a similar trend in ζ is not entirely known. It is possible that the size of a proton is just too small to effectively associate within the 18-Crown-6 cavity, meaning both 15-Crown-5 and 12-Crown-4 can coordinate more effectively. It is quite possible that the hysteresis curve observed for the 18-Crown-6-modified AuNPS is not even related to association between the crown ether cavity and the proton, but protonation of the crown ether moiety itself. The particles are present in an increasingly acidic solution meaning that protonation is more than likely to occur. This change may not be observed for both the 15-Crown-5 and 12-Crown-4-modified AuNPS because they are technically already "protonated" when interacting with protons within their cavity, or quite possible the protonation is simply masked by the change in ζ due to association.

The most interesting aspect of this experiment is the conductivity measurements shown in Figure 3.20. The conductivity for both the 15-Crown-5 and 12-Crown-4-modified AuNPs is upward curving rather than linear, like that seen for the 18-Crown-6-modified AuNPS. A similar effect was observed, although not to such a noticeable extent, between the 18-Crown-6-modified AuNPS and $BaCl_2$, which is known to associate well with 18-Crown-6. The only explanation for a non-linear increase in conductivity is that a portion of the conducting ions are becoming incapable of transferring charge, a case that would be quite likely if the ions were trapped within the cavity of a crown ether, effectively masking their presence. The fact that both 15-Crown-5 and 12-Crown-4-modified

AuNPS show a non-linear conductivity increase and sharp increase in the ζ heavily indicates that the particles are indeed associating with the protons and then proceeding to phase transfer.

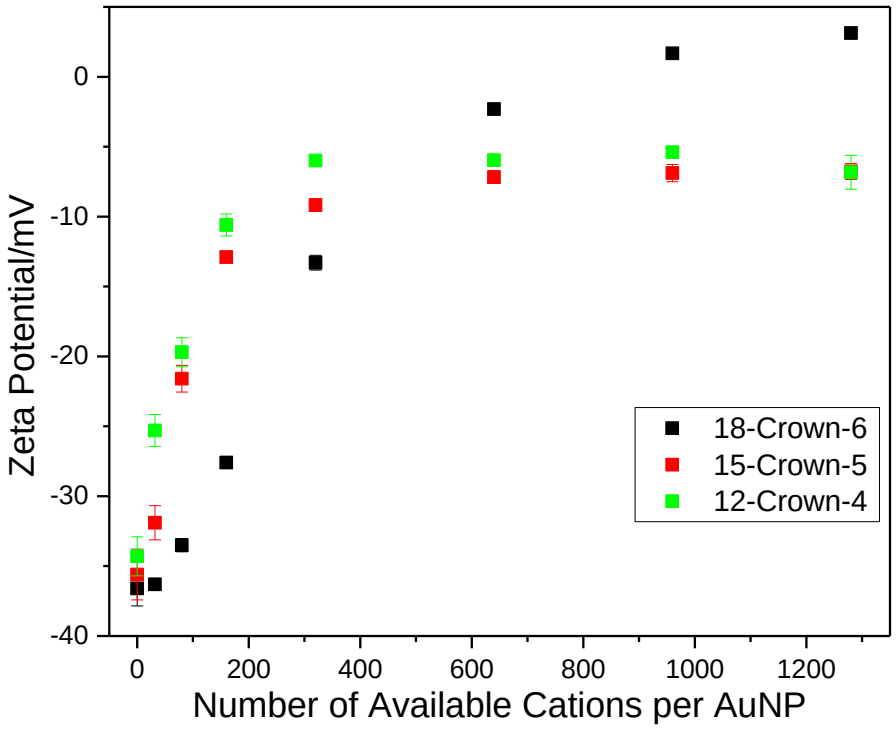

Figure 3.19: *The ⊿ζ of crown ether-coated 3nm AuNPs when in the presence of increasing ratios of H^+*

The results of this experiment were slightly surprising, literature showed that both 18-Crown-6 and 15-Crown-5 had affinities for binding protons; with no literature showing a similar relationship for 12-Crown-4 it was assumed that there was relatively little interaction between the two. These results show that both 15-Crown-5 and 12-Crown-4, when attached to AuNPS, associate strongly with protons and the 18-Crown-6-modified AuNPS show very little interaction, however it cannot be ignored that the situations and environments that these associations are taking place in are vastly different and so alterations in the binding affinities are not entirely surprising.

Due to this line of work not being within the scope of this thesis no further work involving protons association will be discussed. However, the nanoparticles systems are being incorporated in more advanced electrochemical systems involving planar membranes, as mentioned and discussed in chapter 5, are being undertaken by Steven Danks within the Brust research group to develop a better understanding of the system.

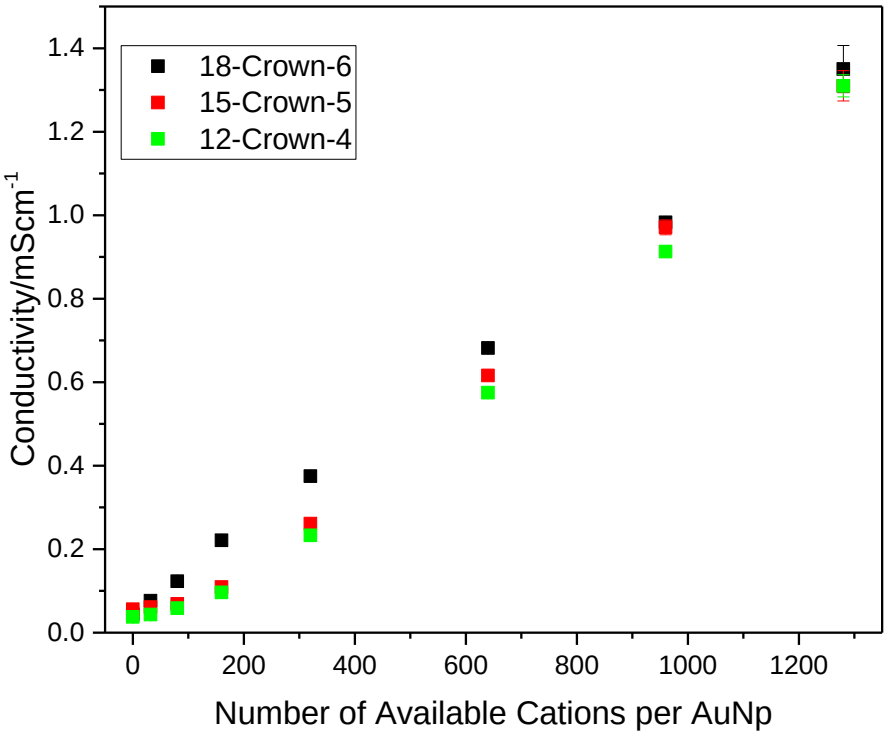

Figure 3.20: The change in conductivity of 3nm crown ether modified AuNPs when in the presence of increasing ratios of HCl

3.4 Phase Transfer of 18-Crown-6 AuNPs with Higher Concentrations of KCl

In Section 3.1 it was determined that the most appropriate crown ether coated AuNP for attempting cation transfer was the 18-Crown-6 AuNP due to its high degree of selectivity for K^+ over Na^+ and Li^+ and relatively fast transfer into the organic phase. Within this chapter it has been shown that the rate of transfer of these particles is strongly related to the charge present upon the particle, monitored in this chapter by ζ, with a faster rate of transfer occurring as the charge tends towards zero. It was noted that this Δζ started to reach a plateau at higher concentrations of KCl (Figure 3.2), postulated to be the saturation of the 18-Crown-6 cavities upon the AuNP surface.

This section describes the experiment set used to develop a better understanding of how the particles behave at even higher concentrations of KCl, to determine whether they still retained their phase transition properties.

3.4.1 Thermodynamic Phase Transfer of 18-Crown-6 AuNPs with KCl

The thermodynamics of phase transfer for the 18-Crown-6 AuNPs was quantitatively determined by the following procedure: An aqueous dispersion of 18-Crown-6 AuNPs (1.52×10^{16} NP/mL, 1.75 ml) was diluted with fresh MQ water (5.25 ml) to achieve a final volume of 7 ml (3.8×10^{15} NP/mL), the solution was separated into 7x1 ml aliquots to which 0, 5, 10, 50, 100, 200 and 400 mM of KCl were added respectively, the solutions were then vortexed for 30 seconds and left for a further 5 minutes to reach equilibrium. Each solution was then placed upon chloroform (1 mL) within a glass vial (4 mL). Upon addition each solution was shaken vigorously for 15 seconds. Upon achieving phase separation, the two phases were separated in order to prevent further particle transfer. Each solution was then analysed with UV-Vis spectroscopy in order to determine the concentration of particles present within solution.

Figure 3.21a shows the equilibrium partitioning of the 18-Crown-6 AuNPs between water and chloroform at different potassium chloride concentrations in the aqueous phase, after intense mixing and subsequent phase separations. This is also shown in terms of UV-Vis absorbance at 400 nm, Figure 3.21b. With increasing salt concentration, the particles initially become more hydrophobic, reaching maximal hydrophobicity at around 50 mM salt concentration. At further increasing salt concentrations this trend is reversed so that the highest salt concentration used (400 mM) results in a large majority of the particles remaining within the aqueous phase, comparable to the situation without salt present. Thus, the empirical optimum of salt concentration for creating hydrophobic particles is at around 50 mM. Note that the change in hydrophobicity is initially very steep (0-5 mM), indicating a dramatic change in the hydrophobicity of the particles. From ζ measurements shown in Figure 3.2, it can be seen that within this salt concentration region the charge upon the particle changes quite rapidly due to cation complexation, tending towards zero. From 5-10 mM KCl the hydrophobicity change appears to be minimal; this is not entirely unexpected as from Figure 3.2 it is apparent that the ζ is reaching a saturation plateau and so any change in hydrophobicity as a result of the particle charge at these salt concentrations will be relatively small. For the nanoparticles used within these experiments a ligand shell coating of anything larger than 300 ligands per AuNP is unlikely, meaning that full saturation with potassium ions is expected at these relatively low concentrations of KCl and is highly suggested by the ζ results shown previously.

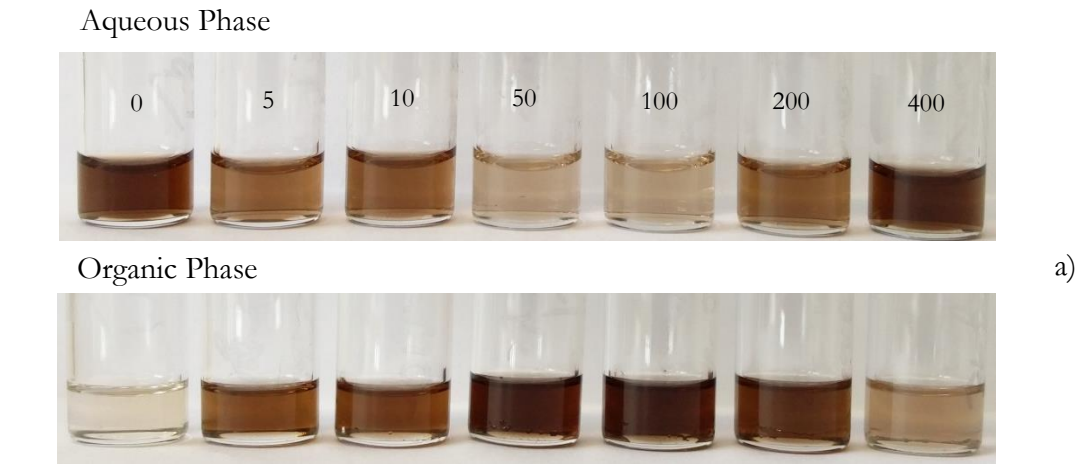

a)

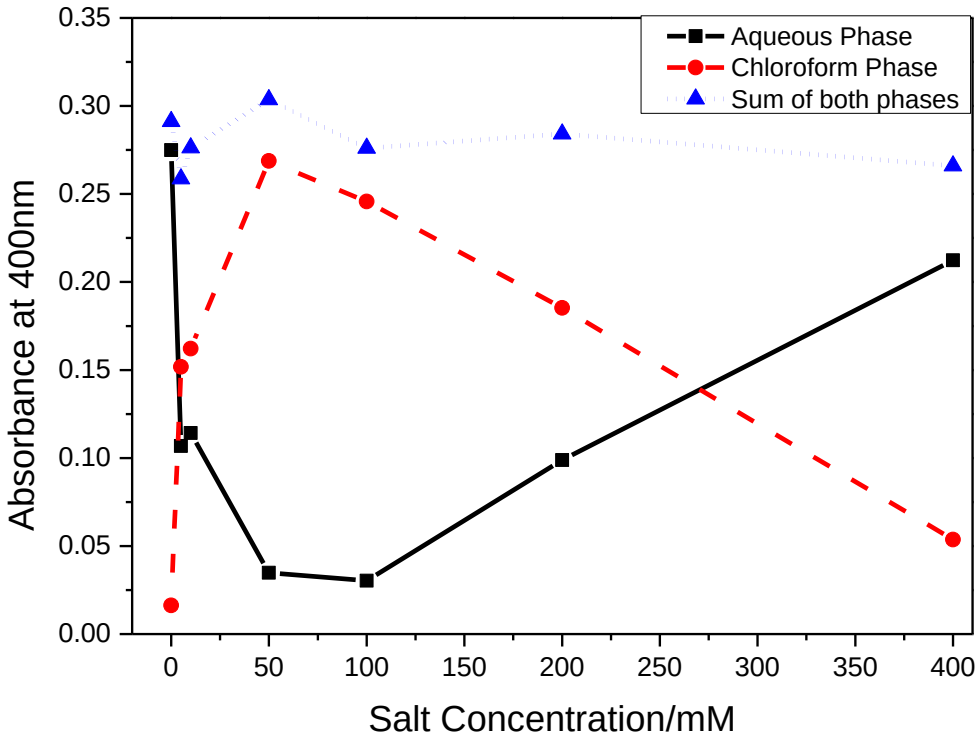

b)

Figure 3.21: a) Equilibrium partitioning of the 18-Crown-6-modified AuNPs with increasing KCl concentrations, b) Partitioning of the aqueous-organic phases stated in UV-Vis absorbance at 400nm.

Above 10 mM KCl concentration the appearance of the graph appears to be quite independent of particle concentration, suggesting an important contribution from other effects that are independent of particle concentration. As stated previously the optimal hydrophobicity of the particle is observed at around 50 mM KCl; at these salt concentrations it is possible that the salting-out effect is being observed, whereby the increased ionic strength of the solution results in the disposition of solutes present within

the aqueous media. The most curious observation here, however, is that as the salt concentration is increased further (100-400 mM) the hydrophobicity of the particles is reduced, with the quantity of particles present in the chloroform phase decreasing in a linear fashion, an opposite trend to that observed previously. This reversal in hydrophobicity could be attributed to the build-up of a large electrochemical double layer around the particles as a result of the aqueous phase becoming saturated with KCl. As the electrochemical double layer grows with increasing salt concentrations the particle becomes "masked", meaning that the properties of the particles are no longer evident, just the properties of the salt ions themselves. This build up in the electrochemical double layer will inherently result in a more highly charged system, giving rise to this reduction in phase transfer.

So within this experiment we observe three effects taking place: 1) The increase in hydrophobicity of the system due to the complexation of a complementary cation (0-10 mM), 2) The increase in hydrophobicity of the system due to the increased ionic strength of the aqueous phase giving rise to "salting out" (50-100 mM) and 3) The decrease in hydrophobicity as the aqueous phase becomes saturated with KCl, resulting in the build-up of an electrochemical double layer around the particles, blocking their path to the chloroform interface.

3.4.2 Kinetic Phase Transfer of 18-Crown-6 AuNPs with KCl

The kinetics of phase transfer for the 18-Crown-6 AuNPs was qualitatively found by following the procedure as described in 3.3.1 but rather than shaking each vial, they were left to allow phase transfer at the interface to occur naturally, Figure 3.22.

It is important to note that whilst the images shown in Figure 3.22 give rise to some interesting observations, which shall be discussed later in this section, the rate of transfer for the 18-Crown-6 AuNPs vs salt concentration was not accurately determined within this thesis, as calculating the multiple factors that can potentially affect this rate of transfer was not within the scope of this project.

Overall the kinetics of phase transfer follow the same trend as the thermodynamic experiment shown in section 3.3.1; increasing KCl concentrations initially resulting in an increased presence of particles in the chloroform, followed by a decreasing presence of particles in the chloroform at even higher KCl concentrations, with the similarities being

most notable in the 6 and 18-hour images in Figure 3.22. However, within the earlier stages of kinetic transfer (far from equilibrium) there are some noticeable differences between the rates of particle phase transfer.

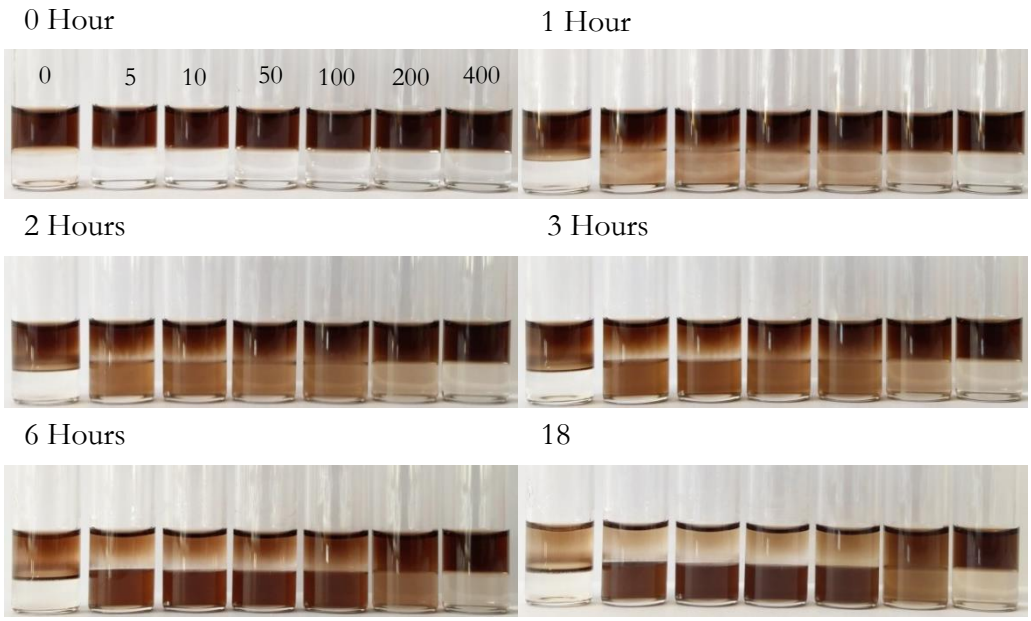

Figure 3.22: Kinetic Phase Transfer of 18-Crown-6 AuNPs with: 0, 5, 10, 50, 100, 200 and 400mM of KCl.

The change in the size of the depletion layer with changes in the KCl concentration is most notable, with 5 mM KCl giving rise to the largest depletion layer which then gradually decreases with increasing salt concentration, resulting in no depletion layer at 200 mM KCl concentration. The exact explanation for this effect is not entirely understood. It is postulated that the gradual reduction within the depletion layer with increasing salt concentration is due to the build-up of the electrochemical double layer surrounding the particles, with the increasing size of the double layer masking the particles environment (including the organic phase boundary), reducing the rate at which the particles can associate with phase boundary, resulting in the rate of depletion reducing, and the rate of diffusion within the aqueous phase staying the same. As to why the salt concentration that shows the most transfer thermodynamically (Figure 3.21 50-100 mM) is not matched kinetically (Figure 3.22 5-10 mM) has not been studied in detail. It does however enforce that there are multiple factors at work when these particles begin phase transferring.

3.5 Transfer of 18-Crown-6 AuNPs into Solvents with Varying Polarity

With the optimum KCl concentration for achieving the highest percentage of transfer being found to be 50 mM, the next step was to determine whether the particles could be effectively transferred into less polar solvents. The reasoning behind this is that less polar solvents such as hexane and toluene are more appropriate for attempting to mimic the conditions within the membrane.

An aqueous dispersion of 18-Crown-6 AuNPs (1.52 $x10^{16}$ NP/mL, 1.25 ml) was diluted with fresh MQ water (3.75 mL) to achieve a final volume of 5 ml (3.8$x10^{15}$ NP/mL), the solution was separated into 5x1 ml aliquots to which 50 mM of KCl was added, and then the solutions were vortexed for 30 seconds and left for a further 5 minutes to reach equilibrium. The solution was placed upon 1mL of organic solvent (Chloroform, Dichloroethane, Diethyl Ether, Toluene and Hexane) with polarity indexes of 4.1, 3.5, 2.8, 2.4 and 0 respectively. The solutions were then shaken vigorously for 30 seconds, followed by each phase being analysed via UV-Vis for the determination of the presence of particles. Images were taken just before mixing, just after mixing and 1 day after mixing, as shown in Figure 3.23, with the percentage transfer into each solvent shown in Table 3.1.

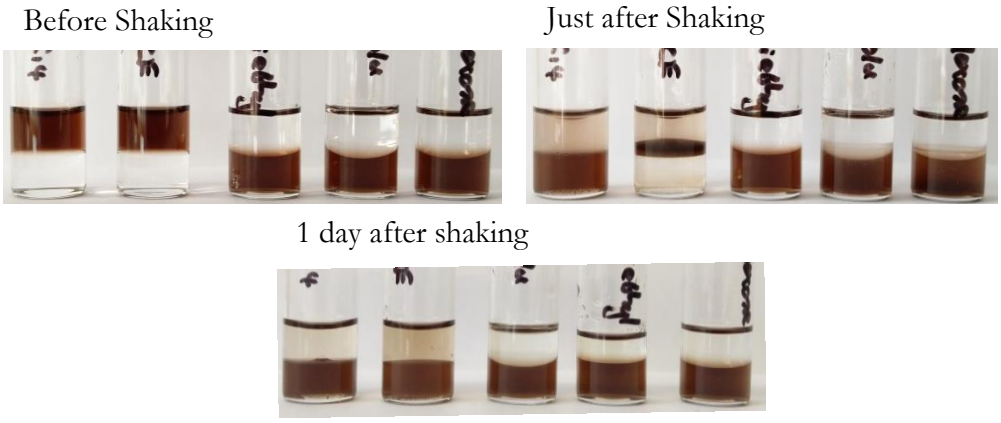

Figure 3.23: Images of 18-Crown-6 AuNPs with a KCl concentration of 50mM attempting transfer into: Chloroform, Di-chloroethane, Di-Ethyl Ether, Toluene and Hexane.

Solvent	Chloroform	Dichloroethane	Diethyl Ether	Toluene	Hexane
Transfer (%)	96	76	0	0	0

Table 3.1: Percentage transfers of 18-Crown-6 AuNPs with a KCl concentration of 50mM into a range of solvents after 1 day.

The transfer into chloroform was highly successful, giving 96% of particles transferred; this was to be expected from previous experiments. In the case of dichloroethane the particles initially associated with only the interface (Figure 3.23), but over the course of a day gradually dispersed into the organic phase, giving a particle transfer of 76%. Diethyl ether, toluene and hexane all showed no presence of particles within the solvent at 0% transfer.

It is evident from the above phase transfer results that even when presented with 50 mM KCl, the concentration of complementary salt that result in the highest hydrophobicity, the 18-Crown-6 AuNPs are incapable of transferring to less polar solvents.

3.5.1 Temperature Dependent Reverse Phase Transfer

Whilst the lack of phase transfer into less polar solvents proved unsuccessful with pure crown ether-modified gold nanoparticles, an interesting property was observed within the dichloroethane system. It can already be seen in Figure 3.23 that the particles adhered strongly to the interface between water and dichloroethane followed by a gradual movement into the organic phase over time. Upon cooling to 2°C the system then behaved unexpectedly, as shown in Figure 3.24.

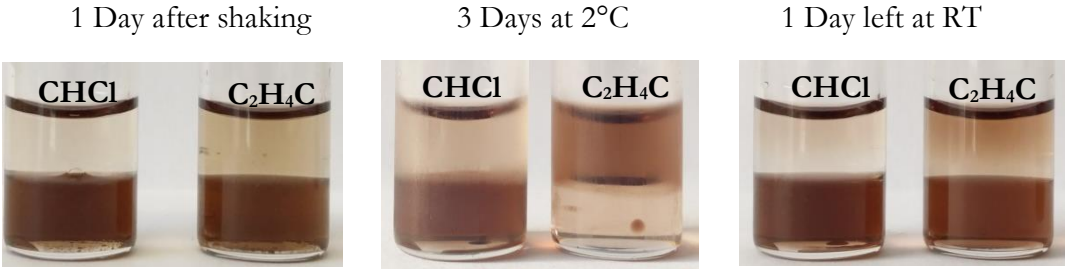

Figure 3.24: Images showing the reversible phase transfer of the 3nm 18-Crown-6-modified gold nanoparticles, when cooled down to 2ºC and left to thaw to room temperature (RT), when in Dichloroethane, Phase transfer is shown to be irreversible in chloroform. Note, the organic phase is at the bottom.

Figure 3.24 compares two solutions of crown ether-modified gold nanoparticles in the presence of 50 mM KCl after being left to settle for 1 day in both chloroform ($CHCl_3$,

left) and dichloroethane ($C_2H_4Cl_2$, right). When cooled down to 2°C the chloroform system shows no signs of the particles returning to the interface/moving back into the aqueous phase. However, within the dichloroethane system we see a very obvious change in the behaviour of the particles; rather than stay in the organic phase they move towards the interface, which can be seen in middle image as a dark inner disk upon the interface; not only do they move back to the interface but start to redistribute back into the aqueous phase. When the solution was left to heat back up to room temperature the particles gradually transferred back into the organic phase, with both the colouration of the aqueous phase and the concentration of particle at the interface depleting and eventually disappearing. This trend of decreasing temperature resulting in increasing hydrophilicity is not only observed here but is also seen to be a unique property of the larger 7.5nm crown ether-modified gold nanoparticles. This is discussed in Chapter 4 of this thesis, whereby the larger particles agglomerate in the aqueous phase at higher temperatures followed by stable re-dispersion at lower temperatures.

The process behind this unique property will be described in detail in Chapter 4 when discussing the 7.5 nm crown ether-modified AuNPs. However, a short explanation shall be replicated here for clarity.

At higher temperatures the entropy gain by removing the hydrophobic particles from the aqueous phase over compensates the positive ΔH associated with transferring the particles from one phase to another, resulting in the phase transfer at room temperature, as seen in Figure 3.24. When the temperature is lowered the absolute value of the '$T\Delta S$' term for transfer to the organic phase is smaller than that of ΔH, resulting in the equilibrium shifting towards the other side (the aqueous phase).

Further research involving this interesting property was not achieved and shall be discussed in future work.

3.6 Potassium Transport Through Vesicle Membranes.

The following work was achieved with the help of Marcin Grzelczak, helping to both use and understand the methodology behind obtaining the fluorometric data, without his input this experiment set would not have been possible. With the 18-Crown-6 modified

3nm gold nano particles showing the highest potential for carrying cations selectively across an aqueous organic-interface (in this case potassium cations into chloroform) it became possible to develop further experiments involving vesicles, where the modified nanoparticles could be capable of acting as a new type of artificial ionophore, resulting in the polarisation of the phospholipid bilayer membrane. In order to achieve this the potassium concentrations inside and outside the vesicles need to be adjusted so that in the presence of an ionophore specific for potassium a membrane potential, $\Delta\psi$, can be established according to the Nernst-Donnan equation.

$$\Delta\psi = \frac{RT}{ZF}\, ln\, \frac{[K^+]_{out}}{[K^+]_{in}}$$

In order to monitor the change in membrane potential via the transport of potassium cations Safranin O was decided upon. Safranin O is a potential-sensitive, lipophilic cationic fluorescent dye which is suitable for spectroscopic detection of membrane potentials in both cellular and vesicular membrane systems, and is extensively used in multiple biological applications such as mitochondrial membrane potentials[20-23] and membrane potentials across other cell membrane preparations[24, 25]. Due to the almost linear association between its absorbance changes and the membrane potential it was deemed a suitable candidate for the testing of the modified crown ether gold nanoparticles. The molecular structure of Safranin O is shown in Figure 3.25a.

So that the dye could be effectively used within these experiments control tests had to be implemented to directly observe this proposed linear relationship between the fluorescent intensity and the membrane potential. To effectively calibrate the system a well-known potassium ionophore must be used, in this case, Valinomycin. Valinomycin is a naturally occurring dodecadepsipeptide used in the transport of potassium. The structure is made of twelve alternating amino acids and esters to form a macrocyclic molecule, with the twelve carbonyl groups being essential for metal ion binding, as shown in Figure 3.25b. The general shape and properties of Valinomycin are relatable to the shape and properties of the crown ether moieties used within this thesis, strongly suggesting that these particles coated in the crown ether could potentially allow for the transfer of cations across a membrane.

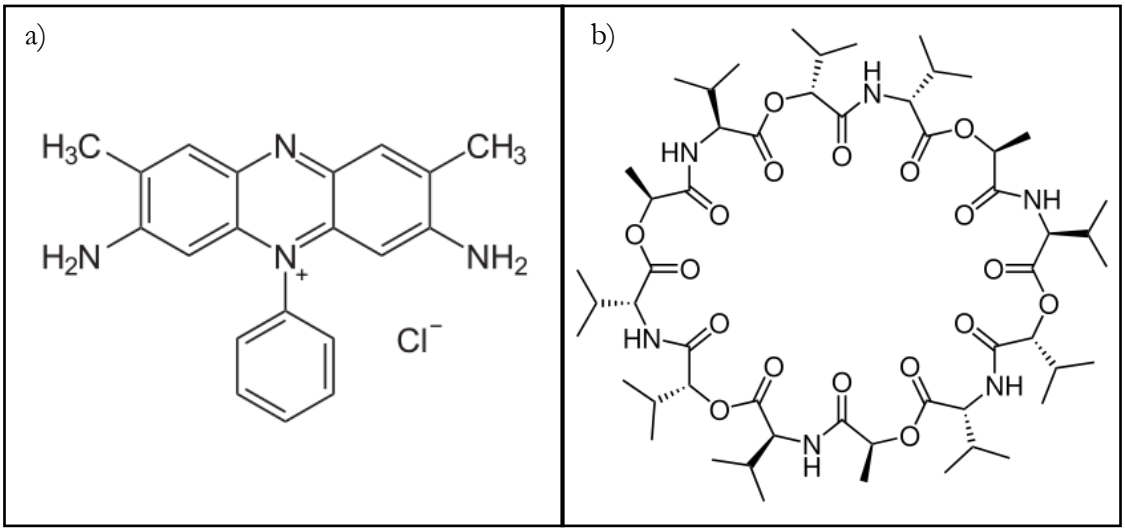

Figure 3.25: a) Molecular structure of the fluorescent dye Safranin O, b) Molecular structure of the potassium ionophore Valinomycin.

3.6.1 Fluorescent Calibration Tests with Safranin O and Valinomycin

The data presented in this section was obtained using the following procedure: Vesicles were prepared by a modified variant of the method described by Newcomb[26] *et al.* Briefly, a 10 mM stock solution of phospholipids was made by the dilution of liposome kit lyophilized powder (cholesterol 9 mmol, L-a-phosphatidylcholine (egg yolk) 63 mmol, stearlyamine 18 mmol) in chloroform. 1 mL aliquots of the stock solution were rotary evaporated for 2 hours to remove all residues of organic solvent and a solution of KCl and NaCl was used to hydrate the phospholipids. The concentration of KCl and NaCl used varied depending on the desired membrane potential which can be calculated using the Nernst-Donnan equation. To make the now white suspension of phospholipids more homogenous the solution was heated to 60°C followed by 8-10 freeze-thaw cycles via the use of liquid nitrogen, with the solution being vortexed for 15 seconds after every thaw cycle. Next the hydrated and homogenous phospholipid solution was extruded 20 times through a mini-extruder (Avanti) with a 100 nm-pore-size polycarbonate filter (Whatman) to form vesicles of about 100 nm in diameter. The vesicle solution was then purified via dialysis using MWCO 12 000-14 000 dialysis tubing (Serva), with the external KCl solution concentration kept constant at 1 mM.

A suspension of vesicles with a final concentration of phospholipids of 1 mM was placed in a fluorometric cuvette followed by the addition of the potential probe dye Safranin O (180 nM final concentration). Then the fluorescence intensity was allowed to equilibrate

for 2 minutes. The kinetic mode was used to detect continuously the fluorescent intensity changes at 589 nm, with an excitation wavelength of 521 nm. Finally, 20 nM of Valinomycin was added and the fluorescent intensity was monitored for 1700s.

The results of the change in fluorescence for Safranin O when Valinomycin is added at varying degrees of membrane potential are shown in Figure 3.26. Providing that the interior membrane charge is negative we observe a change in the fluorescence of Safranin O as Valinomycin is added, with the change in fluorescence increasing as the membrane potential is increased. When the fluorescent maximum is plotted against the membrane potential it can be seen that the relationship is indeed almost linear. It should be noted that the red data points marked in Figure 3.26b are estimated values for the change in fluorescence whilst the black data points are taken from experimental observation. With the calibration data confirming the reliability of using this system to attempt potassium transfer with the modified crown ether gold nanoparticles the next set of experiments were undertaken.

The requirement of the interior membrane to have a negative a charge is generally assumed to be due to the fact that the positively charged dye is driven into the membrane from outside the vesicle by the electric field across the membrane which then allows for quantification of the membrane potential

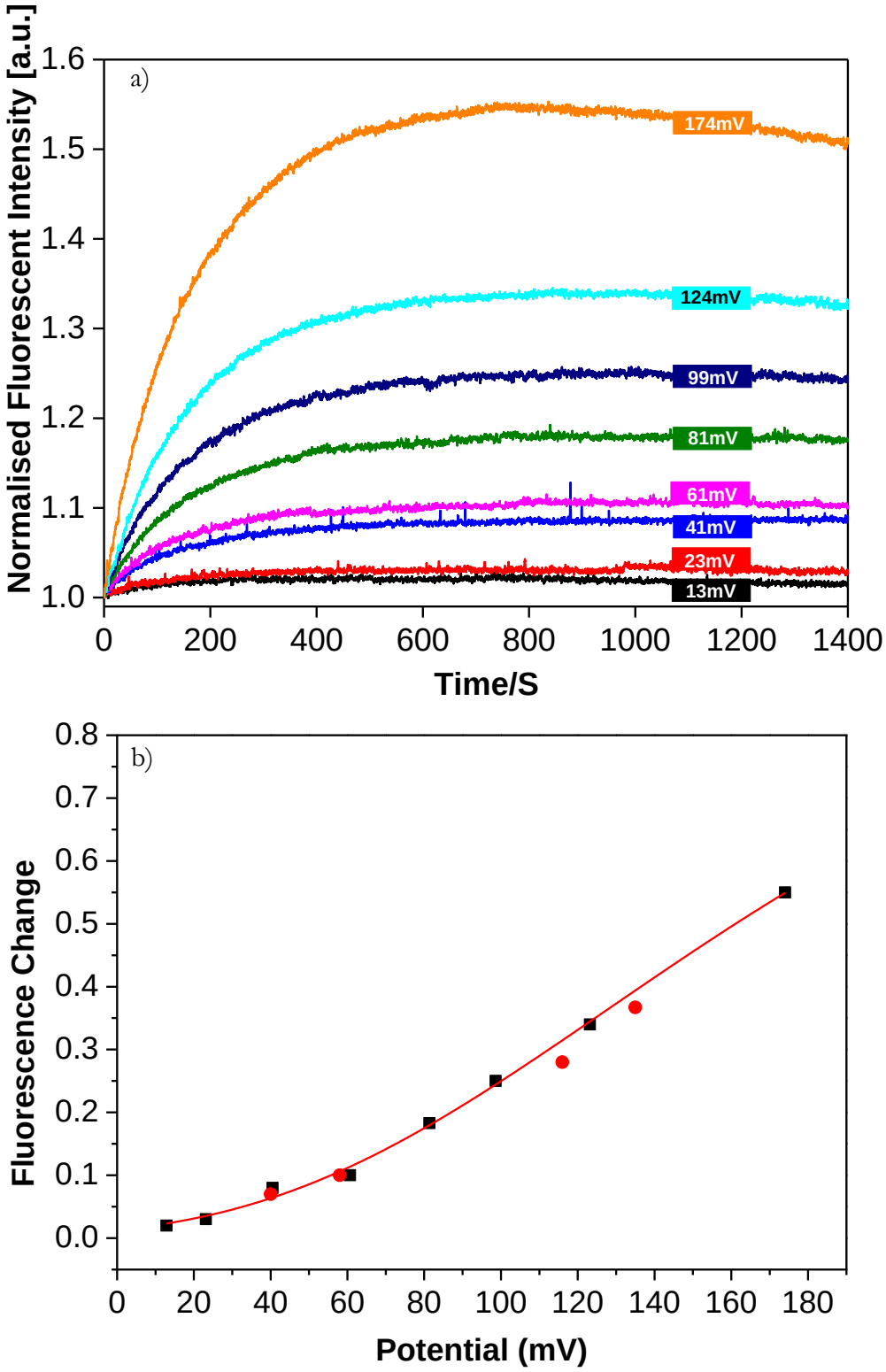

Figure 3.26: a) Fluorescent measurements showing how the fluorescence changes with increasing membrane potential. b) Fluorescent change maxima plotted against membrane potential.

3.6.2 Fluorescent Analysis of Crown Ether Modified 3nm Gold Nanoparticles

The data was collected via application of the experimental process described in section 3.4.1 with modification as follows: The concentrations of KCl and NaCl inside the vesicle were set to 100 mM and 1 mM respectively, whilst the concentrations of KCl and NaCl outside the vesicle were set to 1 mM and 100 mM respectively. The stated experimental set up was then used to monitor the fluorescent changes for three concentrations of crown ether-modified 3 nm AuNPs at 5, 10 and 20 nM.

Figure 3.27a is a model describing the experiment and how it should proceed. Should a suitable ionophore for potassium present itself to the system then the high concentration of potassium inside the vesicle will be allowed to diffuse out, resulting in a membrane potential with a negative charge localised on the interior membrane wall, causing an increase in the fluorescence of Safranin O. The experimental results are shown in Figure 3.27b. As observed in the calibration experiment described in 3.4.1 the addition of 20nM of Valinomycin results in an increase in fluorescence, shown by the black spectra, with the fluorescence increasing gradually until the end of the experiment. This outcome was to be expected due to the reliability of Valinomycin as a potassium ionophore and also ensured that the experiment was working as desired, allowing for testing with the crown ether modified particles. When the system is presented with varying concentrations of crown ether modified gold nanoparticles it becomes apparent that the particles are capable of successfully transporting potassium cations across the phospholipid membrane with the rate of change in fluorescence being dependent upon the concentration of particles within the system; 5 nM is slower, 10 nM shows a similar initial rate and 20nM shows a higher initial rate.

Interestingly, the particles, whilst showing obvious signs of cation transport, do not behave exactly the same as Valinomycin. Instead of showing a gradual increase in fluorescence throughout the entire experimental duration they reach a plateau which is followed by a gradual decrease in the fluorescence intensity. This change can be attributed to the degree of selectivity both Valinomycin and 18-Crown-6 have for potassium and sodium. Valinomycin is known to have exquisite selectivity for potassium cations over sodium, with a binding constant nearly $1x10^5$ higher for potassium over sodium whilst 18-Crown-6 only has a binding constant of $1x10^3$ higher for potassium over sodium. Such a reduction in the degree of selectivity can more than likely result in the allowance for a

small majority of sodium ions to diffuse into the vesicle, lowering the membrane potential, resulting in the observed gradual loss of fluorescence.

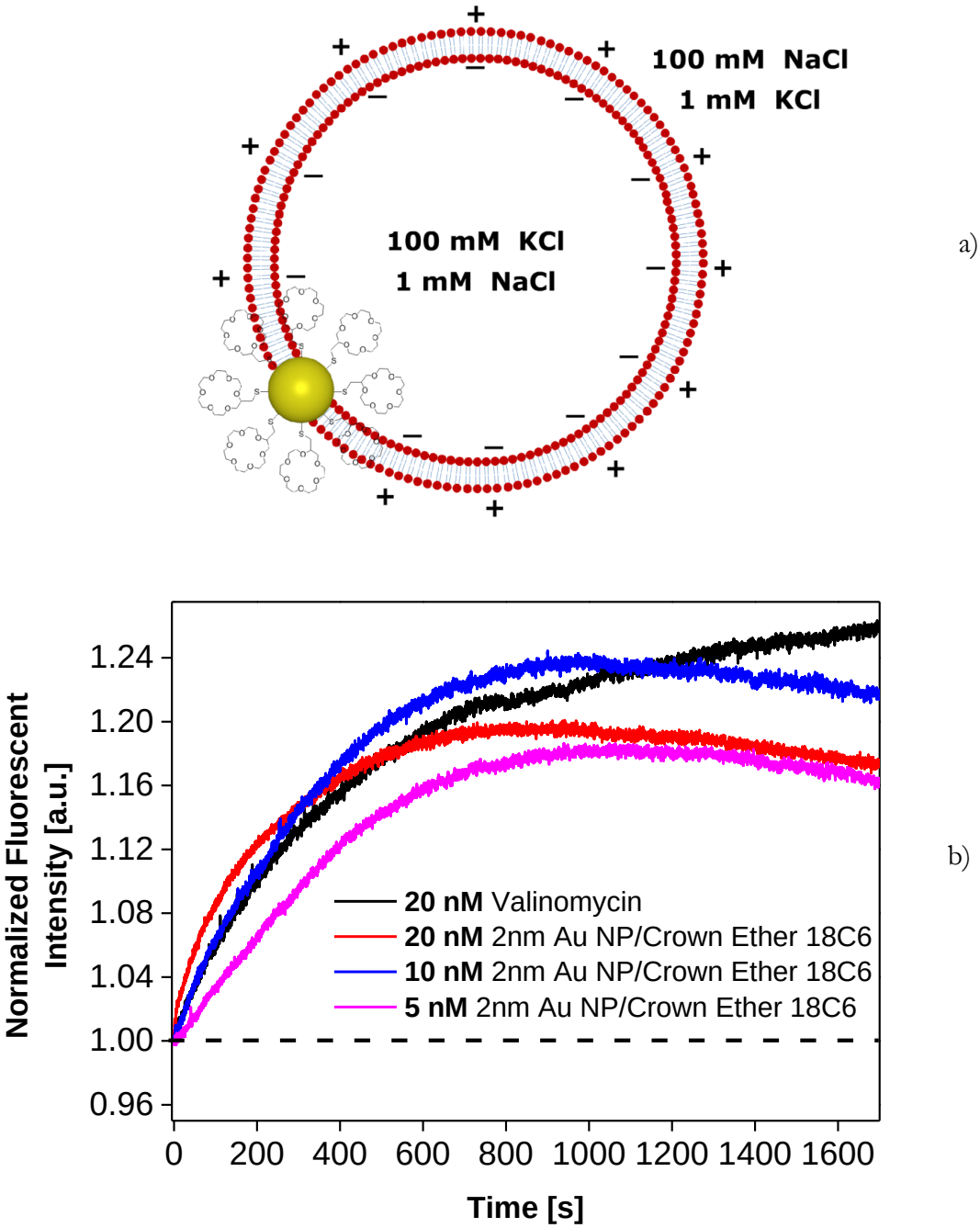

Figure 3.27: a) Model of the polarised phospholipid bilayer membrane with a crown ether modified gold nanoparticle acting as a potassium ionophore. b) Fluorescent spectra showing the change in fluorescence of Safranin O in the presence of either Valinomycin or Crown ether modified gold nanoparticles.

It should also be noted that the 20 nM experiment resulted in an unexpected lowering of the overall fluorescence increase, even though the initial change in fluorescence was higher than that seen for 10nM. Unfortunately, no reliable explanation for such a result

could be confirmed. However, there are a few postulations that can attempt to explain this odd behaviour. One is that an increased population of crown ether-modified gold nanoparticles initially present within the system would result in an overall increased rate of fluorescence due to an increased number of channels, which is clearly seen in Figure 2.37b within the initial stages of the experiment. Secondly, the reduced fluorescence peak could be attributed to an excessive number of particles presenting at the vesicular surface, hindering one another in their ability to transport potassium cations through the membrane; an example of such a hindrance would be when two particles are in contact with one another the crown ethers become preoccupied with associating to one another resulting in few crown ethers capable of acting as ionophore-channels for the potassium. Finally, it is also possible that an increased number of particles could be causing an excessive quenching of the dye, potentially resulting in a lower than expected fluorescence as the quenching of fluorescent dyes is not uncommon in the presence of nanoparticles[27-29]. These are all theories however and there is no solid baseline of data to adhere them too, further research needs to be conducted in order to fully understand potential artefacts/discrepancies within this system.

The previous experiment was repeated with the salt concentrations reversed[30]. A model and the results are shown in Figure 3.28. As stated previously, Safranin O requires that the internal membrane of the vesicle within these experiments becomes negatively charged upon presentation of the ionophore due to the need to pull the dye into the membrane in order to provide quantitative fluorescent data on changes in membrane potential.

In the case of Valinomycin, whereby the potassium selectivity is well known, we should observe no increase in the fluorescence, but in fact a decrease in intensity as the positive charge localised upon the inner membrane forces the Safranin O out of the membrane, preventing fluorescence. In the case of the crown ether-modified gold nanoparticles it was observed that the fluorescence gradually decreased after a certain period of time, indicating a potential to be not as selective as once hoped for potassium over sodium. Whilst this experiment would not provide any quantitative data due to the unreliability of Safranin O when the internal membrane of the vesicle is positive, it can provide quantitative data on whether or not the particles are highly selective for potassium over sodium by following a similar trend as shown by Valinomycin.

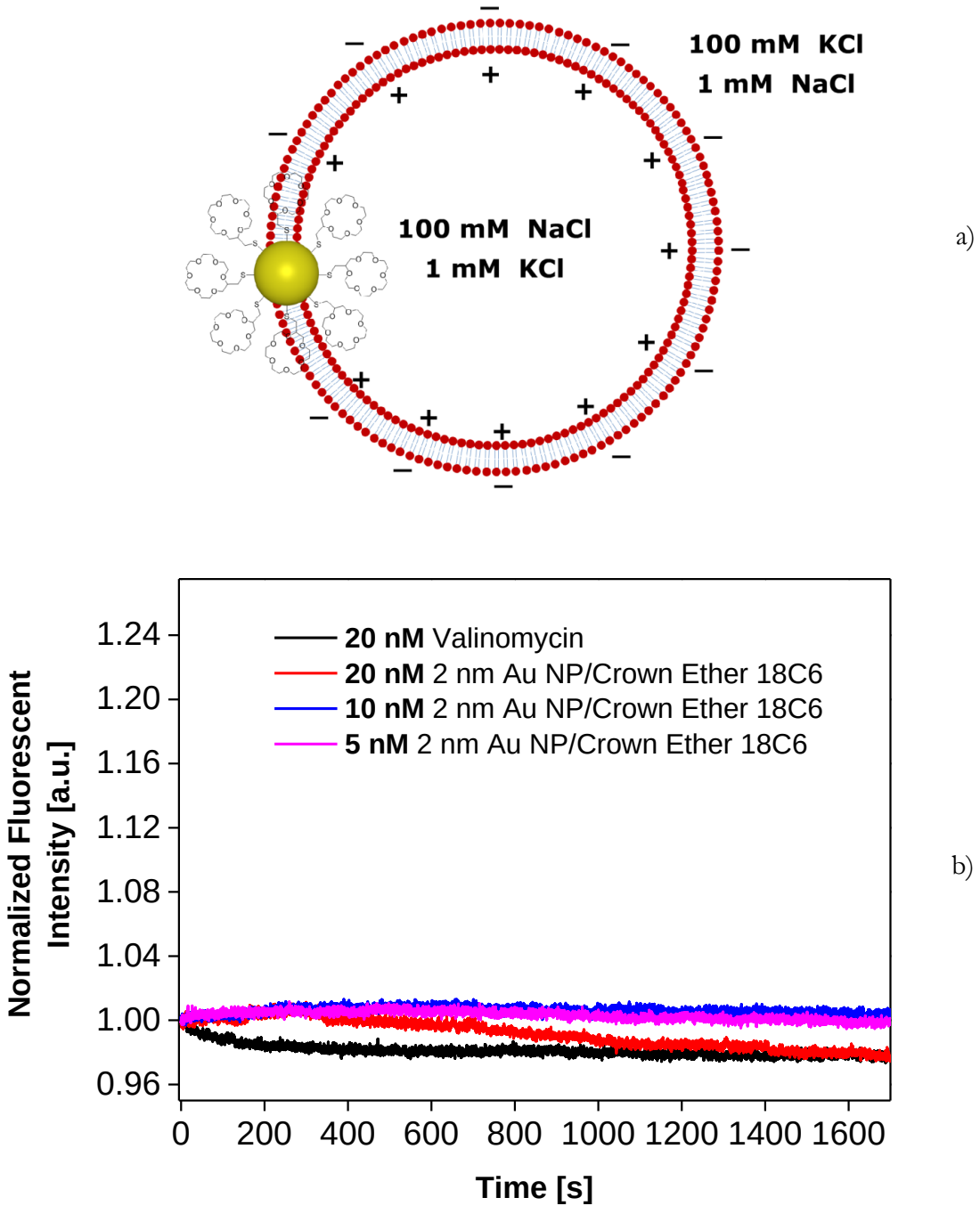

Figure 3.28: a) Model of the polarised phospholipid bilayer membrane with a crown ether modified gold nanoparticle acting as a potassium ionophore, with opposite salt concentrations to Figure 3.24, b) Fluorescent spectra showing the change in fluorescence of Safranin O in the presence of either Valinomycin or crown ether-modified gold nanoparticles.

In Figure 3.28b it is observed that upon the addition of Valinomycin the fluorescence of the system decreases gradually, indicating an opposite polarisation of the membrane as to that shown in Figure 3.27b, resulting in the rejection of the Safranin O from the membrane. The same effect occurs when the system is presented with 20 nM of the crown ether modified gold nanoparticles, again showing a decrease in the fluorescence intensity,

albeit over a longer period than that seen for Valinomycin. This is to be expected however, with Valinomycin having potassium selectivity 100 times greater than that of the 18-Crown-6, some deviations between the two were to be expected.

The outcome of this experiment set is the successful demonstration that these newly-made crown ether-modified nanoparticles are capable of not only selectively binding potassium, which fits nicely with the phase transfer experiments shown earlier in this chapter but are also capable of incorporating into a membrane and allowing for selective cation transfer across the membrane.

It is somewhat surprising that the particles appear to act as near perfect selective ionophores comparable to the standard compound Valinomycin. The mechanism of ion transfer has not yet been studied and still remains open to speculation. It's possible that the complexation of potassium is in relatively fast equilibrium with free potassium and that the transfer of potassium across the membrane is facilitated by a tumbling motion of the particles that randomly exposes crown ether moieties to either side of the membrane. An alternative and perhaps more appealing mechanism could be that the crowns self-organise on the surface of the particle in such a way that a continuous channel is formed, with a comparatively high level of ligand shell organisation as reported previously in work by Rotello[31] et al and Stellacci[32-34] *et al*, although the results of the Stellacci have later been disputed by others[35, 36]. Further experimentation will need to be done in order to better understand and develop a much more refined understanding of the method of transport within this system.

3.7 Phase Transfer with Larger Crown Ether-Modified Gold Nanoparticles

With the 3nm 18-Crown-6-modified gold nanoparticles showing positive results for the successful transport of a complimentary cation (K^+) and after deciding they were the most promising candidate, the next logical step for the project was to determine whether the transfer of electrons was also possible with these particles. Successfully accomplishing this to any high degree of transport is not trivial as there are a few factors that strongly hinder electron transport across AuNPs. The first is the size of the capping agent coating the gold core, which is typically particles that are capable of dispersing and remaining

stable within organic media coated with long organic chains. Additionally, the terminating group of these capping agents can be highly hydrophilic, giving rise to amphiphilic particles[37-40]. This does not remove the presence of the hydrophobic chain dwelling closer to the gold core and typically these chains struggle with effective conduction of electrons to the gold core[41-43]. This gives rise to a dilemma when attempting to transport electrons across a gold core situated within a membrane, as the low conductivity capping agents results in too large an energy barrier to overcome.

The second limiting factor for the transport of electrons through an artificial membrane via a AuNP is the size of the gold nanoparticle itself. Gold, being a highly metallic substance, is highly conductive[44] but upon reaching the nanoscale the ease by which electrons could flow through gold becomes restricted. This is clear in the case of small gold clusters[45-47], where the coulomb blockade effect arises. Essentially the particle in question has become so small that even single electrons residing upon the core create a strong enough coulombic repulsion to prevent further electrons from moving through the system. Coulomb blockading is the extreme example of this however, and typically only occurs on gold clusters smaller than 2 nm in diameter. This does not mean that anything larger than 2nm in diameter is exempt from restricted electron flow however; the 3 nm 18-Crown-6-modified gold nanoparticles discussed in this chapter would still exhibit restrictions upon electron flow as their capacitance is relatively low.

To overcome this restriction upon the flow of electrons, the size of the gold core needs to be increased, to raise the capacitance of each AuNP and lower the energy barrier for the transport of electrons across the gold core situated within an artificial membrane. The challenge that now presents itself is to develop a particle of a suitable size such that it was able to accommodate the flow of electrons through its core and accommodate the flow of cations through the capping agent, yet also be capable of integrating into a membrane to allow these transport processes to flow between previously confined environments.

Chapter 2 of this thesis describes and discusses both successful and failed attempts at developing larger 18-Crown-6-modified AuNPs. Within this section we shall discuss the first success for larger particles, the 15.7 and 25.5nm 18-Crown-6-modified AuNPS developed by the two-step functionalisation involving PEG 5000 as an intermediary step.

The 15.7 and 25.5 nm 18-Crown-6-modified AuNPs were subjected to the same phase transfer experiments as the 3 nm 18-Crown-6-modified gold nanoparticles to determine whether they can achieve phase transfer across an aqueous-organic interface and whether the rate of transfer was on par with their smaller counterparts, this is shown in Figure 3.29.

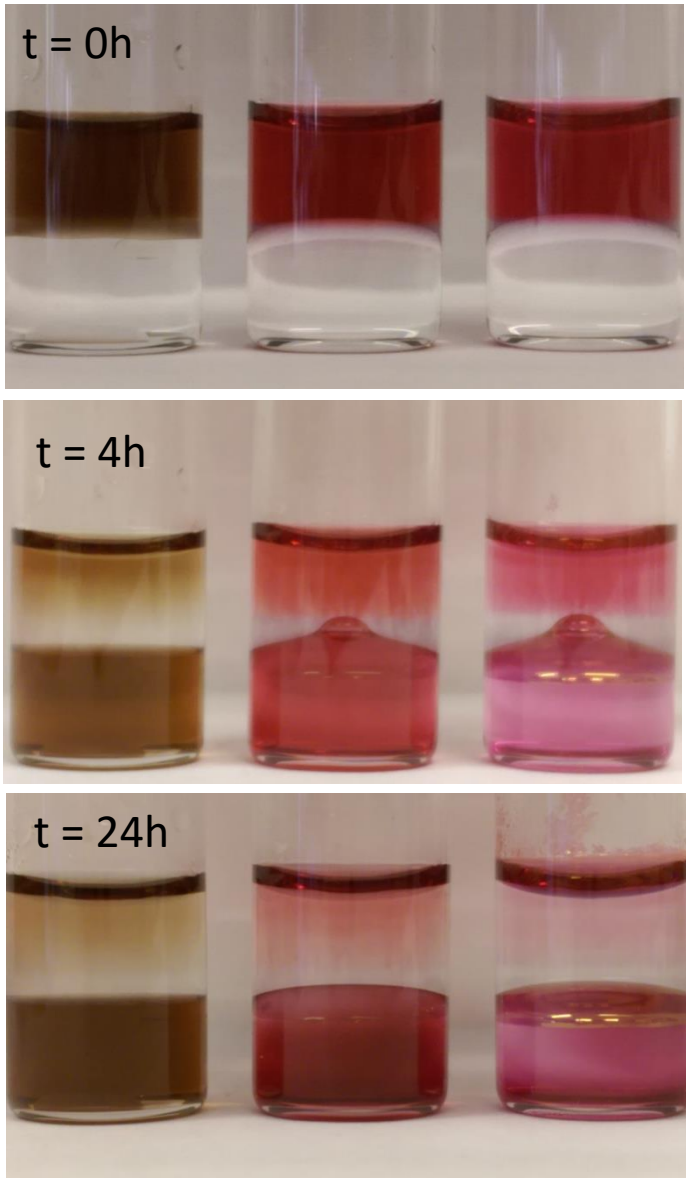

Figure 3.29: Phase transfer of 3.5nm, 15.7nm and 25.5nm 18-Crown-6-modified gold nanoparticles after this addition of 4mM KCl. The concentrations of gold nanoparticles were calculated such that the number of crown ether ligands in each solution was approximately the same.

The concentrations for each particle solution were modified so that the total number of 18-Crown-6 ligands in each solution was approximately the same, this was done to try and prevent any discrepancies from occurring due to differing ratios of cation : 18-

Crown-6. It can be seen in Figure 3.29 that after the addition of the complimentary cation the 15.7 and 25.5 nm 18-Crown-6-modified gold nanoparticles follow a similar phase transfer process as the 3nm variety; with the depletion layer forming above the aqueous-organic interface as the rate of transfer overcomes the rate of diffusion within the aqueous phase.

With the larger particle variants showing promising phase transfer properties in the presence of the complimentary cation the stability of the 15.7 and 25.5. 18-Crown-6-modified AuNP within the aqueous phase needed to be checked, which is shown in Figure 3.30.

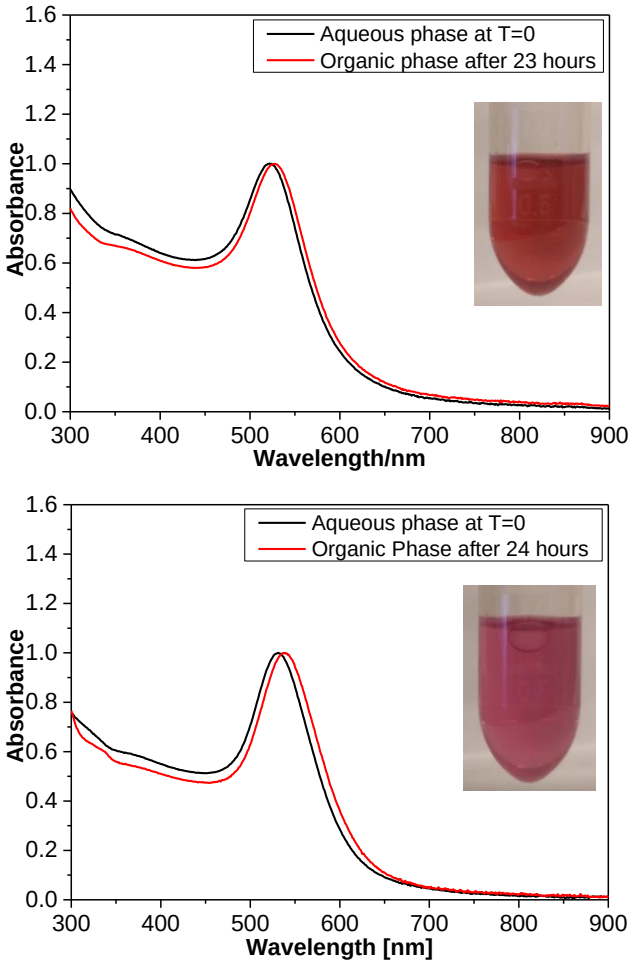

Figure 3.30: UV-Vis of a) 15.7 nm18-Crown-6-modified gold nanoparticles, b) 25.5nm 18-Crown-6-modified gold nanoparticles in both the aqueous phase (Black) and the organic phase (Red). With optical images of the particles present in the chloroform phase.

For both larger sizes of particle, the stability within the organic phase (chloroform) appears to be as good as the smaller particles. Within the organic phase, the UV-Vis spectra showing no broadening of the plasmon peak and only minor red shifts which can be attributed to the change in the solvent polarity index when moving from water to chloroform. The optical images show no aggregation or discolouration of the particles, indicating a high degree of stability within the organic media.

Whilst both larger sets of particles showed very promising results with regards to phase transfer and organic phase stability, the extent to which they worked was surprising; when large particles are functionalised with small ligands such as the 18-Crown-6 ligand they are inherently unstable and a large majority of the time the functionalisation would not even work, resulting in rapid aggregation due to the small size of the ligand of interest. This raised a suspicion about just how much of the PEG 5000 that was used as an intermediary step for functionalisation was remaining upon the nanoparticle surface. To determine whether the particles were phase transferring purely because of the 18-Crown-6 associating with its complimentary cation or just by the presence of some remaining intermediary stabilising agent the phase transfer experiment was repeated for the PEG 5000 intermediary particles, as shown in Figure 3.31.

In the presence of 4 mM KCl, the 15.7 nm PEG 5000 AuNPs show a degree of phase transfer from the aqueous phase to the organic phase. The overall process is quite different to the 18-Crown-6-modified AuNPs however. Within two hours the 18-Crown-6-modified AuNPs showed a strong degree of transfer into the organic phase with the characteristic depletion layer being shown (Figure 3.29). After the same amount of time the PEG 5000 modified AuNPs showed very little to no transfer into the organic phase, and instead of a depletion layer a destabilisation layer is observed, which is obvious from the change in colouration between the top and bottom of the colloidal solution. This destabilisation does progress further, with the eventual transfer of some particles into the organic phase.

The same experiment was attempted on the larger 25.5 nm PEG 5000 AuNPs but due to their inherent instability within the aqueous phase (the stock is kept in pure ethanol) it was not possible to compare the result.

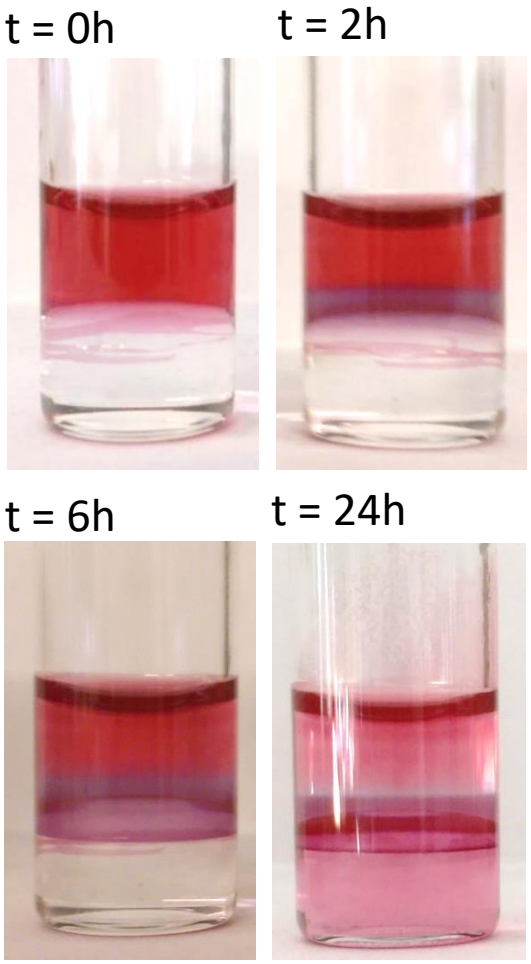

Figure 3.31: Phase transfer of 15,7nm PEG 5000 gold nanoparticles in the presence of 4mM KCl.

So, whilst the intermediary PEG 5000 AuNPs do show evidence of phase transfer into the organic phase in the presence of 4 mM KCl, the time it takes it is significantly increased in comparison to the final 18-Crown-6-modified AuNPs and the mechanism of transfer seems to be altered, with the PEG 5000 showing a destabilisation layer rather than a depletion layer. Whilst it would have been better to observe that the PEG 5000 AuNPS show no evidence of phase transfer, the difference between the two is enough to validate that the larger 15.7 nm and 25.5 nm 18-Crown-6-modified gold nanoparticles are phase transferring largely due to the association of a complimentary cation.

Unfortunately, when the 15.7 nm and 25.5 nm 18-Crown-6-modified AuNPs particles were used in the vesicle experiments as discussed in section 3.5.2, there was no evidence of cation transfer in either case; the phase transfer experiments positively indicate that these particles are capable of associating with the crown ethers complimentary cation

(K^+), just like their smaller counterparts, but are unable to effectively shuttle the cations through an artificial membrane. Even though the vesicle experiment gave a negative result, it does not provide information on just how the particle is interacting with the membrane, which could provide insight, it was therefore decided to investigate the interaction further using Cryo-TEM.

3.8 Cryo-TEM of Vesicle and 18-Crown-6-modified Gold Nanoparticles

The previous sections of this chapter showed that the 3 nm, 15.7 nm and 25.5 nm 18-Crown-6-modified AuNPs were all capable of achieving aqueous-organic phase transfer when in the presence of a complimentary cation (K^+), with all three sizes of particle exhibiting similar properties such as the rate of transfer and the development of a depletion layer. Upon moving to proper artificial membranes in the form of vesicles only the 3 nm 18-Crown-6-modified gold nanoparticles showed any sign of effective cation transport. To try and uncover what caused this lack of transport for the 15.7 and 25.5 nm particles Cryo-TEM was utilized. This technique allows the observation of the interaction between particle and vesicle in-situ, rather than having to dry the sample out, resulting in vesicle destruction and therefore unreliable evidence.

3.8.1 Cryo-TEM of 3nm 18-Crown-6-modified gold nanoparticles

Samples for cryo-TEM were prepared by pipetting approximately 10uL of solution, onto a holey support film carbon grid, freshly glow-discharged using argon plasma. After 10 minutes of incubation the grids were quickly blotted on each side twice for two seconds and instantly plunged into a liquid ethane bath, freezing the sample in a thin layer of ice. This process was achieved using a FEI Vitrobot Mk2 system working at >98% humidity. The frozen sample was then quickly transferred onto a cryo-holder (626 Gatan cryo-holder) with a small liquid nitrogen tank attached to keep the sample arm chilled. The samples were then imaged using the same TEM as described previously.

Two samples were prepared for the 3 nm 18-Crown-6-modified gold nanoparticles: 1) 0.5 mM of vesicle stock, 0.25 ml was mixed with $1.52x10^{16}$ NPs/mL, 100uL, 2) 0.5 mM of vesicle stock, 0.25 ml with 4 mM KCl was mixed with $1x52x10^{16}$ NPs/mL.

Images were taken of the two frozen samples containing vesicles and 3 nm 18-Crown-6-modified gold nanoparticles, with the second sample containing the 4 mM of KCl. The best images were selected that gave the broadest impression of the sample overall and had enough resolution to compare the interactions. These are shown in Figure 3.32

Figure 3.32a shows how the particles and vesicles react in the absence of K^+. It can be seen that a large proportion of the particles are sitting upon the edge of the carbon film coating the TEM grid, whilst there are a select few particles sitting upon the vesicles and thus it can be confidently stated that majority are seemingly uninterested in the vesicles. (The resolution of the vesicles is limited in the image due to attempting to focus upon the particle more to effectively locate them; due to the vesicle being large it is still possible to observe their location when out of focus and so a compromise had to be made.)

Figure 3.32b shows how the particles and vesicles interact in the presence of K^+. It becomes obvious very quickly that the interaction is quite different. Instead of most of the particles sitting upon the edges of the carbon grid, seemingly uninterested in the vesicles, almost all the particles are interacting with the vesicle membranes, readily observable around the edges and in the membranes. The addition of KCl into the system has triggered the particles into moving into the membrane of each vesicle. This coincides nicely with the phase transfer experiments discussed previously, as well the vesicle experiments showing evidence of cation transport. It can be confidently stated now that when in the presence of K^+ the 3 nm 18-Crown-6-modified AuNPs successfully integrate within the vesicle membrane and allow for the transport of K^+ across the system.

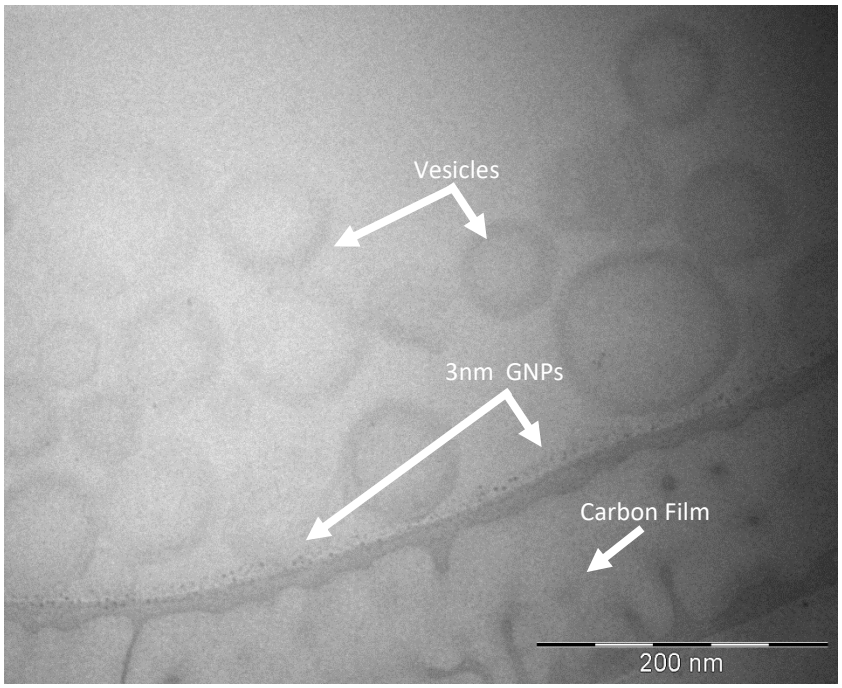

a)

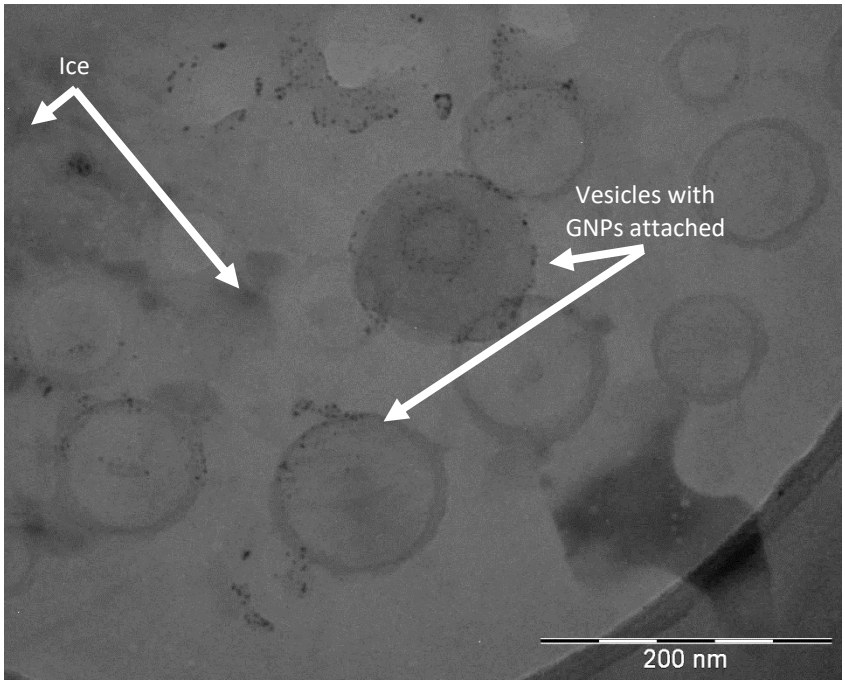

b)

Figure 3.32: Cryo-TEM images showing the interaction between 3nm 18-Crown-6-modified gold nanoparticles with: a) Vesicles + 3nm 18-Crown-6-modified gold nanoparticles, b) Vesicles + 3nm 18-Crown-6-modified gold nanoparticles + 4mM KCl.

3.8.2 Cryo-TEM of 15.7 nm and 25.5 nm 18-Crown-6-modified Gold Nanoparticles

Samples were prepared as stated in section 3.7.1 except 3 nm 18-Crown-6-modified gold nanoparticles were replaced with 15.7 nm/25.5 nm 18-Crown-6-modified gold nanoparticles and the total time left to incubate was increased from 10 minutes to 1 hour.

Section 3.7.1 described how when in the presence of 4mM K^+ the 3 nm 18-Crown-6-modified gold nanoparticles readily interfaced with vesicle membranes, helping to validate that those particles were capable of transporting K^+ through a vesicle. As stated previously, the vesicle experiments involving the 15.7 nm 18-Crown-6-modified gold nanoparticles resulted in no evidence of K^+ transfer through the membrane. This correlates with what is observed when using Cryo-TEM as shown in Figure 3.33. In the absence of K^+ the particles do not interact with the vesicle membranes, much like the 3 nm particles. The same is observed when the particle are left to incubate for 1 hour with 4 mM KCl present, which is the opposite of what happens with the 3 nm particles. No definitive attachment is observed; there are perhaps two or three particles that appear to be sticking to the membrane, but many of the particles within the system do not show any interest. This fits well with the particles showing no transport of K^+ within the vesicle experiments.

The same situation is also evident for the 25.5 nm 18-Crown-6-modified gold nanoparticles, shown in Figure 3.34, with the particle behaviour with and without 4 mM KCl remaining constant and not interacting with the vesicle membranes. This again correlates with no observable K^+ transport from earlier vesicle experiments.

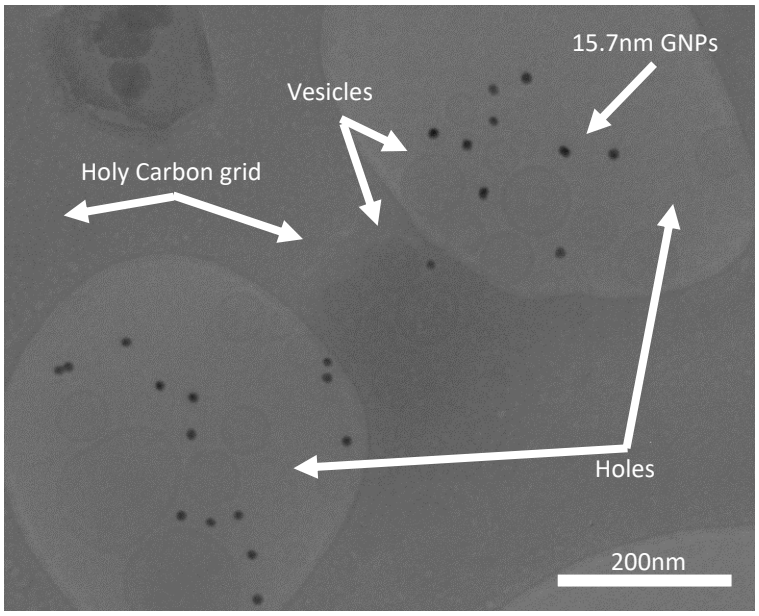

a)

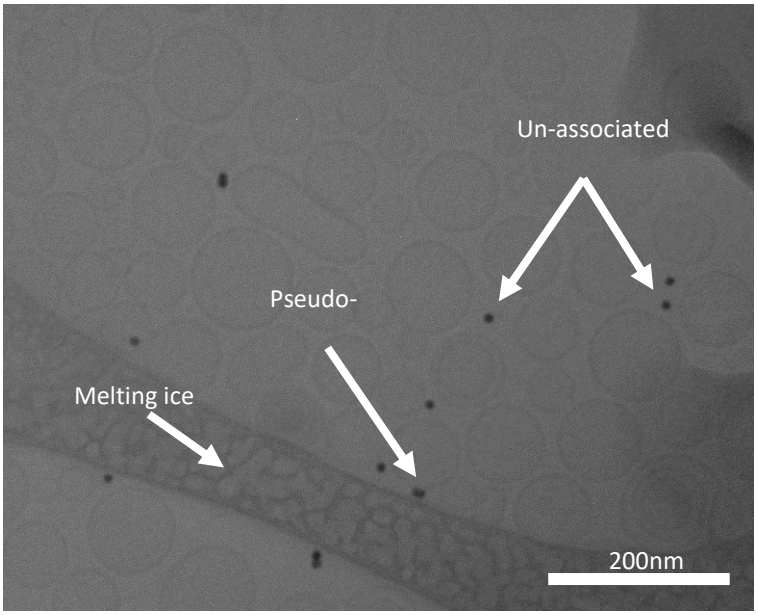

b)

Figure 3.33: Cryo-TEM images showing the lack of interaction between 15.7nm 18-Crown-6-modified gold nanoparticles with: a) Vesicles + 15.7nm 18-Crown-6-modified gold nanoparticles, b) Vesicles + 15.7nm 18-Crown-6-modified gold nanoparticles + 4mM KCl.

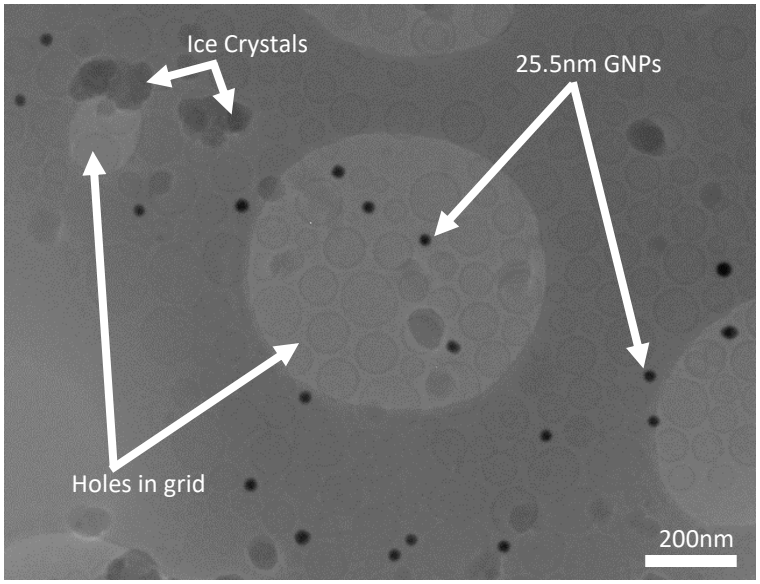

a)

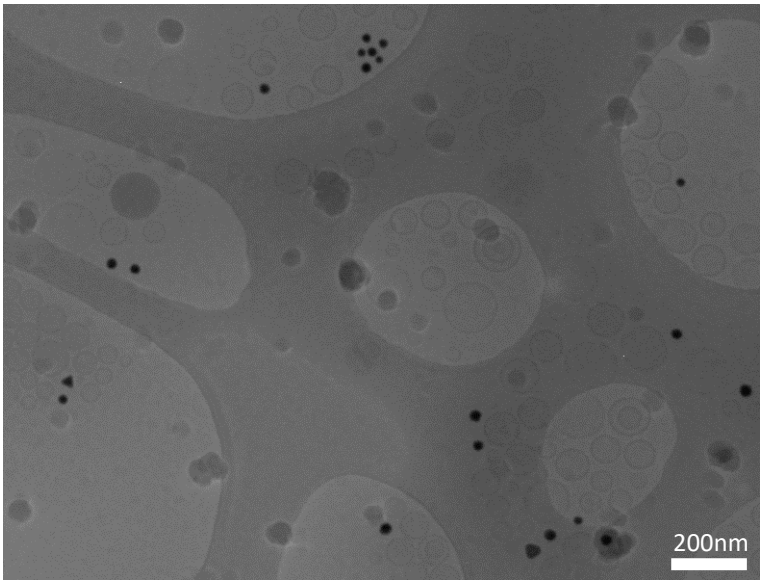

b)

Figure 3.34: Cryo-TEM images showing the lack of interaction between 25.5nm 18-Crown-6-modified gold nanoparticles with: a) Vesicles + 25.5nm 18-Crown-6-modified gold nanoparticles, b) Vesicles + 25.5nm 18-Crown-6-modified gold nanoparticles + 4mM KCl.

With the aid of Cryo-TEM it becomes possible to understand why the larger particles (15.7 nm and 25.5 nm) showed no cation transport during vesicle membrane experiments, simply due to them showing little to no association with the vesicles even though they behaved similarly to the 3 nm 18-Crown-6-modified gold nanoparticles when it came to the phase transfer experiments.

The two most prominent reasons behind this change in behaviour are, firstly, the change in interface, switching from a simple water-chloroform interface to a phospholipid bilayer, and the difference in the energetic barrier associated with integrating with a vast planar surface, experienced within the glass vial phase transfer experiments, compared to a relatively small vesicle surface. It is shown in the literature that as nano-structures increase in size, the favourability of integrating into a membrane is altered dramatically[48, 49]. This fits with other observed results as the larger particles did indeed show no interest in properly associating with the vesicle membranes, yet the 3 nm 18-Crown-6-modified particle can be seen to be heavily integrated within the vesicle membrane, being small enough to not disrupt the structure of the bilayer in an unfavourable way. Secondly, another potential reason as to why the 15.7 nm and 25.5 nm 18-Crown-6-modified gold nanoparticles were unsuccessful in membrane integration could be due to the presence of PEG 5000 left over from the intermediary step during synthesis. Completely removing an original thiol capping agent in exchange for a new one is not trivial and near impossible. The sizes of PEG 5000 could more than likely prevent these particles from integrating with a membrane.

So even though 15.7 nm and 25.5 nm 18-Crown-6-modified gold nanoparticles were created, large enough to potentially allow a generous flow of electrons across the gold core, they proved ineffective in successfully integrating with the vesicle membranes in order to facilitate the transport of ions. This unsuccessful attempt is put down to a combination of the sheer size of the gold core, as well as potential remnants of the intermediary PEG 5000 during synthesis, with both factors potentially making integration unfavourable. This means that in order to achieve cation transfer and electron transfer, a sweet spot must be found; the particle must be large enough to allow for the electron transportation but also small enough to still be favourable for membrane insertion. Additionally, it needs to have only 18-Crown-6 present upon the surface, without the presence of overly large capping agents. A particle with these characteristics was

successfully developed, see Chapter 2, Section 2.23, and is characterised in Chapter 4 of this thesis.

3.9 Summary

The role of this chapter was to discuss whether the 3 nm 18-Crown-6, 15-Crown-5 and 12-Crown-4 modified AuNPs developed in Chapter 2 were capable of incorporating their well-known aqueous-organic cation phase transfer properties onto an AuNP.

Initial phase transfer tests with potential complimentary cations, such as K^+, Na^+, Li^+ and Ba^{2+}, were undertaken to determine which of the crown ether modified AuNPs gave the highest potential for selective cation transfer across artificial membranes. These phase transfer results were further validated by the application of ζ to observe the change in charge of the particles upon interaction with cations present within the solution.

Upon successfully finding the most promising candidate, 3 nm 18-Crown-6-modified AuNPs, which not only had the highest degree of selectivity between cations, but also resulted in one of the highest rates of transfer; further testing with a wide range of KCl concentrations (0-400mM) was completed to try and fully understand how the particles were interacting with ions present in solution. Upon obtaining the salt concentration (50mM) with the most effective transfer rate into chloroform, studies involving the transfer of particles in less polar organic solvents were initiated. With only dichloroethane showing any transfer of particles, less polar solvents showed no apparent interest in accommodating the particles. These experiments did, however, allow the observation of a unique and interesting property of the 3 nm 18-Crown-6-modified AuNPs when in dichloroethane, which was the reversible phase transfer between the aqueous and organic phase when the solution was cooled and heated.

The 3 nm 18-Crown-6-modified AuNPs were then put to the test, by incorporating them into a vesicle system, to determine whether they were capable of transporting their complimentary cation (K^+) through an artificial membrane. This turned out to be highly successful; not only were the particles capable of transferring K^+ through the vesicle membranes, but they also showed a rate of transfer like that of Valinomycin, albeit a lower selectivity with regards to other cations such as Na^+. This was a milestone for the project,

demonstrating that cations could be transferred selectively by incorporating specially functionalised AuNPs into a confined compartment system.

The remaining section of this chapter discussed attempts at developing larger particles (15.7 and 25.5 nm 18-Crown-6-modified AuNPs), in the hopes of retaining the selective cation transfer through an artificial membrane while opening the gold core to effective electron transport at the same time, with the hopes of coupling electron and cation transfer across an artificial membrane. Whilst the development of larger 18-Crown-6-modified particles was achieved via the use of an intermediary functionalisation ligand (PEG 5000), neither of the two types of larger particles (15.7 and 25.5 nm) showed cation transfer across the vesicle membranes, even though they showed initially very promising phase transfer when in the presence of the complimentary cation (K^+). This lack of success regarding these larger particles was put down to the size of the particles being too large to effectively attach to the vesicle membranes to allow any kind of transport through them to be possible. This was also thought to have been affected by using the bulky intermediary functionalisation ligand 5000.

In short, cation transfer through an artificial membrane was achieved by 3 nm 18-Crown-6-modified gold nanoparticle when using the complimentary cation K^+. When larger particles were developed to improve electron transferral this resulted in the loss of the cation transferral and so further research had to be undertaken to try and find the "Sweet spot" to allow both of these processes to occur simultaneously across one particle. This is discussed in Chapter 4, where the 7.5nm 18-Crown-6-modified gold nanoparticles are investigated, including some of their highly unique reversible agglomeration properties when subjected to temperature changes.

3.10 References

1. P. C. J., *Angewandte Chemie International Edition in English*, 1988, **27**, 1021-1027.
2. Y. Marcus, *Journal of the Chemical Society, Faraday Transactions*, 1991, **87**, 2995-2999.
3. I. Persson, *Journal*, 2010, **82**, 1901.
4. L. X. Dang, *Journal of the American Chemical Society*, 1995, **117**, 6954-6960.
5. K. A. T. Silverstein, A. D. J. Haymet and K. A. Dill, *Journal of the American Chemical Society*, 1998, **120**, 3166-3175.
6. U. Domańska, *Measurement and correlation of the solubility of crown ethers in selected organic solvents*, 1998.
7. C. J. Pedersen, 1988, **27**, 1021-1027.
8. S. Blair, E. Kempen and J. Brodbelt, *Journal of the American Society for Mass Spectrometry*, 1998, **9**, 1049-1059.
9. G. W. Gokel, W. M. Leevy and M. E. Weber, *Chemical Reviews*, 2004, **104**, 2723-2750.
10. C.-Y. Chen, C.-T. Cheng, C.-W. Lai, P.-W. Wu, K.-C. Wu, P.-T. Chou, Y.-H. Chou and H.-T. Chiu, *Chemical Communications*, 2006, DOI: 10.1039/B512677K, 263-265.
11. S.-Y. Lin, S.-W. Liu, C.-M. Lin and C.-h. Chen, *Analytical Chemistry*, 2002, **74**, 330-335.
12. A. F. Danil de Namor, J. C. Y. Ng, M. A. Llosa Tanco and M. Salomon, *The Journal of Physical Chemistry*, 1996, **100**, 14485-14491.
13. M. Takeshi, Y. Shozo, I. Akira and O. Mitsuo, 1982, **55**, 2005-2009.
14. L. S. Mizoue and J. Tellinghuisen, *Biophysical Chemistry*, 2004, **110**, 15-24.
15. E. Karkhaneei, M. H. Zebarjadian and M. Shamsipur, *Journal of Solution Chemistry*, 2001, **30**, 323-333.
16. B. Tanmay, S. Moorthy, G. H. N. and D. Amitava, *European Journal of Inorganic Chemistry*, 2011, **2011**, 4680-4690.
17. T. I. Petrenko, *Theoretical and Experimental Chemistry*, 1985, **20**, 597-600.
18. P. Hurtado, F. Gámez, S. Hamad Gomez, B. Martínez-Haya, J. Steill and J. Oomens, *Crown Ether Complexes with H3O+ and NH4+: Proton Localization and Proton Bridge Formation*, 2011.
19. R. R. Julian and J. L. Beauchamp, *Journal of the American Society for Mass Spectrometry*, 2002, **13**, 493-498.
20. Å. K. E.O. and W. M. K.F., *FEBS Letters*, 1976, **68**, 191-197.
21. A. Zanotti and G. F. Azzone, *Archives of Biochemistry and Biophysics*, 1980, **201**, 255-265.

22. G. Krumschnabel, A. Eigentler, M. Fasching and E. Gnaiger, in *Methods in Enzymology*, eds. L. Galluzzi and G. Kroemer, Academic Press, 2014, vol. 542, pp. 163-181.
23. T. R. Figueira, D. R. Melo, A. E. Vercesi and R. F. Castilho, in *Mitochondrial Bioenergetics: Methods and Protocols*, eds. C. M. Palmeira and A. J. Moreno, Humana Press, Totowa, NJ, 2012, DOI: 10.1007/978-1-61779-382-0_7, pp. 103-117.
24. A. P. Singh and P. Nicholls, *Journal of Biochemical and Biophysical Methods*, 1985, **11**, 95-108.
25. A. S. Waggoner, *Annual Review of Biophysics and Bioengineering*, 1979, **8**, 47-68.
26. C. J. Newcomb, S. Sur, J. H. Ortony, O.-S. Lee, J. B. Matson, J. Boekhoven, J. M. Yu, G. C. Schatz and S. I. Stupp, *Nature Communications*, 2014, **5**, 3321.
27. M. El-Kemary and H. El-Shamy, *Journal of Photochemistry and Photobiology A: Chemistry*, 2009, **205**, 151-155.
28. C. Lofrumento, F. Arci, S. Carlesi, M. Ricci, E. Castellucci and M. Becucci, *Spectrochimica Acta Part A: Molecular and Biomolecular Spectroscopy*, 2015, **137**, 677-684.
29. M. El-Kemary, Y. Abdel-Moneam, M. Madkour and I. El-Mehasseb, *Journal of Luminescence*, 2011, **131**, 570-576.
30. S. Wen, L. Zhan-Ting and H. Jun-Li, *Angewandte Chemie International Edition*, 2014, **53**, 4578-4581.
31. A. K. Boal and V. M. Rotello, *Journal of the American Chemical Society*, 2000, **122**, 734-735.
32. A. M. Jackson, J. W. Myerson and F. Stellacci, *Nature Materials*, 2004, **3**, 330.
33. M. Yu and F. Stellacci, *Small*, 2012, **8**, 3720-3726.
34. Q. K. Ong, J. Reguera, P. J. Silva, M. Moglianetti, K. Harkness, M. Longobardi, K. S. Mali, C. Renner, S. De Feyter and F. Stellacci, *ACS Nano*, 2013, **7**, 8529-8539.
35. Y. Cesbron, C. P. Shaw, J. P. Birchall, P. Free and R. Levy, *Small*, 2012, **8**, 3714-3719.
36. J. Stirling, I. Lekkas, A. Sweetman, P. Djuranovic, Q. Guo, B. Pauw, J. Granwehr, R. Lévy and P. Moriarty, *PLOS ONE*, 2014, **9**, e108482.
37. J. Song, J. Zhou and H. Duan, *Journal of the American Chemical Society*, 2012, **134**, 13458-13469.
38. O. Uzun, Y. Hu, A. Verma, S. Chen, A. Centrone and F. Stellacci, *Chemical Communications*, 2008, DOI: 10.1039/B713143G, 196-198.
39. J. J. Brown, J. A. Porter, C. P. Daghlian and U. J. Gibson, *Langmuir*, 2001, **17**, 7966-7969.
40. M. Prabaharan, J. J. Grailer, S. Pilla, D. A. Steeber and S. Gong, *Biomaterials*, 2009, **30**, 6065-6075.

41. W. Y. Lee, M. J. Hostetler, R. W. Murray and M. Majda, *Israel Journal of Chemistry*, 1997, **37**, 213-223.
42. R. H. Terrill, T. A. Postlethwaite, C.-h. Chen, C.-D. Poon, A. Terzis, A. Chen, J. E. Hutchison, M. R. Clark and G. Wignall, *Journal of the American Chemical Society*, 1995, **117**, 12537-12548.
43. *Applied Physics Letters*, 1998, **72**, 1781-1783.
44. S. Peter, *Angewandte Chemie International Edition*, 2003, **42**, 1892-1895.
45. R. P. Andres, T. Bein, M. Dorogi, S. Feng, J. I. Henderson, C. P. Kubiak, W. Mahoney, R. G. Osifchin and R. Reifenberger, *Science*, 1996, **272**, 1323-1325.
46. N. W. Martin , C. Laura, Y. Mingdi, X. C. Sui , O. B. Leif , H. James and F. W. K. John *Japanese Journal of Applied Physics*, 1997, **36**, 7796.
47. M. Dorogi, J. Gomez, R. Osifchin, R. P. Andres and R. Reifenberger, *Physical Review B*, 1995, **52**, 9071-9077.
48. R. C. Van Lehn, P. U. Atukorale, R. P. Carney, Y.-S. Yang, F. Stellacci, D. J. Irvine and A. Alexander-Katz, *Nano Letters*, 2013, **13**, 4060-4067.
49. A. Akthakul, A. I. Hochbaum, F. Stellacci and A. M. Mayes, *Advanced Materials*, 2005, **17**, 532-535.

Chapter 4 Entropy Driven Reversible Agglomeration of Crown Ether Capped Gold Nanoparticles

In Chapter 3 of this thesis it was shown that the use of thiolated crown ethers as capping agents for small AuNPs allowed the control of the hydrophilicity via complexation of complementary cations, resulting in phase transfer between aqueous and organic solvents[1] followed by evidence of cation transfer across a phospholipid membrane. In this chapter it shall be demonstrated that the same ligand can also be used to prepare thermal-responsive particles that exhibit entropy driven reversible agglomeration, with controllable transition temperatures directly related to the degree of cation complexation of the crown ether moiety, with the overall process being briefly summarised in Figure 4.1. The research discussed here is published in *Chemistry – A European Journal* (Chem. Eur. J. 2018, 24, 3151-3155)[2].

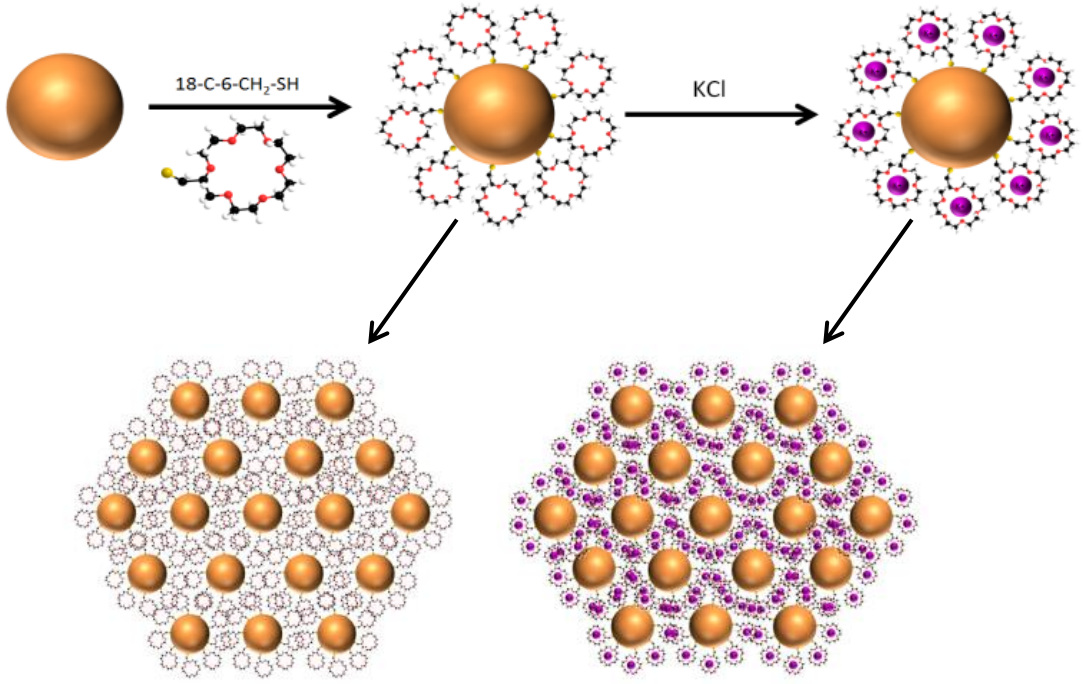

Figure 4.1: Illustration showing how the LCST of crown ether coated gold nanoparticles changes depending on the concentration/type of salt added to the local environment.

Interparticle plasmon coupling resulting from the agglomeration of AuNPs can readily be exploited to create simple colorimetric test formats for analytical or diagnostic purposes[3-5]; in particular, the body of work by Mirkin and colleagues[6, 7] on the use of plasmon coupling in AuNPs for DNA and RNA analysis stands out as a significant

ongoing development with many scientific and commercial ramifications. In recent years, a plethora of chemical and physical stimuli that can trigger the agglomeration of AuNPs have been identified including light[8], pH[9, 10], metal ions[11-13] and temperature[14, 15].

Nanoparticles that assemble upon cooling have been developed by functionalising with polymers (Figure 4.2) that have upper critical solution temperatures (UCSTs), such as poly(N-acrlyoylglycinamide)[16] and poly(N,N'-dimethyl-(methacrylamido propyl) ammonium propanesulfonate)[17]. On the other hand, nanoparticles that assemble upon heating are typically functionalised with polymers with lower critical solution temperatures (LCSTs), such as poly(N-isopropylacryamide), better known as pNIPAm[18], and oligo(ethylene glycol) terminated polymers such as poly(ethylene oxide-st-propylene oxide)[19]. Nanoparticles with thermo-responsive behaviour can prove useful to a wide range of applications such as cellular internalisation[20], controlled drug release[21], catalysis[22] and colorimetric sensors[23]. pNIPAm, one of the best-known thermo-responsive LCST polymers, has a phase transition that occurs at 31-32°C[24]. It has been observed that during this process pNIPAm forms coils within aqueous media followed by their collapse to form large insoluble globular structures, resulting in precipitation. A similar property has been seen in both PEG AuNPs[25] when at suitably high temperatures/ionic concentrations and oligo ethylene glycol (OEG) AuNPs when presented with suitable alkyl terminating groups[26]. The agglomeration of functionalised nanoparticles at elevated temperatures is somewhat counterintuitive but typical for entropy driven processes such as hydrophobic interactions.

Crown ethers[27], which are cyclic oligomers of ethylene oxide, are known for their ability to strongly bind to specific cations, whilst being completely inert to others. This unique property is due to the hole-size cation-diameter relationship[28] and has resulted in their use for a variety of applications such as sensing[29, 30], phase transfer catalysis[31-33] and ion encapsulation[34], with particular note given to Kotov[5] *et al* who developed long-chained 18-Crown-6 capped AuNPs capable of detecting melamine via the forced agglomeration of the AuNP system. Further information involving the historic background of crown ethers and their functional uses can be found in Chapter 1 of this thesis.

Characterising the temperature dependant properties of the 7.5nm 18-Crown-6-modified gold nanoparticles would potentially open pathways to successful membrane insertion for a system previously incapable of doing so with particles larger than 3nm.

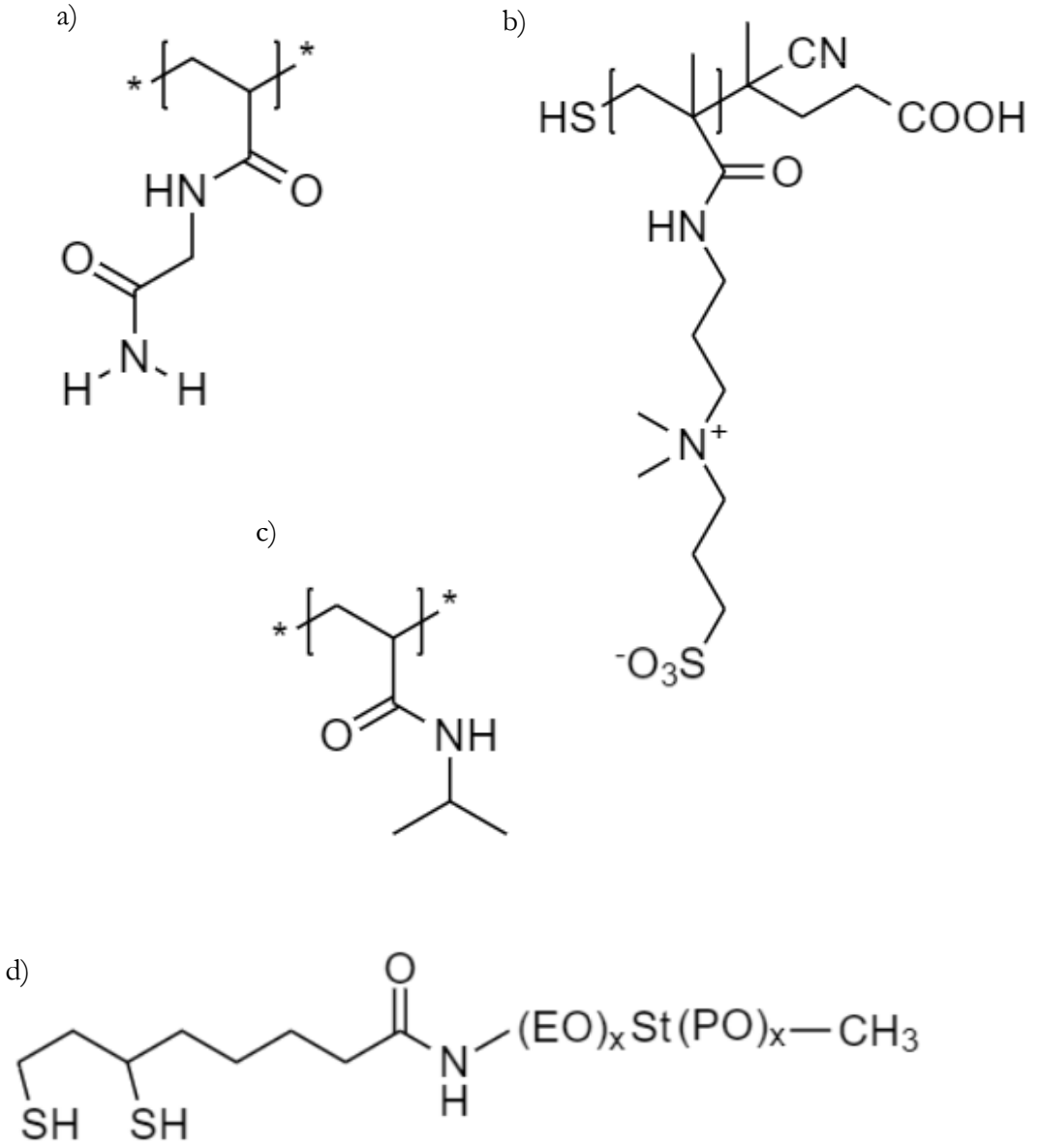

Figure 4.2: UCST Polymers: a) poly(N-acrlyglycinamide, b) poly(N,N'-dimethyl-(methacrylamido propyl) ammonium propanesulfonate, LCST Polymers c) poly(N-isopropylacrylamide), d) poly(ethylene oxide-st-propylene.

4.1 Temperature Cycling Experiments

4.1.1 UV-Visible Spectroscopy

An aqueous dispersion of the 18-C-6-CH_2-SH coated AuNPs ($4.0x10^{14}$ Np/mL) prepared as synthesised in Chapter 2 Section 2.2.3 was subjected to a series of temperature cycles from 5ºC to 35ºC, with a UV-Vis spectrum taken at 5ºC and 35ºC for every cycle. The heating of the sample was achieved via immersion in a water bath set to 35ºC and cooling was achieved by placement into a fridge set at 5ºC. Figure 4.3 shows the UV-Vis spectra obtained, along with images showing the colours of the particle solutions at the three temperatures.

In Figure 4.3a it should be noted that the colour of the line is related to the cycle number, whereby the first temperature cycle is indicated by the black lined spectra for both 5ºC and 35ºC, whilst the tenth cycle is indicated by the bright red lined spectra for both 5ºC and 35ºC, with the gradual colour shift from black to red indicating the cycles (2-9) in between.

When the aqueous solution was kept at 5ºC the particles are stable as singular entities within solution, resulting in the plasmon peak being observed at 518 nm, typical for AuNPs of 7.5 nm in diameter[35]. As the temperature is increased to 35ºC the particles become unstable as singular entities and gather together to form a more stable structure, resulting in larger particulates and shifting the plasmon peak to a higher wavelength. This can be seen in figure 4.3a as the plasmon resonance changes from 518 nm to 555 nm, along with a much broader shoulder heading into the 700-900 nm wavelength region, indicative of much larger structures (1000+ nm) being present. The presence of an increased agglomerate size becomes obvious when the aqueous solution is subjected to even higher temperatures of 50ºC, as shown in figure 4.3b, where the solution becomes deep blue in colour and opaque, with a slight gold tint via the scattering of reflected light. This increase in scattered light is typical of much larger AuNPs[36-38] and is further proof that large agglomerates are forming within this system. As the temperature is decreased back to 5ºC the AuNPs once again become stable as singular entities, resulting in a shift of the plasmon peak back to 518 nm, and so returning to their original deep red colour.

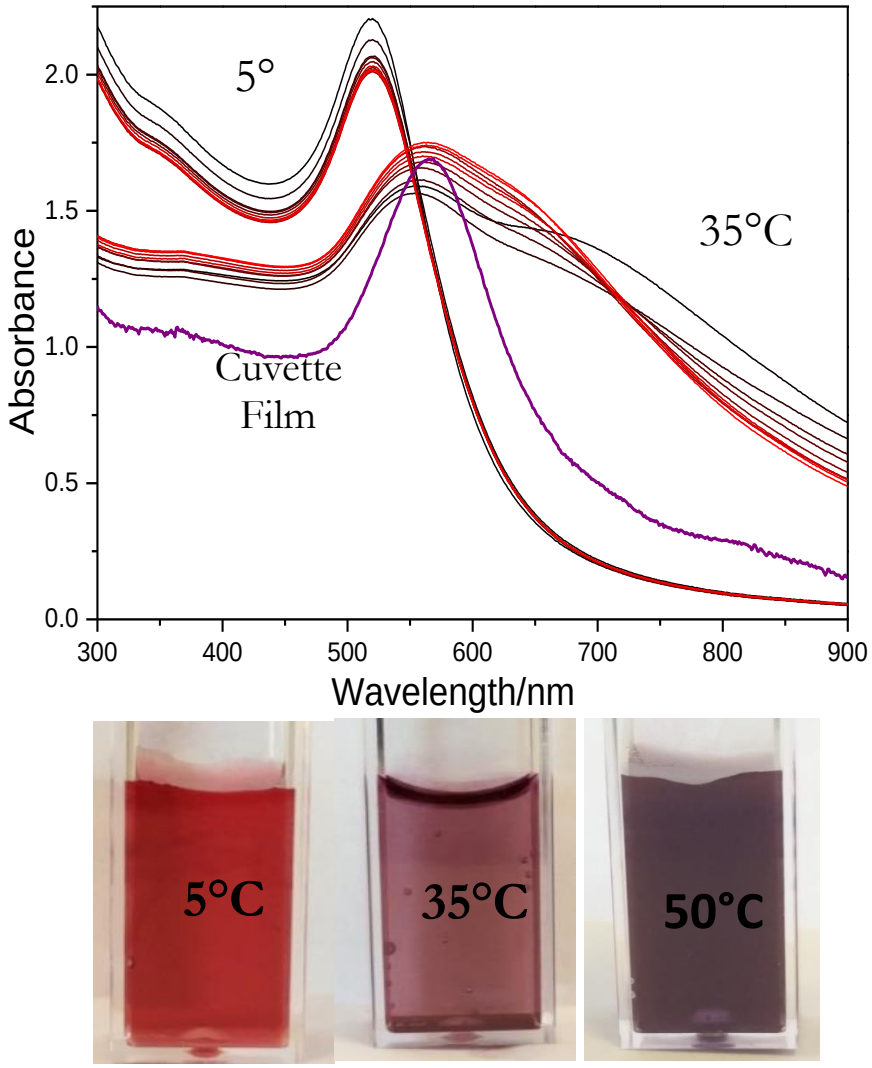

Figure 4.3: a) UV-Vis spectra of the particle solution taken at 5 and 35ºC over the course of 10 temperature cycles, b) Images showing the colour of the particle solution at 5, 35 and 50ºC

After every temperature cycle the spectrum taken at 5ºC shows a gradual decrease in absorbance, Figure 4.3, with the overall change in absorbance decreasing with every cycle, indicating a saturation limit is being reached. The reverse trend is seen in the spectra taken at 35ºC, with the plasmon peak at 555 nm increasing gradually with every cycle, with a similar saturation point occurring as seen for the 5ºC spectra. This change in absorbance for both spectra can be attributed to a slow film formation process, which begins at 35ºC and is not reversible in aqueous media. It should also be noted that the plasmon peak shifts from 555 nm to 560 nm, shown in Figure 4.4, where the change in the plasmon peak during each cycle is shown. This can be attributed to an increasing film thickness of AuNPs which has been observed and noted on by Brust *et al* [39].

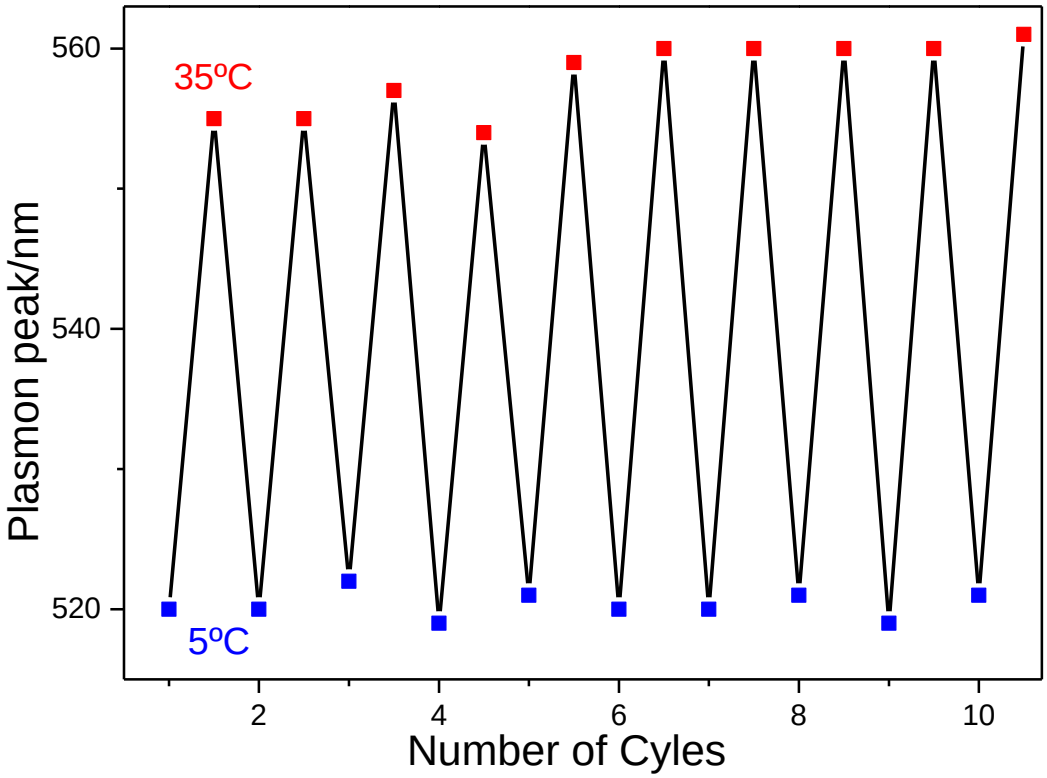

Figure 4.4: A graph showing the reversibility of the plasmon peak during temperature cycling between 5 and 35ºC.

To confirm that these changes in absorbance are the formation of a film and not just loss of particulate matter due to aggregation, a picture of the cuvette was taken after the 10 temperature cycles, as shown in Figure 4.5. It is obvious from this image that there is layer of particles presenting at the surface of the plastic. The cuvette film was analysed directly with UV-Vis in air, resulting in the purple spectrum shown in Figure 4.3a, with the spectrum being enhanced to better compare it to the aqueous dispersion spectrum. The cuvette film spectrum has a plasmon peak at 560 nm, the exact same as the final plasmon peak of the aqueous dispersion spectrum shown in Figure 4.5. The film was dissolvable in chloroform, the resulting solution being analysed via UV-Vis, giving the spectrum also shown in Figure 4.5. When compared to the spectra of the aqueous dispersion, presented at 5ºC, it showed a very similar absorbance spectrum, with the only difference being a slight shift in the plasmon peak, which can be attributed to the change in the solvent refractive index [40] rather than any kind of loss in stability [41].

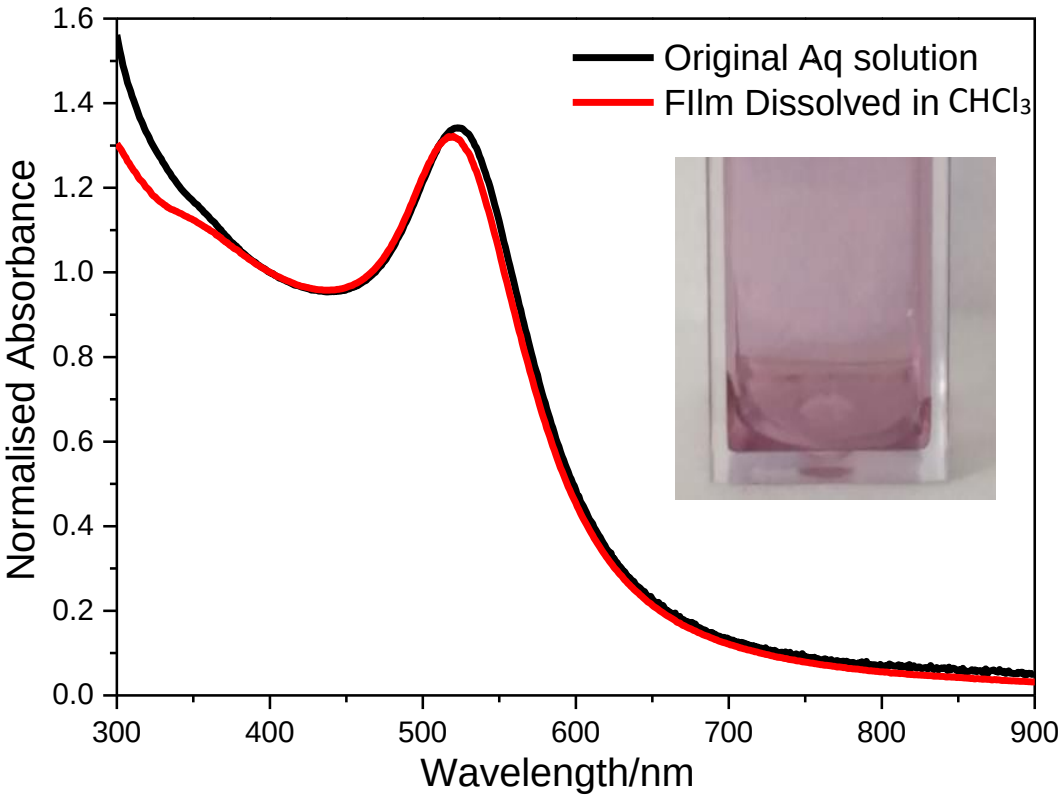

Figure 4.5 UV-Vis spectra comparing the plasmon peak of the particle solution when dispersed in water and chloroform, (inset) Image showing the presence of a particle film upon the cuvette after temperature cycling.

With evidence of film formation occurring within the system the changes in absorbance in various locations can be better explained. After each cycle a population of particles that was present in solution adhere to the walls of the cuvette, with the initial population of particles that adhere being relatively large due to having a clean surface to adhere to. These particles are now lost to the bulk solution and begin to absorb light at 555-560 nm. When the particles are present at 5ºC this loss of material to the film results in a lower concentration of particles within solution, giving rise to a reduced plasmon peak intensity.

A similar effect is seen within the 700-900 nm region, where once again the loss of material results in fewer particulates capable of absorbing the transmitted light, lowering the overall absorbance. This increase in absorbance at 555-560 nm is due to the film absorbing at the same wavelength, and so contributes to the plasmon peak additively. It is interesting that the film is not completely saturated within the first cycle, but steadily becomes saturated over the course of multiple cycles, indicating that there is a steady build-up of particles upon the surface, Figure 4.6. Brust *et al* [42] observed a similar effect when experimenting with the self-assembly of nonane-1, 9-dithiol AuNPs onto an Au coated quartz crystal and it has been demonstrated that only 50-60% of the total available

surface area is accessible[43], with the increase in thickness of the next few cycles resulting from the increased roughness of the first initial monolayer

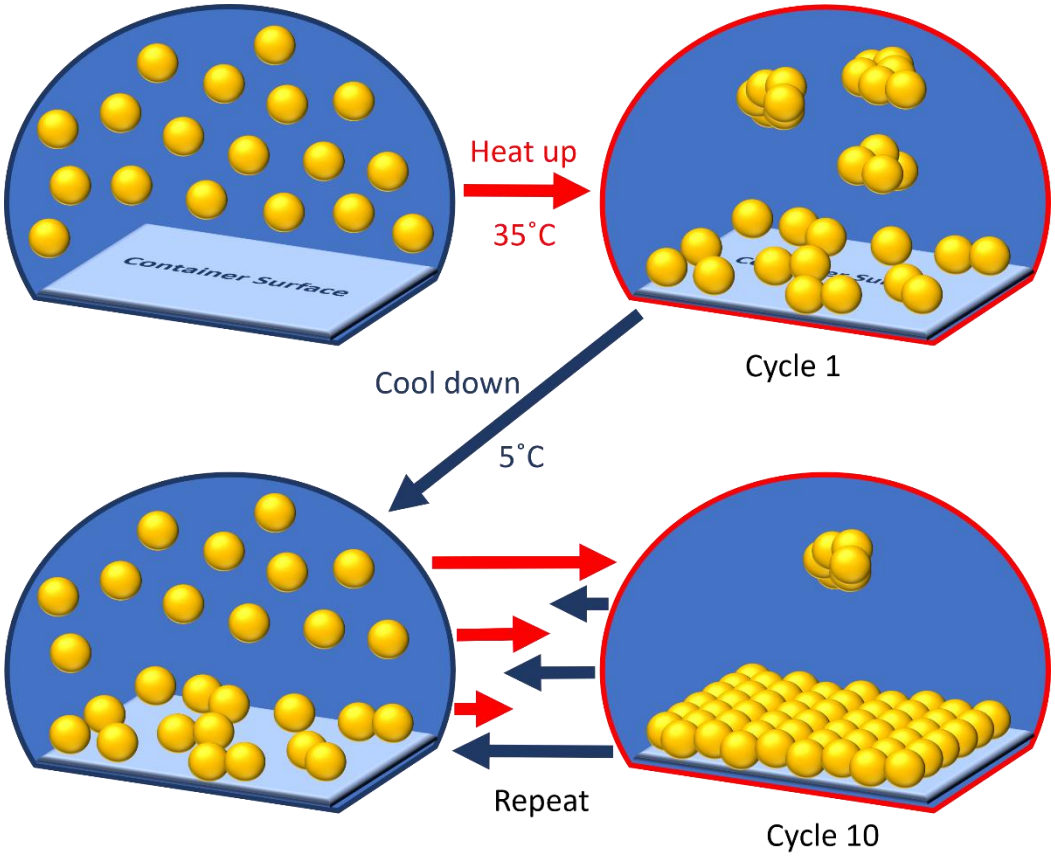

Figure 4.6: The state of 7.5nm 18-Crown-6-modified gold nanoparticles are: a) Kept beneath the phase transition point, resulting in all particle being stable within the aqueous media, b) Heated up to 35˚C, resulting in agglomeration within solution or partial coverage of the container wall, c) Cooled back down to 5˚C, reversing the solution agglomeration but some particle remain upon the surface, d) Cycled between 35 and 5˚C numerous times, resulting in an increasingly thick film of particles upon the container wall.

4.1.2 Transmission Electron Microscopy

To better understand and explain the results that were observed when undertaking the temperature cycling experiments electron microscopy was used to try and observe these thermo-responsive effects on the microscopic scale rather than the macroscopic. To obtain the TEM images shown in Figure 4.7 and 4.8 the following procedures were used: An aqueous dispersion of the 18-C-6-CH_2-SH coated AuNPs ($5.8x10^{13}$ Np/mL, 4 µl) was drop-cast upon two carbon-coated 400 mesh copper grids, one grid was left to slowly evaporate at 5ºC whilst the second grid was left to evaporate at 30ºC. To obtain a more reliable image of the particles at 50ºC (Figure 4.9) a different approach was used; a carbon coated 400 mesh copper grids was heated up to 50ºC followed by 4 µl of the particle

solution being drop cast onto it, resulting in a very fast evaporation of the solution whilst preventing any cooling of the particles during evaporation.

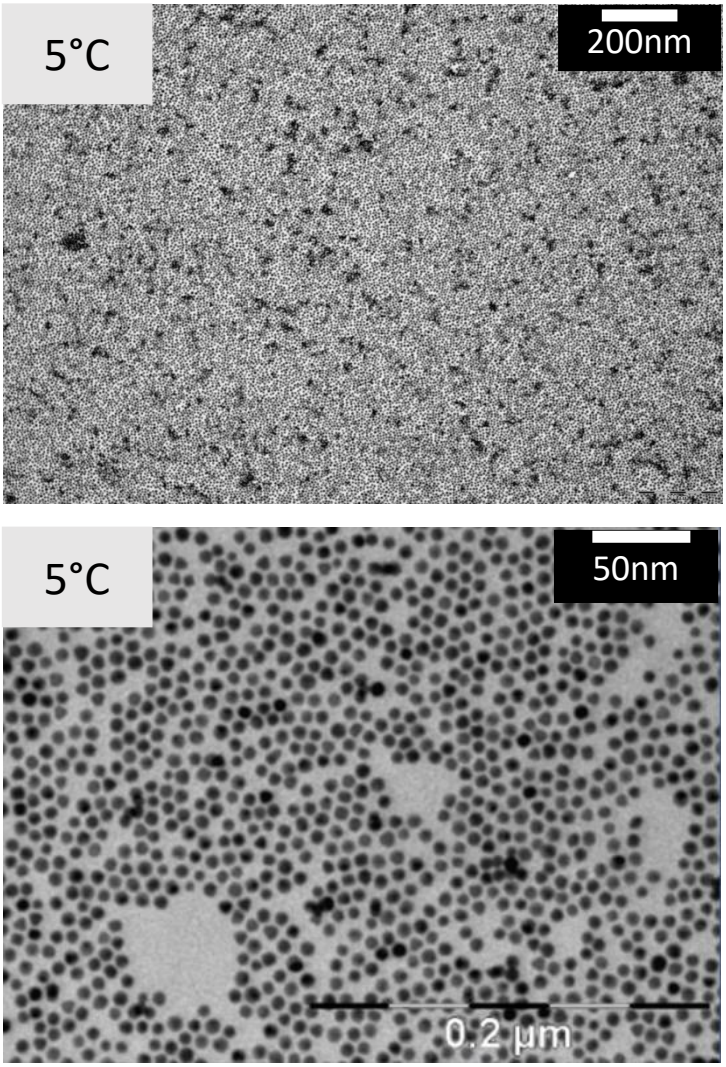

Figure 4.7: TEM images showing the crown ether coated particles when prepared at 5ºC, with varying levels of magnification.

The aqueous AuNP dispersion evaporated at 5ºC shows a nice even distribution of particles upon the grid when viewed with a lower magnification (Figure 4.7a), with a couple of dark spots observed throughout the sample where a small quantity of particles has agglomerated. However, the majority of particles presented upon the grid show an even coverage. This is especially obvious once the magnification is increased (Figure 4.7b). At this magnification it becomes obvious that each particle is separated from its neighbour, which is to be expected for particles considered stable within their liquid media.

The TEM images shown in Figure 4.8 were taken at 30ºC to catch the beginning of the agglomeration process before the phase change occurs, which would result in the development of large agglomerates. This was a success; at a lower magnification (Figure 4.8a) the particles appear much more disorganised upon the grid surface, with multiple areas of the grid void of particles whilst other sections show increased populations.

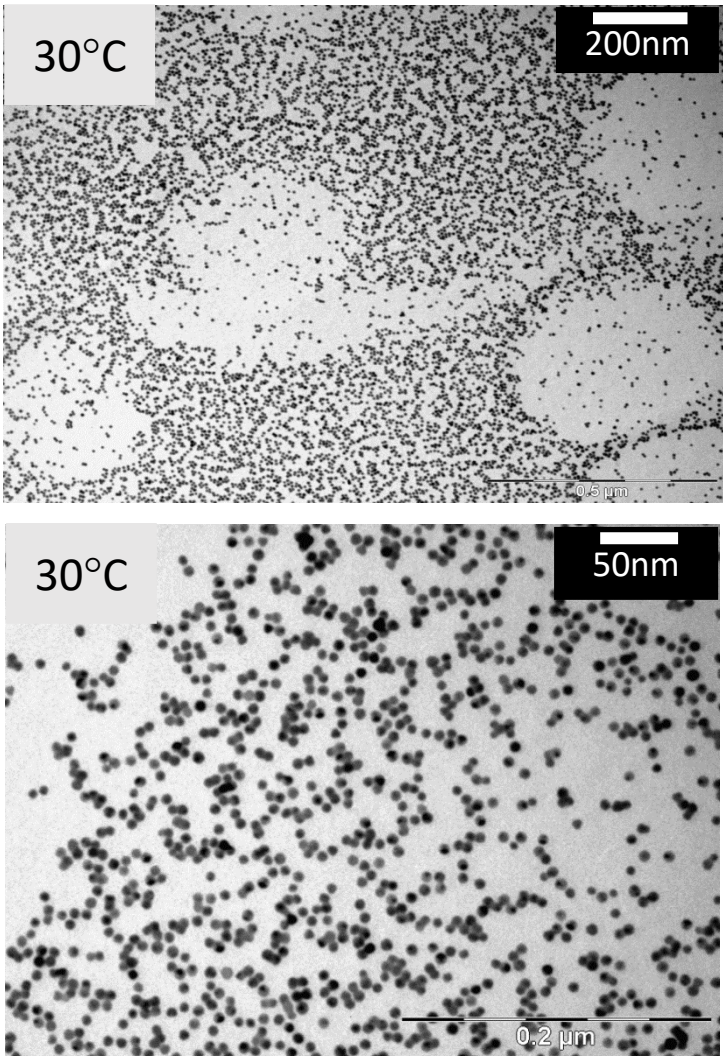

Figure 4.8: TEM images showing the crown ether particles when prepared at 30ºC, with varying levels of magnification.

The cause of this change in the nanoparticle dispersion across the grid becomes apparent when a higher magnification is used, Figure 4.8b; the particles presented in this image are no longer separated from their neighbours, but actively adhering to them, forming dimers, trimers and sometimes larger groupings, which shall be discussed further on in this section. Whilst a change in nanoparticle composition is observed when comparing TEM

images between 5ºC and 30ºC, the overall effect is relatively minor due to it being the beginning of the phase transition. In this regard the experiment was a success, observing the beginning of the phase transition process as the particles being to adhere one another.

The most dramatic change in the nanoparticle compositions is when comparing the 5ºC images to the 50ºC images, as seen in Figure 4.9.

It is immediately obvious even at lower magnification, Figure 4.9a, that there has been a dramatic change within the solution. On first sight the grid appears to be covered with a large polymeric structure that could quite easily be mistaken as an organic impurity. At higher magnifications, Figure 4.9b and **c,** it becomes apparent that the structure potentially arising from an organic impurity is not the cause, but large populations of particles adhering to one another in huge frameworks that span across the grid. The agglomeration of the particles to one another becomes highly apparent when looking at Figure 4.9c, where the formation of long branched lines of particles is observed; these chains of particles appear to then wrap around one another and become part of a much larger overall structure seen in Figure 4.9a.

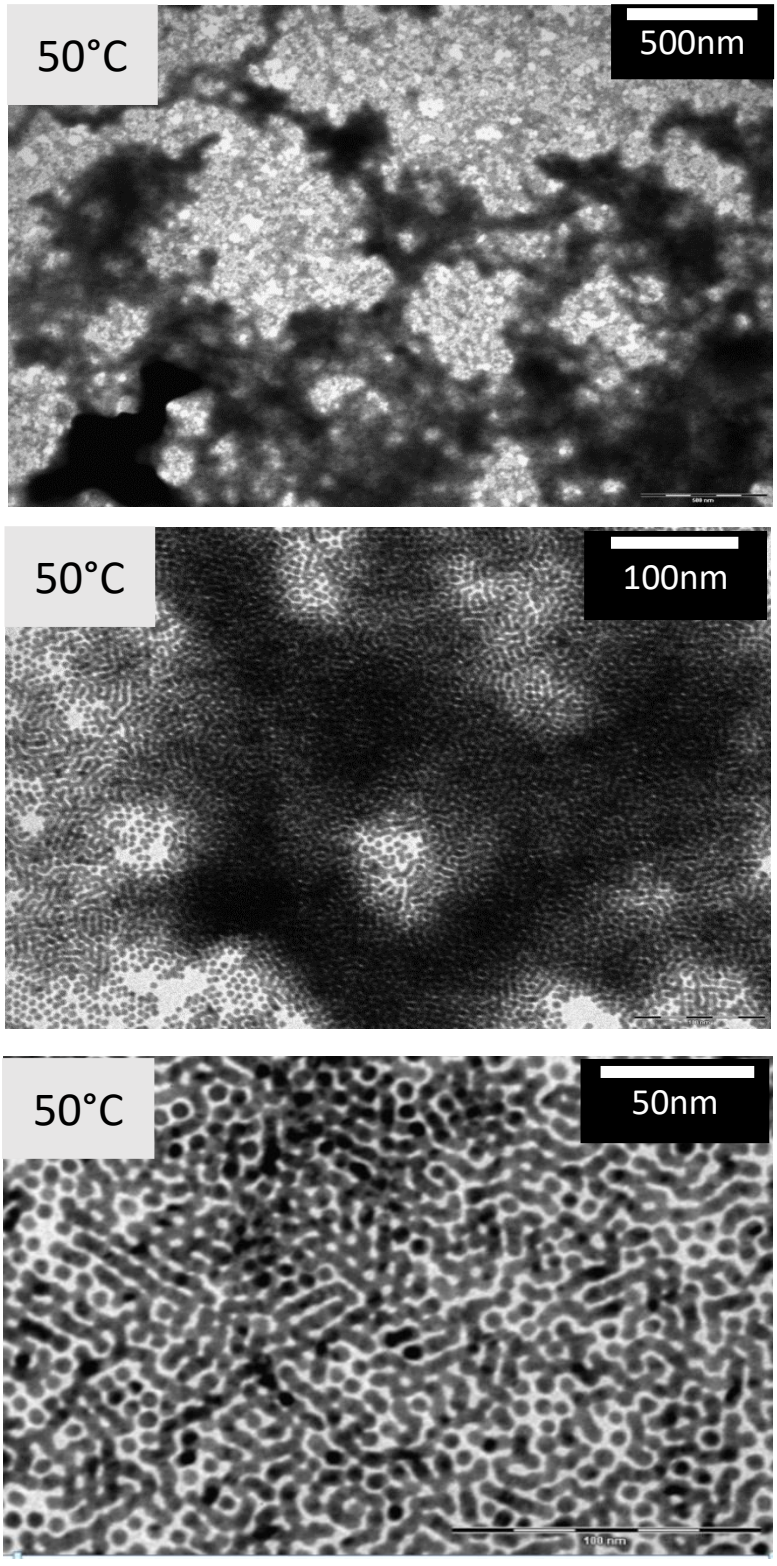

Figure 4.9: TEM images showing the crown ether particles when prepared at 50ºC, with varying levels of magnification.

4.1.3 Dynamic Light Scattering Analysis

Unfortunately, due to the nature of TEM, where the sample is effectively dried out, the actual size of these large agglomerated structures is impossible to determine unless further experimental techniques are used. To try and obtain a better understanding of the particulate size changes occurring within the system with increasing temperature, DLS was employed. An aqueous dispersion of the 18-C-6-CH_2-SH coated AuNPs (3.95x10^{13} Np/mL, 1 mL) was placed in a quartz cuvette and for each temperature measurement the AuNP solution was allowed to equilibrate for five minutes before the measurement was taken. A total of four measurements were taken at: 5, 30, 40 and 50ºC. The results of this experiment can be seen in Figure 4.10.

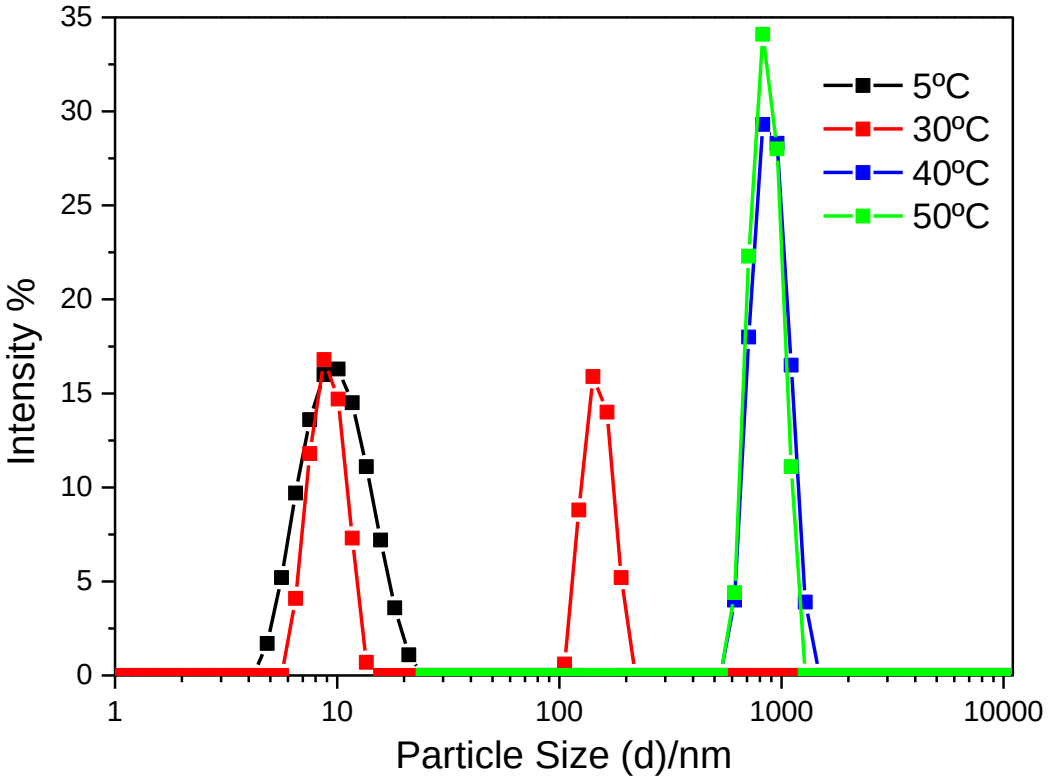

Figure 4.10: A graph showing the change in particulate size at various temperature levels when observed using Dynamic Light Scattering.

When the aqueous AuNP solution is at a temperature of 5ºC DLS shows the estimated particulate size to be around 9 nm in diameter, slightly larger than both TEM and UV-Vis suggest (around 7 nm in diameter). However it is well known that the accuracy of DLS for small particles is not precise due to the measurement of size relying on the intensity ratio of scattered light between the particle and the solvent, resulting in only a small difference between these two when smaller particles are involved[44]. This effect is

described in greater detail in Chapter 1- Introduction; This slight deviation in particle diameter is due to instrumental error with regards to this particle size.

Upon heating the solution up to 30ºC a secondary peak emerges, giving two peaks in total, one stating a diameter of 9 nm and the other stating a diameter of 150 nm. It has been discussed previously in this section that at 30ºC populations of particles begin to agglomerate, forming dimers, trimers and larger structures. Having a secondary peak arising at this temperature point was to be expected. The appearance of two peaks within DLS can be attributed to the presence of anisotropic shapes of particles or agglomerates. For example, it is also observed in Au nanorods[45]. It is already apparent from Figure 4.9c that these particles initially develop long chains, which then collect together to form much larger structures, allowing us to better interpret this double peak at 30ºC as the initial assembly of long linear chains of particles before further agglomeration occurs, this is often the case in destabilising charged colloidal systems [46].

Upon heating the solution up to 40ºC there is now only a single peak at 1000 nm particle diameter. At this temperature the solution is past the phase transition point of the AuNPs and so only the presence of large agglomerates of particles is observed. This is reinforced by the peak remaining at a particle diameter of 1000 nm upon heating to 50ºC. This fits nicely with the image shown in Figure 4.3 where heating the particles up to 50ºC results in a deep blue colouration and high degrees of light scattering, indicative of large AuNP.

4.1.4 Environmental Scanning Electron Microscopy

4.1.4.1 In-situ Droplet Observation

Whilst TEM is an exceptional tool for observing AuNP particles in high resolution when dried and encapsulated upon a grid, it proves ineffective at providing insight into how the particles behave and interact when in solution. To build up a more refined picture of the agglomeration behaviour within the aqueous media, attempts to observe the particles whilst still present within a droplet and heated up to 50ºC were undertaken. This process proved immensely challenging however; if the droplet was placed within the SEM chamber under a low enough humidity (<50%) that an acceptable resolution of the system could be obtained, the droplet rapidly evaporated over a period of a minute, as can be seen in Figure 4.11. On the other hand, if a suitable humidity was used that

prevented the droplets evaporation or at least slow it down enough to observe the sample in dispersion (>50%) the resulting resolution incapable of discerning anything of value.

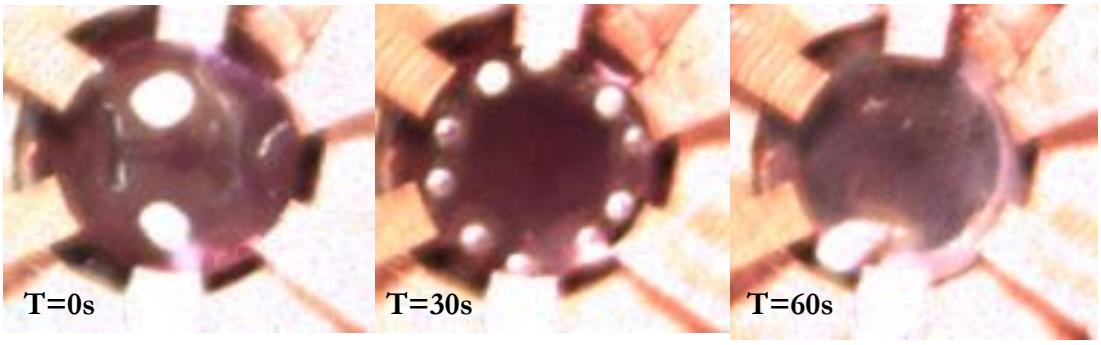

Figure 4.11: Images showing the rapid evaporation of the aqueous droplet containing crown ether particles when attempting to observe them in situ.

The images shown in Figure 4.12 were the most successful results obtained from this set of experiments. Unfortunately, due to the difficult nature of this process, only the presence of a thin film of water upon the grid surface was observed, rather than a large water droplet. Whilst the overall outcome of this experiment set was not entirely as desired, the ability to observe the particles present even in a thin film upon the surface was still interesting and informative.

To achieve the images shown in Figure 4.12 the SEM was used in transmission mode, to see events occurring within the droplet, rather than analysing the surface. Figure 4.12a was taken at a lower magnification to show how the thin film looks from a broader perspective, with darker patches indicating the presence of particles. With increased magnification (Figure 4.12b) it is observed that the particles are developing a similar agglomerated structure as seen in the TEM images previously (Figure 4.9), with the particles attaching to one another to form long branched structures. When attempting to further increase the magnification to better resolve the structure (Figure 4.12c) it becomes apparent that obtaining singular particle resolution would be impossible in the presence of water upon the surface along with humidity of 50% or above within the chamber, once again defining the limitations we observed with this experiment. In Figure 4.12d the surface boundary of the water layer (left) compared to the dried-out grid (right) is observed and it becomes obvious that the presence of water upon the surface greatly effects the ability to observe exactly how the particles interact with one another upon increasing temperature.

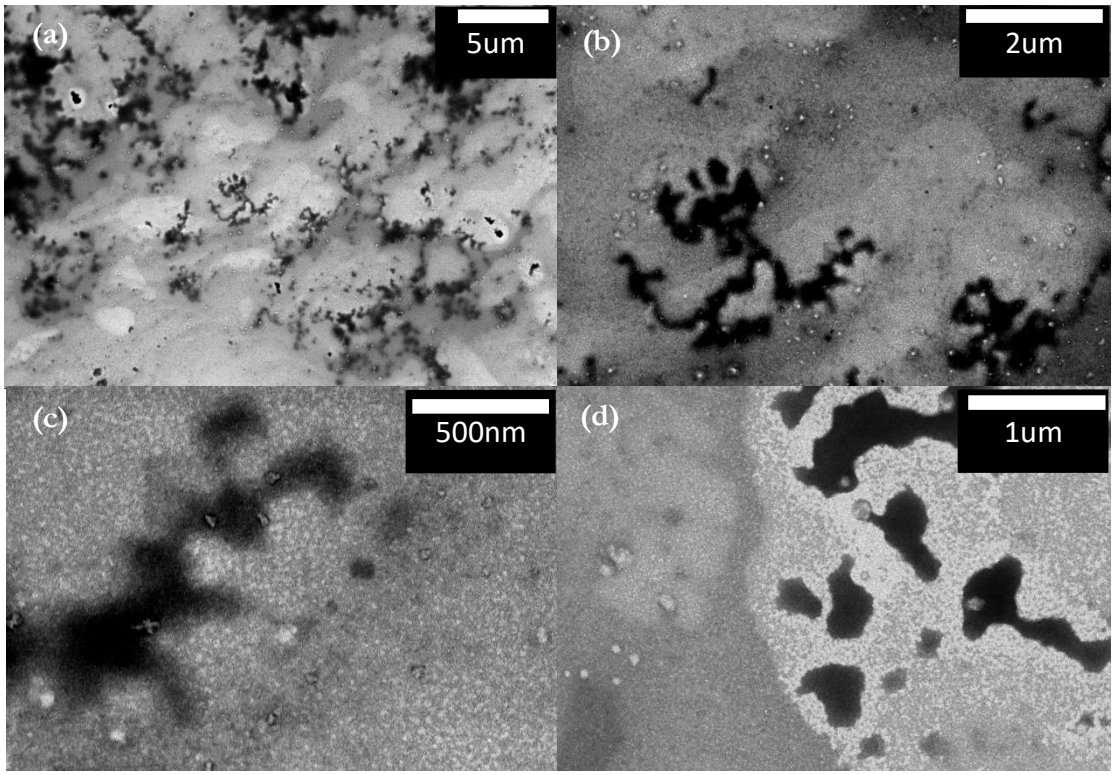

Figure 4.12: SEM images in transmission mode attempting to show the presence of particle within a water droplet present upon the grid.

A more appropriate method to observe the structures that these particles create upon agglomeration when heated would be cryogenic TEM. Unfortunately, due to time constraints this procedure could not be attempted

4.1.4.2 Thin Film Formation on Hydrophilic and Hydrophobic Surfaces

As observed in section 4.1.1 of this chapter the 7.5 nm 18-Crown-6-modified AuNPs tend to coat their external environment when heated above their transition temperature. In this section the observations of this film formation on both hydrophobic and hydrophilic surfaces will therefore briefly be discussed. In this case Highly Orientated Pyrolytic Graphite (HOPG) was used as the hydrophobic surface and Au coated glass as the hydrophilic surface. Both substrates were placed into the same particle solution at 5ºC. The solution was then steadily heated up to 50ºC, then cooled back down to 5ºC, at which point the two substrates were removed, rinsed with MQ water and allowed to dry at room temperature. Each substrate was then placed into the SEM and analysed under high vacuum with an electron beam of 10.00 kV, resulting in the images shown in Figure 4.13 and Figure 4.14.

Due to the hydrophobic nature of the surface of HOPG[47] the particles were expected to disperse across the surface in a relatively even distribution due their increase in hydrophobicity upon heating. The prediction appears to hold true in observation. Figure 4.13a shows the surface of the HOPG coated in the AuNP film, with a high density of AuNPs appearing in the crevices and shelves present upon the HOPG surface. On closer inspection of these higher density areas (Figure 4.13b) relatively smooth layers of AuNPs are seen to be present upon the surface; unfortunately, due to the handling of the HOPG (layers of HOPG placed upon scotch tape) the film of particles has become damaged during transport, resulting in the large cracks as seen in Figure 4.13c. Upon closer inspection of the more planar areas of the HOPG (Figure 4.13c) it is observed that whilst the density of gold particles is much reduced the formation in which the film forms remains the same. Whilst observing the build-up of large populations of AuNPs within the high energy crevices and shelves is still interesting, the coverage in these areas masks the underlying initial film formation, resulting in the lower populated planar areas of the HOPG providing greater insight into the formation of the film. It becomes obvious in Figure 4.13d that film that is created upon the hydrophobic surface of HOPG is very ordered and has extremely good surface coverage, with only a few small gaps exposing the underlying surface.

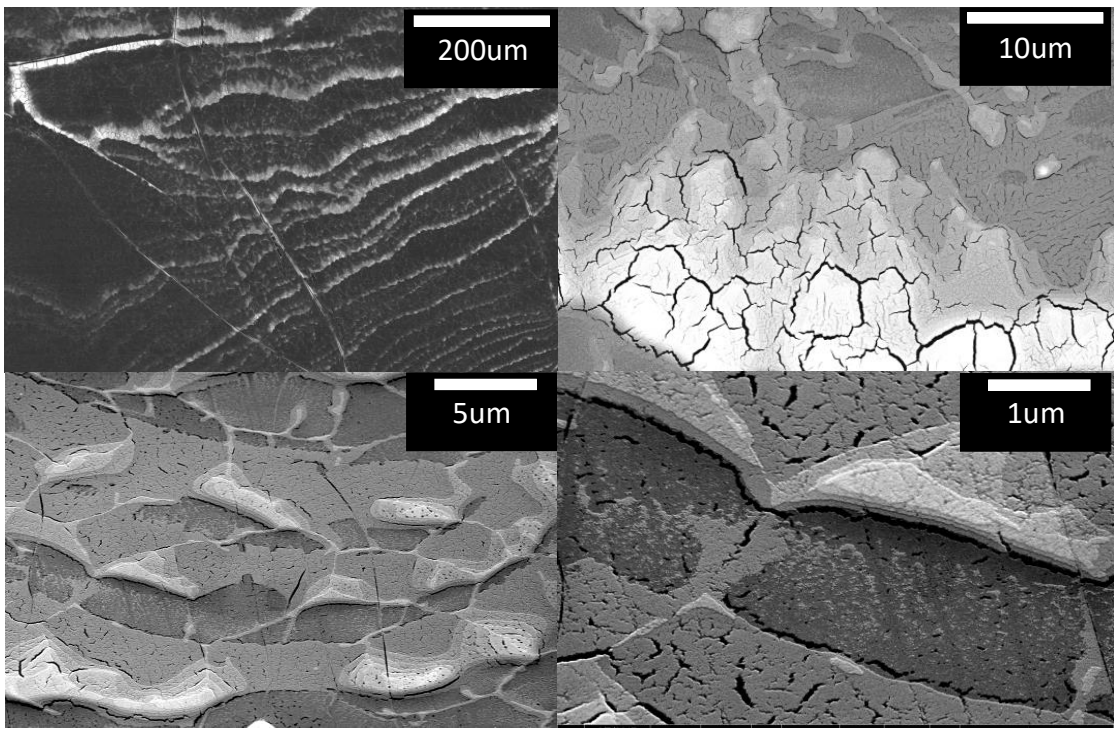

Figure 4.13: SEM images in reflectance mode showing the film formation of crown ether coated particles upon a HOPG surface.

When the particles were allowed to build up a film upon a more hydrophilic surface, in this case Au coated glass, the formation of the film changes drastically as can be seen in Figure 4.14a and b; rather than observing smooth layers of particles upon the surface we see the formation of varying sizes of "islands", the result of the particles being unable to effectively stabilise themselves upon the hydrophilic surface and agglomerating together in order to more effectively lower their energy. When attempting to resolve the film further by increasing the magnification it becomes increasingly difficult to distinguish between the substrate surface and the AuNPs (Figure 4.14c and d). This is a result of there being little contrast between the substrate surface (gold) and the AuNPs. This does not detract from the obvious differences between the two films however, with HOPG showing a strong degree of coverage with an overall smooth build-up of particles, and the Au coated glass showing the formation of islands across the entire surface where a large majority of the AuNPs agglomerate together.

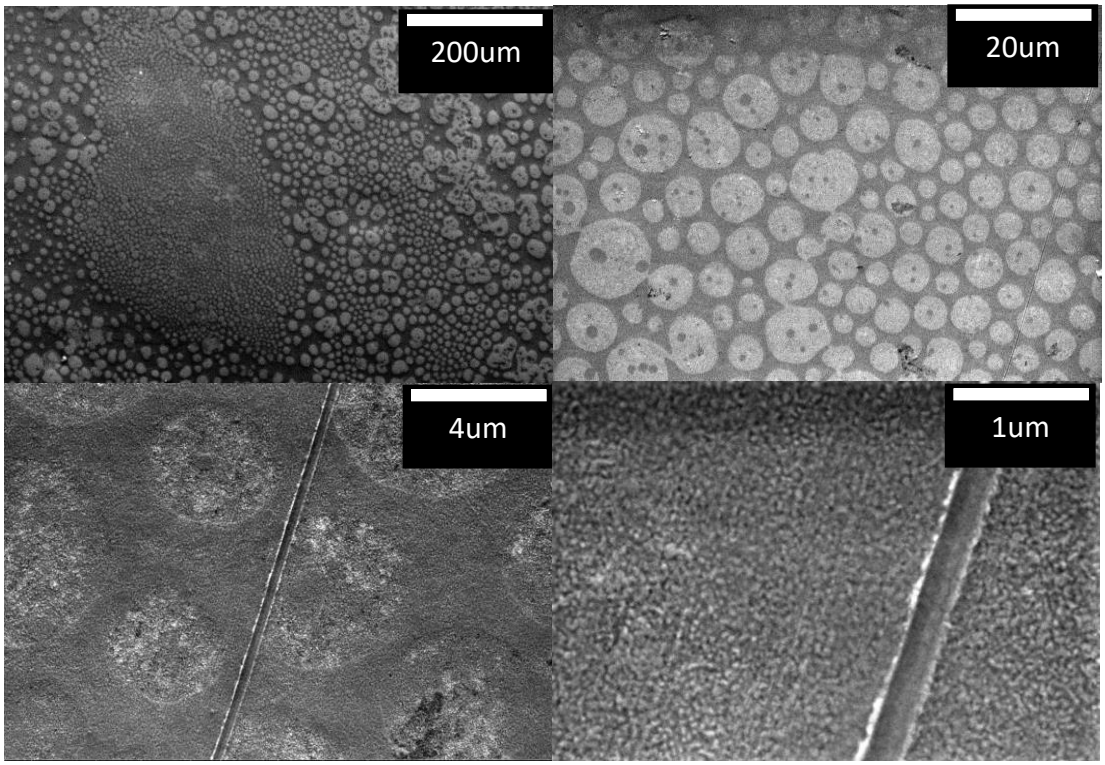

Figure 4.14: SEM images in reflectance mode showing the film formation of crown ether particles upon an Au coated glass surface.

In summary, it was possible directly to observe the change in the film formation structure of the AuNPs upon heating by changing the hydrophilicity of the substrate on which they form the film. This is what was expected due to the particles showing increased hydrophobicity upon heating and fits nicely with the overall data set collected.

4.1.5 Phase Transition Temperature vs Cation Complexation

As discussed in Chapter 1 of this thesis 18-Crown-6 has a strong degree of selectivity for binding to K^+ due to a multitude of reasons[28] including: 1) The cation-diameter-hole-size relationship, 2) The solvation enthalpies and entropies of the cation and ligand, 3) The number of donor atoms participating in binding, and 4) the conformation of the bound and unbound macrorings, but most noticeably the complementarity between the cavity size (260-320 pm) and the ionic radii of the K^+ cation (276 pm). This was further proved in Chapter 3 in this thesis when the change in zeta potential of 18-C-6-CH_2-SH coated 3 nm AuNPs in relation to selective cation binding and how that affected the rate of transfer between the aqueous and organic phases was observed. Now we shall move on to exploring how these complementary binding states affect the phase transition temperature of the larger 7.5nm 18-Crown-6-modified AuNPs.

The data shown in Figures 4.15 and 4.16 was obtained by the following experimental procedure:

Figure 4.15**:** An aqueous dispersion of 7.5 nm 18-Crown-6-modified AuNPs ($5.8x10^{13}$ Np/mL) was separated into six fractions of 0.5 mL, each being placed into a cuvette and left to equilibrate at 5ºC for 30 minutes. Concentrations of salt were added to the separate cuvettes in the following order, 0 mM, 1 mM, 2 mM and 5 mM of KCl, 1 mM NaCl and 1 mM LiCl. Each solution was thoroughly mixed for 1 minute and then left to equilibrate at 5ºC for 10 minutes.

Separately, each solution was placed into a water bath set at 5ºC, an initial UV-Vis spectrum was taken at this point. The temperature of the water bath was steadily increased by 0.5ºC a minute with a UV-Vis spectrum being taken at 5ºC intervals, the temperature intervals at which the UV-Vis spectra was taken was changed to 2ºC upon observing the beginning of the phase transition process. Once it was apparent that the phase transition was complete, the temperature interval was reverted to every 5ºC. The experiment was stopped after observing and extended period of no change within the plasmon peak.

Figure 4.16: An aqueous dispersion of 7.5 nm 18-Crown-6-modified AuNPs ($5.8x10^{13}$ Np/mL) was separated into three fractions of 1 mL, each being placed into a Lo-Bind Eppendorf (2 mL) and left to equilibrate at 5ºC for 30 minutes. Before addition of salt one of the solutions was placed into a DTS 1070 disposable cuvette and had the ζ measured for a minimum of 10 scans per run for three runs. This solution was then

removed and placed back into its Lo-bind Eppendorf. All solutions after the addition of salt were thoroughly mixed for 1 minute and left to equilibrate within the Zetasizer in a DTS 1070 disposable cuvette at 5°C for 5 minutes before measurements were taken, with each measurement having a minimum of 10 scans per run for three runs. To the first solution 0.25 mM of KCl was added and the ζ measured, the same solution had further additions of KCl resulting in final concentration of: 0.5, 1, 2, 4 and 8 mM of KCl with each concentration having the ζ measured. To the second and third solutions a similar approach was used as the first with the final concentrations being 1, 4 and 8 mM of NaCl and LiCl respectively.

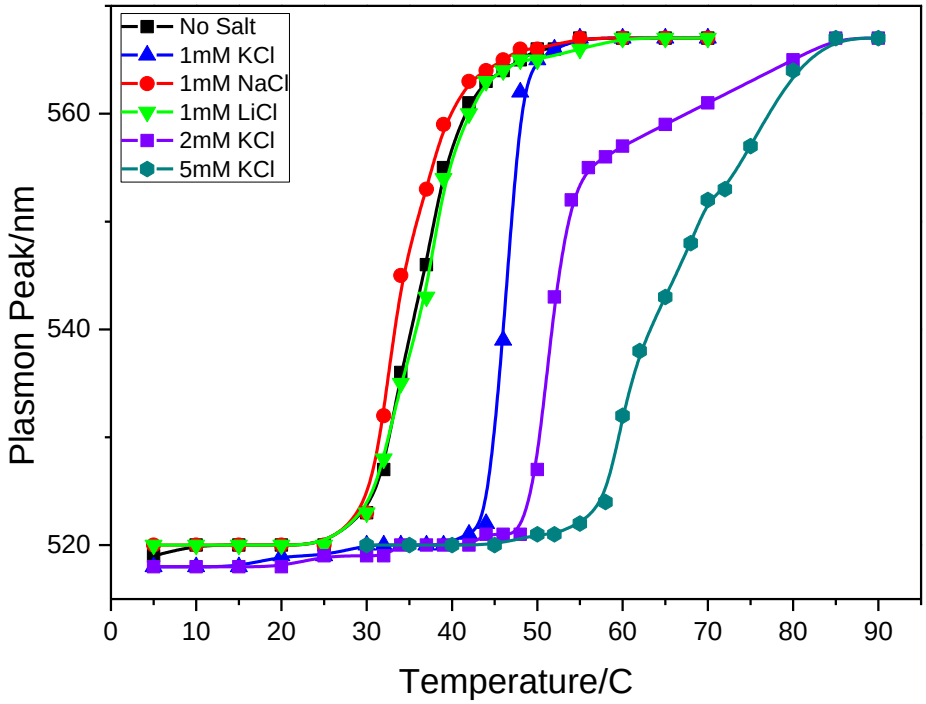

Figure 4.15: A graph showing the change in plasmon peak versus the change in temperature in the presence of different salt concentrations

It should be noted that the change in the plasmon peak wavelength observed within Figure 4.15 is not the change of the bulk solution into large agglomerates, as ~1000 nm particulates absorb within the UV-Visible spectra in the 700-900 nm range and typically show a very broad hump, as can be seen in Figure 4.3a at 35°C. What is being observed is believed to be the formation of more stable structures that builds up upon the surface of the cuvette, again seen in Figure 4.3a, which was explained as film formation. It was decided that due to the inaccuracy of attempting to obtain a plasmon peak from the broad hump of the large agglomerates, as well as the rapid sedimentation of such large structures, it was better to compare the build-up of the surface structures due to their

consistent nature and the fact that they are still entirely reversible (apart from the film), as seen in Figure 4.3a. The build-up of the surface structures is still entirely reliant on the temperature change as well as the salt present within the solution as the particles that cause it are still present within the bulk solution before they adhere, and so it was deemed to be a good indicator of the overall effect occurring in the bulk solution.

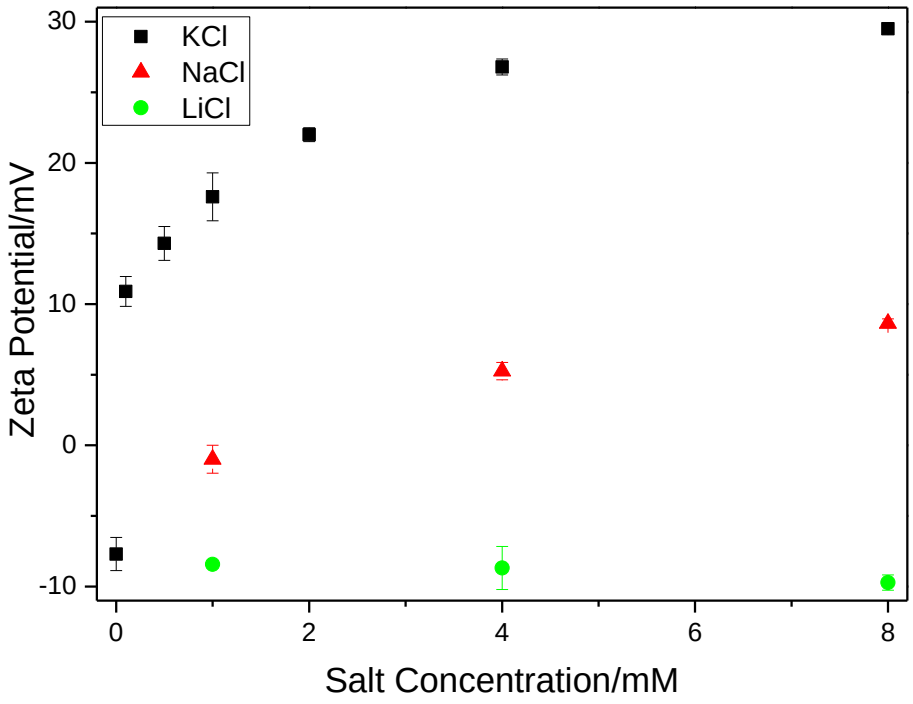

Figure 4.16: A graph showing the change in zeta potential of the crown ether nanoparticles when subjected to different salt concentrations.

In Figure 4.2 the AuNP solutions that have no salt, 1 mM NaCl and 1 mM LiCl have an initial phase transition point at 30ºC, with the centre point occurring at 35ºC for both no salt and 1 mM LiCl and at 33ºC for 1 mM NaCl. The phase transition then plateaus for all three solutions at 50ºC. This data coincides nicely with what was previously seen in Figure 4.3 where an obvious change in the solution is seen at 35ºC and then a dramatic change at 50ºC. By looking at Figure 4.16 the ζ of the particles with no salt present occurs at -7.7 mV. In the presence of 1 mM LiCl the zeta potential becomes slightly more negative at -8.83 mV resulting in practically no change, which was to be expected as seen in previous experiments in Chapter 3, Section 3.1.1, Figure 3.1, where very little binding of Li^+ was seen, which also agrees with the literature for 18-Crown-6 [48]The addition of 1 mM NaCl results in a small change in the ζ, going from -7.7 mV to -1 mV. This change

also agrees with data shown in Chapter 3, Section 3.1.1, Figure 3.1, where the slight binding of Na^+ is observed, which also agrees with the literature[48]. Interestingly it appears that the change in the phase transition temperature of the AuNP solution is related to the change in the ζ of the system, with the presence of LiCl showing no change in the phase transition temperature and the presence of NaCl resulting in a steeper phase transition slope as the ζ tends towards zero. This becomes especially obvious when observing the change in phase transition temperature in the presence of K^+, the cation that has the highest binding affinity to 18-C-6 as stated by literature and seen in Chapter 3, Section 3.1.1, Figure 3.1.

Upon the addition of 0.25 mM KCl a very large change in the ζ is seen, (-7.7 mV to +10.9 mV), a change that is in the order of magnitudes higher when compared to both NaCl and LiCl. Upon increasing the salt concentration to 0.5 mM KCl the ζ increases from +10.9 to +14.3 mV and when 1 mM of KCl is present the ζ becomes +17.6 mV, a change of 25.3 mV in total. Comparing this to the changes in ζ for NaCl and LiCl at 6.7 and 0 respectively it becomes obvious that these particles have a much higher affinity to bind K^+ over both Na^+ and Li^+ which was to be expected. What is interesting is that this large change in ζ has resulted in a large change in the phase transition temperature as seen in Figure 4.15 where the initial phase transition point has gone from 30ºC to 45ºC. In the presence of 2 mM KCl the phase transition temperature increased further to 48ºC (+22 mV), reaching 53ºC (+28 mV) when the 5 mM KCl is present, with the ζ for 5 mM KCl being calculated by observing the general trend of the ζ data.

With increasing concentrations of KCl the returns on the change in phase transition temperature gradually reduce. This makes sense with respect to the ζ as a saturation of the charge upon the particle as the ratio of crown ether is being seen; K^+ becomes overly large. This same trend was also observed for the 3nm particles discussed in Chapter 3.

Plotting the change in ζ (ΔZP) versus the change in phase transition temperature (ΔT), as seen in Figure 4.17, it is observed that the relationship between these two parameters is close to being linear; even with only three points present the strong correlation helps support the hypothesis on how this process is believed to occur. Unfortunately, it was not possible to add extra data points to the graph.

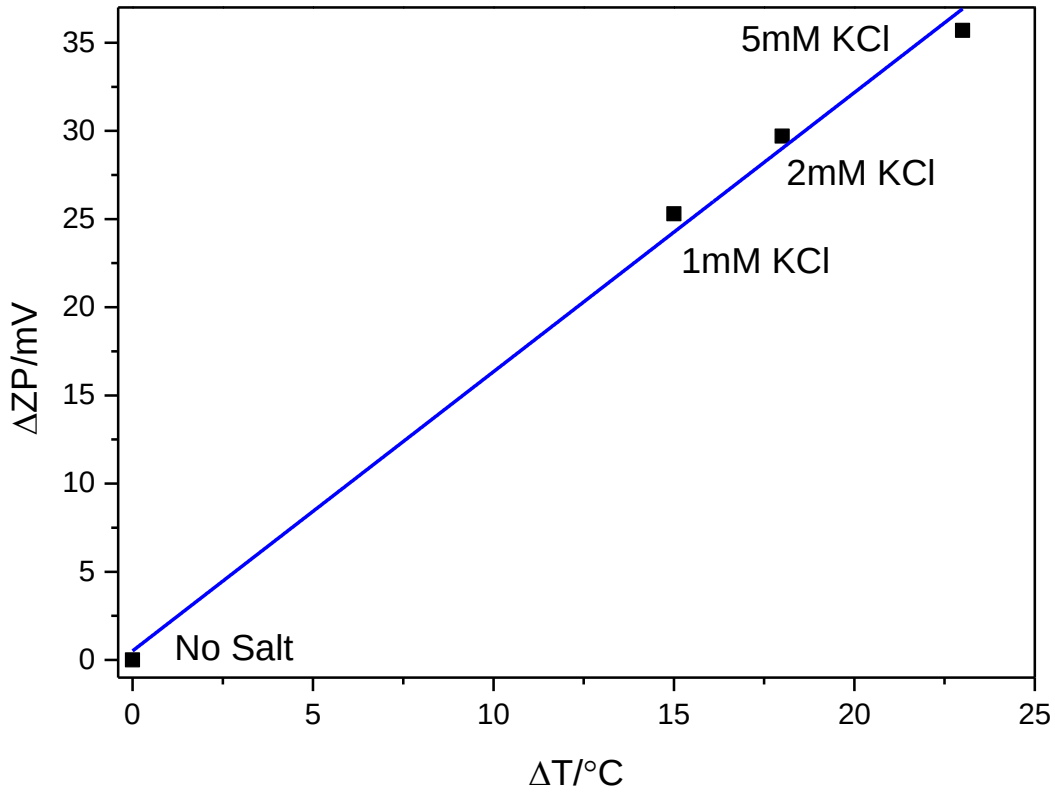

Figure 4.17: A graph showing the roughly linear trend between the changes in phase transition temperature and zeta potential when increasing concentration of KCl are present within solution.

What is nice about this system is that whilst other effects do most likely play a part, the major contributor that can explain the observations in the simplest manner is the hydrophobic effect. The hydrophobic effect describes the phenomenon whereby non-polar solutes present within water tend to separate out from the aqueous media. The unfavourable free energy change accompanying the dissolution of these non-polar solutes results from structural changes in the solvent around each solute molecule. The explanation behind this process is that the number of water molecules required to create an ordered solvent cage around two separate non-polar solutes is greater than that of having to create a solvent cage around two combined non-polar solutes. This is due to the reduced surface area of the solutes, resulting in an overall increase of free water molecules within the system resulting in an increase in entropy (ΔS) of the system, which readily obeys the second law of thermodynamics *"all spontaneous processes produce an increase in the entropy of the universe"*. This effect has long been recognised to be of great importance

in physical[49] [50]and bio chemistry[51] and this theory will now be applied in order to better explain the system in this chapter, and which is visually represented in Figure 4.18.

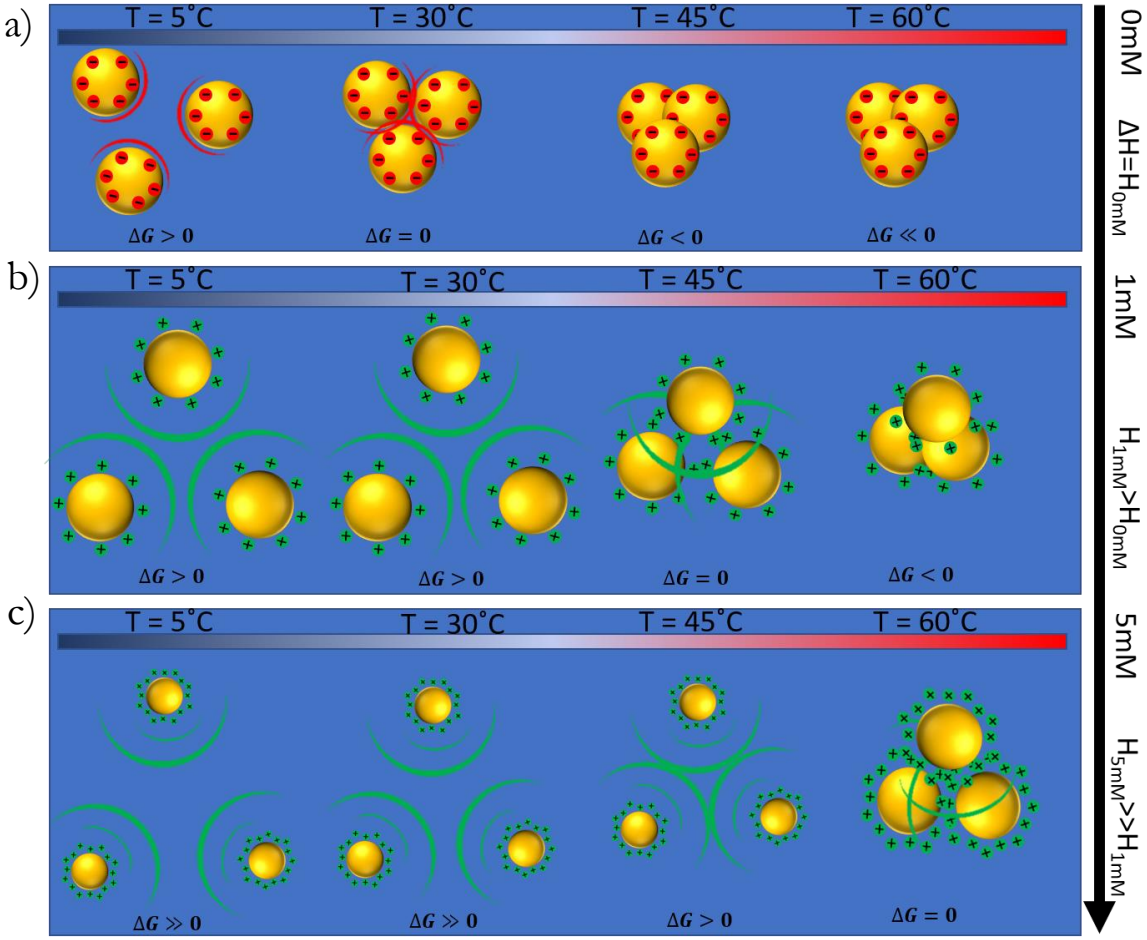

Figure 4.18: A schematic showing how the temperature at which the 7.5nm 18-Crown-6-modified gold nanoparticle undergo agglomeration is related to the concentration of KCl present at: a) 0mM, b) 1mM and c) 5mM. With the concentration of KCl directly altering the ζ of the particles, resulting in increased ⊿H values and therefore increased temperature to achieve agglomeration. This model assumes that the entropy of the system remains unchanged, at the point of discussing this work this value was not determined.

By taking the second law of thermodynamics:

$$\Delta S_{univ} = \Delta S_{sys} + \Delta S_{surr} \geq 0$$

and rearranging it such that:

$$\Delta S_{total} = \Delta S_{univ} = \Delta S_{surr} + \Delta S_{sys}$$

the formula for entropy changes in the surroundings, which is: $\Delta S_{surr} = \frac{\Delta H_{sys}}{T}$, can be applied which gives rise to the following equation:

$$-T\Delta S_{univ} = \Delta H_{sys} - T\Delta S_{sys}$$

which is better described as the Gibbs Free Energy Equation:

$$\Delta G = \Delta H - T\Delta S$$

With this equation the agglomeration process of the 18-C-6-CH_2-SH coated 7nm AuNPs can be explained.

As discussed in Chapter 1 of this thesis the stabilisation of gold nanoparticles in solution is not trivial; exposed metal cores of such sizes naturally occupy a high energy state and so will gather together to lower their energy state. To prevent this process, capping agents must be present around the particle resulting in energy being required to overcome this new boundary being greater than the energy release upon combining. The enthalpy (ΔH) of such systems is positive and, as such, energy must be placed into the system to overcome the stabilisation boundary. It is easy to therefore state that the AuNP system must also have a positive ΔH, seeing as the AuNPs are being stabilised by the presence of the thiolated crown ether.

It has already been made clear with the data shown in this chapter so far that the AuNPs are stable in solution at cooler temperatures, and agglomerate in much larger structures at high temperatures. By applying the Gibbs Free Energy Equation and knowing that a process is only spontaneous when $\Delta G \leq 0$ it can be surmised that the entropy changes of the system (ΔS) is positive. This fits in with the original discussion of the hydrophobic effect whereby the agglomeration of the AuNPs in solution results in an increase in the number of free water molecules present within the system, giving a positive ΔS. Now that the base states both ΔH and ΔS has been determined it is possible better to explain why the phase transition temperature increases with increasing concentrations of complementary cations (K^+) present.

As previously discussed in Chapter 3, Section 3.1.1 we know that the charge of the AuNPs in solution is altered in the presence of a complementary cation, with the charge tending towards positive. This is strongly reinforced by the zeta potential results obtained within this system, Figure 4.16; the increase in charge surrounding each particle will result in an increased electrostatic repulsion between a singular particle and its neighbours, which can be better described as an increase in the value of ΔH for the system. If the value of ΔH

within the AuNP system becomes more positive, then either the temperature (T) or ΔS of the system must also increase in order to make $\Delta G \leq 0$.

At present time it is being assumed that the overall entropy of the system remains constant, and so the only parameter that can change is T. This fits perfectly with the current set of experiments. It is seen that the system requires an increase in T to make the agglomeration process spontaneous when the charge of the nanoparticle becomes more positive.

To gain a better understanding of the system an attempt was made to obtain quantitative values for ΔG, ΔH and ΔS via the use of Isothermal Titration Calorimetry (ITC).

4.2 Isothermal Titration Calorimetry (ITC)

The previous section of this chapter described how the change in phase transition temperature for the reversible agglomeration of the 7.5 nm 18-Crown-6-modified gold nanoparticles was due to cation association with the crown ether moiety, resulting in an increased electrostatic repulsion between the particles. This process was then postulated to correlate well with the Gibbs free energy equation, ITC analysis would therefore prove useful in attempting to fully understand the energetics occurring within the nanoparticle system and provide greater insight into further understanding how to utilise the system for cation transport across membranes.

The following procedure was followed to obtain the preliminary ITC data showing in this section: A standard volume (1.2 mL) 24 carat gold isothermal chamber within a NanoITC calorimeter was rinsed thoroughly with both water and ethanol (300 ml) using a specialised vacuum pump related to the machine. Once cleaned the 24 carat 1.2 ml reference cell was filled with fresh Milli Q water, followed by the insertion of a metal syringe needle to mimic the presence of the injection syringe within the main cell. 1.2 ml of fresh milli Q water was slowly injected into the analysis cell, taking care to prevent the formation of any air pockets. A specialised interval injection syringe was then filled with 11.6 mM KCl solution and carefully placed into the analysis cell. The syringe was set to stir at 400 rpm and the system was left to equilibrate for 45 minutes at 45°C. Upon completion the injection process was initiated, with 15.1 uL of 11.6 mM KCl solution

being injected every 5 minutes for a total of 15 injections. Upon completion of the procedure the results were analysed using the NanoAnalyse software.

The same procedure as above was repeated except instead of 1.2 ml of Milli Q water being injected into the analysis cell, 1.2 ml of 7.5 nm 18-Crown-6-modified AuNPS ($1x10^{15}$ Np/mL) was injected instead.

The goal of the above experiments was to determine whether the system can detect the reversible agglomeration process that occurs during the phase transition point of the particles, this was achieved by slowly raising the salt concentration of the solution above the determined concentration of salt required for the particles to phase transition after 45°C (Figure 4.15), which was just over 1 mM in concentration. The reason why fresh water was used first was as a control experiment. The injection of dissolution peaks as the two fluidic volumes mix together and equilibrate. The control experiment was needed to confirm whether the peaks observed during salt injection were that of crown ether-cation association, or just salt dissolution peaks.

The data for these two experiments can be seen in Figure 4.19 and Figure 4.20.

Figure 4.19 shows that upon injection of 11.6 mM KCL solution into pure water within the NanoITC we observe what can be only be attributed to dissolution peaks, with initial injections resulting in nearly 90 uJ input from the machine to retain the same temperature of 45°C. It can also be observed that as the experiment progresses with increasing injections the total amount of energy input necessary to retain the same temperature reduces, this is due to the concentration gradient of KCl between the two solutions reducing as more salt is present within the analytical cell already. It was confirmed by this control experiment that the injection of 11.6 mM KCl will certainly result in dissolution peaks when it comes to running experiments with the particles also present.

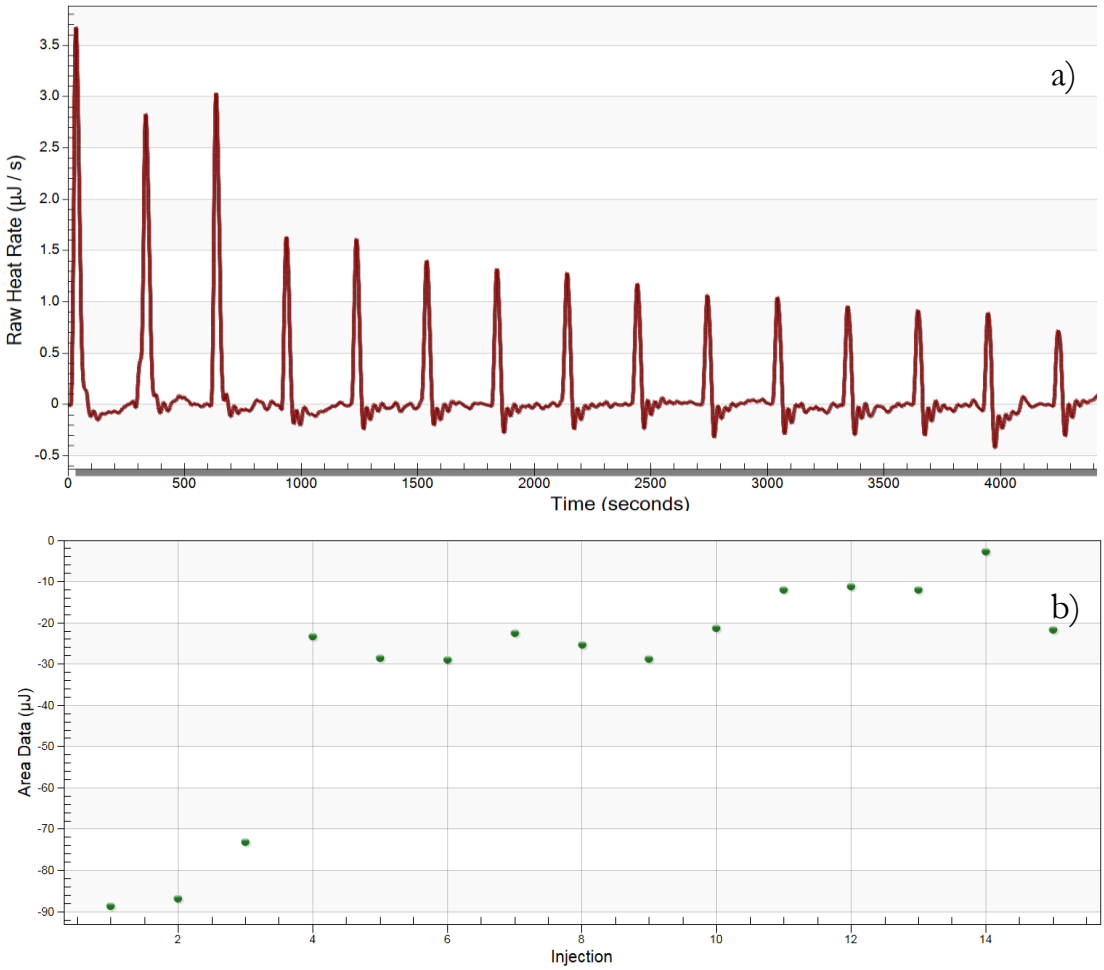

Figure 4.19: ITC data showing: a) The raw heat rate (uJ/s) of injecting 11.6mM KCl solution into pure water (1.2ml), in 15.1uL intervals every 5 minutes, b) The total energy amount of energy per injection (uJ) the ITC system had to input to retain an equivalent temperature to the reference cell.

Figure 4.20 shows how the system changes when in the 7.5 nm 18-Crown-6-modified AuNPs are present within the analysis cell, not only was it hoped to observe a dramatic change in the initial injection peaks in order to indicate a binding association between the crown ether moiety and the complimentary cation, but also to observe a change around injection 7, 8 and 9 (1800s-2500s) as this would be the point where the particles are suitably complexed with K^+ that they become stable at 45°C. Unfortunately, neither of these observations appear to have occurred. The overall trend of the injection data follows that of the control experiment shown in Figure 4.19, with initially large peaks followed by a gradual decline and plateau. There are a few minor changes in the system such as the overall energy input requirements for the first few injections (60uJ) being lower than that of the control experiment (~90 uJ), and the peaks in the final series of injections showing an increased energy input (~25 uJ) compared to the control

experiment (~10 uJ). It should also be noted at this point that the solution that came out of the cell upon removal was bright red, indicating that the particle had indeed de-agglomerated over the course of the experiment.

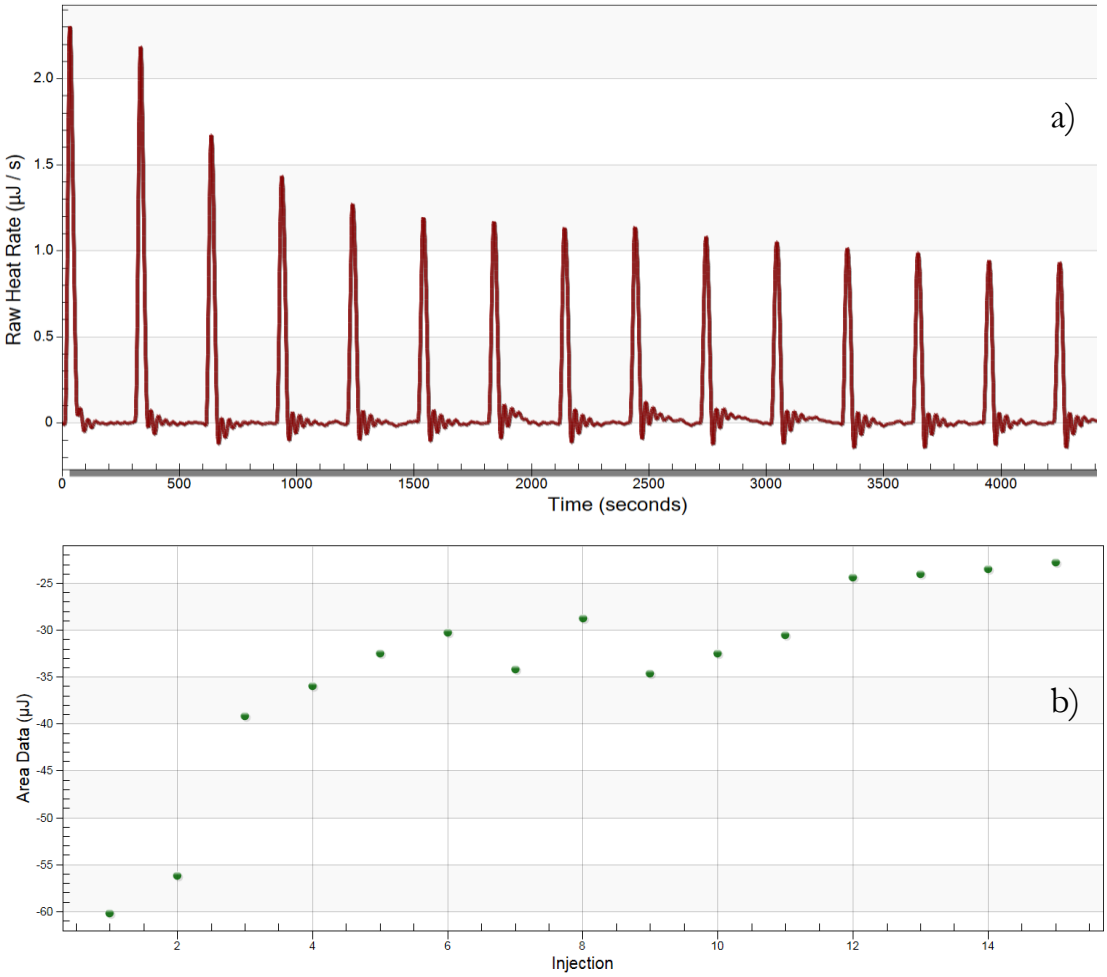

Figure 4.20: ITC data showing: a) The raw heat rate (uJ/s) of injecting 11.6mM KCl solution into 7.5nm 18-Crown-6-modified AuNPs ($1x10^{15}$) (1.2ml), in 15.1uL intervals every 5 minutes, b) The total energy amount of energy per injection (uJ) the ITC system had to input to retain an equivalent temperature to the reference cell.

There are multiple potential causes for the experiments described above to have not given rise to any significant temperature changes within solution. The first reason is that the amount of time spent working with the machine was extremely limited, and therefore experience in refining parameters to produce a substantial result was lacking. This was especially prevalent due to the complexity of the system that was being investigated. The second reason could simple be that the machine is not sensitive enough to detect these changes that are experienced by the nanoparticles. The concentration of nanoparticles within the solution is in nano molars, resulting in the estimated crown ether concentration being approximately 10-50 uM. Literature has shown that even with 0.5 mM of 18-

Crown-6 present in solution[52, 53] the associative binding constant between it and complimentary cations is challenging to observe. Unfortunately creating more concentrated stocks of the 7.5 nm 18-Crown-6-modified AuNPS is not trivial. Centrifugation of the colloidal solution typical results in a noticeable loss of particles due to the difficulty of pelleting them completely, the amount of processing that was required to increase the concentration of the stock solution by ~20% was not considered valuable enough to follow for this thesis work. The final reason is that the particles are within an environment that has never been directly observed throughout the rest of this research. The presence of a pure gold surface could influence the interaction between the particles, or perhaps the syringe being present in solution throughout the entire injection process.

Another potential cause for not being capable of observing any notable temperature changes within solution is that the agglomeration process is not a first order phase transition but a second order phase transition. First order phase transitions result in a rapid (and normally large) change in the thermodynamics of the system. The change in phase occurs at the critical temperature (Tc) and so a large amount of energy is gained/lost at a singular point in time, resulting in an observable thermodynamic change. For second order phase transitions the order parameter rises continuously from zero up to the Tc and has a continuous entropy at Tc. What this physically means is that the change from one phase to another occurs very smoothly and does not change the thermodynamics of the system abruptly, making it challenging to see the change in conventional systems.

So, preliminary analysis using ITC to gather more definitive details upon the enthalpy and entropy of the 7.5 nm 18-Crown-6-modified AuNPs proved unsuccessful. This does not mean that the technique should not be pursued further however, with more experience in the technique combined with an appropriate amount of time could bear fruit for this system. With the hope of further validating that this system does indeed correlate well with the Gibbs free energy equation.

4.3 Cryo-TEM of 7.5nm 18-Crown-6-modified Gold Nanoparticles

In previous sections of this chapter it is discussed as to why the 7.5 nm 18-Crown-6-modified gold nanoparticles exhibit reversible agglomeration with increasing temperature. With the particles coming together at higher temperatures to produce more favourable larger agglomerates in solution. The observation that during these agglomeration cycles particle that are near an external surface, such a glass/plastic container will readily adhere to them, forming thin films. It is thought that these particles are doing so to experience a less polar surface than that of the water molecules in solution. If this is the case, then the presence of vesicles within the system could result in the 7.5 nm 18-Crown-6-modified gold nanoparticles interacting with the membrane instead of themselves/container surfaces.

The experimental tools used for this experiment are laid out in Chapter 3, Section 3.7.1 with the following modifications. 0.5 mM of vesicles stock (2x250 ml) were placed into separate Lo-bind Eppendorfs, $4x10^{14}$ NP/ml, 100 uL of 7.5 nm 18-Crown-6-modified gold nanoparticles was added to each vesicle solution at 10ºC. The solutions were mixed thoroughly and left to incubate for 1 hour; after this period one sample was prepped for Cryo-TEM whilst the other was quickly heated up to 50º and left to incubate further for 10 minutes. After this period the sample was also prepped for Cryo (Section 3.7.1).

The highest quality images obtained from this experiment are shown in Figure 4.21. Figure 4.21a shows the 7.5 nm 18-Crown-6-modified gold nanoparticle left to incubate at only 10ºC. The image shows the majority of the particles surrounding the carbon film edge, with a minute number of particles seemingly associating with the vesicles. This fits well with previous data as at 10ºC the particles are stable within aqueous media.

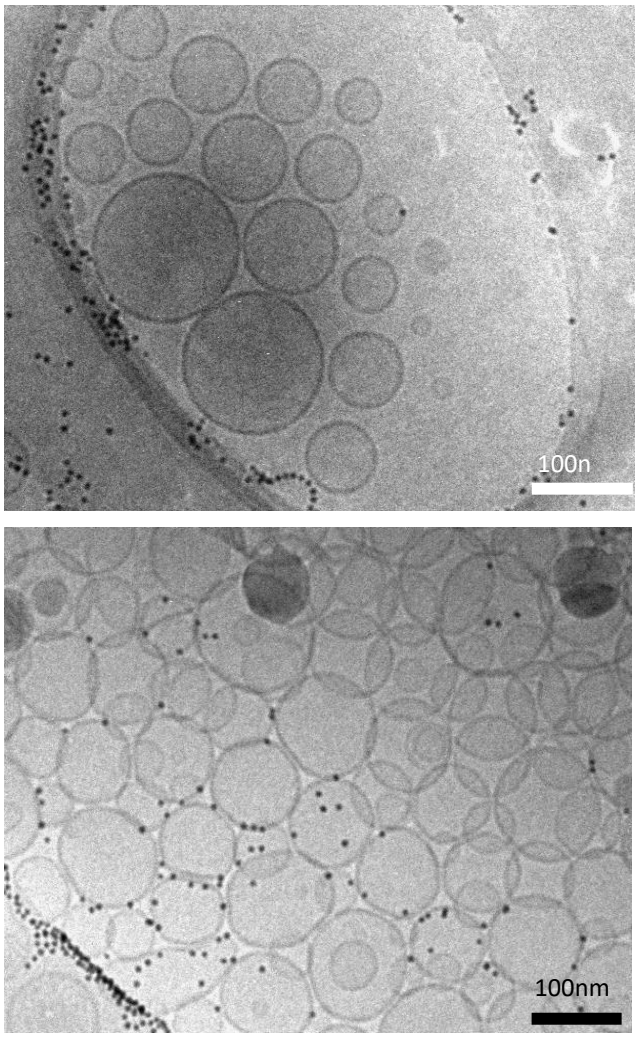

Figure 4.21: Cryo-TEM pictures showing the change in interaction between 7.5nm 18-Crown-6-modified gold nanoparticles and the membranes of vesicles when: a) The particles are incubated at 10ºC for 1 hour, b) The particles are incubated at 10ºC for 1 hour and then a further 50ºC for 10 minutes.

The behaviour of the particle is seen to change in Figure 4.21b, where the sample was left to incubate for a further 10 minutes at 50ºC, whilst there still appears to be a large number of particles presenting themselves at the carbon film coating the TEM grid there is a much more prominent number of particle seemingly associating with the vesicle membranes; Indicating that if the 7.5 nm 18-Crown-6-modified gold nanoparticle is heated up with organic interfaces present then they are capable of associating with them.

Association between the vesicle membranes and 7.5 nm 18-Crown-6-modified gold nanoparticles could prove useful in achieving both cation and electron transport through an artificial membrane as being able to successfully incorporate the particle into the membrane at increased sizes was proving a challenge. From previous TEM imaging showing the particles at 50ºC to be forming large complexes it was a bit surprising to see

that the particles that were not directly associated with the vesicle membranes did not have the agglomerated clumped up line structures as previously discussed within the chapter. It is believed that this is attributed to the preparation time required to get the sample ready for freezing, typical taking 5 minutes, a droplet of 10 uL in size could easily dissipate heat within that time, especially when in contact with a metallic TEM grid. As the agglomeration process is reversible the lower temperature droplet would now have singular particles existing once again, such as those observed within Figure 4.21b.

Unfortunately, due to time constraints, further work and Cryo-TEM imaging was unable to be achieved for this section of the research, nevertheless, this potential association of the 7.5 nm 18-Crown-6-modifed gold nanoparticles when cycling the temperature of the solution could be useful in furthering the development of a particle capable of achieving both cation and electron transport through an artificial membrane.

4.4 Phase transfer of 7.5nm 18-Crown-6-modified Gold Nanoparticles

With the development of the 7.5 nm 18-Crown-6-modified AuNPs resulting in not only a stable colloidal system when using only the crown ether ligand, but also the potential for successful integration into phospholipid bilayers via just a change in the temperature of the solution; the ability of the particles to achieve a similar effect but via the use of complementary cations came into question.

To effectively build an understanding of whether the 7.5 nm 18-Crown-6-modified AuNPs could achieve this, preliminary experiments like those seen in chapter 3 for the 3 nm 18-Crown-6-modified AuNPs had to be completed.

4.4.1 Phase Transfer in the Absence of Salt

A 1 ml solution of 18-Crown-6-modified gold nanoparticles ($4.0x10^{14}$ Np/mL) synthesised as stated in Chapter 2 of this thesis was placed on top of 1ml of chloroform within a glass vial (4 mL) followed by observation via optical imaging over the course of 6 hours, with these images being shown below in Figure 4.22.

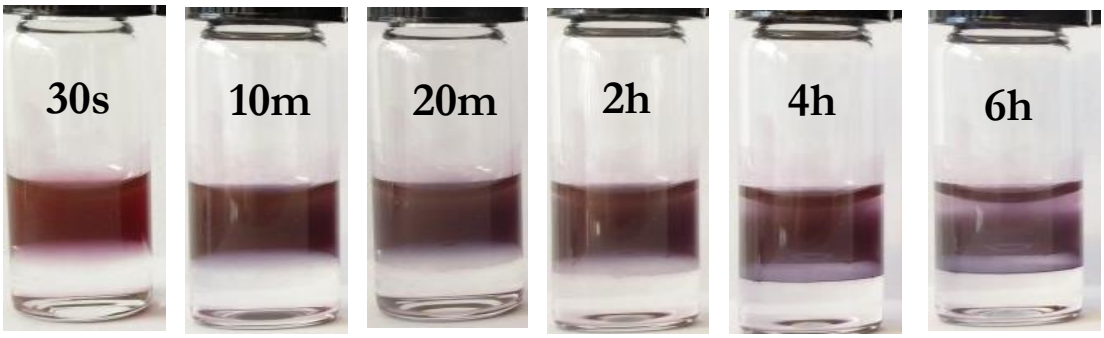

Figure 4.22: Attempted phase transfer of 7.5nm 18-Crown-6-modified gold nanoparticles in to chloroform in the absence of complementary salts.

Interestingly rather than the particles remaining stable in the aqueous phase, or moving gradually to the organic phase, it is observed that the colloidal system slowly destabilises within the aqueous phase over time, with the deep red solution gradually turning purple, followed by the gradual precipitation of the particles upon the interface. A similar interaction was observed with the smaller 18-Crown-6-modified gold nanoparticles presented in Chapter 3 when in the absence of salt, with a gradual precipitation of the particles upon the interface, but in this case, there was no obvious change in colour. This was attributed to two major differences between the colloid systems: 1) The zeta potential (ζ) of the larger particles is -7.72 mV whilst the ζ of the smaller modified particles is -33 mV, so in the absence of salt the larger particles are less inclined to stay within the aqueous phase, 2) The difference in size between the two particle systems, resulting in a much more dramatic change in colour due to the extinction coefficients of the constituent plasmon resonances. This process is not due to an inherent instability when in the presence of chloroform however. Within section 4.1.1 of this chapter showed that a thin film formed during temperature cycling in water can easily be dissolved in chloroform, resulting in a stable colloidal solution which is identical to the original water colloid system. What is believed to be occurring here is the diffusion of a small quantity of chloroform into the aqueous phase (chloroform has a solubility of 8.09 g/L at 20ºC); due to the preference of the particles for the chloroform phase they start to crowd around the chloroform molecules, resulting their gradual agglomeration. This is an effect very similar to that seen when these particles are heated past their phase transition point, turning purple as large agglomerates begin to develop.

4.4.2 Phase Transfer in the Presence of K+, Na+ and Li+

With the phase transfer behaviour of the particles in the absence of salt observed to show no transfer, only destabilisation and sedimentation, the next step was to determine whether the particles behave similarly to their small counterparts when in the presence of their complimentary cation (K^+) as well as the other two most prominent alkaline salts, Na^+ and Li^+.

The experimental for the following experiment is the same as stated in section 5.1.1 except 1 mM of the desired salt was added to each solution. The results are shown in Figure 4.23.

It becomes immediately apparent that the presence of the different salts causes a substantial change in relation to the absence of salt and effectiveness of phase transfer. When in the presence of the complimentary salt (K^+) the solution retains its ruby-red colouration, followed by a very gradual transfer of the particles into the chloroform phase. Conversely, the presence of Na^+ not only results in a seemingly quicker destabilisation of the colloidal solution within the aqueous phase, but also a very prominent transfer of the solution into the chloroform phase. A similar effect occurs in the presence of Li^+ but the overall rate of transfer is slower with respect to Na^+ addition.

The changes in the interactions of the particles with the organic interface become much clearer when referring to Figure 4.16 in Section 4.1.5. The addition of 1 mM of K^+ results in a $\Delta\zeta$ of -7.72 mv to +17.6 mV, indicating that the crown ether has readily taken up K^+ into its cavity and subsequently developed a positive charge (for a more detailed hypothesis of why this potentially occurs please see Chapter 3, section 3.1. With such a high affinity for K^+ resulting in the crown ethers located upon the gold surface saturating their cavities, hence resulting in such a high charge, the solution is now no longer as influenced by the chloroform interface, or chloroform solutes, within the aqueous phase, resulting in a highly stable colloidal solution with a gradual diffusion process very similar to that as seen by the smaller 18-Crown-6 modified gold nanoparticles discussed in Chapter 3.

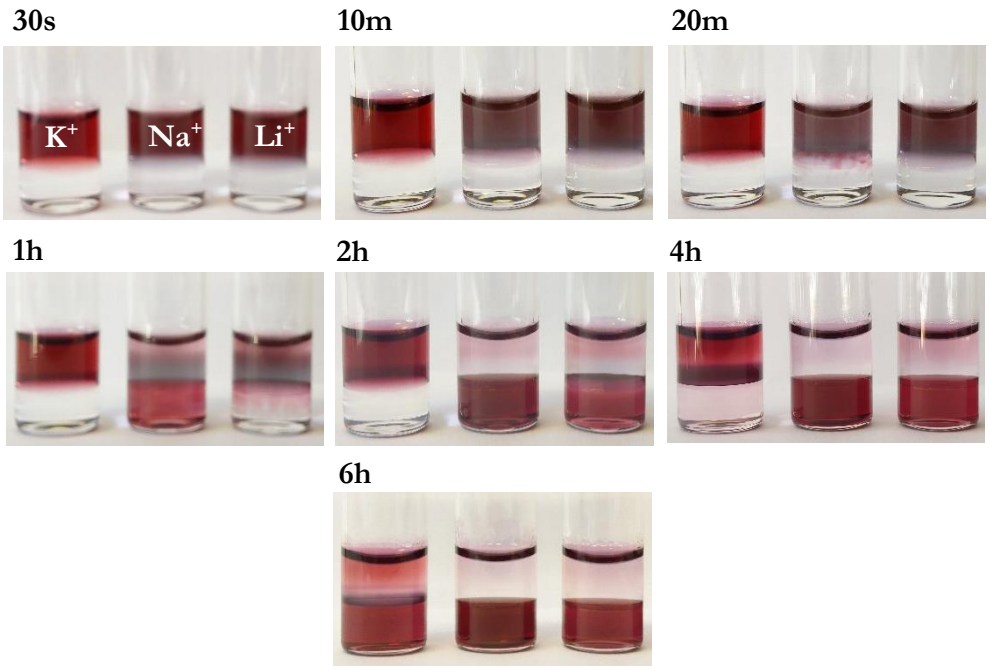

Figure 4.23: Optical Images showing the phase transfer of 18-Crown-6-modified gold nanoparticles when presented with K^+, Na^+ or Li^+ and left for a period of 6 hours.

The most interesting observation of these phase transfer experiments is the relatively fast rate of phase transfer for the Na^+ system. This can be attributed to the $\Delta\zeta$ observed in Chapter 4, Section 4.1.5, Figure 4.16, resulting in a $\Delta\zeta$ of -7.72 mV to -1 mV. The lower-degree complexation within the presence of Na^+ results in a ζ that is much closer to zero. This gives rise to an increase in the particle hydrophobicity, lowering the energy barrier associated with interacting and crossing the aqueous-organic interface, resulting in the increased rate of aggregation and phase transfer. In the case of the Li^+ system the $\Delta\zeta$ is negligible, giving rise to a similar ζ as seen in the absence of any salt. Interestingly the particles still start to phase transfer quite readily into the organic phase, unlike the system without any salt. This was an unexpected observation as it sits outside the expected behaviour of the particles from what has been seen before. A theory to potentially describe this unique behaviour could be that even though there seems to be very little association between the 18-Crown-6-modified gold nanoparticles and the lithium, there is enough interaction with the oxygens within the crown ether ring to lower the energy requirements for phase transfer, allowing for the particles to push through the interface rather than sit upon it. Unfortunately, this property was not able to be researched further and shall have to be undertaken at a later date.

The result of this preliminary experiment is that the 7.5 nm 18-Crown-6-modified AuNPs are still capable of transferring to the organic phase (whilst retaining stability within the aqueous phase) when in the presence of K^+, whilst Na^+ and even Li^+ resulted in faster rates of transfer, the loss of stability within the aqueous phase is an unwanted side effect. With the ability to transfer ions cross phase boundaries confirmed, the next logical step was to see if the property that these particles were made for, their ability to more effectively conduct electrons, could be exploited.

4.4.3 Phase Transfer with Ba^{2+} and Potassium Ferro/Ferri cyanide

Previous results discussed in Chapter 3, Section 3.2, Figure 3.15 show that 18-Crown-6 is also capable of readily binding Ba^{2+}. Ba^{2+} can be readily exploited as a strong exothermic reaction, or downhill reaction, by allowing it to form the highly stable complex $BaSO_4$. Should the particles be capable of transporting Ba^{2+} from one confined aqueous phase to another, one containing the SO_4^{2-} anion, then the first stage of coupling a downhill process to an uphill process is complete.

Another important aspect of this postulation is to find a suitable redox couple to attempt to combine the downhill reaction of the $BaSO_4$ formation with the uphill process of electron transfer. In this case potassium ferro (II)/ferri (III) cyanide was determined to be the most viable candidate due to a combination of factors such as solubility in aqueous media, stability in the presence of oxygen, price and a relatively low redox potential (E_0') of +0.43 V at 30ºC[54-56]

The experimental for the following procedure is the same as stated in Section 4.4.2 with the following changes: No salt, 1 mM $BaCl_2$, 1mM potassium ferro (II) cyanide, 1 mM potassium ferri (III) cyanide, 1 mM $BaCl_2$ + 1 mM potassium ferro (II) cyanide, and 1 mM $BaCl_2$ + 1 mM potassium ferri (III) cyanide were added to separate vials. The results of this phase transfer experiment are shown in Figure 4.24

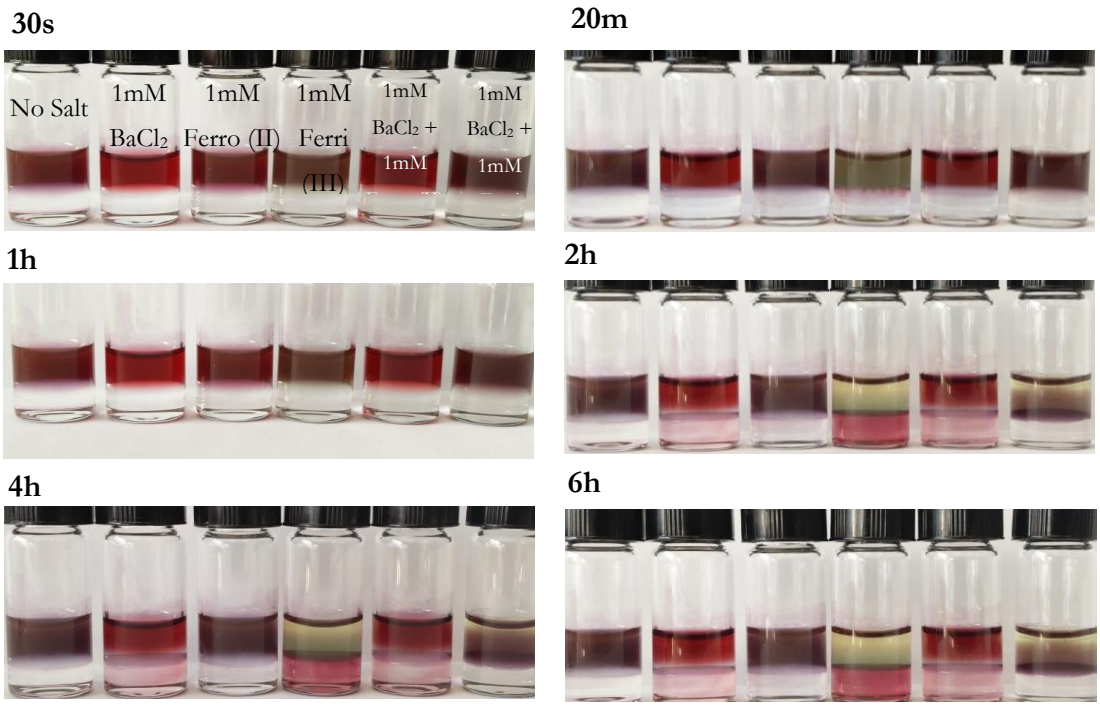

Figure 4.24: Optical images showing the effect of $BaCl_2$ and the potassium ferro (II)/ferri (III) cyanide compounds upon the aqueous phase stabilisation and the rate of phase transfer into the chloroform phase. From left to right: No salt, 1mM $BaCl_2$, 1mM potassium ferro (II) cyanide, 1mM potassium ferri (III) cyanide, 1mM $BaCl_2$ + 1mM potassium ferro (II) cyanide, 1mM $BaCl_2$ + 1mM potassium ferri (III) cyanide.

With no salt the present the 18-Crown-6-modified gold nanoparticles behave as seen previously, with no phase transfer and gradual stabilisation within the aqueous phase.

In the presence of $BaCl_2$ the particles behave similarly to those in the presence of K^+, with the colloidal solution showing increased stability when in the presence of the chloroform phase followed by a gradual phase transfer into the organic phase.

When subjected to potassium ferro (II) cyanide the colloidal solution behaves almost identically to the system with no salt present within solution, showing no sign of phase transfer and destabilisation within the aqueous media; with the counterion of the ferro (II) cyanide being potassium it was slightly unexpected to see practically no change in the system whilst the complimentary cation was present. This could mean one of two things: 1) The ferro (II) complex's association to its K^+ counterions is greater than that of the binding energy gained by associating within the crown ether cavity, essentially ignoring the crown moiety entirely, or 2) The crown ether moiety is picking up the K^+ counterions but is combined with the donation of an electron from the ferro (II) cyanide complex,

resulting in the formation of ferro (III) cyanide. Current observations would suggest that it is the first of the two as no colour transition to yellow (the colour of Fe (III)) was observed in the aqueous phase after 24 hours. It should be noted, however, that this does not prove that the latter effect is not occurring as the concentration of crown ether within the colloidal solution is barely into the μM range so the amount of ferro (II) converted to ferri (III) would be extremely small.

In the presence of potassium ferri (III) cyanide the colloid shows a dramatic increase in the rate of destabilisation, with the particle aggregating and settling upon the aqueous-organic interface 20 minutes after addition. The particles then swiftly disperse into the chloroform phase, with there being no sign of any particles left in the aqueous phase after 6 hours.

The combination of $BaCl_2$ and potassium ferro (II) cyanide results in a similar process as seen when the particles are in the presence of just Ba^{2+}; Similar to the addition of just ferro (II), which resulted in very little change from when no salts were present within solution. Indicating that there is very little to no interaction between the AuNPs and the potassium ferro (II) cyanide complex. Why there is such a drastic change in behaviour in the AuNPs when interacting with the redox couple is currently not known and should be researched further to fully understand the system and allow for progress to be made in coupling the redox couple with the formation of $BaSO_4$

The combination of $BaCl_2$ and potassium ferri (III) cyanide shows a dramatic change in the overall process, with the particles aggregating and eventually resting upon the aqueous-organic interface with no indication of transferring to the organic phase. The reduced rate of destabilisation within the aqueous phase with respect to the sample containing only ferri (III) cyanide indicates that the crown ether moiety upon the particle surface is still achieving complexation with Ba^{2+} but becomes overwhelmed by the degree of destabilisation caused by the presence of ferro (III) cyanide resulting in the precipitation of the particles. These two effects are counteracting one another in such a way that the particles are no longer stable within either media and so results in the sedimentation layer seen in Figure 5.3. The mechanism for this process is once again not entirely understood. There are some odd but interesting interactions occurring within these preliminary phase transfer experiments, some of which could potentially lead to a successful fusion between electron and cation transfer via the use of these 7.5nm 18-Crown-6-modified AuNPs, research to be undertaken at a later date.

4.5 Summary

The purpose of this chapter was to discuss the unique properties of the 7.5nm 18-Crown-6-modified AuNPs, with their synthesis and basic characterisation discussed in Chapter 2 Section 2.2.3. Through the use of temperature cycling, UV-Vis, DLS and TEM the 7.5 nm 18-Crown-6-modified AuNPs were shown to effectively demonstrate reversible agglomeration upon reaching a certain phase transition temperature point. That tipping point was also analysed and discussed, showing that phase transition point to be easily altered via the addition of the 18-Crown-6 –complimentary cation K^+, but showing no change when in the presence of other cations such as Na^+ and Li^+. The phase transition point data was then supported by ζ values showing that the 7.5nm 18-Crown-6-modified AuNPs behaved in a similar fashion to the 3nm 18-Crown-6-modified AuNPs described in Chapter 3; With a large increase in the positive charge present around/upon the particle being suggested to be responsible for the increase in stability upon addition of the complimentary cation.

Isothermal titration calorimetry (ITC) was attempted to try and observe the energetic changes in the system during the agglomeration process. Unfortunately, either through lack of experience upon the machine or the machine not being sensitive enough to detect this phase change, no reliable data involving the agglomeration process was attained, only what seemed to be salt dissolution peaks upon injection of the KCl solution. This technique should not be abandoned however, with proper experience and/or more sensitive equipment it is more than likely possible to detect the changes in enthalpy and entropy for the agglomeration process. This data would prove useful in understanding whether the system is behaving as is currently believed, or whether a completely different process is occurring that has not been thought of at present. Either way, further work involving the use of ITC should be done.

The 7.5 nm 18-Crown-6-modified AuNPs were then integrated into solutions containing vesicles like those used in Chapter 3 to achieve show cation transport through an artificial membrane. It was observed via the use of Cryo-TEM that when below the phase transition point the particle showed little to no interaction with the vesicle membrane, yet when subjected to temperatures above the phase transition point the particles appeared to integrate with the vesicle membrane much more effectively; Indicating that the instability cause by increasing heat can be used to push the 7.5nm 18-Crown-6-modified AuNPs into membranes instead of agglomerating together. A promising initial result that

could provide a starting pathway to developing a "sweet spot" particle capable of sitting within an artificial membrane and transport both cations and electrons.

Preliminary experiments for phase transfer were then initiated, attempting to achieve cation transfer from the aqueous phase to the organic phase, mimicking the characteristics of the smaller 3nm 18-Crown-6-modified AuNPs, with the results showing promise for both stability and transfer with regards to K^+, the expected complimentary cation. This mimicking of the 3 nm 18-Crown-6-modified AuNPs ability to transfer complimentary cations was then used to instigate some very preliminary phase transfer experiments to observe how the particle behave when in the presence of Ba^{2+}, the desired downhill reaction via the formation of BaSO4, and the redox couple, potassium ferro/ferri cyanide. In the hopes of starting to develop an understanding of how the two species interact, both together and with the 7.5 nm 18-Crown-6-modified AuNPS. With more advanced experiments currently being undertaken outside of this thesis as first steps towards achieving the desired goal; an AuNP capable of achieving both electron and cation transfer through an organic interface.

4.6 References

1. M. P. Grzelczak, A. P. Hill, D. Belic, D. F. Bradley, C. Kunstmann-Olsen and M. Brust, *Faraday Discussions*, 2016, **191**, 495-510.
2. H. A. P., K. O. Casper, G. M. P. and B. Mathias, *Chemistry – A European Journal*, 2018, **24**, 3151-3155.
3. K. Saha, S. S. Agasti, C. Kim, X. Li and V. M. Rotello, *Chemical reviews*, 2012, **112**, 2739-2779.
4. S.-Y. Lin, S.-W. Liu, C.-M. Lin and C.-h. Chen, *Analytical Chemistry*, 2002, **74**, 330-335.
5. H. Kuang, W. Chen, W. Yan, L. Xu, Y. Zhu, L. Liu, H. Chu, C. Peng, L. Wang, N. A. Kotov and C. Xu, *Biosensors and Bioelectronics*, 2011, **26**, 2032-2037.
6. R. Elghanian, J. J. Storhoff, R. C. Mucic, R. L. Letsinger and C. A. Mirkin, *Science*, 1997, **277**, 1078-1081.
7. C. A. Mirkin, R. L. Letsinger, R. C. Mucic and J. J. Storhoff, *Nature*, 1996, **382**, 607-609.
8. R. Klajn, K. J. Bishop and B. A. Grzybowski, *Proceedings of the National Academy of Sciences*, 2007, **104**, 10305-10309.
9. C. J. Orendorff, P. L. Hankins and C. J. Murphy, *Langmuir*, 2005, **21**, 2022-2026.
10. J. Song, J. Zhou and H. Duan, *Journal of the American Chemical Society*, 2012, **134**, 13458-13469.
11. Y. Kim, R. C. Johnson and J. T. Hupp, *Nano Letters*, 2001, **1**, 165-167.
12. H. N. Kim, W. X. Ren, J. S. Kim and J. Yoon, *Chemical Society Reviews*, 2012, **41**, 3210-3244.
13. J. S. Lee, M. S. Han and C. A. Mirkin, *Angewandte Chemie*, 2007, **119**, 4171-4174.
14. A. Housni and Y. Zhao, *Langmuir*, 2010, **26**, 12933-12939.
15. Y. Liu, X. Han, L. He and Y. Yin, *Angewandte Chemie International Edition*, 2012, **51**, 6373-6377.
16. F. Liu and S. Agarwal, *Macromolecular Chemistry and Physics*, 2015, **216**, 460-465.
17. C. Durand-Gasselin, R. Koerin, J. Rieger, N. Lequeux and N. Sanson, *Journal of colloid and interface science*, 2014, **434**, 188-194.
18. S. Chakraborty, S. W. Bishnoi and V. c. H. Pérez-Luna, *The Journal of Physical Chemistry C*, 2010, **114**, 5947-5955.
19. C. Durand-Gasselin, M. Capelot, N. Sanson and N. Lequeux, *Langmuir*, 2010, **26**, 12321-12329.
20. S. Salmaso, P. Caliceti, V. Amendola, M. Meneghetti, J. P. Magnusson, G. Pasparakis and C. Alexander, *Journal of Materials Chemistry*, 2009, **19**, 1608-1615.
21. M. Pernia Leal, A. Torti, A. Riedinger, R. La Fleur, D. Petti, R. Cingolani, R. Bertacco and T. Pellegrino, *ACS nano*, 2012, **6**, 10535-10545.

22. X.-Y. Liu, F. Cheng, Y. Liu, H.-J. Liu and Y. Chen, *Journal of Materials Chemistry*, 2010, **20**, 360-368.
23. X.-Y. Liu, F. Cheng, Y. Liu, W.-G. Li, Y. Chen, H. Pan and H.-J. Liu, *Journal of Materials Chemistry*, 2010, **20**, 278-284.
24. D. Roy, W. L. Brooks and B. S. Sumerlin, *Chemical Society Reviews*, 2013, **42**, 7214-7243.
25. D. n. Zámbó, G. r. Z. Radnóczi and A. s. Deák, *Langmuir*, 2015, **31**, 2662-2668.
26. R. Iida, H. Mitomo, Y. Matsuo, K. Niikura and K. Ijiro, *The Journal of Physical Chemistry C*, 2016, **120**, 15846-15854.
27. C. J. Pedersen, *Angewandte Chemie International Edition*, 1988, **27**, 1021-1027.
28. G. W. Gokel, D. M. Goli, C. Minganti and L. Echegoyen, *Journal of the American Chemical Society*, 1983, **105**, 6786-6788.
29. G. W. Gokel, W. M. Leevy and M. E. Weber, *Chemical reviews*, 2004, **104**, 2723-2750.
30. J. Li, D. Yim, W.-D. Jang and J. Yoon, *Chemical Society Reviews*, 2017, **46**, 2437-2458.
31. M. E. Childs and W. P. Weber, *The Journal of Organic Chemistry*, 1976, **41**, 3486-3487.
32. D. Landini, F. Montanari and F. M. Pirisi, *Journal of the Chemical Society, Chemical Communications*, 1974, 879-880.
33. A. E. Visser, R. P. Swatloski, W. M. Reichert, S. T. Griffin and R. D. Rogers, *Industrial & Engineering Chemistry Research*, 2000, **39**, 3596-3604.
34. F. Lucio-Martínez, B. Bermúdez, J. M. Ortigueira, H. Adams, A. Fernández, M. T. Pereira and J. M. Vila, *Chemistry-A European Journal*, 2017, **23**, 6255-6258.
35. J. Piella, N. G. Bastús and V. Puntes, *Chemistry of Materials*, 2016, **28**, 1066-1075.
36. M.-C. Daniel and D. Astruc, *Chemical Reviews*, 2004, **104**, 293-346.
37. S. Link and M. A. El-Sayed, *The Journal of Physical Chemistry B*, 1999, **103**, 4212-4217.
38. K. L. Kelly, E. Coronado, L. L. Zhao and G. C. Schatz, *The Journal of Physical Chemistry B*, 2003, **107**, 668-677.
39. M. Brust, D. Bethell, C. J. Kiely and D. J. Schiffrin, *Langmuir*, 1998, **14**, 5425-5429.
40. P. Mulvaney, *Langmuir*, 1996, **12**, 788-800.
41. G. C. Papavassiliou, *Progress in Solid State Chemistry*, 1979, **12**, 185-271.
42. M. Brust, R. Etchenique, E. J. Calvo and G. J. Gordillo, *Chemical Communications*, 1996, DOI: 10.1039/CC9960001949, 1949-1950.
43. L. Finegold and J. T. Donnell, *Nature*, 1979, **278**, 443.
44. H. Ruf, *Advances in Colloid and Interface Science*, 1993, **46**, 333-342.

45. X. Liu, Q. Dai, L. Austin, J. Coutts, G. Knowles, J. Zou, H. Chen and Q. Huo, *Journal of the American Chemical Society*, 2008, **130**, 2780-2782.
46. G. S. C., S. M. J. and K. N. A., *AIChE Journal*, 2004, **50**, 2978-2985.
47. D.-S. Yang and A. H. Zewail, *Proceedings of the National Academy of Sciences of the United States of America*, 2009, **106**, 4122-4126.
48. L. X. Dang, *Journal of the American Chemical Society*, 1995, **117**, 6954-6960.
49. Y. Marcus, *Journal of the Chemical Society, Faraday Transactions*, 1991, **87**, 2995-2999.
50. M. D. Tissandier, K. A. Cowen, W. Y. Feng, E. Gundlach, M. H. Cohen, A. D. Earhart, J. V. Coe and T. R. Tuttle, *The Journal of Physical Chemistry A*, 1998, **102**, 7787-7794.
51. R. A. Alberty, 1969, **244**, 3290-3302.
52. L. S. Mizoue and J. Tellinghuisen, *Biophysical Chemistry*, 2004, **110**, 15-24.
53. J. R. Horn, D. Russell, E. A. Lewis and K. P. Murphy, *Biochemistry*, 2001, **40**, 1774-1778.
54. J. E. O'Reilly, *Biochimica et Biophysica Acta (BBA) - Bioenergetics*, 1973, **292**, 509-515.
55. I. M. Kolthoff and W. J. Tomsicek, *The Journal of Physical Chemistry*, 1934, **39**, 945-954.
56. C. Beriet and D. Pletcher, *Journal of Electroanalytical Chemistry*, 1993, **361**, 93-101.

Chapter 5 Conclusions and Future Work

In this chapter potential experiments/methodology that could be implemented to further improve upon the research presented in this thesis shall be discussed. With a summary of the negatives and positives that arose from the work; followed by some suggestions on how to improve. The overall thesis will then be summarised briefly in a conclusion stating which milestones were reached and how the overall project can be taken further.

5.1 The flocculation of 3 nm 18-Crown-6-modified AuNPs

In Chapter 3 section 3.1.2 the increased rate of transfer from the aqueous phase to the organic phase (chloroform) was discussed; when 15-Crown-5-modified AuNPs were in the presence of a non-complimentary cation K^+. It was determined via the analysis of the zeta potential (Figure 3.18) and UV-Vis spectroscopy (Figure 3.19), as well as literature study, that this increased rate of transfer could be due to the sandwiching of a singular cation between multiple crown ethers. This process would explain both the dramatic changes in zeta potential and the rate of transfer, a property that should be exploited further to potentially increase the rate of cation transfer across organic interfaces.

A suitable experiment set to provide further insight into this unexpected trait is to determine whether the effect is reproducible for a non-complimentary cation that is large than the crown ether in question; Meaning Na^+ for 12-Crown-4 (this property was potentially already observed as described in Chapter 3 but should not be considered fact until tested again) and Rb^+/Cs^+ 18-Crown-6. If the theory proves correct and increased rates of transfer can be shown for larger non-complimentary cations, it could prove useful for increasing the overall rate of cation transfer.

Vesicle experiments as described in Chapter 3 section 3.6.2 should follow these results as they would further validate this process as a method of increasing the rate of transfer, providing that the particles are still suitably inclined to reside within the membrane when the particles experience the sandwich effect. This can only be found out through testing however.

5.2 Cyclic Voltammetry as a method of observing charge transfer across a membrane.

Whilst the preliminary phase transfer experiments combined with the vesicle membrane cation transfer provide a convincing argument for the transfer of cations across a membrane. An approach that would not only reinforce these results but provide a strong set of quantitative data, is the use of cyclic voltammetry across a planar membrane to observe the rate of charge transfer electrochemically. This technique is currently being developed by Stephen Danks within the Brust research group, not only perfecting the method of developing the planar membranes, but also beginning to collect informative data on the behaviour of the particles when in solution and presented with various salts/positive charges (H^+). Such a process could progress the project by allowing fine tweaks to be made to the system to optimise the rate of transfer, whilst also allowing for a high degree of reproducibility and increasing throughput of future results.

5.3 Control of 3nm 18-Crown-6-modified AuNPs partitioning between aqueous and organic phase via changes in temperature.

A property of the 3 nm 18-Crown-6-modified AuNPs that was found late on during the project, which was unfortunate due to it being quite a fascinating property that was briefly discussed in Chapter 3 section 3.5.1, whereby the concentration of particles present within: the aqueous phase, the interface and the organic phase (dichloromethane) could be controlled by a change in temperature. The most logical way to progress this experiment set would be to attempt ITC, much like that which was attempted on the 7.5 nm 18-Crown-6-modified AuNPs in Chapter 4.

This task would not be trivial however, attempting to observe the thermodynamic changes of a system involving both an aqueous and an organic phase would be extremely difficult, especially as most ITC instruments deteriorate when subjected to organic solvents, meaning the acquirement of quantitative data would be a challenge. Gaining more insight into the system via the use of a live UV-Vis spectrum could show promise however, with both the aqueous and organic phase being monitored in real time as the temperature is changed. This would allow for the portioning of the particles to be

qualitatively measured, providing insight into how to optimise the temperature control of the system. Ocean Optics sell portable UV-Vis spectrometers that can be used to analyse a solution within a cuvette in real time, a suitable appliance capable of achieving these results.

5.4 Further experimentation with cryo-TEM on vesicle incubation

Cryo TEM was a staple analytical tool used within this thesis to directly observe the interaction between vesicles and the crown ether particles. The major issues were its failure rate (2 in 3 grids were unsuccessful) and the preparation time, even when in the hands of a highly skilled user (Dr Domagoj Belic). This resulted in the experiments done within this thesis being very "to the point", attempting to gather the vital information that was required to confirm whether they particles were in the membrane or not. This did not allow for interesting experiments to be run such as: observing how the change in particle concentration affects interactions with the vesicles, how changes in the vesicle size affects vesicle and particle interaction and how changes in the media (addition of small quantities of ethanol for example) could alter the interaction. These experiments, whilst not vital to the project would have certainly been interesting to try, potentially providing useful insight into how factors such as concentration play a role.

5.5 Optimisation of the Environmental SEM to observe the 7.5nm 18-Crown-6-modified AuNPs in situ when altering the temperature

In Chapter 4 Section 4.1.4 attempts to observe how the 7.5 nm 18-Crown-6-modified AuNPs behaved in situ when subjected to changes in temperature were attempted. Whilst the result proved insightful into how the particles dried down onto a grid under vacuum, the true intent of the experiment was never reached. However, that is not to say that this occurred because of limitations with the machine, but more about finding just the right environment in which to successfully observe the droplet at up to 50°C, whilst under vacuum, yet retaining the right humidly level to prevent the droplet from evaporating but

also allowing for an acceptable resolution of the particles themselves. Chapter 4 showed how the particles look when dried out on a TEM grid, very much like a large polymeric network, which, whilst backed up by both DLS and UV-Vis spectroscopy, would have been nice to observe the formation of in a more visual way. A similar effect could also be achieved by cryo-TEM, albeit with a similar level of experimental optimisation to bear fruit. Being able to observe the development of the large 3D structure would be both extremely interesting from a visual perspective, but also allow for the thermodynamics of the system to be better understood. It was postulated that the system initially developed strings of particles which then eventually collapsed into one another to create the much larger structures, being able to prove this via an SEM "video" is something that could further the understanding of the particles used within this thesis.

5.6 ITC calorimetry as a method for determining the thermodynamics of the 7.5 nm AuNP 'reversible agglomeration'

In Chapter 4 ITC was used in an attempt to collect values for ΔH, ΔS and ΔG for the 'reversible' agglomeration' observed when the 7.5 nm 18-Crown-6 modified AuNPs were subjected to changes in temperature. This set of experiments resulted in not being able to provide such data, with multiple factors being the cause for this: The ITC used (NanoITC) did not have the correct specifications to detect the change in state for the colloidal solution, the concentration of particles was not high enough to be able to see an observable change; linking in with the previous limitation, and the lack of experience with using such an analytical tool.

The insight that ITC data could provide with regards to this interesting 'reversible agglomeration' characteristic would prove invaluable in furthering our understanding of exactly how it occurs, which would provide the information needed to fully exploit the effect and allow for a more successful interaction with organic interfaces.

The major factor believed to result in not obtaining substantial data was sensitivity limitations within the machine, either because it is simply not possible to detect this interaction (unlikely), or the combination of sensor limitation/particle concentration was not correct. Solutions for this are to use a more sensitive machine such as the Affinity

ITC provided by TA instruments, capable of detecting heat changes of 0.04 uJ, or to increase the concentration of the colloidal solution. The limitation for this is that upon centrifugation a large proportion of particles can be lost to the walls of the centrifuge tube, resulting in increasing the concentration of the solution by even 10-20% becoming a very time-consuming task, with potential for particle destabilisation as the solution is subjected to multiple centrifugations. The most effective solution for this would be to find centrifuge tubes capable of providing an entirely non-stick coating, allowing for no loss of particles during the centrifugation steps.

The next factor believed to be responsible for not achieving substantial data for this experiment set was lack of experience with the tool itself; the experiment should be repeated with a more experienced hand, capable of tweaking the parameters, allowing for the experiment to be optimised for the colloidal solution in question.

It was also believed that the use of a 24-carat gold cell could be causing unwanted interactions between the colloidal solution and the cell wall. To combat this a more suitable material such as Hastelloy should be used in order to provide a more sufficient barrier between the solution and adhering to the cell walls.

If these changes could be implemented, then the gathering of the thermodynamic data for the 'reversible agglomeration' effect could be possible.

5.7 Use of 7.5 nm 18-Crown-6-modified AuNPs in achieving both cation and electron transfer

In the final section of Chapter 4 preliminary phase transfer data was discussed with regards to starting to develop a procedure/technique of being able to transport not only cations (specifically the complimentary cation), but also electrons via the introduction of a redox couple (potassium ferro/ferri cyanide), in the hopes of coupling the two processes together and develop the desired final goal system. This preliminary data is currently being used within the research group to further this goal and some interesting experiments have been postulated.

Figure 5.1 is an illustration provided by Casper Kunstmann[1] a researcher within the Brust group. The illustration is a simplified model being used to describe how both electron

and cation transport could occur between aqueous droplets that had differing environments, by incorporating the 7.5 nm 18-Crown-6-modified AuNPs inside and allowing them to shuttle between the two environments through an organic phase (chloroform).

This experiment set is still in the making and will require tweaking and optimisation to fully realise whether the hybridisation of the two processes is possible, but the process is advancing and is believed to be using the 7.5 nm 18-Crown-6-modified AuNPs as the transporting shuttle, the process the particles were designed for.

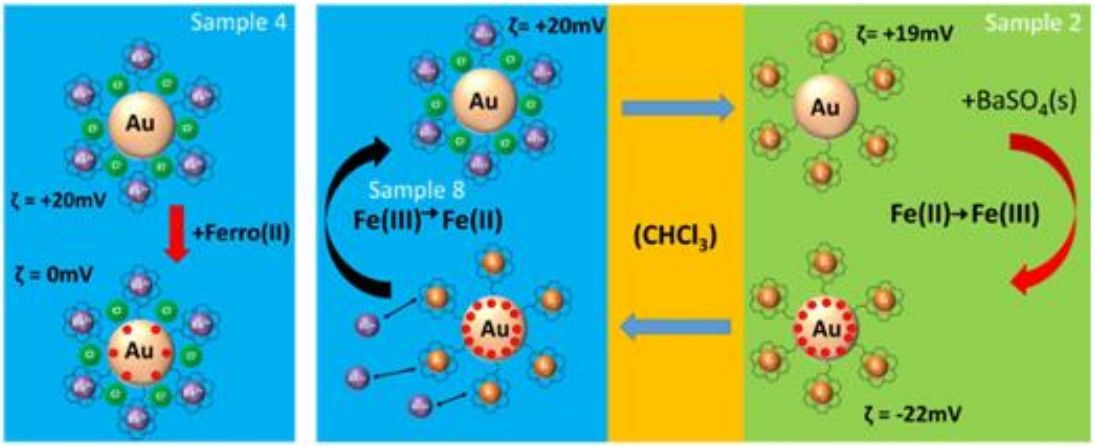

Figure 5.1: Illustration provided by Casper Kunstmann showing how the 7.5nm AuNPs developed within this thesis are being used within water in chloroform emulsion experiments to demonstrate that both cation and electron transport are potentially occurring.

5.8 Complimentary Cation sensitive electrodes by coating with 7.5 18-Crown-6-modified AuNPs

Chapter 4 discussed interesting property of the 7.5 nm 18-Crown-6-modified AuNPs whereby upon heating they would not only agglomerate with one another, but also readily stick to the container surface, resulting in increasingly thick layers of AuNPs upon the surface.

It may be possible to exploit this property and combine this surface adherence with the cation selectivity that these particles exhibit. If an electrode is left within a solution of the 7.5 nm 18-Crown-6-modified AuNPs throughout a series of heating cycles it would be possible to develop a thin film of cation selective AuNPs upon the surface. Due to the insolubility they have within aqueous solutions after adhering to a surface it may be possible to use the modified electrode to detect changes in salt concentration within a

body of water. With the charge located near the surface of the electrode being dependant on the effective binding of cations present within the crown ether AuNPs, resulting in an observable change in voltage measured.

This is of course only a postulation and has not actively been tested but is a potential idea for which these particles may have an application for.

5.9 Final Conclusions

To conclude, the main goal of the project was to initiate the development of AuNPs capable of selectively transporting charge across organic interfaces; with the first milestone being the transfer of cations, and the second being the transfer of electrons. The first milestone was readily achieved with 3 nm AuNPs; starting from simple preliminary phase transfer experiments with various crown ether types, giving rise to a greater understanding of the system and how it behaves, to developing vesicle systems capable of showing the effective transport of cations via the use of fluorescence dyes; with the ability to observe this interaction between vesicle and particle directly via the use of cryo-TEM. These successes were then transferred to the larger 7.5 nm 18-Crown-6-modified AuNPs, the development of which was no easy task, resulting in not only the potential for cation transfer, but also electron transfer. Throughout the progression of both particle systems, unique and interesting properties were observed; some being studied extensively, whilst others ran short on time, no doubt interesting work for future research.

The second milestone, the successful transfer of electrons, was not fully realised, headway was made into starting to develop systems capable of achieving this via the use of redox couples. With the work in this thesis pathing the way for the future, it is certain that the development of an AuNP capable of achieving both cation and electron transfer as a coupled system is on the horizon.

5.10 References

1. C. Kunstmann, personal communication.